INFORMATION TO USERS

The most advanced technology has been used to photograph and reproduce this manuscript from the microfilm master. UMI films the text directly from the original or copy submitted. Thus, some thesis and dissertation copies are in typewriter face, while others may be from any type of computer printer.

The quality of this reproduction is dependent upon the quality of the copy submitted. Broken or indistinct print, colored or poor quality illustrations and photographs, print bleedthrough, substandard margins, and improper alignment can adversely affect reproduction.

In the unlikely event that the author did not send UMI a complete manuscript and there are missing pages, these will be noted. Also, if unauthorized copyright material had to be removed, a note will indicate the deletion.

Oversize materials (e.g., maps, drawings, charts) are reproduced by sectioning the original, beginning at the upper left-hand corner and continuing from left to right in equal sections with small overlaps. Each original is also photographed in one exposure and is included in reduced form at the back of the book. These are also available as one exposure on a standard 35mm slide or as a 17" x 23" black and white photographic print for an additional charge.

Photographs included in the original manuscript have been reproduced xerographically in this copy. Higher quality 6" x 9" black and white photographic prints are available for any photographs or illustrations appearing in this copy for an additional charge. Contact UMI directly to order.

U·M·I

University Microfilms International
A Bell & Howell Information Company
300 North Zeeb Road, Ann Arbor, MI 48106-1346 USA
313/761-4700 800/521-0600

Order Number 9000065

Computational model of velocity generation from patterns of otolith activation during off-vertical axis rotation (OVAR)

Schnabolk, Charles, Ph.D.

City University of New York, 1989

U·M·I
300 N. Zeeb Rd.
Ann Arbor, MI 48106

COMPUTATIONAL MODEL OF VELOCITY GENERATION FROM PATTERNS OF OTOLITH ACTIVATION DURING OFF-VERTICAL AXIS ROTATION (OVAR)

by

CHARLES SCHNABOLK

A dissertation submitted to the Graduate Faculty in Computer Science in partial fulfillment of the requirements for the degree of Doctor of Philosophy, The City University of New York.

1989

This manuscript has been read and accepted for the Graduate Faculty in Computer Science in satisfaction of the dissertation requirement for the degree of Doctor of Philosophy.

January 19, 1989
date

Theodore Raphan
Chairman of Examining Committee

January 19, 1989
date

T C Wendlberger
Executive Officer

Professor Michael Anshel

Professor Bernard Cohen

Professor Theodore Raphan (Chairman)

Professor Fred Thau

Professor Chaim Ziegler

Supervisory Committee

The City University of New York

Abstract

COMPUTATIONAL MODEL OF VELOCITY GENERATION FROM PATTERNS

OF

OTOLITH ACTIVATION DURING OFF-VERTICAL AXIS ROTATION

(OVAR)

by

Charles Schnabolk

Advisor: Professor Theodore Raphan

Rotation about an off vertical axis (OVAR) causes continuous unidirectional horizontal nystagmus in darkness (Guedry, 1965). Evidence from a wide range of studies suggest that the otoliths are the primary effectors in generating the continuous nystagmus. The purpose of the dissertation was to develop a model which would show how the continuous nystagmus during OVAR might be generated by estimating the velocity of the head from changing patterns of otolith excitation and inhibition. The model examined how noise and the distribution of the polarization vectors affect the estimation. We also examined how the model might be extended to three dimensions to gain an understanding of how position signals are processed to obtain

an estimate of head velocity.

In one dimension the estimation of velocity is based on a "template matching" algorithm. It is assumed that a signal arising in each cell of the macula is delayed by a certain time (T). Thus, as the head rotates in the gravitational field a delayed pattern representing a previous position of the head is available as a "template" that can be compared to the pattern associated with the present position of the head.

The extension of the model to three dimensions shows that:

1. two patterns do not contain sufficient information to uniquely specify the velocity,
2. An estimate utilizing four patterns computes an accurate estimate of head velocity based on otolith position information,
3. the estimator and velocity storage integrator form a robust compensator for head rotations in gravitational environments.

Acknowledgements

I wish to express my warm gratitude to my mentor, Professor Theodore Raphan. If not for his support and encouragement I would not be earning this degree. Each time I needed his help, he took the time to help me complete this dissertation. We spent many hours together in which he kindly gave me some of his insights and guidance. Almost all of my work on this dissertation was done in the laboratory that he designed at Brooklyn College.

I wish to thank all the members of my committee, Professors Michael Anshel, Bernard Cohen, Fred Thau, and Chaim Ziegler for their time and effort in guiding and examining me, as well as reading and constructively criticizing this dissertation. I appreciated the personal time each of the committee members gave me.

I wish to thank the members of the Department of Computer and Information Science and of the Department of Physics at Brooklyn College for their support and encouragement. In particular I wish to thank Professors Patrick Sterbenz, Keith Harrow, Robert Fanelli, and Gerry Weiss, and Ms. Deborah Sturm and Ms. Gilder Shani, and others who gave up some of their time in support of my fulfilling some of the requirements needed to earn the Ph.D. degree. I also wish to thank Professor Kenneth McAloon for his time and effort in his administration of the language exam.

Finally, I wish to acknowledge the support given to me by The National Institute of Health under Grant No. EY04148 to Theodore Raphan and the PSC-CUNY research award program Award No. 6-63231 to Theodore Raphan.

TABLE OF CONTENTS

Chapter		Page
1	INTRODUCTION	1
	1.1 Rationales and Motivation	1
	1.2 Organization of Dissertation	4
2	MODELS OF THE VESTIBULO-OCULAR REFLEX AND VISUAL-VESTIBULAR INTERACTION	10
	2.1 The Semicircular Canals: Coordinate Frame and Dynamical Models	10
	2.2 Eye Movements in Response to Rotations about a Vertical Axis	25
	2.3 Biophysics of the Otolith Organs	35
	2.4 Eye Movements and OVAR	46
3	MODEL FOR SLOW PHASE EYE VELOCITY ESTIMATION FROM PATTERNS OF OTOLITH ACTIVATION DURING OVAR	50
	3.1 Modelling the Estimation as a One-Dimensional Process	50
	3.1.1 Conceptual Basis for Model	50
	3.1.2 Computation of Head Velocity Estimate During OVAR	60
	3.1.3 Model Simulations and Comparison with Physiological Data	80

Chapter Page

3.1.4 Effects on Estimation of Nonuniform Otolith Polarization Angle Spacing 92

3.1.5 Effects of Nonideal Time Delay on the Estimator 101

3.1.6 Effects of Noise on the Estimation of Head Velocity 155

3.2 Modelling the Three-Dimensional Properties on Velocity Estimation 165

3.2.1 Polarization Vectors: Space and Head Representations 173

3.2.2 Three-Dimensional Estimation by Combining Three One-Dimensional Ideal Noise Free Models 180

3.2.3 Estimation as a Function of Gravity, Head Angular Velocity, and Canal Orientation 198

3.2.4 Analysis of the Three-Dimensional Estimator for Head Angular Velocity Parallel to a Canal Axis 221

3.2.5 Two-Pattern Estimator, Simulations and Results 224

Chapter Page

3.2.6 Approaches to Multiple Pattern Estimation 249

4 SUMMARY CONCLUSIONS AND FUTURE RESEARCH 274

4.1 Summary 274

4.2 Discussion 279

4.3 Recommendations for Future Research 287

APPENDIX A: REDUCTION OF THE COMPUTATIONAL COMPLEXITY OF VELOCITY ESTIMATION 289

APPENDIX B: IDENTITIES AND FORMULAE USED IN DERIVING ESTIMATION ALGORITHM 292

APPENDIX C: COMPUTER PROGRAMS USED TO GENERATE EYE VELOCITY COMMAND IN FIGURES 3.1.10, 3.1.14, and 3.2.16 295

BIBLIOGRAPHY 323

LIST OF ILLUSTRATIONS

Figure		Page
2.1	Orthogonality of the semicircular canal planes	12
2.2	Three-dimensional model of the VOR and the orientation of the semicircular canals with respect to the head axes	13
2.3	Dynamical model of a semicircular canal	15
2.4	Illustrations of the vestibular organs and their responses to acceleration	17
2.5	A single bundle of cilia in the utricular macula	18
2.6	Displacement of a bundle of cilia in the saccular macula	20
2.7	Directional sensitivity of a hair cell in the saccular macula	21
2.8	Sinusoidal canal stimulation in monkey	22
2.9	One-dimensional model of the VOR	27
2.10	VOR due to rotations about a vertical axis	28
2.11	Otolith unit response to a slow pitch angular velocity	37
2.12	Evidence for a biological realization of a delay operator	38
2.13	Schematic of the utricular and sacular polarization vector distributions	40
2.14	Polarization vector distribution in monkey	41
2.15	Dynamical model of an otoconium and a bundle of cilia	43
3.1.1	Effects of rotating the utricular macula in a gravitational force field	51
3.1.2	Model of the spatial ordering of otolith cells and an N-dimensional pattern vector	55

Figure		Page
3.1.3	The association of a unit polarization vector with a particular cell and a representation of the otolith activation pattern	57
3.1.4	Spatio-Temporal relation between patterns of otolith cell activation	62
3.1.5	Estimate of the spatial displacement by template pattern matching	67
3.1.6	Formula and implementation of the velocity estimator	74
3.1.7	Response to off-vertical axis rotation	81
3.1.8	Effects of delay time on the steady state estimate of head velocity	84
3.1.9	The dynamic response of the system to a step in head velocity during off-vertical axis rotation	87
3.1.10	The dynamic response of the velocity storage integrator to a sudden tilt when driven by the estimator	90
3.1.11	Functional polarization vector distribution in the left utricule	93
3.1.12	Estimate of the head angular velocity given a nonuniformly spaced polarization vector distribution	95
3.1.13	The average, the maximum, and the minimum of the estimate for one head rotation as a function of the head angular velocity given a nonuniformly spaced polarization vector distribution	97
3.1.14	The eye velocity command as a function of time given a nonuniformly spaced polarization vector distribution	98
3.1.15	Estimate of velocity given a first order system replacing the ideal delay operator	118
3.1.16	Eye velocity command given a first order system replacing the ideal delay operator	120
3.1.17	Steady state estimate of velocity given a first order system replacing the ideal delay operator	124

Figure		Page
3.1.18	Estimate of velocity given a second order system replacing the ideal delay operator	141
3.1.19	Eye velocity command given a second order system replacing the ideal delay operator	145
3.1.20	Steady state estimate of velocity given a first order system replacing the ideal delay operator	149
3.2.1	Time dependence of a macular normal do to misalignment with head velocity	166
3.2.2	Three-dimensional system responding to OVAR	168
3.2.3	Correspondence between a gravity vector and an otolith activation pattern	171
3.2.4	There are many head velocities corresponding to two activation patterns or two gravity vectors	172
3.2.5	Space, head and canal coordinate systems	174
3.2.6	First stage of processing to obtain three functional planes of polarization vectors	181
3.2.7	Functional polarization vector obtained from unit polarization vectors	186
3.2.8	Polar coodinate representation of a functional polarization vector	188
3.2.9	In the two-pattern estimator, normalization depends on tilt angles of the canal axes	193
3.2.10	The estimate as a function of the head angular velocity, the orientation of the canal axes, and gravity	199
3.2.11	Estimate of velocity given a two-pattern three-dimensional estimator	225
3.2.12	The number of extremum, generated by the two-pattern three-dimensional estimator, is four at a head angular velocity magnitude of 90 degrees/second	227

Figure		Page
3.2.13	The average, the maximum, and the minimum estimates over one head rotation as a function the head angular velocity magnitude	229
3.2.14	The average, the maximum, and the minimum estimates over one head rotation as a function of the angle between the head yaw axis and the space vertical	232
3.2.15	A canal component of the average, the maximum, and the minimum estimates over one head rotation as a function of the angle between the canal axis and the head angular velocity	235
3.2.16	Eye velocity command generated by the three-dimensional velocity storage integrator with input from the two-pattern estimator	238
3.2.17	Slow phase eye velocity using a two-pattern estimator	241
3.2.18	Magnitude of the slow phase eye velocity (or eye velocity command) as a function of time.	244
3.2.19	The left lateral component of the eye velocity command from the three-dimensional velocity storage integrator with a head yaw time constant of 6 seconds	245
3.2.20	The head yaw component of the slow phase eye velocity generated by the three-dimensional velocity storage integrator with the head yaw time constant of 6 seconds	246
3.2.21	A gravity vector difference is perpendicular to the head angular velocity	254
3.2.22	Model of the 1^{th} component of the four-pattern three-dimensional estimator	256
3.2.23	Steady state estimate of velcoity generated by the four-pattern three-dimensional estimator	260
3.2.24	Dynamic estimate of velocity in canal coordinates after a sudden tilt	266
3.2.25	Dynamic estimate of velocity in head coordinates after a sudden tilt	268
3.2.26	Eye velocity command generated by a three-dimensional gravity dependent velocity storage integrator with input from the four-pattern estimator	272

CHAPTER 1

INTRODUCTION

1.1 Rationales and Motivation

The vestibulo-ocular reflex (VOR) is important for generating compensatory eye movements that maintain stable gaze. An understanding of the functional aspects of the vestibulo-ocular reflex should prove useful in interpreting the effects of lesions and in diagnosing and treating patients whose vestibular system has been impaired. The purpose of this research is to contribute towards that understanding by developing computational models of how the central nervous system estimates the velocity of the head from otolith information as it rotates in a gravitational environment. A great deal of work has been done in characterizing the VOR for head rotations about a vertical axis. Such rotations activate the semicircular canals and produce nystagmus whose slow phase velocity decays to zero as rotation continues (See Wilson & Melvill-Jones, 1979; Henn, Cohen & Young, 1980 for review). In contrast, the response to off-vertical axis rotation (OVAR) generates continuous horizontal nystagmus in darkness (Guedry, 1965; Benson & Bodin, 1966a). The mechanism for producing this response is not well understood.

Attempts to model nystagmus generation during off-vertical axis rotation have involved considering both the effects of gravity on the semicircular canals (Benson & Bodin, 1966a; Steer, 1970) and on the otolith organs (Guedry, 1965). There is now considerable evidence that the otolith organs are the more likely candidates for producing the bias component of slow phase velocity. They are continuously stimulated by yaw rotation about off-vertical axes (Guedry, 1965; Graybiel & Miller, 1968; Benson, 1974; Guedry, 1974) and canal plugging does not abolish the response characteristics (Cohen, Suzuki & Raphan, 1983; Correia & Money, 1970; Janecke, Jongkees & Oosterveld, 1970). In addition, recordings from eight nerve canal afferents do not show maintained direction specific responses during constant velocity rotation (Goldberg & Fernandez, 1981; Raphan et al, 1983).

It has been suggested that the velocity command signal that produces the bias component during OVAR is formed in the central nervous system by detecting the moving pattern that occurs as otolith afferents with different polarization vectors (Flock, 1964; Flock & Wersall, 1962; Lowenstein & Wersall, 1959) sequentially excited by a rotating gravity vector (Guedry, 1965; Raphan et al. 1981; Schnabolk & Raphan, 1986). However, a precise mathematical description of how the sequential activation of hair cells by gravity is transduced to give an estimate of head velocity has not yet been formulated. In addition, there needs to be established a relationship between the dynamics of eye velocity and unit activity during OVAR and the model

predictions.

The purpose of this thesis is to model how the central nervous system processes changing patterns of otolith activation to estimate the velocity of the head as it moves in a gravitational environment. The proposed algorithms have been examined for robustness with regard to noise as well as the cellular polarization distribution in the macula. We have also examined the extension of the model to three dimensions. These analyses are important for interpreting unit activity in the central vestibular system during OVAR (Reisine et al, 1988) and relating it to the behavioral responses. The effects of velocity storage on the estimated command signal have also been evaluated as it plays an important role in generating the bias component of slow phase velocity during OVAR (Raphan et al, 1981; Raphan & Cohen, 1985; Hain, 1986). The model explains many of the steady state and dynamic characteristics of nystagmus during OVAR and provides a theoretical basis for studying otolith-oculomotor processing during sustained motion of the head in a gravitational field.

1.2 Organization of Dissertation

This dissertation is organized into essentially three parts. The first part (chapter 2) gives a description of the prominent aspects of the biophysics of the vestibular apparatus, the velocity characteristics of eye movements generated by the vestibular ocular reflex (VOR) and the work that has been done to understand its function. Evidence is reviewed which indicates that the brain carries out its internal processing in canal coordinates. In section 2.1, the biophysics of semicircular canal transduction is examined. It is shown that a first order system can be used to model the canal transduction process. It is then shown how this simple model is used to excite a velocity storage mechanism to model the prominent features of the vestibulo-ocular reflex (VOR) (sec. 2.2). In section 2.3 the biophysics of the otolith transduction is examined and the work showing that the otolith transduction can be approximated by a first order system with a 16 millisecond time constant is summarized. This indicates that the otoliths essentially code the position of the head when it is moved with regard to gravity. In section 2.4 eye movments due to off-vertical axis rotation (OVAR) and associated models are examined.

The second and third parts of the dissertation (chapter 3) develop a head angular velocity estimator using the distributed nature of the cells in the otolith macula. In section 3.1.1 the conceptual

basis for the angular velocity estimator, is developed. In section 3.1.2 an idealized one-dimensional model is constructed assuming that the estimate is derived from patterns of otolith activation. The model assumes noiseless signals, uniformly spaced polarization vectors, and an ideal time delay constant. Two patterns of otolith activation such that one pattern is delayed relative to the other are used in a "template" matching algorithm to obtain the estimate of head velocity as the head rotates relative to gravity. The estimate is proportional to the sampling function of the product of the head velocity and the time delay constant and closely approximates the eye velocity versus head velocity curve for the monkey.

In section 3.1.3 the results and simulations for the one dimensional model are presented. It is shown that a value of 0.85 seconds for the parameter, T, explains both the steady state and dynamic properties of eye velocity during OVAR. The one-dimensional model simulated data from an OVAR experiment in which a subject was suddenly tilted after rotating about a vertical axis. Simulations of the estimator with a distribution of nonuniformly spaced polarization vectors (section 3.1.4) showed that the steady state estimate oscillates with twice the head frequency. It indicates that the oscillations in horizontal eye velocity during OVAR may in part be due to the oscillations in the estimator. When the estimate is processed through the velocity storage integrator a significant amount of the oscillations are damped. It shows that velocity storage smooths the

velocity command coming from the estimator.

In section 3.1.5 the effects of replacing the ideal delay of section 3.1.1 by a first or second order system is examined. The steady state output from either the first or second order system for small head velocities is approximately a delayed version of the input. In either case for small head velocities, the steady state output from the estimator is approximately equal to the head velocity. For both the first and second order system approximations to the delay, increases in head velocity cause the steady state output from the estimator to rise to a maximum and then decay to zero. In section 3.1.6 the effects of additive noise are considered to test the robustness of the model due to perturbations which are inherent in the system. It is shown that the average value of a one-sided estimate contains a term proportional to the number of cell groups. A modification of the ideal estimator to compute an unbiased spatial difference causes the average value of the estimate to be less prone to noise perturbations. The utilization of a bilateral estimator also enhances the noise immunity of the estimator.

The third part of the dissertation (section 3.2) extends the model to three dimensions. In section 3.2.1, a space reference frame determined by gravity and a corresponding coordinate system is represented. A head reference frame and a corresponding coordinate system is also represented, because slow phase eye velocities are measured relative to the head and polarization vectors are fixed in

the head. In 3.2.2 a three-dimensional estimate based on three idealized models from section 3.1.1 is developed. The model assumes that the estimate is formed in canal coordinates. Therefore, the canal coordinate system is represented in the head reference frame. If the complementary canal planes are not parallel then there would be six canal coordinates, three associated with each side of the head. The left and right side estimates would then be appropriately combined (Pellionisz, 1986). However, the complementary canal planes are approximately parallel (Robinson, 1982) and this simplified approach has been taken in this study.

The limitations of the information content of the otolith patterns are then examined. It is shown that the patterns of otolith activation do not contain enough information from which an accurate estimate of the head velocity can be obtained and an estimate of the head velocity based on the patterns will be in error with respect to direction as well as magnitude. For small head velocities, the three-dimensional estimator computes the component of the head velocity perpendicular to gravity. The estimator then normalizes each component of the result of the computation.

In section 3.2.3 the estimate generated from the two-pattern estimator is described as a function of gravity, the head angular velocity, and the orientation of the canal axes. From this analysis it is shown that the estimate can be decribed in terms of the component of the head angular velocity perpendicular to gravity and

the vector cross product of the space vertical and the head angular velocity. In section 3.2.4 it is shown that if the head angular velocity is along a canal axis then, the component of the estimate along the canal axis reduces to the one-dimensional result. In section 3.2.5 model simulations and their comparison to physiological data are presented. The simulations showed that the estimates oscillated as the head rotated. The frequency of oscillations were equal to the frequency of head rotation. The simulations showed that usually a pair of components of the estimate were 90 degrees out of phase with one another. The phase relations depends on the orientation of the canal axes relative to the head angular velocity and gravity.

For experimental conditions in which the head angular velocity is parallel to the head yaw axis, the angle between the left lateral canal axis and the head angular velocity is approximately 15 degrees. Under these conditions the left lateral canal component of the estimate, generated by the two-pattern model, is in good agreement with the experimental data. However, recordings in a right anterior (or posterior) canal unit show that the brain is obtaining an estimate which oscillates about a nonzero bias. The bias is a good estimate of the right anterior (or posterior) canal component of the head angular velocity. The angle between the head angular velocity and the anterior (or posterior) canal axis is approximately 100 degrees. Under these conditions the left anterior (or posterior) canal

component of the estimate, generated by the two-pattern model, oscillates with a bias of approximately zero. Therefore, the corresponding steady state component of the eye velocity command generated by the two-pattern three-dimensional velocity storage integrator has a bias of approximately zero. Unit recordings in the central vestibular system suggest that the bias component of slow phase velocity is coded approximately along all axes.

In section 3.2.6 a four-pattern three-dimensional model is developed. This estimator utilizes difference patterns which represent three-dimensional vectors which are perpendicular to the head angular velocity. If the head angular velocity is constant this model generates an estimate that is parallel to the head angular velocity with a magnitude equal to wSa(wT), where w is the head angular velocity, T is the time delay constant, and Sa(.) is the sampling function. This estimator predicts that the three components of head velocity are estimated accurately and that the oscillations in frequency of vertical canal activity during OVAR is mainly due to oscillations in the velocity storage integrator.

In chapter four, we present a summary and recommendations for future reseach.

CHAPTER 2

MODELS OF THE VESTIBULO-OCULAR REFLEX AND VISUAL-VESTIBULAR INTERACTION

Modelling the vestibulo-ocular reflex has proven to be important for understanding visual-vestibular interactions as well as the effect of lesions and drugs (Raphan et al, 1979; Waespe et al, 1983; Cohen et al, 1987). To understand the effects of gravity on the vestibulo-ocular reflex such as during OVAR, it is first necessary to have an understanding of the system organization in three dimensions. The purpose of this chapter is to review models that have been developed in one dimension and their extension to three dimensions. We will review work which establishes the coordinate bases and the dynamical properties of the VOR that determine the central processing of the signals related to movement of the head and visual surround. The aim is to show how the model of the velocity estimator developed in this thesis fits into the overall three-dimensional model of the vestibular ocular reflex.

2.1 The Semicircular Canals: Coordinate Frame and Dynamical Models:

The semicircular canals respond to angular acceleration and

generate compensatory eye movements when the head is rotated (see Wilson & Melvill-Jones, 1979, for review). There are three semicircular canals: the lateral, anterior, and posterior canals, on each side of the head that lie in planes approximately orthogonal to one another (Fig. 2.1B). The orientation of the canal planes are tipped up approximately 15 degrees and rotated 45 degrees with regard to the steriotaxic, frontal and sagittal planes. Eye movements have been generally measured in this frame which has been designated a "head based" coordinate frame. If a right handed coordinate system is utilized the orientation of the canal based coordinate frame with respect to the head is given by the following matrix transformation (Fig. 2.2B, Raphan & Cohen, 1985):

$$T_{can} = \begin{vmatrix} 0.707 & 0.683 & -0.183 \\ -0.707 & 0.683 & -0.183 \\ 0.0 & 0.259 & 0.966 \end{vmatrix}. \qquad (2.1.1)$$

There are complementary semicircular canals on the right side of the head whose planes are approximately parallel to those on the left (Robinson, 1983; Pellioniez, 1986; Curthoys, et al, 1977; Reisine et al, 1988) and represent a mirror image coordinate system. The nonorthogonality of the canal system on both sides of the head have been considered and have led to a representation of their transformation properties by higher dimensional matrices or tensors

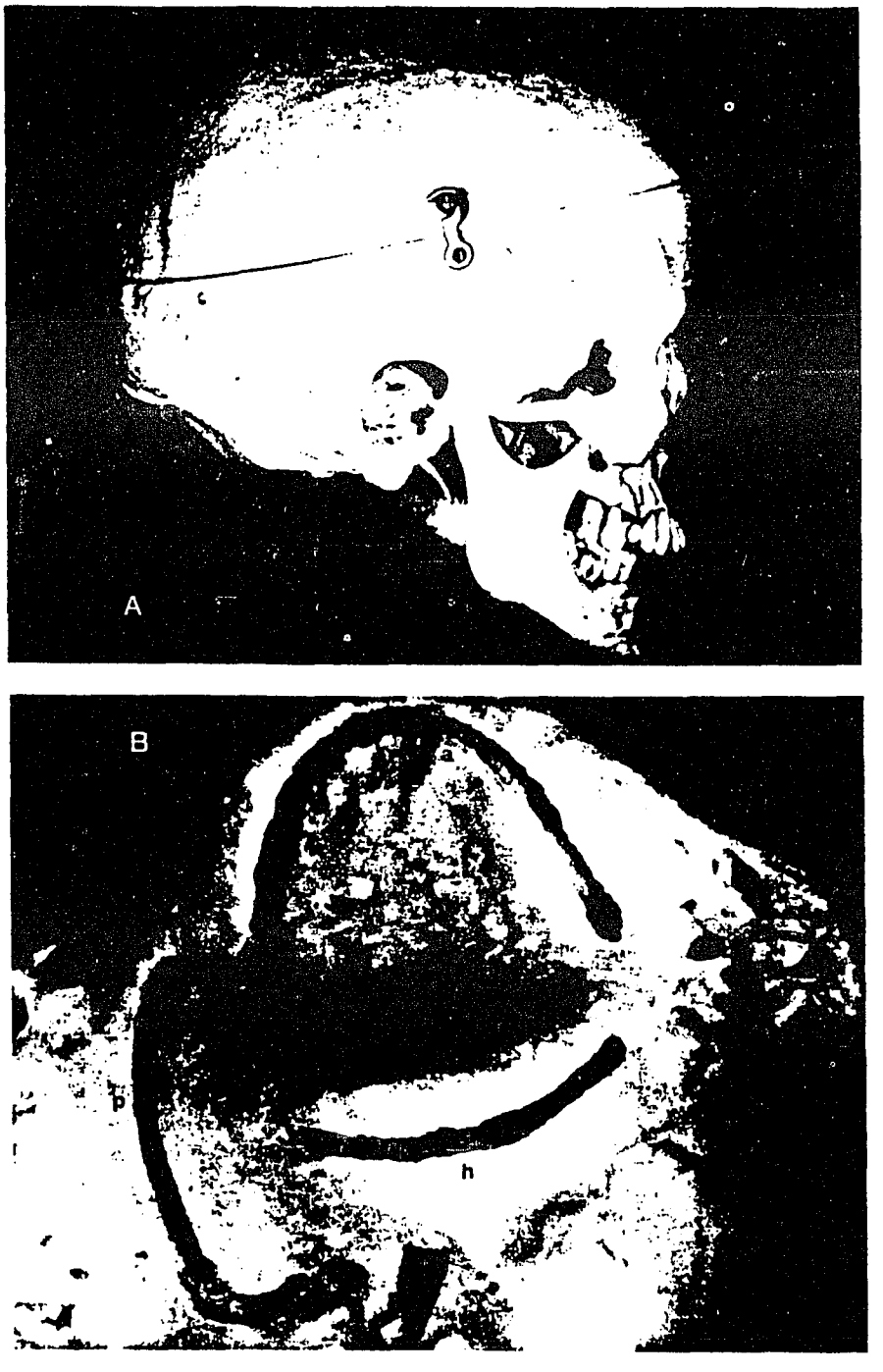

Fig. 2.1 A. Location of the semicircular canals with respect to the human skull.
B. The semicircular canals showing that each canal is approximately orthogonal to each of the other two canals. Taken from Blanks et al, 1975.

A

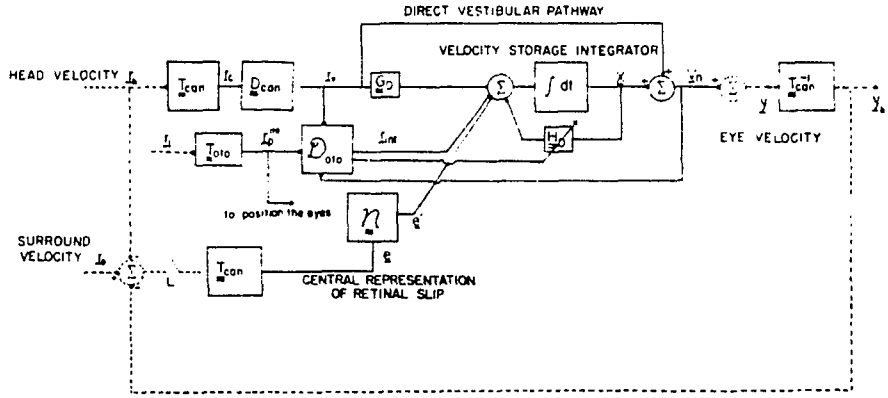

B

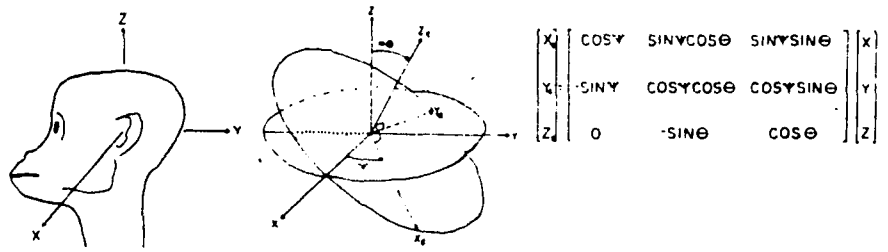

XYZ - HEAD BASED CO-ORDINATES
$X_c Y_c Z_c$ - CANAL BASED CO-ORDINATES

X_c - NORMAL TO ANTERIOR CANAL PLANE
Y_c - NORMAL TO POSTERIOR CANAL PLANE
Z_c - NORMAL TO HORIZONTAL CANAL PLANE

Fig. 2.2 A. A three-dimensional model of the vestibular ocular reflex.
B. The orientation of the semicircular canals with respect to the head system of axes. Taken from Raphan & Cohen, 1985.

(Pellionisz & Llinas, 1982). However, a close approximation to the coordinate representation between canal and head coordinates can be given by a three-by-three matrix (Robinson, 1982; Raphan & Cohen, 1985). Recent evidence has suggested that the semicircular canal coordinate system is also utilized in the processing of signals in the visual system (Simpson & Graf, 1981). Thus, this coordinate frame appears to be of fundamental importance in governing the behavior of the vestibular ocular reflex and the visual vestibular interaction.

The semicircular canals also have dynamic properties and behave as if they were torsion pendulums (Steinhausen, 1933). The canal can be represented by a thin circular tube with center c (Fig 2.3). The radius of curvature of the tube is R with an internal radius r where $r \ll R$. The tube is completely filled with a fluid with constant moment of viscous friction per relative angular velocity of fluid flow B. The moment of inertia of the fluid about an axis through c and perpendicular to the plane containing the fluid is I. Within the tube is a membrane, the cupula, that is assumed to act as an ideal spring with spring constant K. It is assumed that the cupula is like an elastic drum maintaining complete physical separation of the fluid on either side of the cupula.

An equation describing the displacement of the semicircular canal fluid can be derived from rotational dynamics and is given by: (see Wilson & Melvill-Jones, 1979)

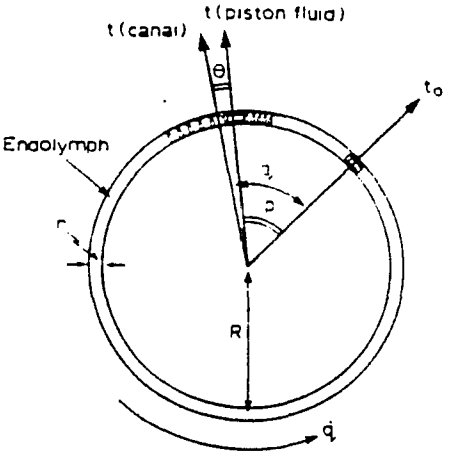

$$\begin{pmatrix}\text{Inertial}\\ I\ddot{\theta}\\ \text{Moment}\end{pmatrix} = \begin{pmatrix}\text{Viscous}\\ B\dot{\theta}\\ \text{Moment}\end{pmatrix} - \begin{pmatrix}\text{Elastic}\\ k\theta\\ \text{Moment}\end{pmatrix}$$

$$\begin{pmatrix}\text{Canal}\\ \text{Ang}\\ \text{Accel}\end{pmatrix} \ddot{q} = \ddot{\theta} + \frac{B}{I}\dot{\theta} + \frac{k}{I}\theta$$

Fig. 2.3 Dynamical model of a semicircular canal:
q, the angular position of the canal relative to space;
p, the angular position of the cupula relative to space;
θ or h, the angular position of the canal relative to the head. Taken from Wilson & Melvil-Jones, 1979.

$$D_t^2 q = D_t^2 h + (B/I) D_t h + (K/I) h, \qquad (2.1.2)$$

where q is the angular displacement of the canal relative to space and h is the angular displacement of the fluid relative to the head. Examination of this algebraic equation reveals that it is an overdamped system governed by two time constants, T_1 and T_2 where $T_2 >> T_1$ (Steinhausen, 1933) and are given by T_1=0.003 seconds and T_2=10 seconds. Therefore, for times greater than a few T_1's, the fluid displacement is governed by T_2. Therefore, an approximate first order system can be developed to describe the cupula displacement and in turn the activation of the associated afferents (see Raphan & Cohen, 1981 for review).

Beneath the cupula (Fig. 2.4), is a layer of sensory epithelium that contains bundles of cilia (Fig. 2.5) projecting into the cupula. Each bundle (Fig. 2.5) consists of a large number of stereocilia and one kinocilium. The kinocilium is the longest or one of the longest cilia in a bundle. The kinocilium contains nine double tubular filaments surrounding two single tubular filaments. The stereocilia are arranged so they are approximately located to one side of the kinocilia. The length of a stereocilium is related to the distance between the stereocilium and the kinocilium. As the distance decreases the length increases. A vector with a direction from the short stereocilia toward the kinocilium represents the morphological polarization vector. Within an ampulla of the semicircular canal,

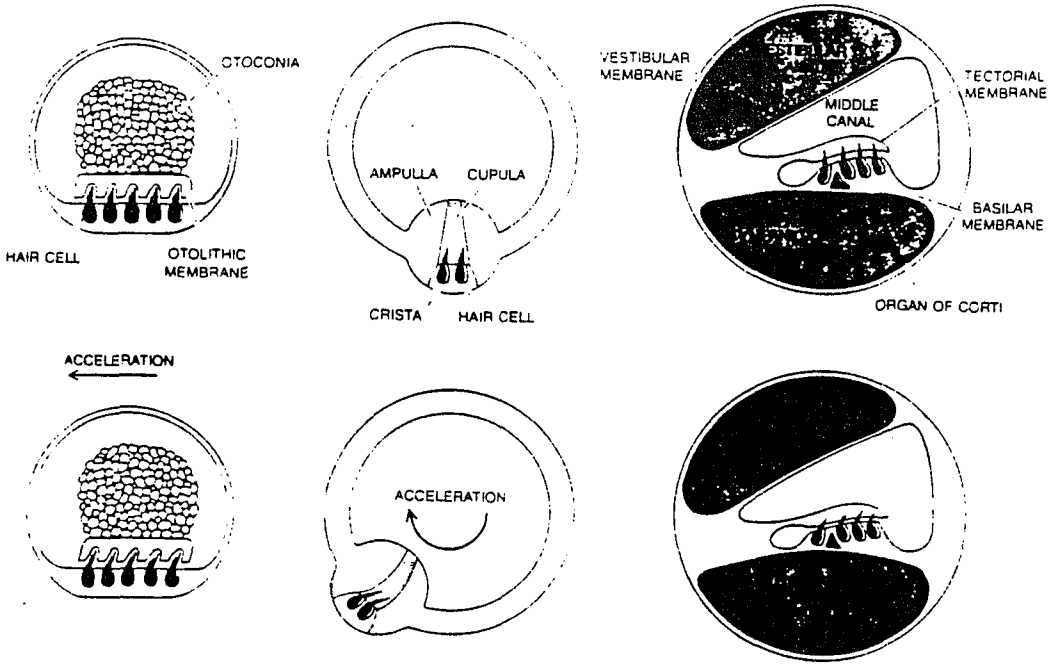

Fig. 2.4 Illustrations of the vestibular organs, utricle and saccule (left), and the semicircular canals (right), that respond to linear and angular acceleration respectively.
Top left. The cilia project into the otoconia.
Bottom left. The bending of the cilia due to the relative motion of the otoconia with respect to the cilia. The fluid that surrounds the otoconia is much less dense than the otoconia.
Top middle. The cilia project into the cupula of a semicircular canal.
Bottom middle. The bending of the cilia due to the motion of the canal fluid relative to the canal.
Top right and bottom right. Show the cilea in the cochlea. Taken from Hudspeth & Corey, (1977).

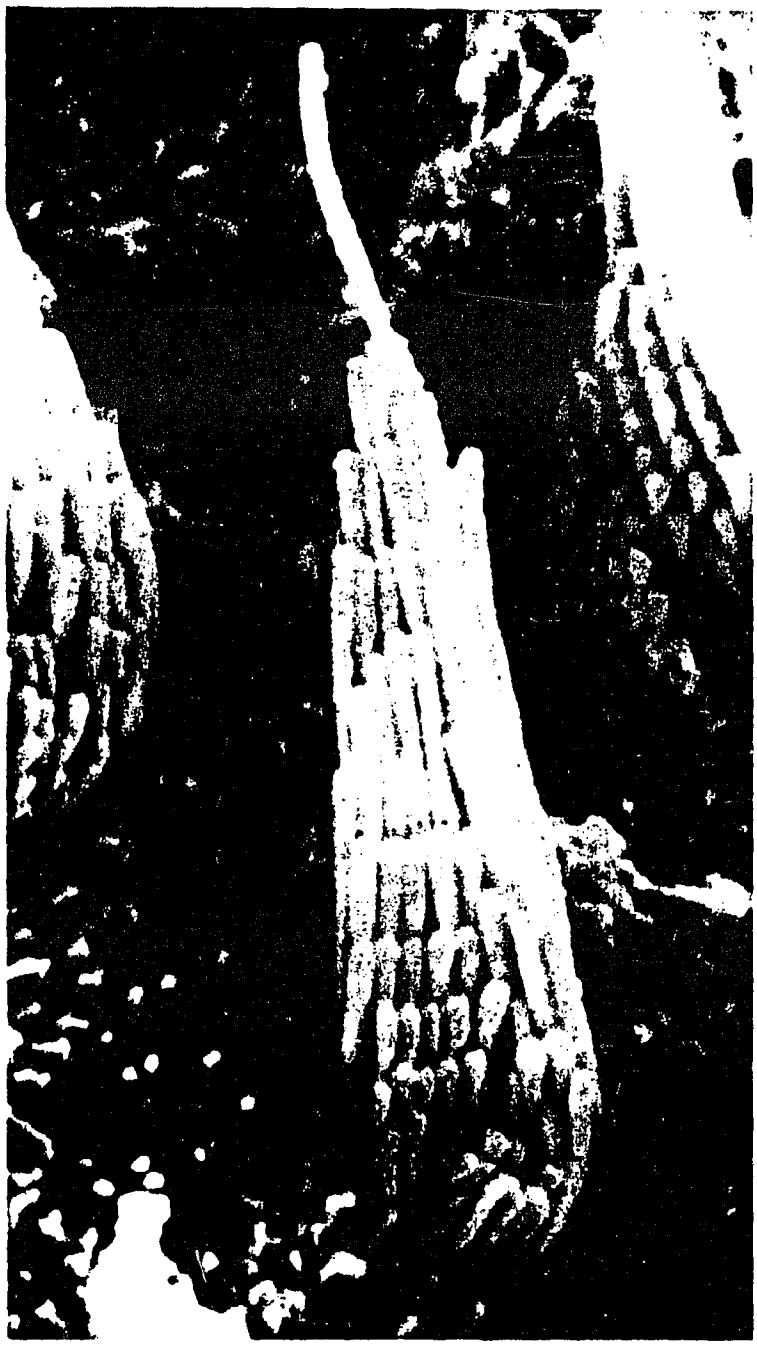

Fig. 2.5 A single bundle of cilia in the utricular macula of guinea pig. Taken from Lindeman, 1973.

almost all of the morphological polarization vectors are parallel. The mechanical bending of a bundle of cilia (Fig. 2.6) in the direction of the morphological polarization vector is associated with excitation of the primary afferent signal while the mechanical bending of a bundle of cilia in the direction opposite to the morphological polarization vector is associated with inhibition of the primary afferent signal (see top trace of Fig. 2.7). The mechanical bending of a bundle in a direction perpendicular to the morphological polarization vector does not change the primary afferent signal (see bottom trace of Fig. 2.7) (Hudspeth & Corey, 1977). Movement of semicircular canal fluid will be matched by movement of the cupula which in turn will bend the bundles of cilia (Fig. 2.4).

Recordings of discharge patterns from primary afferents in monkey in response to angular head rotation support the torsion pendulum model (Fernandez & Goldberg, 1976; Shor et al, 1985). Fig 2.8A shows an example of an afferent response due to sinusoidal rotation that stimulates the semicircular canals. The upper trace in Fig. 2.8A (Hudspeth & Corey, 1977) represents the head position of a monkey as it oscillates about a vertical axis with a frequency of 0.3Hz and an amplitude of approximately 15 degrees. The lower trace represents the instantaneous impulse rate from the ampulla of a regularly firing unit. The bias of the firing rate of the unit is approximately equal to its resting firing rate (the dashed line). Comparing the the lower trace to the upper trace of Fig 2.8A, the phase of the firing rate of

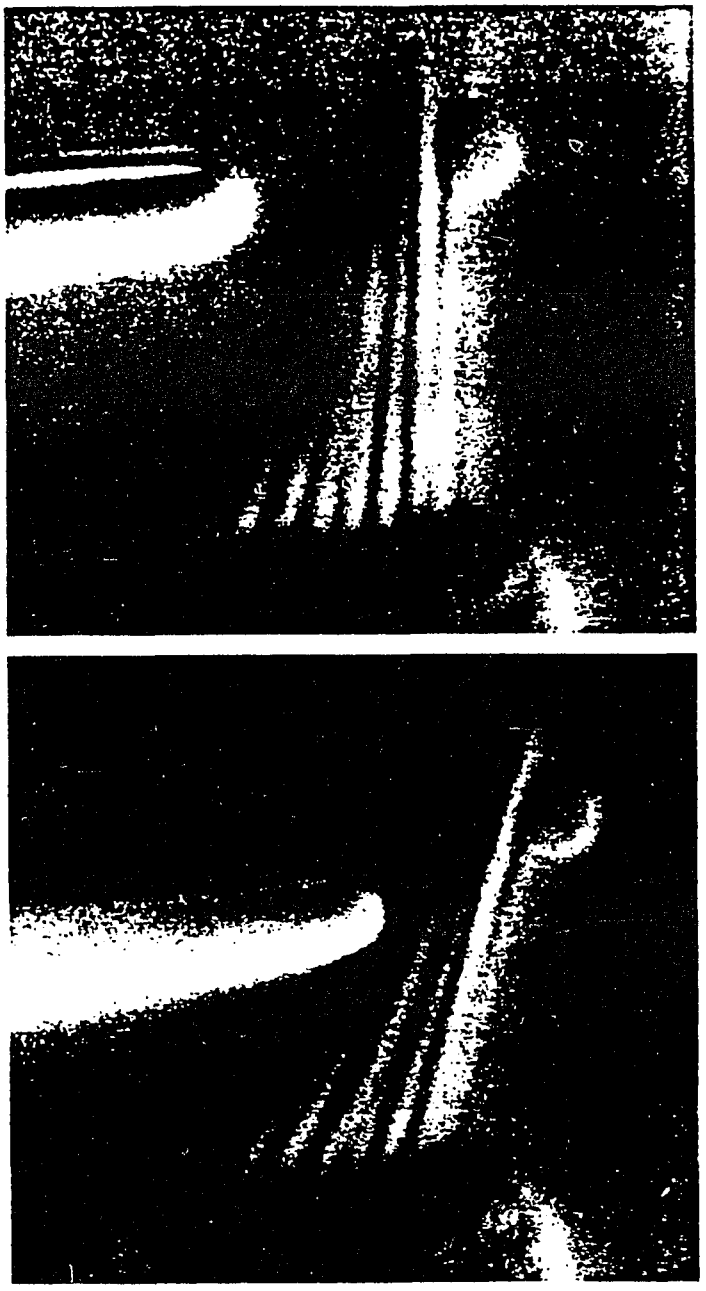

Fig. 2.6 The shape of a bundle of cilia, from the saccule of the American bullfrog, before and during displacement by a glass microprobe. Taken from Hudspeth & Corey, (1977).

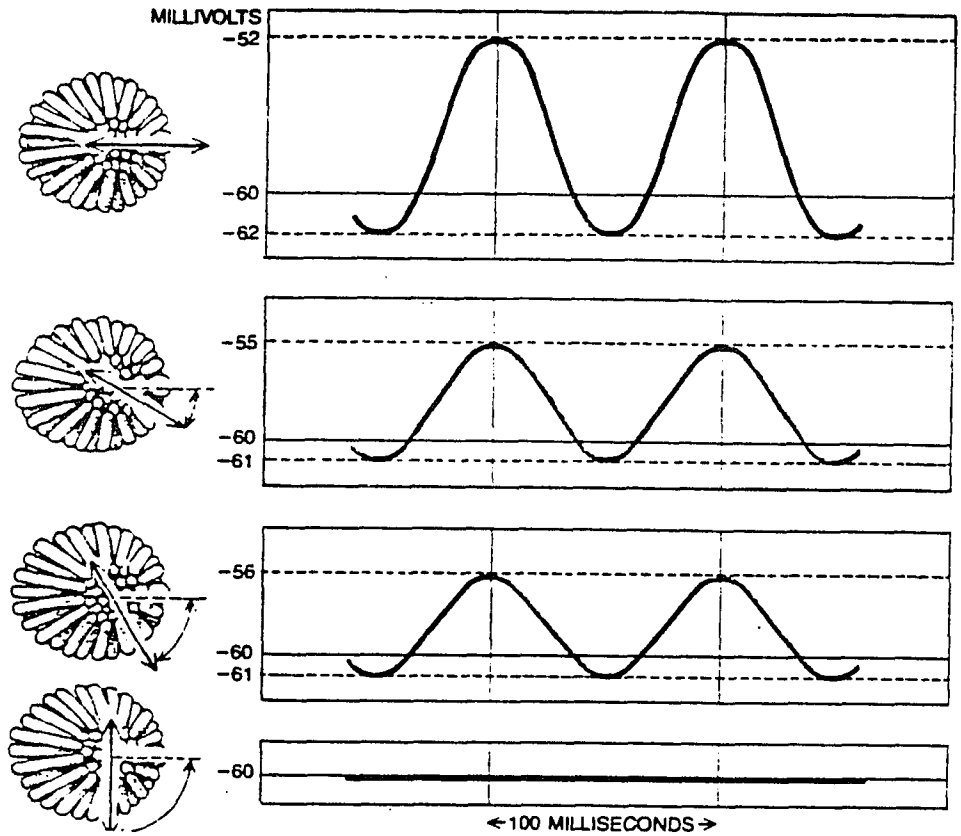

Fig. 2.7 The directional sensitivity of a hair cell, from the saccule of the bullfrog, due to the bending a a bundle of cilia. An electrode was inserted into the hair cell. The resting or unperturbed state corresponded to a membrane potential of -60 millivolts (relative to the fluid surrounding the saccule.)
Top trace. Displacements of the bundle of cilia in the direction of the polarization vector of the hair cell increase the membrane potential or activate the hair cell. Displacements of the bundle in the opposite direction decrease the membrane potential or inhibit the hair cell.
Two middle traces. The peak-to-peak response of the hair cell decreases as the direction of the displacements of the bundle deviate from zero to 90 degrees from the polarization vector.
Bottom trace. The hair cell is insensitive to displacements of the bundle of cilia perpendicular to the polarization vector. Taken from Hudspeth & Corey, (1977).

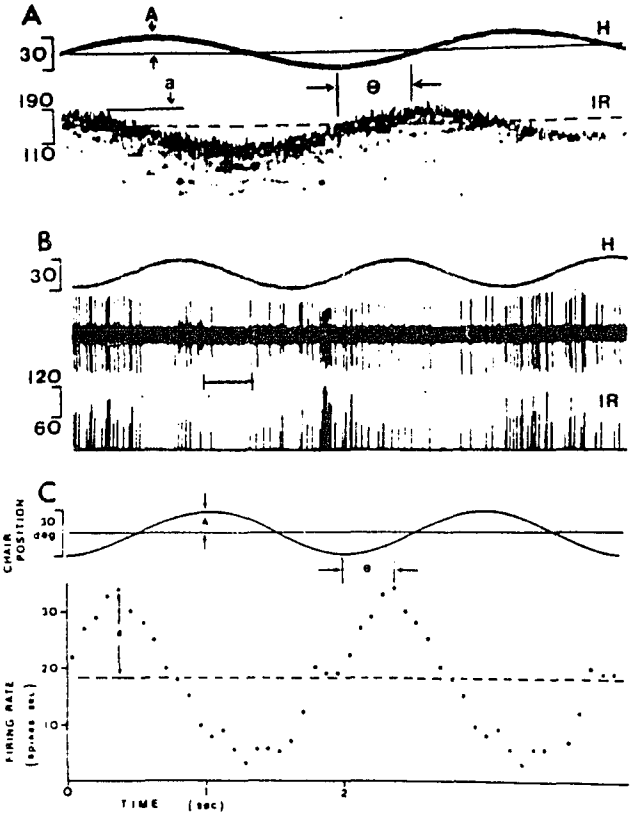

Fig. 2.8 Sinusoidal canal stimulation in monkey. The sinusoidal stimulation is characterized by an amplitude of approximately 15 degrees and a frequency of 0.3 Hz.
H: Head Position
IR: Instantaneous Discharge Rate
A. Regularly firing unit.
Top trace. The orientaion of the monkey with respect to time.
Bottom trace. The firing rate from the ampullar unit. The dashed line represents the resting firing rate.
B. Irregularly firing unit.
C. Averaged response of unit B. Taken from Keller, 1976.

the unit leads the phase of the monkey's head position by approximately 90 degrees. This suggests that the firing rate of this unit represents the monkey's angular velocity and that the canal related subsystem of the VOR can be reprsented as an integration of the monkey's angular acceleration.

The two sets of parallel morphological polarization vectors in each pair of complementary canals point in opposite directions. A step in head angular velocity to the left about a head vertical axis will excite the left horizontal canal and inhibit the right horizontal canal. A step in head angular velocity, such that the head instantaneously and simultaneously pitches forward and rolls to the left about a horizontal axis, will excite the left anterior vertical canal and inhibit the right posterior vertical canal. A step in head angular velocity, such that the head instantaneously and simultaneously pitches backward and rolls to the left about a horizontal axis, will excite the left posterior canal and inhibit the right anterior canal.

In summary, the semicircular canals have dynamic inertial properties, they establish a coordinate frame for processing motion signals from the vestibular and visual systems, and drive the oculomotor system in that coordinate frame. We will be using this concept in developing the computational model of compensatory eye velocity generation during OVAR.

In the next section we review the work that has been done in

characterizing compensatory eye movements for rotations about a vertical axis.

2.2 Eye Movements in Response to Rotations about a Vertical Axis:

Head rotations generate compensatory eye movements which tend to maintain gaze stability (Mach, 1886; Ter Braak, 1936; Mowrer, 1937; Robinson, 1977; Raphan et al, 1979). The compensatory eye velocity relative to the head can be decomposed into three components: pitch (or vertical), roll, and yaw (or horizontal). Under normal circumstances, the head is rotated rapidly and the dynamical parameters of the vestibular-ocular-reflex (VOR) are not apparent. However, when there is continuous rotation about an axis, the eyes execute a rhythmic motion consisting of a slow movement in one direction followed by a rapid movement in the other direction, referred to as nystagmus. The slow component is the compensatory eye movement, while the rapid phase resets the eyes. This thesis is concerned with modelling how slow phase eye velocity signals are generated during off vertical axis rotation (OVAR) from patterns of otolith activation due to gravity. As a point of reference, we will consider how present models are able to account for the vestibular-ocular-reflex (VOR) due to rotations of the head or environment about a vertical axis.

A number of models have been presented that simulate the operation of the VOR and visual-vestibular interaction for rotations about a vertical axis (Raphan et al, 1977; Robinson, 1977; Raphan et al, 1979; Robinson, 1980; Waespe et al, 1983; Buizza & Schmid, 1985).

A model which has been explored in particular detail and compared to physiological data has been developed by Raphan Fig. 2.9 (Raphan et al, 1979; Waespe et al, 1983; Cohen et al, 1987). We will summarize the experimental basis for the model and the major functional elements which explain the behavior of the VOR. The data that will be described were obtained from experiments on monkeys (Cohen et al, 1977; Raphan et al, 1977; Raphan et al, 1979; Raphan et al, 1981; Waespe et al, 1983; Raphan & Cohen, 1985).

When the head is given a step of velocity about a vertical axis in darkness the yaw component of eye velocity compensates immediately with a gain close to one in the monkey. The pitch and roll components of the eye velocity are zero. This is known as the per-rotatory nystagmus and is shown in Fig. 2.10A (taken from Raphan et al, 1979). The slow phase eye velocity is maintained at a gain close to one for a time, on the order of two to three seconds, known as the plateau phenomenon (Raphan et al, 1979). As the rotation continues, the compensatory yaw component of eye velocity decays to zero with a time constant of 15 seconds (Fig. 2.10A). When the head is suddenly stopped, the eye velocity jumps in the opposite direction equal to the step in head velocity. Eye velocity then decays toward zero, relative to the head, with characteristics similar to that of the per-rotatory response and is known as post-rotatory nystagmus (see Wilson & Melvill-Jones, 1979; Henn, Cohen & Young, 1980 for review).

A complementary kind of behavior is observed during optokinetic

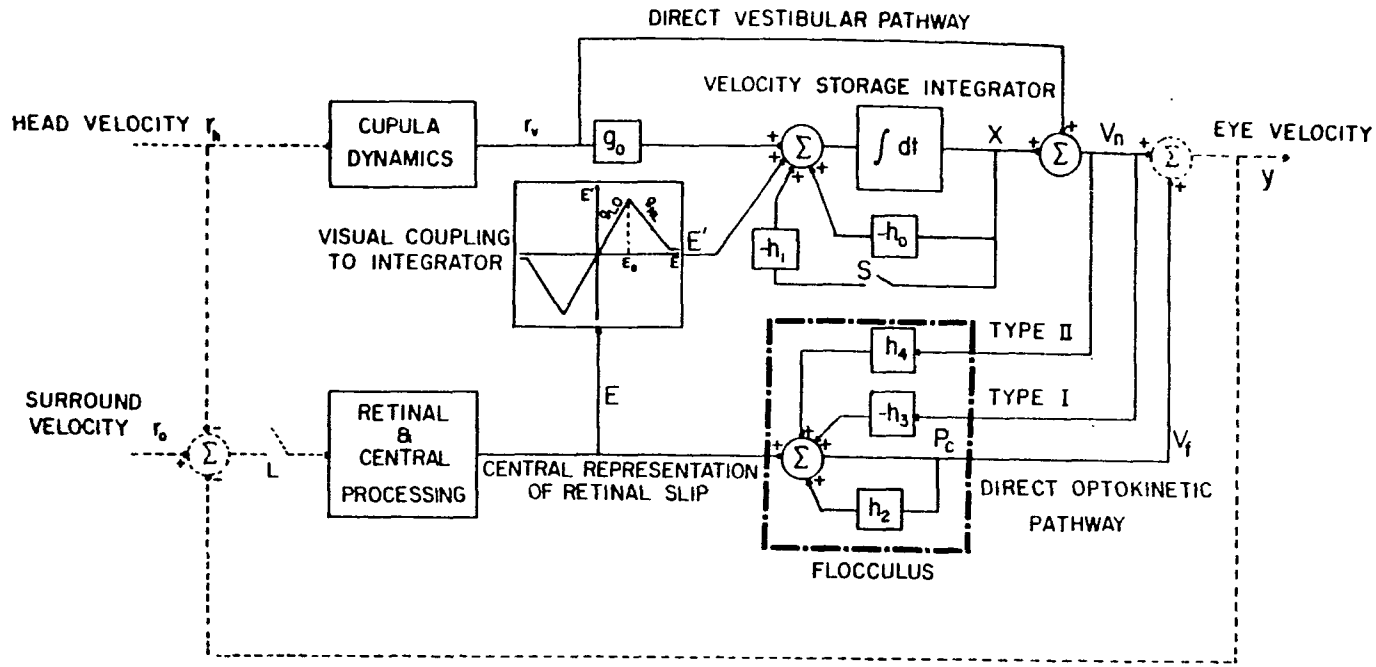

Fig. 2.9 A one-dimensional model which is able to account for many of the prominent features of the VOR due to rotations of the head or surround about a space vertical axis. Taken from Waespe et al, 1983.

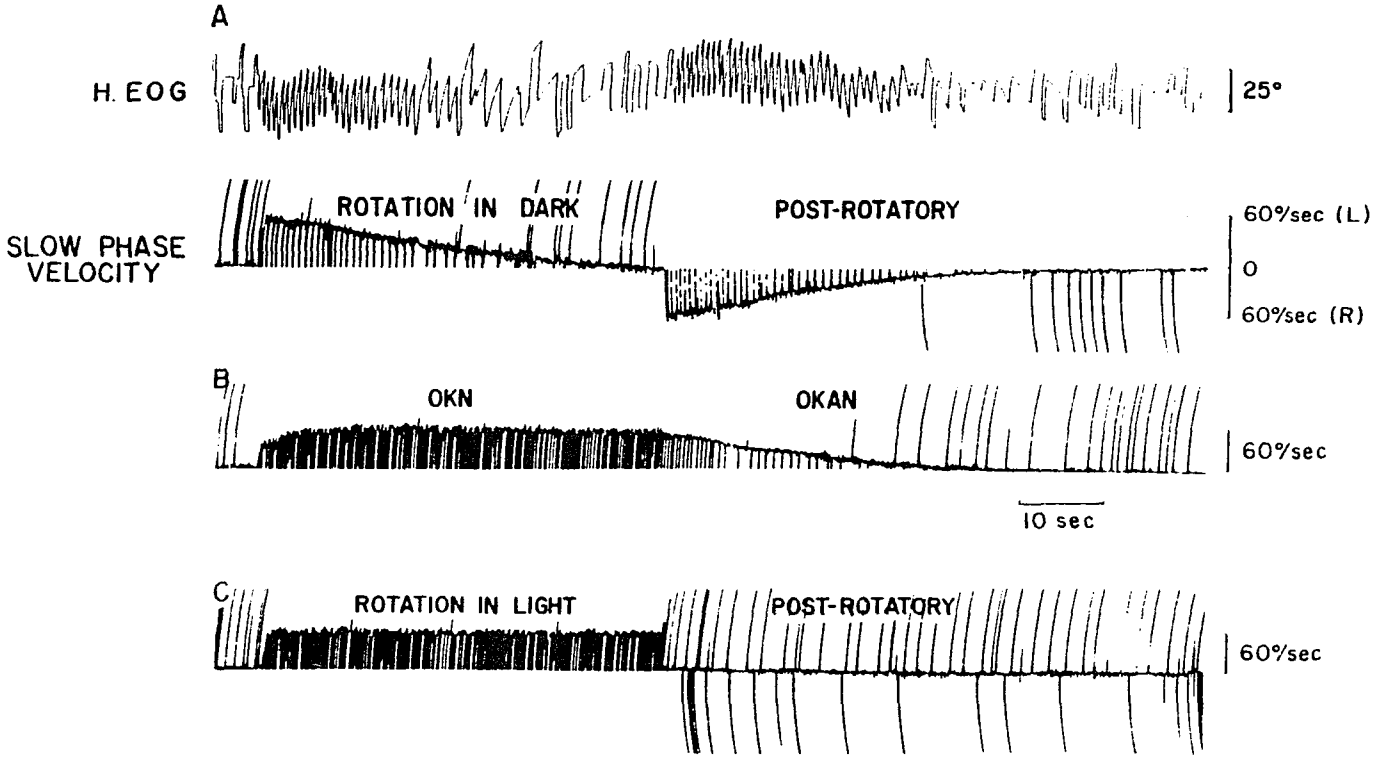

Fig. 2.10 A. The first region of the bottom of the two figures shows the per-rotatory nastagmus in which the head is rotating to the left in the dark. The post-rotatory region shows the nystagmus of the stopped head.
B. The OKN region shows the nystagmus of a fixed head viewing the pattern which is rotating to the right about the head. The OKAN region shows the nystagmus of the fixed head in the dark.
C. The first region shows the nystagmus of the head rotating to the left about the fixed pattern. The post-rotatory region shows the nystagmus of the stopped head in the dark. Taken from Raphan et al, 1979.

stimulation when the head is held in an upright position. If a drum containing a sequence of alternating black and white vertical stripes is rotated at a constant angular speed about the head, eye velocity approximates the velocity of the moving pattern of stripes. When the lights are first turned on the slow phase eye velocity rapidly increases to approximately 60% of the speed of the moving pattern (Fig. 2.10B; Cohen et al, 1977). Eye velocity is maintained for as long as the stimulus persists. When the lights are switched off, eye velocity decays toward zero with a time constant of approximately 12-15 seconds and is called optokinetic after-nystagmus (OKAN) (Ter Braak, 1936; Mowrer, 1937; Cohen et al, 1977).

Combined optokinetic and vestibular activation cause a superposition of these responses (Fig. 2.10C). A drum containing a sequence of alternating black and white vertical stripes is held in a steady position. As the head starts to move to the left at an angular speed of w relative to space, the eyes move toward the right relative to the head with a velocity of approximately w. This eye speed is maintained for as long as the lights stay on and the head rotates. When the lights go out and the head is suddenly stopped, eye velocity is reduced to approximately zero (Raphan & Cohen, 1981).

Next we will describe a model developed by Raphan (Fig. 2.9) to explain the above findings (Cohen et al, 1977; Raphan et al, 1979; Waespe et al, 1983; Cohen et al, 1987). This model has two inputs each of which is measured relative to space: a head angular velocity,

r_h, and a surround angular velocity, r_o. The output is an eye velocity signal relative to the head, y.

The model contains various system components, including a first order dynamical system representing the cupula and associated canal fluid used to transduce the head angular acceleration into a vestibular signal, r_v. The cupula system component includes a cupula state (memory), x_c, representing the angular velocity of the cupula. The vestibular signal is an internal representation of the difference between the head angular velocity, r_h, and the cupula state, x_c. The time constant of the cupula system has been approximated to be about 4 seconds.

Another system component in the model is a nonlinear retinal slip operator. The retinal slip, e, is the difference between the surround angular velocity and the eye velocity both measured with respect to the head reference frame. The retinal slip is processed through a nonlinearity whose output is e'. As the retinal slip increases from zero to a value of E_s (E_s is approximately 24 degrees/second), which delineates the linear region, the output, e', is proportional to e with a slope of approximately 0.25. As the retinal slip continues to increase from E_s, the output decreases linearly from E_s with a slope of approximately -0.025. As the retinal slip continues to increase, e' levels off at zero.

The output from the cupula system contributes to the output, y, via two paths; an indirect pathway that contains a velocity storage

integrator and a direct pathway. The output from the visual system and the otolith system contribute to y via the indirect pathway. The retinal slip also contributes to y via a optokinetic direct pathway. The direct pathway allows for a rapid response while the indirect pathway allows for a delayed response. The velocity storage integrator contains a state x (memory), which also contributes to y. The state of the integrator allows for the system to have a (leaky) memory of the head angular velocity. The output y is equal to the sum of the integrator state, the vestibular signal, and the direct optokinetic output.

For head motions performed in the dark, as the head accelerates to a steady angular velocity, the vestibular signal drives the eyes via the direct path. After the initial acceleration, the vestibular signal decreases with a time constant of about 4 seconds. The model therefore predicts that the initial motion of the eyes compensate for the head motion so that the eye speed is approximately zero relative to space. The vestibular signal via the indirect path charges the velocity storage integrator. The sum of the vestibular signal and the integrator output continues to drive the eye relative to the head such that the eye speed relative to space is approximately zero. This compensatory eye movement lasts for about one second during which the vestibular signal is decaying and the integrator output is increasing. Similarly the integrator output will begin to decrease with time since the vestibular signal is decaying to zero. The time constant of the

velocity storage integrator is approximately 13 seconds (Raphan et al, 1979). Therefore, the model predicts that as time increases the eye velocity relative to the head will decrease with a time constant of approximately 13 seconds, which is the time constant of the integrator.

The model is also able to explain the ocular response due to a drum rotating about a vertical axis with the head fixed. The model predicts that when the lights are turned on the retinal slip signal via a direct path drives the eye. The intial motion of the eye compensates for the motion of the drum so that the speed of the eye is approximately equal to the speed of the drum. The retinal slip signal, via the indirect path, charges the velocity storage integrator. The sum of the retinal slip signal and the integrator output drives the eye. So long as the lights remain on, the slow phase signal, y, remains constant. When the lights go out the eye velocity relative to the head decays to zero. The time constant of decay is that of the velocity storage integrator.

The model is able to explain the VOR response due to the rotation of the head in light about a vertical axis. Note that when the head is rotated to the left the vestibular and the retinal slip signals both drive the eyes to the right as the head starts to move to the left. As the head continues to rotate the model predicts that the vestibular signal will decay to zero and that the slow phase eye velocity will continue to compensate for the head motion due to the

retinal slip signal. When the lights go out and the head stops the vestibular signal now drives the eye to the left while the integrator output drives the eye to the right. The superposition of the eye velocity response to the vestibular signal and the initial condition of the integrator produce an output approximately equal to zero.

An extension of the above model to three-dimensions has been developed (Fig. 2.2A; Raphan & Cohen, 1985). In this model there are three inputs each of which is a three-dimensional vector and is measured with respect to space: a head angular velocity, $\underline{r}_h$, a surround angular velocity, $\underline{r}_o$, and a force, $\underline{r}l$. The output is an eye velocity signal relative to the head, $\underline{y}$. In the three-dimensional model there are system components corresponding to the system components of the one-dimensional model: a three-dimensional cupula dynamical system represented by three uncoupled first order systems, a three-dimensional retinal slip operator, and a three-dimensional velocity storage integrator. The behavior of the three-dimensional velocity storage integrator is believed to be a function of the orientation of the head with respect to gravity (Raphan & Cohen, 1988; Sturm & Raphan, 1988). In addition, there is an otolith operator. The input to the otolith operator is the force $\underline{r}l$. The otoliths convert this force into a pattern of otolith activation. From this pattern, a direct signal can be generated representing the direction of gravity. If the head is rotating about an off vertical axis an estimate of the head velocity can be computed from the changing

pattern of otolith activation. This head angular velocity estimate is used as another input to the velocity storage integrator. This dissertation is conserned with the generation of a head velocity estimate from the changing patterns of otolith activation.

The properties of the otolith organs are considered next.

2.3 Biophysics of the Otolith Organs

The otolith organs consist of the utriculus and the sacculus which respond to linear acceleration (Fig. 2.4). The macula associated with the utricule lies in a plane approximately parallel to the horizontal semicircular canal plane. The rest of the utricular macula bends into a frontal plane. The saccular macula approximately lies in a sagittal plane. Thus, the otoliths can detect linear acceleration in three dimensional space. Part of the macula contains a layer of sensory epithelium and bundles of cilia project from this layer into the otolith membranes (Fig. 2.4). The otolith membranes contain a dense layer of otoconia (calcium carbonate crystals). A bundle of cilia (Fig. 2.5) in the macula is similar to the bundle of cilia in an ampula of the semicircular canals (see section 2.1). Each bundle of cilia is composed of a large number of stereocilia and one kinocilium. A vector with a direction from the short stereocilia to the kinocilium in a bundle of cilia projecting from a macula determines the morphological polarization vector for that bundle. The functional significance of the morphological polarization vector is that force fields along a polarization vector maximally excite the afferents projecting from the bundle (Figs. 2.6 & 2.7; Hudspeth & Corey, 1977).

The activation of a cell will vary sinusoidally with head orientation. In support of this, consider the recordings of a cat's

peripheral neural unit spike frequency versus the cat's orientation made by Loe et al, (1973). A cat was pitched at an angular velocity of approximately 10 degrees/second. The unit's firing rate varies sinusoidally with orientation (see Fig. 2.11). This suggests that the unit's firing rate represents the component of gravity along the associated polarization vector(s). Therefore, if the head is rotated in a gravitational field, the otolith cells will be sequentially activated and generate patterns of activation.

The model that is developed in this dissertation depends on two patterns of activation, one delayed approximately one second relative to the other. Evidence for the direct pattern of activation, which represents the present head orientation with respect to gravity, is given in work by Fernandez & Goldberg, (1976c). They show that the transduction of a linear force into a firing rate, by a hair cell can be represented by a "first-order lag system". The system pole (or time constant) is approximately 16 milliseconds. This supports the existence of an otolith pattern that approximately represents the present orientation of the head with respect to gravity. Evidence for the existance of an indirect or delayed pattern of activation, which represents a previous head orientation with respect to gravity, is given in work by Schor et al, (1985). They show a phase versus frequency plot (Fig. 2.12A) obtained from recordings (from a decerebrate and canal plugged, cat) of vestibular neurons in and around the lateral vestibular nucleus of Deiters. The slope of the

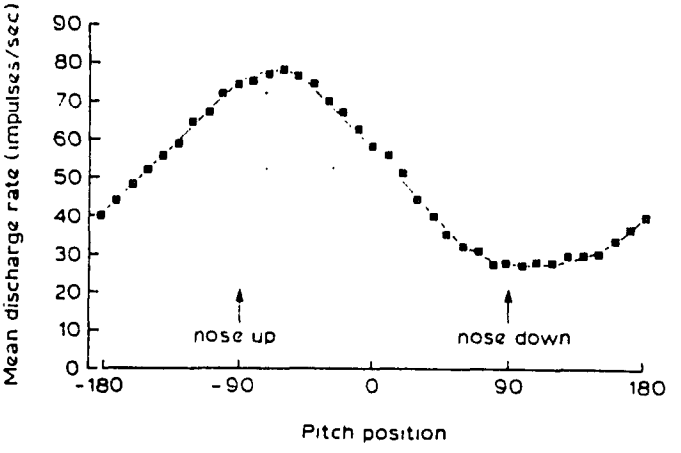

Fig. 2.11 The discharge rate of a cat's otolith unit during a pitch angular velocity of 10 degrees/second in a uniform gravitational field. Each data point is an average over a period of approximately 100 milliseconds. Taken from Wilson & Melvill-Jones, 1979, as modified from Loe et al, 1973.

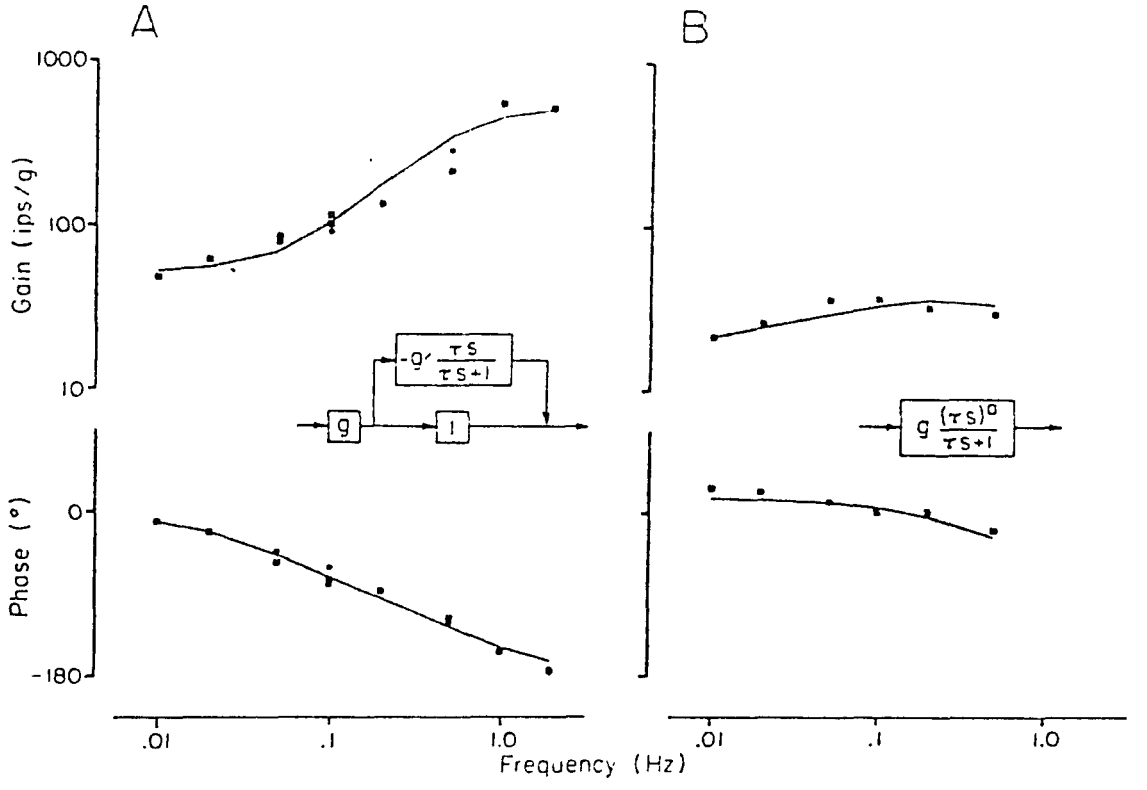

Fig. 2.12 The figure was obtained from recordings, from a canal plugged decerebrate cat, of the lateral vestibular nucleus of Deiters. The responses from two neurons are shown in A and B.

A. The top figure shows an increase in gain as the stimulus frequency increases. The bottom figure shows an increasing phase lag which is approximately characteristic of an ideal delay with a delay time constant of 0.5 seconds.

B. The response characteristics of a second neuron. Taken from Schor et al, 1985.

plot is approximately characteristic of the phase plot of an ideal delay operator with a time delay constant of approximately 0.5 seconds.

The utricular macula is divided into two regions separated by a curved line called the striola (Fig. 2.1.13A). Almost all of the morphological polarization vectors, on either side of the striola, point toward the striola. Similarly, the saccular macula (Fig. 2.1.13B) is also divided into two regions by a striola. However, almost all of the morphological polarization vectors of the saccular macula point away from the striola. From studies of primary afferent neuron signals in monkey Fernandez & Goldberg (1976a) found that the polarization vectors fanned out into the three spatial dimensions consistent with anatomical findings (Fig. 2.14; Fernandez & Goldberg, 1976a).

An idealized model of a macula is shown in Fig. 2.15. The model consists of a number, N, of spherical masses of mass M and density p_m (otoconial mass), each contained in a cylindrical tube fixed to the head. The internal radius of a tube is larger than the radius of a mass M. Each tube is filled with a fluid (endolymph) of density p_e and a coffecient of viscous friction per unit of velocity B'. Two bundles of cilia projecting into the otoconial layer are modeled as springs each with spring constant K'. Each spring axis is coincident with the axis of the tube. Each spring is attached to an end of the tube and to the mass M such that the mass is between the springs. A

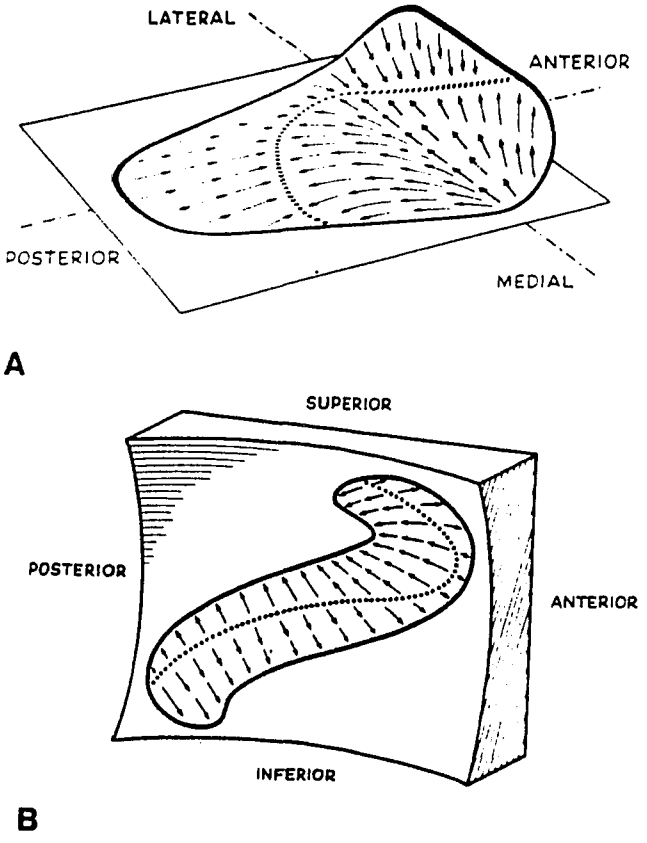

Fig. 2.13 A. The utricular macula: Almost all of the polarization vectors point toward the striola.
B. The saccular macula: Almost all of the polarization vectors point away from the striola. Taken from Spoendlin, 1966.

Fig. 2.14 Functional polarization vector distribution in monkey. The xyz head coordinate frame axes are defined in Fig. 2.2B. Circled points represent unit recordings after the superior nerve had been sectioned. A dot represents a polarization vector which is tilted out of the page and a cross represents a polarization vector which is tilted into the page. A radial line specifies an azimuthal angle (similar to a longitude) measured about the axis which is perpendicular to the page. A concentric circle specifies a copolar angle (similar to a latitude) measured from the plane of the page. A dot or cross detemines a corresponding radial line and concentric circle, both of which specify the polarization vector direction. The radial lines and concentric circles demarcate 30 degree intervals of direction.
A-C. Recordings from superior nerve units. The recordings shown in figure B are from the utricular afferents in the left side of the head.
D-E. Recordings from inferior nerve units.
F. Recordings from unassigned neurons. Taken from Fernandez & Goldberg, 1976a.

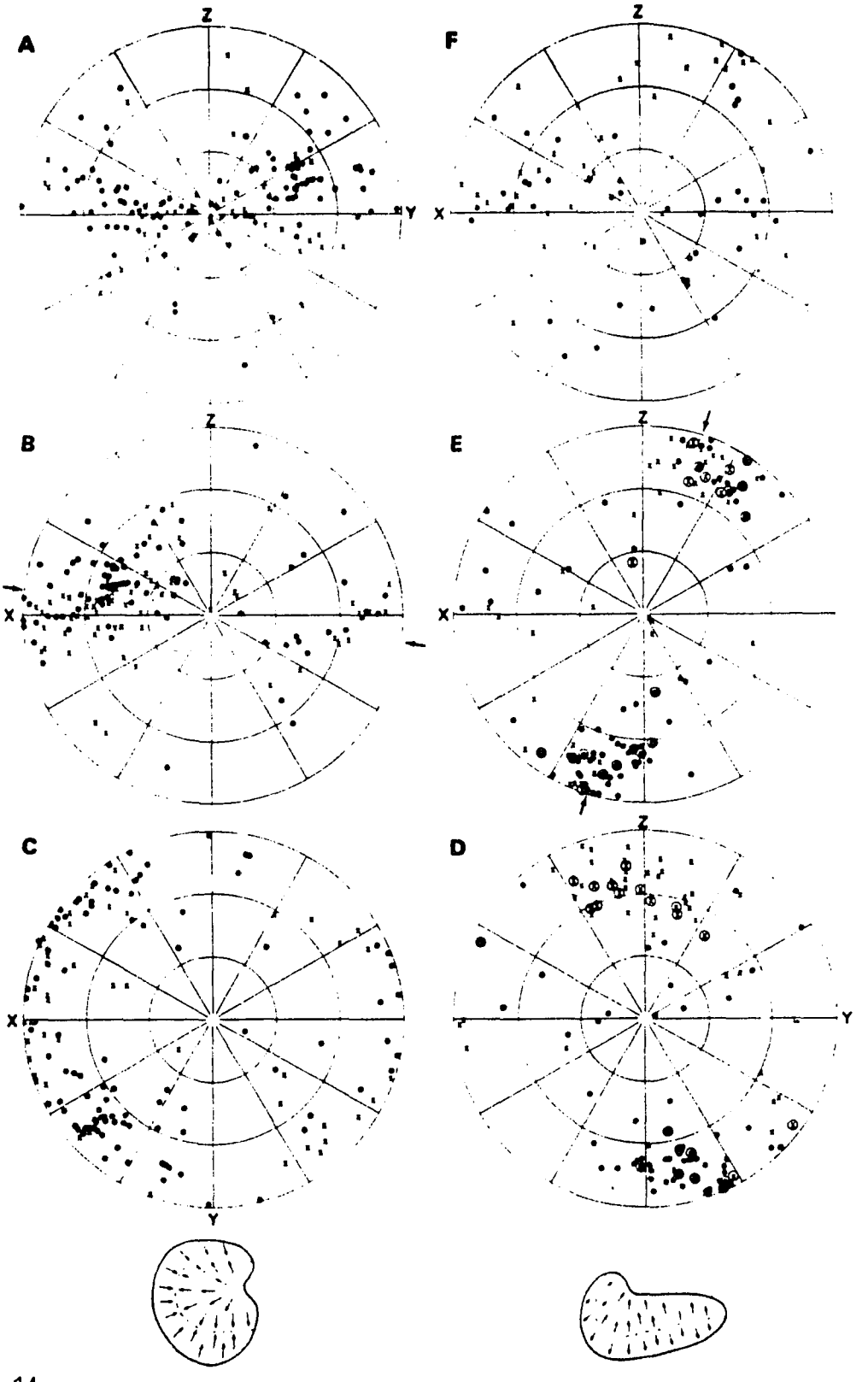

Fig. 2.14

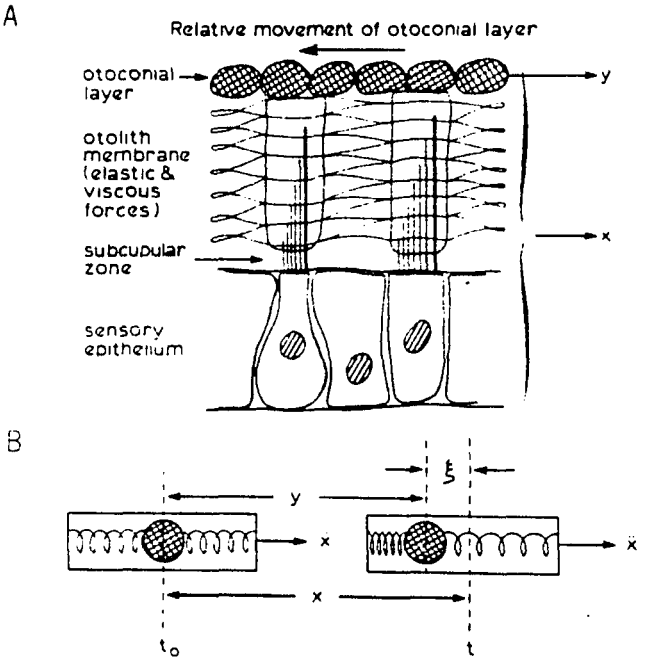

Fig. 2.15 Dynamical model of an otoconium and a bundle of cilia: D_t^2x or $\ddot{x}$, linear acceleration (such as gravity) of the head relative to space; D_t^2y or $\ddot{y}$, acceleration of an otoconium relative to space; z or ξ, relative displacement (bending of the bundle of cilia) of otoconium and macula.
A. Shows a pictorial representation of the relation among a bundle of cilea, the endolymph, and the otoconial layer.
B. Simplified one-dimensional representation of the dynamics of an otoconial mass. Taken from Wilson & Melvill-Jones, 1979.

reference position for each otoconial mass is defined as the position of the mass M when, the external force along the axis of the tube is zero and the mass M is stationary relative to the tube.

Each mass M with its tube, two springs, and fluid, responds to the component of the net force along the axis of the tube and not to components perpendicular to the axis of a tube. The response of the system consists of N values. Each of the values represents the displacement of an otoconial mass along the tube. Wilson & Melvill-Jones, from Newton's laws of physics, develop an equation

$$(1-[p_e/p_m])D_t^2x=D_t^2z+(B'/m)D_tz+(K'/m)z \qquad (2.3.1)$$

describing the displacement of an otoconial mass, M. In Eq (2.3.1), x is the component of the displacement of the head along the axis of the tube, z is the displacement of the otoconial body relative to the tube, m is the equivalent mass of an otoconial body, and D_t is the differential operator. The equivalent mass, m, not only includes the mass M but also includes the effects of accelerating fluid local to the otoconial body.

Values for the relavent parameters in Eq (2.3.1) are not known due to the complexity of the system, and therefore the time constants associated with Eq (2.3.1) were not calculated. However, direct observation of otolith membrane movement showed that the steady state response z (otolith displacement) was proportional to a stimulus, D_t^2x,

when the stimulus was in the range from -g to g (g is the acceleration due to gravity) (de Vries, 1950). Fernandez & Goldberg (1976c), from studies of primary afferent neuron signals in monkey, identified a first order system approximating a delay operator, representing the possible mechanics of otolith activation. They determined that the time constant of the first order system was approximately 16 milliseconds. This suggests, that given a sinusoidal stimulus with a small angular frequency, that the steady state response will be approximately proportional to the stimulus.

In summary, the otoliths respond to linear force fields such as gravity. The direction of the polarization vector with regard to the force field determines the activation of a particular afferent. A given force field determines a pattern of excitation and inhibition which represents the force field in this space. The dynamics are rapid and respond in 16 milliseconds (Fernandez & Goldberg, 1976a). Thus, when the head is oriented with regard to gravity, the otolith activation pattern represents the orientation of the head with regard to gravity. There are also central neurons that code the head orientations as well as delayed signals related to head orientation.

2.4 Eye Movements and OVAR

In this section we will consider eye movements associated with off vertical axis rotation (OVAR). When the head is rotated about a vertical axis the nystagmus decays to zero. If the head is suddenly tilted, there is a slow increase in the yaw component of the slow phase eye velocity. For as long as the off vertical axis rotation persists the yaw component of the eye velocity remains constant. When the head is tilted back to its original orientation such that the head is again rotating about a vertical axis, the yaw component of the eye velocity begins to decay to zero with a time constant of the order of 13 seconds (Benson and Bodin, 1966; Guedry, 1965; Raphan et al, 1981; Young and Henn, 1975).

Various models have been proposed to explain this response characteristic. Benson and Bodin (1966a) proposed that the semicircular canals were responsible for the bias component of the nystagmus slow phase velocity. They postulated that since the canal walls are flexible, they are capable of being constricted by gravitational forces, the "roller pump" theory. By this mechanism, rotation in a gravitational field would cause pressure gradients that would result in constant deflection of the cupula.

Steer (1970) derived equations that support this notion. The physical model consists of a fluid rotating at a constant velocity. The centripetal force on any portion of the fluid maintains this

circular motion. The force has three basic components, that due to the membrane on the outer rim of the fluid, that due to the membrane on the inner rim of the fluid, and the gravitational force. It is the changing components of the centripetal force due to the membranes that give rise to the pressure gradients that produce a pinched roller pump effect.

It has been reported that the semicircular canals respond to linear acceleration (Ledoux, 1949; Goldberg & Fernandez, 1975; Perachio & Correia, 1983). However, these responses are unidirectional, asymmetric, and have no systematic response characteristics over any class of canal afferents (Perachio & Correia, 1983). The responses may to a large extent be artifactual (Goldberg & Fernandez, 1975) or related to the efferent system (Goldberg & Fernandez, 1980). In addition, recordings from eighth nerve canal afferents do not show maintained, direction specific responses during constant velocity rotation (Goldberg and Fernandez, 1981; Raphan, Waespe & Cohen, 1983). Therefore, it is unlikely that the signal producing the bias component of the slow phase velocity of nystagmus during OVAR originates in the semicircular canals.

One of the first models to consider how the otoliths generate a continuous signal during OVAR was developed by Benson and Barnes (1970). The model consists of a concentrated mass, the statoconia, in the form of a disk with an elastic restraint provided by the stereocilia. The statoconia is separated from the sensory epithelium

(also in the form of a disk) by a viscoelastic stem. The bending of the stereocilia is proportional to the movement of the stem. In a gravitational force the sensory epithelium is anchored to the body. The force on the statoconia due to gravity has two basic components, a shearing component and a compressional or tensional component. The visoelastic stem resists compressional forces due to the movements of the statoconia and the stereocilia resists shearing forces due to the movements of the statoconia. Benson and Barnes (1970) considered the head rotating such that the axis of rotation is normal to the plane containing the statoconia. They showed that the deflection of the statoconia lags the rotating linear acceleration vector (gravity) causing the statoconia to twist with respect to the macula. Twisting of the statoconial membrane in turn would excite receptors that are sensitive in the direction tangential to the macula, generating a constant signal proportional to the angle of twist. Unit recordings from otolith afferents, however, do not show any bias component related to the velocity during OVAR in their frequency of firing (Goldberg & Fernandez, 1981; Raphan et al, 1983).

Another model to consider how the otoliths generate a continuous signal during OVAR was developed by Hain (1986). Information from the otoliths is used to determine the linear acceleration experienced by the head in a gravitational field. This model proposes that the information from the computed linear acceleration is used to determine the jerk vector (or the derivative of the linear acceleration.) A

nonlinear combination of the computed linear acceleration, the retinal slip, the eye velocity, and the jerk vector is formed. This nonlinear combination involves multiplying components of the linear acceleration vector with the jerk vector. The combination is then used as input to the velocity storage integrator. In effect, the time constant of the integrator is modified. The correlation, the multiplication of two signals followed by an integration, of the jerk vector with some computed component of the linear acceleration vector yields a signal proportional to the angular speed. Therefore, a signal related to the angular speed can be produced by the integrator.

Neither this model nor the Benson & Barnes model considered the distributed nature of the information processing by the cells in the otolith macula. In addition, these models do not explain the dynamic responses to sudden tilts while rotating. Neither do they explain the steady state eye velocity characteristics as a function of stimulus velocity (Benson & Bodin, 1966a; Raphan et al, 1981). In the next section, we develop a one-dimensional model of a head velocity estimator using the distributed patterns of otolith activation as the head rotates in a gravitational force field.

CHAPTER 3

MODEL FOR SLOW PHASE EYE VELOCITY ESTIMATION FROM PATTERNS OF OTOLITH ACTIVATION DURING OVAR

3.1 Modelling the Estimator as a One-Dimensional Process

3.1.1 Conceptual Basis for Model

The otolith organs, utricle and saccule, respond to a force vector which is produced by linear acceleration or gravity. Each cell of the utricular macula is maximally excited if the force is along its polarization vector (Fernandez, Goldberg & Abend, 1972; Fernandez & Goldberg, 1976a,b,c; Hudspeth & Corey, 1977; Flock, 1964; Shotwell, Jacobs & Hudspeth, 1981). Thus, when the head is tilted, the gravitational force field activates those cells which have a component of its polarization vector along the gravitational field (Fig. 3.1.1A). Those cells which have polarizations othogonal to the gravitational field will not be activated. The polarization vectors are distributed over all angles (Fernandez & Goldberg, 1976a) and the dynamics of the otolith afferents are very rapid, responding to a sudden head tilt in 15 miliseconds (Fernandez & Goldberg, 1976c). Thus, the vector that excites the central nervous system from the transduction by the otolith organs is a pattern of activation representing the outputs from the individual hair cells (Fig. 3.1.1B). Under normal circumstances, this pattern gives a good estimate of head

Fig. 3.1.1 A. Effects of rotating the utricular macula in a gravitational force field. When the macula is in position I the cells in the medial portion have their polarizations orthogonal to the component of the gravity vector, $\underline{g}$. Cells in the anterior portion are excited or inhibited depending on whether they are lateral or medial to the striola. When the macula is rotated to position III, cells in the medial portion of the macula will have their polarization vectors aligned with the gravity vector. Thus, as the macula rotates through 360 degrees (I-IV) all cells are sequentially activated in approximately a sinusoidal fashion. Each cell has a maximal firing rate whose phase is dependent upon its polarization angle.
B. Frequency of firing distribution of utricular macula cells as a function of polarization angle and the relative position of the component of gravity to these cells. (I) The gravity vector in an arbitrary position which maximally excites the cells having zero degree polarization angle. Cells which are maximally inhibited are designated by a polarization angle of 180 degrees. Other groups of cells are activated between these levels. When there is relative movement of the gravity vector (II), a different class of macula cells are maximally excited while the zero degree polarization class has a lowered frequency of firing. Thus, the peak of the distribution moves with the relative movement of the gravity vector (I-IV). This has the effect of generating a traveling wave of excitation and inhibition of the cells of the macula.

A

UTRICULAR MACULA ROTATION IN CONSTANT FORCE FIELD

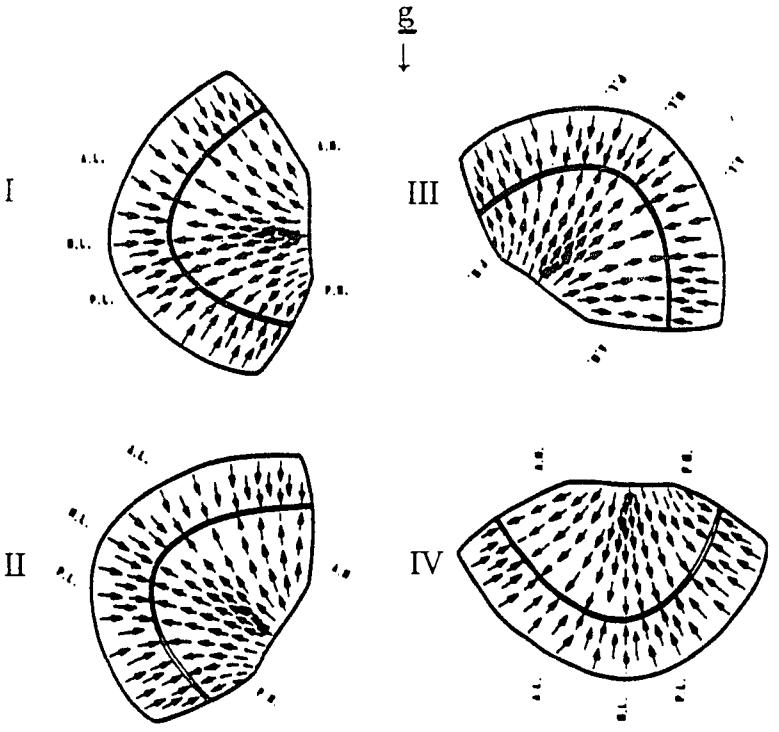

B

PATTERNS OF OTOLITH ACTIVATION DURING OFF-VERTICAL AXIS ROTATION

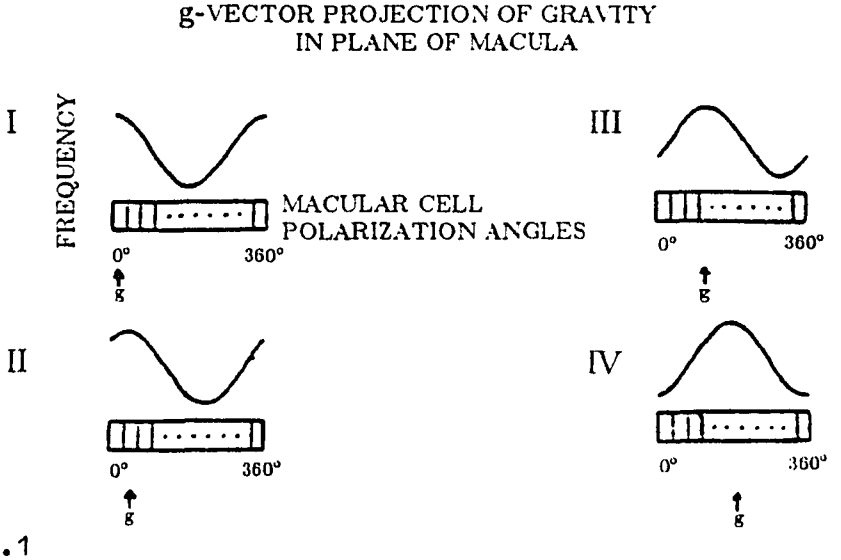

Fig. 3.1.1

orientation with regard to gravity and can generate direct compensatory eye position changes as the head moves into different positions in the gravitational field (Diamond et al, 1979; Wall & Black, 1984).

If there is relative rotation of a force field with respect to the macula, such as occurs during off-vertical axis rotation, there will be a shift in the pattern (Fig. 3.1.1B,I-IV). For example, cells which have their polarizations in a plane orthogonal to the gravitational field when the macula is in the position shown in Fig. 3.1.1A-I are maximally excited when the macula has been rotated to the position shown in Fig. 3.1.1A-III. Thus, all of the cells whose polarization vectors have components perpendicular to the angular velocity, $\underline{w}$, are sequentially excited as the macula rotates through 360 degrees (Fig. 3.1.1A,I-IV). This spatio-temporal relationship would induce a traveling wave of excitation and inhibition in the firing patterns of the cells in the macula (Fig. 3.1.1B). The velocity of the wave is equal to the relative angular velocity of the head with respect to the gravitational field. We postulate that this traveling wave is detected centrally, its velocity estimated and the signal used to excite the velocity storage integrator to generate continuous nystagmus. It will be assumed that the velocity estimate will have three components corresponding to the normal directions of the semicircular canal planes. A model of the mechanism which estimates the velocity in each of these directions is considered next.

The operational model of the otolith cellular organization for sensing head position during OVAR is chosen as an ordered collection of cells with ordering according to the angles of the polarization vectors over a range of 360 degrees (Fig. 3.1.2A). The ordering will be described for the left macula; the ordering of the cells in the right macula is the mirror image. Cell number zero is arbitrarily chosen to correspond to that cell which is maximally excited when the head is positioned with the nose down (Fig. 3.1.2A), with corresponding signal component r_0. As the head is rotated to the left, the next cell to be maximally excited is cell number one, corresponding to component r_1 (Fig. 3.1.2B). As we continue the leftward rotation, the last cell to be maximally excited before cell number zero is again maximally excited is cell number N-1, corresponding to component r_{N-1}. This ordering defines the N-vector $\underline{r}(t)$ (Fig. 3.1.2B). Because of the mirror symmetry about the midsaggital plane a similar excitation vector can be obtained for the right macula. The positive direction of rotation is, however, toward the right rather than the left. Using this ordering, cells corresponding to components r_i and r_{i+1} for i=0, ..., N-2 are adjacent. In addition, cells corresponding to components r_{N-1} and r_0 are adjacent.

The polarization vectors, $\hat{\underline{P}}(\phi(t),h)$, associated with the cells of the otolith macula point radially outward from the center of a circle in a space fixed frame of reference (Fig. 3.1.3A). The component of

Fig. 3.1.2 A. Model of the spatial ordering of otolith cells for a particular plane. An animal is in a barbicue-spit position with its nose down. As the animal is rotated the orientation of the animal's head is given by the angle between the directions defined by its nose and gravity. The polarization angles, h, are defined with respect to the nose. For the left utricular macula the otolith cell which is maximally excited when the animal's nose is down is number zero and its polarization angle, h_0, is zero. As the head is rotated to the left the next cell which is maximally excited is cell number 1 and its polarization angle, h_1, is equal to the present head orientation. As the head continues to rotate to the left the cell which is maximally excited just before cell number zero is again maximally excited is cell number N-1. The numbering of the cells in the right macula is the mirror image of the left macula.

B. An N-dimensional pattern vector of otolith cell activation, $\underline{r}(t)$, defined by the ordering of the cells in A. Component $r_i(t)$ corresponds to the activation of cell number i at polarization angle h_i for $0 \leq i < N$. Cells numbered i and i+1 are adjacent for $0 \leq i < N-1$ as are cells numbered N-1 and zero.

A

SPATIAL ORDERING
OF OTOLITH CELLS

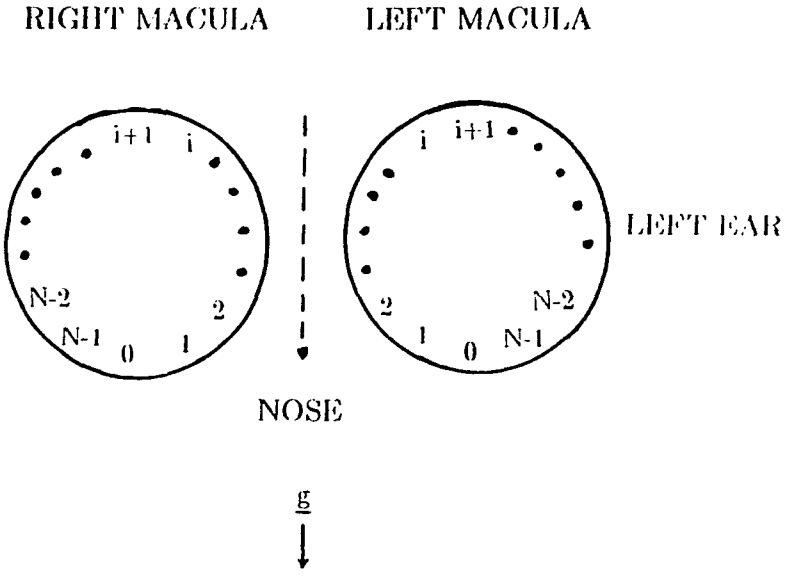

B

N-DIMENSIONAL VECTOR REPRESENTATION
OF OTOLITH MACULA ACTIVATION

$$\underline{r}(t) = \begin{bmatrix} r_0(t) \\ r_1(t) \\ r_2(t) \\ \cdot \\ \cdot \\ \cdot \\ r_{N-3}(t) \\ r_{N-2}(t) \\ r_{N-1}(t) \end{bmatrix}$$

Fig. 3.1.2

Fig. 3.1.3 A. The association of a unit polarization vector with a particular cell (h) in a space fixed reference frame. As the head rotates such that $\phi(t)$ increases, $\underline{P}(\phi(t),h)$ will change direction for a given polarization angle, h, in the head reference frame. The activation of a cell is related to the component of gravity along the cell's unit polarization vector. The cell activation is a function of its polarization angle, h, and, head orientation, ϕ. If $\phi(t)$ and h are changed in an identical fashion, $\underline{P}(\phi(t),h)$ will be constant.

B. A representation of the otolith activation pattern. For a given position of the head this pattern is also a representation of head orientation relative to gravity. The pattern is realized by a sampling of the gravitational field by the cells of the macula in a given plane. The length of each line represents the magnitude of the component of gravity as measured along the polarization vectors in space. Each arrow pointing toward the center of the circle represents an inhibition while each arrow pointing away from the center of the circle represents an excitation. The activation depends only on the angle between the corresponding polarization vector and gravity.

A

UNIT POLARIZATION VECTOR
IN A SPACE FIXED
FRAME OF REFERENCE

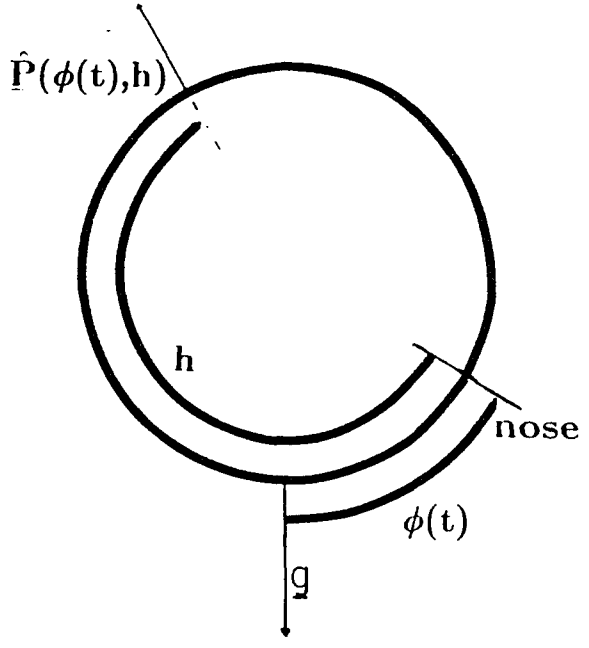

B

COMPONENT OF GRAVITY ALONG
POLARIZATION VECTORS
OF OTOLITH MACULA

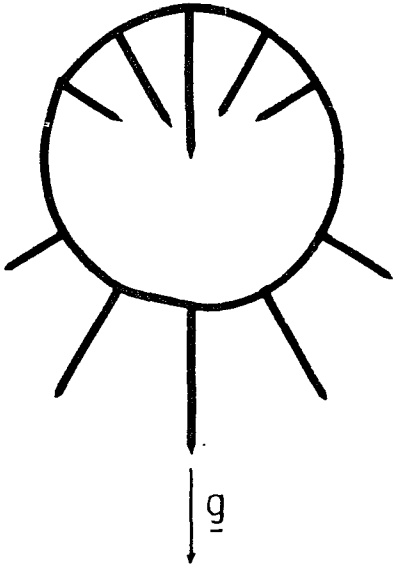

Fig. 3.1.3

force due to gravity as measured along these polarization vectors is shown in Fig. 3.1.3B and is represented by the vector $\underline{r}(t)$ (Fig. 3.1.2B). Arrows pointing toward the center of the circle represent inhibitions while arrows pointing away from the center of the circle represent excitations.

The vector $\underline{r}(t)$ can be interpreted as a pattern of excitation of all otolith cells for any given head position. As the head moves, the pattern will change such that the time variation of each component coupled with the spatial relationship between adjacent components can be used to compute an estimate of head velocity. Consequently, it is necessary to compare two patterns which correspond to head orientations at different times. Therefore, it will be assumed that there are two signals generated centrally from each otolith cell. Each signal is proportional to the bending of the cilia in a prefered direction and reaches the central processing area such that one is delayed by T seconds relative to the other. A mathematically simplifying assumption is that during rotation with constant angular velocity, $\underline{w}$, the head will be positioned such that a normal to the plane of these polarization vectors is parallel to the rotational axis which in turn is perpendicular to gravity. This would correspond to barbecue-spit rotation. Different angles of tilt effectively reduce the magnitude of the component of the force which excites the cells by the sine of the tilt angle. This would effect the amplitudes but not the phases of the cellular excitations during rotation.

3.1.2 Computation of Head Velocity Estimate During OVAR

Consider $\hat{\underline{P}}(\phi(t),h_i)$, the radially outward directed unit vector field in a space fixed coordinate basis (Fig. 3.1.3A). Its direction is a function of the instantaneous angular position of the head with respect to gravity, $\phi(t)$, and the angular orientation, h_i, of a cell in a head fixed coordinate system where $0 \leq h_i < 2\pi$. The angular orientation, h_i, of a given cell is associated with the polarization vector for that cell. As the head rotates, $\hat{\underline{P}}(\phi(t),h_i)$ for a given cell will change its direction in space as $\phi(t)$ changes with time. The projection of gravity onto $\hat{\underline{P}}(\phi(t),h_i)$ for all h_i gives the excitation vector $\underline{r}(t)$ (Fig. 3.1.2B). If we define $\langle , \rangle$ to be an inner product operator which gives the projection of one vector onto the other, a mathematical description of the present and delayed patterns of otolith activation representing head orientation can be given by

$$r(\phi(t),h_i)=\langle \hat{\underline{P}}(\phi(t),h_i),\underline{g}\rangle = r_i(t) \text{ for } i=0, \ldots, N-1 \qquad (3.1.1A)$$

$$r(\phi(t-T),h_i)=\langle \hat{\underline{P}}(\phi(t-T),h_i),\underline{g}\rangle = r_i(t-T) \text{ for } i=0, \ldots, N-1. \qquad (3.1.1B)$$

The delayed function $r(\phi(t-T),h_i)$ for all i supplies information about the position of the head T seconds prior to the present and can be used as a "template" which is compared to the present pattern of cellular activation.

The fundamental equation which implements the template matching approach is derived by assuming that the activation of any cell depends only on the spatial angle, S, with regard to gravity (Fig. 3.1.4). Thus, at angle S the activation of a cell h_i at time t-T must be equal to the activation of cell h_i+d at time t where d is the angle the head has rotated in time T. This relationship can be expressed as follows:

$$r(\phi(t),h_i+d)=r(\phi(t-T),h_i) \text{ for } i=0, \ldots, N-1 \qquad (3.1.2)$$

where $r(\phi(t-T),h_i)$ is the activation of cell h_i when the head is in position $\phi(t-T)$ and $r(\phi(t),h_i+d)$ is the activation of the cell at h_i+d when the head is in position $\phi(t)$. In a head fixed coordinate frame, this is characteristic of a traveling wave whose velocity is d/T.

In order to obtain the velocity of rotation, the displacement, d, must be estimated from Eq (3.1.2). There are certain contraints that the solution must satisfy. Firstly, because of the circular periodicity of the model, Eq (3.1.2) remains valid if d is replaced by d+2nπ where n=0, $\pm$1, $\pm$2, ... Thus, there is no unique solution. In addition, if it is assumed that the estimate of head displacement in one direction is the negative of the displacement in the opposite direction, then the estimate of head displacement, $\hat{d}$, has the property that $\hat{d}(-d)=-\hat{d}(d)$. Furthermore, since the relationships between present and delayed patterns are identical for phase shifts of $\pm$180

Fig. 3.1.4 Spatio-Temporal relation between patterns of otolith cell activation. A cell with polarization angle h at a delayed time t-T is shown by the dotted triangle. The angle between its polarization vector and gravity in a space fixed reference frame is S. Another cell with polarization angle h+d at time t such that the angle between its polarization vector and gravity in a space fixed reference frame is also S. Both cells are assumed to have the same activation (see equation).

SPATIO-TEMPORAL RELATION OF OTOLITH CELL ACTIVATION

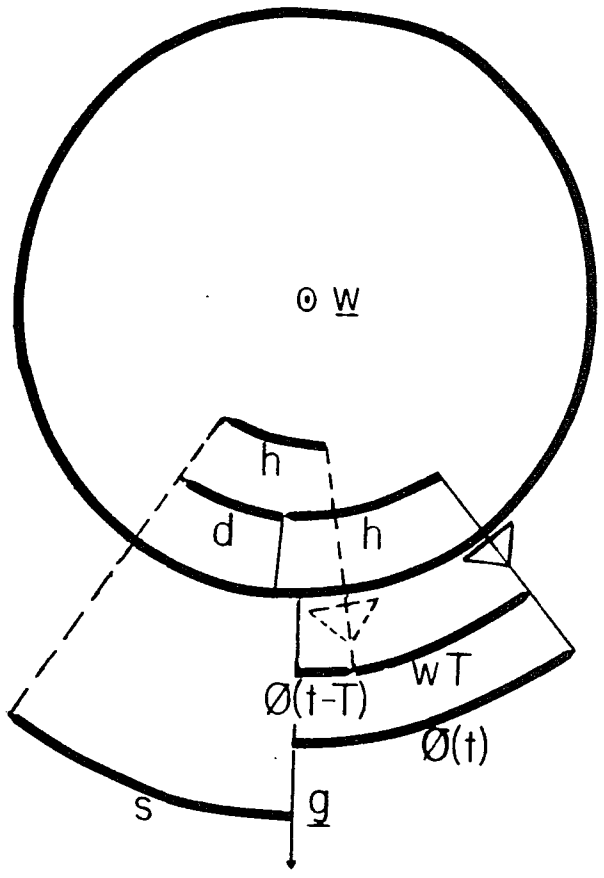

$d = \omega \cdot T$

$r(\phi(t), h+d) \cdot r(\phi(t-T), h)$

S - spatial angle of observation relative to gravity.

▽- nose as viewed from above the top of the head at time t-T.

▽- nose as viewed from above the top of the head at time t.

ϕ - angular position of nose relative to gravity shown at times t-T and t.

ω - constant angular head velocity in a space fixed frame of reference.

$\omega \cdot T$ - angular displacement of head in time interval T.

h - angle of a cell relative to nose (polarization angle).

d - difference in spatial angular orientations of cell with polarization angle h at times t and t-T.

$r(\phi(t-T), h)$ = Excitation of cell with polarization angle h at time t-T.

$r(\phi(t), h+d)$ = Excitation of cell with polarization angle h+d at time t.

Fig. 3.1.4

degrees, $\hat{d}(-\pi)=\hat{d}(\pi)$ and the estimation, $\hat{d}(\pi)$, must be zero. Thus, a solution can be obtained such that $-\pi<\hat{d}<\pi$ subject to the constraints mentioned above.

To solve Eq (3.1.2) we must only utilize the present excitation vector, $\underline{r}(t)$, and the delayed excitation vector $\underline{r}(t-T)$. The excitation, $r(\phi(t-T),h_i)$, in Eq (3.1.2) is equal to the delayed cell excitation, $r_i(t-T)$. However, $r(\phi(t),h_i+d)$, is the projection of gravity onto the polarization vector at angle h_i+d in the head fixed coordinate system. This information may not be available since the only gravity projection information at time t available to the central nervous system is:

$$r(\phi(t),h_i)=r_i(t) \text{ for } i=0, \ldots, N-1 \qquad (3.1.3)$$

corresponding to discrete cell locations. One way to find an estimate of d is to replace $r(\phi(t),h_i+d)$ in Eq (3.1.2) by an approximation to it using the components of $\underline{r}(t)$.

At a given instant of time the spatial distribution of the signal $r(\phi(t),h_i+d)$ for each i is a sinusoidal function of d. However, we can locally approximate the function by a straight line, $Y_i(d,t)$, utilizing the information from the cells at angles h_i and h_{i+1}, corresponding to vector components $r_i(t)$ and $r_{i+1}(t)$ (Fig. 3.1.5). Substituting $Y_i(d,t)$ for $r(\phi(t),h_i+d)$ in Eq (3.1.2), we obtain

$$Y_i(d,t) \simeq r_i(t-T), \text{ for } i=0, \ldots, N-1. \tag{3.1.4}$$

We further constrain each straight line, $Y_i(d,t)$, such that its functional value is equal to the signal values of the cells at h_i (where d=0) and h_{i+1} (where $d=h_{i+1}-h_i$, the angular distance between adjacent cells). That is,

$$Y_i(0,t)=r_i(t) \text{ for } i=0, \ldots, N-1 \tag{3.1.5A}$$

$$Y_i(h_{i+1}-h_i,t)=r_{i+1}(t) \text{ for } i=0, \ldots, N-1 \tag{3.1.5B}$$

where

$$h_N=h_0 \text{ and } r_N(t)=r_0(t) \tag{3.1.6}$$

because of the circular periodicity of the cellular structures.

The equation for Y_i at any time, t, is that of a straight line passing through the points $(h_i, r_i(t))$ and $(h_{i+1}, r_{i+1}(t))$ in a head based coordinate frame and is given by

$$Y_i(d,t)=\{r_{i+1}(t)-r_i(t)\}/\{h_{i+1}-h_i\}d+r_i(t). \tag{3.1.7}$$

If we assume that the cells are uniformly spaced then

$$h_{i+1}-h_i=H \text{ (a constant) for } i=0, \ldots, N-1. \tag{3.1.8}$$

Using Eqs (3.1.7) and (3.1.8) we obtain

$$Y_i(d,t)=\{r_{i+1}(t)-r_i(t)\}/\{H\}d+r_i(t), \text{ for } i=0, \ldots, N-1. \tag{3.1.9}$$

It should be noted that each $Y_i(d,t)$ will be a reasonable approximation of a sinusoid if the angular distance between any two neighboring cells, $H=h_{i+1}-h_i$, and the estimate of head displacement, $\hat{d}$, are small compared to π. If we consider the sequence $Y_i(d,t)$ i=0, ..., N-1 given in Eq (3.1.9) for a given d as a vector approximation to $\underline{r}(t-T)$, we can obtain an estimate of the head displacement, $\hat{d}$, by minimizing the mean square error between $\underline{r}(t-T)$ and $\underline{Y}(d,t)$ with respect to d. Let

$$\underline{E}=\underline{Y}(d,t)-\underline{r}(t-T) \tag{3.1.10}$$

where $\underline{E}$ is an N-vector, the i^{th} component of which is the error in approximating $r_i(t-T)$ by $Y_i(d,t)$ (Fig. 3.1.5). The mean square error is given by

$$F(d,t)=(1/N)\langle\underline{E},\underline{E}\rangle=(1/N)\sum_{i=0}^{N-1} E_i^2. \tag{3.1.11}$$

Fig. 3.1.5 Estimate of the spatial displacement of the present pattern of otolith cell activation from the template pattern (delayed pattern) of otolith activation, d, is obtained by approximating the "delayed pattern" i^{th} activations from present pattern values. The i^{th} component of the approximation is chosen to be a linear function Y_i of a variable d using the present time activations of cells i and i+1. For a given d, Y_i represents an approximation to the activation of cell i at the delayed time, t-T, given by the template pattern. The error in this approximation is given by, E_i. The d that minimizes the mean square error for all i is the best estimate of the head displacement, d.

TEMPLATE MATCHING PROCEDURE

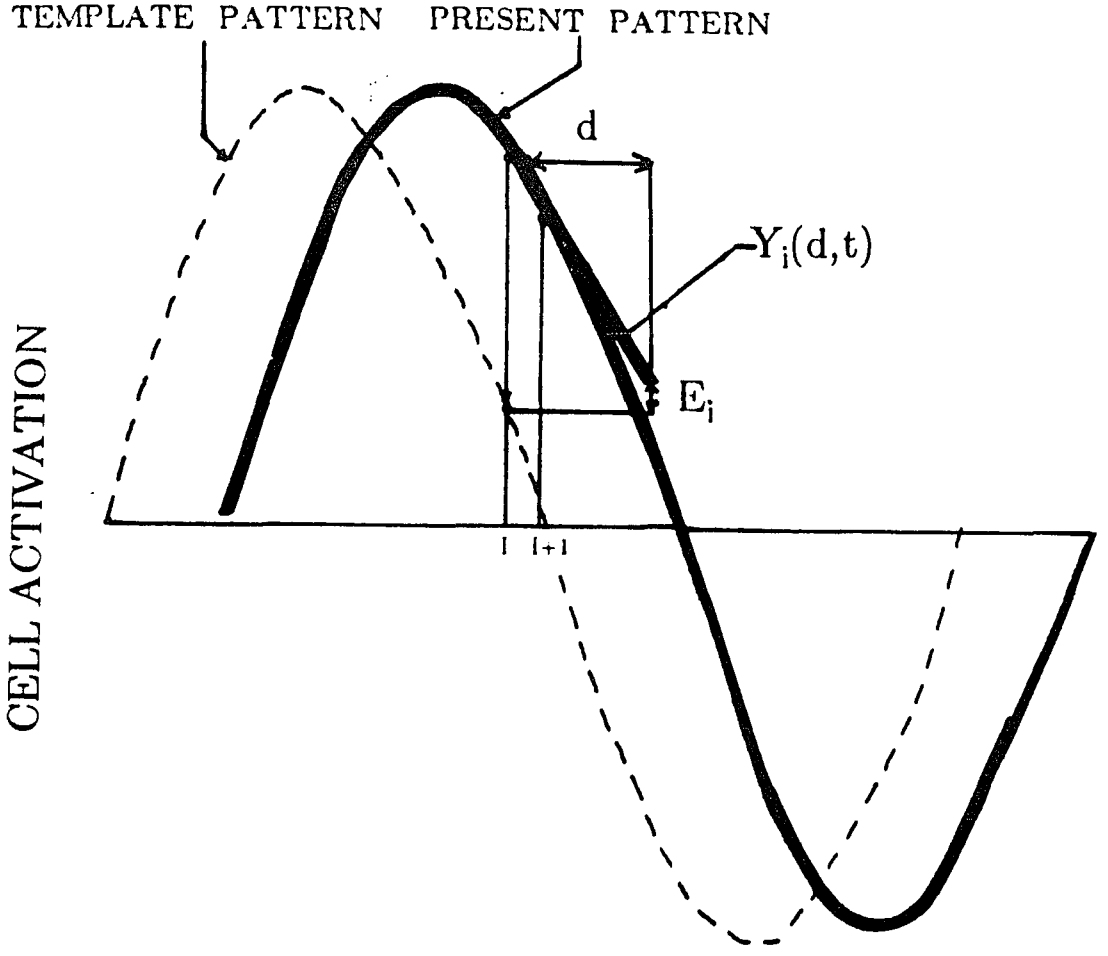

$$\hat{d} = \frac{<\{\text{Delay}(T)\text{-}I\}[\underline{r}(t)], \{\text{RotateUp-}I\}[\underline{r}(t)]>}{\pi g^2}$$

Fig. 3.1.5

To obtain an optimal estimate of d we will minimize F with respect to $\hat{d}$. To help simplify the expression for $\hat{d}$ the following definitions will be made:

Let RotateUp[$\underline{r}$] be an operator which transforms $\underline{r}(t)$ and yields a vector of N numbers such that

$$\text{RotateUp}\left[\begin{matrix} r_0(t) \\ r_1(t) \\ r_2(t) \\ \cdots \\ r_{N-3}(t) \\ r_{N-2}(t) \\ r_{N-1}(t) \end{matrix}\right] = \begin{matrix} r_1(t) \\ r_2(t) \\ r_3(t) \\ \cdots \\ r_{N-2}(t) \\ r_{N-1}(t) \\ r_0(t) \end{matrix} \qquad (3.1.12)$$

Let Delay(s) be another operator which transforms $\underline{r}(t)$ and yields a vector of N numbers such that

$$\text{Delay(s)}\left[\begin{matrix} r_0(t) \\ r_1(t) \\ r_2(t) \\ \cdots \\ r_{N-3}(t) \\ r_{N-2}(t) \\ r_{N-1}(t) \end{matrix}\right] = \begin{matrix} r_0(t-s) \\ r_1(t-s) \\ r_2(t-s) \\ \cdots \\ r_{N-3}(t-s) \\ r_{N-2}(t-s) \\ r_{N-1}(t-s) \end{matrix} \qquad (3.1.13)$$

Define $I[\underline{r}]$ as the identity operator such that

$$I[\underline{r}(t)]=\underline{r}(t). \tag{3.1.14}$$

We now redefine the operator, <,>, to be a generalized inner product defined by a bilinear form (Lang, 1966) such that

$$\langle \underline{X},\underline{Y}\rangle=\underline{X}^{t}K\underline{Y}, \tag{3.1.15}$$

where K is a diagonal N by N matrix and represented by

$$K=\begin{vmatrix} K_0 & 0 & 0 & . & . & . & 0 \\ 0 & K_1 & 0 & . & . & . & 0 \\ & & . & . & . & & \\ 0 & . & . & . & 0 & K_{N-2} & 0 \\ 0 & . & . & . & 0 & 0 & K_{N-1} \end{vmatrix} \tag{3.1.16}$$

The norm of a vector, $||\underline{C}||$, is given by

$$||\underline{C}||= (\langle \underline{C},\underline{C}\rangle). \tag{3.1.17}$$

Using these definitions to find the estimate of head displacement, $\hat{d}$, we begin by letting the i^{th} component of the error vector $\underline{E}$ be given by

$$E_i = d\{\text{RotateUp-I}\}[\underline{r}(t)]_i/(h_{i+1}-h_i)+\{\text{I-Delay}(T)\}[\underline{r}(t)]_i, \quad \text{for } i=0 \text{ to } N-1. \tag{3.1.18}$$

The mean square of the error is given by Eq (11) and can be written succinctly as

$$F(d,t)=(1/N)\langle \underline{E},\underline{E}\rangle. \tag{3.1.19}$$

To find the value of d which minimizes F(d,t) at any time t, we set the partial derivative of F(d,t) with respect to d equal to zero and solve for d.

$$\frac{\partial F(d,t)}{\partial d}=(2/N)\langle \underline{E}, \frac{\partial \underline{E}}{\partial d}\rangle=0. \tag{3.1.20}$$

Therefore,

$$\langle \underline{E}, \frac{\partial \underline{E}}{\partial d}\rangle=0, \tag{3.1.21}$$

where

$$\frac{\partial E_i}{\partial d}=(\text{RotateUp-I})[\underline{r}(t)]_i/(h_{i+1}-h_i), \text{ for } i=0 \text{ to } N-1. \tag{3.1.22}$$

Therefore,

$$\left\langle \underline{E}, \frac{\partial \underline{E}}{\partial d} \right\rangle = \sum_{i=0}^{N-1} \Big(\hat{d}\{(\text{RotateUp-I})[\underline{r}(t)]_i/(h_{i+1}-h_i)\}^2 + [\text{I-Delay}(T)][\underline{r}(t)]_i(\text{RotateUp-I})[\underline{r}(t)]_i/(h_{i+1}-h_i) \Big) = 0. \quad (3.1.23)$$

Solving for $\hat{d}$ we obtain

$$\hat{d} = \Big(\sum_{i=0}^{N-1} \{[\text{Delay}(T)-I][\underline{r}(t)]_i(\text{RotateUp-I})[\underline{r}(t)]_i/(h_{i+1}-h_i)\} \Big) / \Big(\sum_{i=0}^{N-1} \{(\text{RotateUp-I})[\underline{r}(t)]/(h_{i+1}-h_i)\}^2 \Big). \quad (3.1.24)$$

If the polarization angles, h_i for i=0 to N-1, are uniformly spaced then, using Eq (3.1.8) in Eq (3.1.24) we obtain

$$\hat{d} = H\langle[\text{Delay}(T)-I][\underline{r}(t)],(\text{RotateUp-I})[\underline{r}(t)]\rangle / \|(\text{RotateUp-I})[\underline{r}(t)]\|^2. \quad (3.1.25)$$

Insight into the nature of the estimate, $\hat{d}$, can be obtained by assuming that each K_i is a function of tilt angle, a, such that

$$K_i = k(a) \text{ for } i=0, \ldots, N-1 \quad (3.1.26)$$

and

$$k(a)\sin^2(a) \simeq 1. \tag{3.1.27}$$

Using Eqs (3.1.26), (3.1.27), and the set of values $r_i(t)$, for i=0,..., N-1, which are samples from a sinusoid at angles iH, we simplify the denominator in Eq (3.1.25) for large N (see Appendix A), as follows:

$$H/\|\{\text{RotateUp-I}\}[\underline{r}(t)]\|^2 \xrightarrow[N\to\infty]{} 1/(\pi g^2), \tag{3.1.28}$$

where $NH=2\pi$. The estimate of angular head velocity is given by

$$\hat{w}=\hat{d}/T \tag{3.1.29}$$

and by using Eqs (3.1.25), (3.1.28), and (3.1.29) we obtain $\hat{w}(t)$ (in radians/second)

$$\hat{w}(t)=<\{\text{Delay(T)-I}\}[\underline{r}(t)],\{\text{RotateUp-I}\}[\underline{r}(t)]>/\{\pi Tg^2\}. \tag{3.1.30}$$

The model of the velocity estimator is shown in Fig. 3.1.6 where each K_n for n=0, ..., N-1 is a diagonal element of the matrix representing the inner product. Each K_n would be a function of tilt angle and act

Fig. 3.1.6 The pattern velocity estimation formula and the implementation of the velocity estimator. The estimate of the head displacement found in Fig. 3.1.5 is divided by the time to make the displacement, i.e. the delay time, T. It is a generalized inner product between temporal and spatial differences. This is a one-sided model using information from one utricular macula. The difference between the left macula and the right macula estimation is due to mirror symmetry of the numbering of cells. A small leftward rotation of the left macula gives a positive estimate of head velocity while a small leftward rotation of the right macula gives a negative estimate of head velocity. The k_n's in the model implement a generalized inner product or bilinear form and account for the fact that the bias component of velocity due to OVAR is approximately independent of tilt angle after about 10 degrees of tilt.

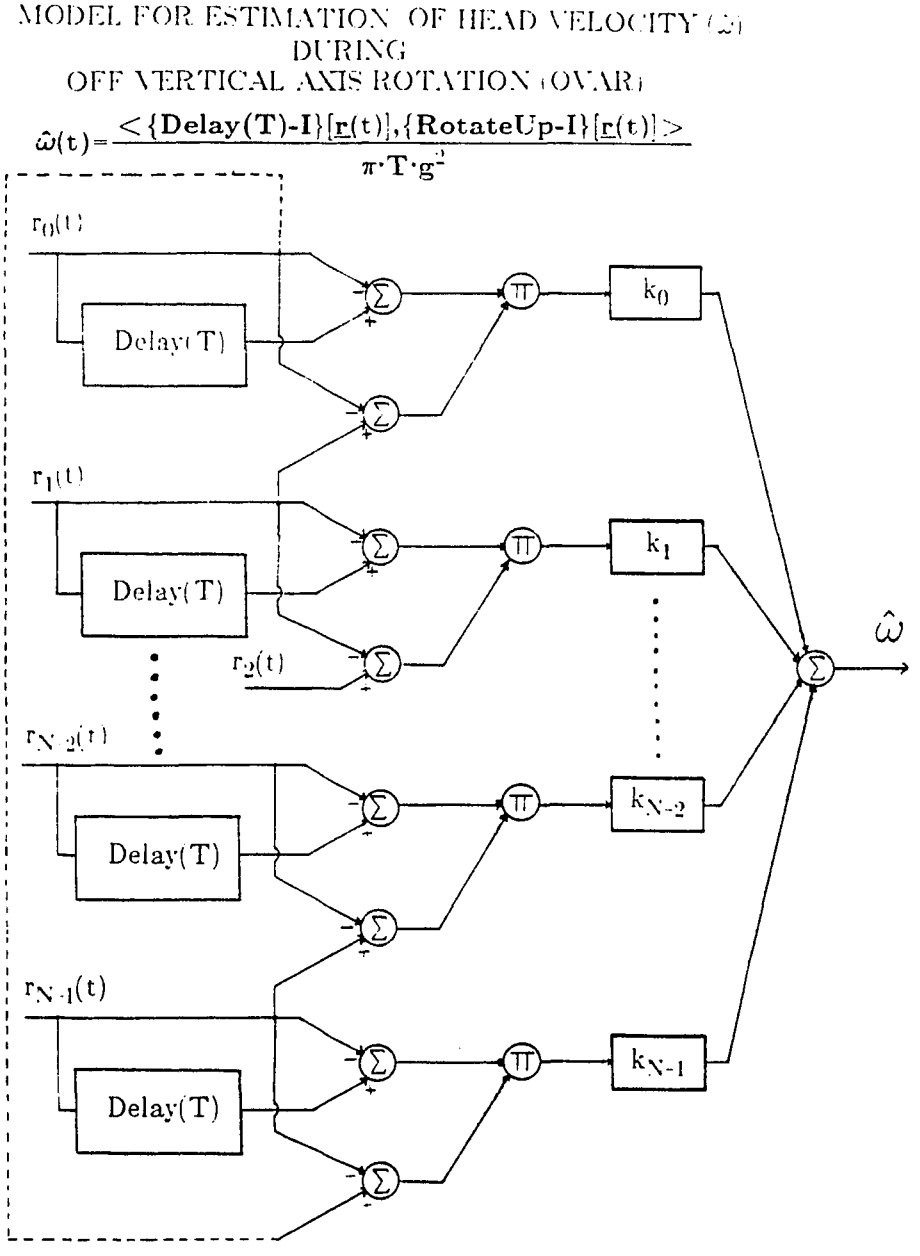
MODEL FOR ESTIMATION OF HEAD VELOCITY (ω̂)
DURING
OFF VERTICAL AXIS ROTATION (OVAR)
ω̂(t)=<{Delay(T)-I}[r(t)],{RotateUp-I}[r(t)]>
π·T·g²
r0(t)
Delay(T)
k0
r1(t)
Delay(T)
k1
r2(t)
rN-2(t)
Delay(T)
kN-2
rN-1(t)
Delay(T)
kN-1
ω̂

Fig. 3.1.6

as a normalizing factor when the head is at different angles of tilt. It should be noted that Eq (3.1.30) represents the estimate of head velocity by each macula. The positive direction for the estimate is to the left for the left macula and to the right for the right macula. Therefore, Eq (3.1.30) can be generalized such that the estimate of head velocity utilizing information from the left macula is given by

$$\hat{w}_l(t)=<\{\text{Delay}(T)-I\}[\underline{r}_l(t)],\{\text{RotateUp}-I\}[\underline{r}_l(t)]>/\{\tilde{T}\tilde{T}Tg^2\} \quad (3.1.31)$$

where $\underline{r}_l$ is the pattern excitation vector of the left macula. The estimate of head velocity utilizing information from the right macula is given by

$$\hat{w}_r(t)=<\{\text{Delay}(T)-I\}[\underline{r}_r(t)],\{\text{RotateUp}-I\}[\underline{r}_r(t)]>/\{\tilde{T}\tilde{T}Tg^2\} \quad (3.1.32)$$

where $\underline{r}_r$ is the pattern excitation vector of the right macula. The estimate of head velocity due to both otoliths is therefore given by

$$\hat{w}=(\hat{w}_l-\hat{w}_r)/2. \quad (3.1.33)$$

If the estimate of head velocity utilizing information from a single macula (Eq (3.1.30)) is simplified it can be shown that the computation of the estimate is independent of time, t. Using the definitions of the operators given in Eqs (3.1.12), (3.1.13), and

(3.1.14), an estimate of velocity utilizing information from the left macula is given by

$$\hat{w}_1(t)=\sum_{n=0}^{N-1}\{r_n(t-T)-r_n(t)\}K_n\{r_{n+1}(t)-r_n(t)\}/(\tau\tau Tg^2). \qquad (3.1.34)$$

For the case where the angular head velocity vector, $\underline{w}$, is along a normal to the plane of the macula which in turn is at an angle of tilt, a, relative to the vertical we have

$$r_n(t)=g\sin(a)\cos(nH-wt) \qquad (3.1.35)$$

where $\phi(t)=wt$ and $h=nH$. Therefore,

$$\hat{w}_1(t)=\sum_{n=0}^{N-1}\{\cos(nH-w[t-T])-\cos(nH-wt)\}K_n\sin^2(a) \qquad (3.1.36)$$
$$\{\cos([n+1]H-wt)-\cos(nH-wt)\}/(\tau\tau T).$$

Expanding the products in Eq (3.1.36) we obtain

$$\hat{w}_1(t)=\sum_{n=0}^{N-1}\{\cos(nH-wt+wT)\cos(nH-wt+H)-\cos(nH-wt+wT)\cos(nH-wt) \qquad (3.1.37)$$
$$-\cos(nH-wt)\cos(nH-wt+H)+\cos^2(nH-wt)\}K_n\sin^2(a)/(\tau\tau T).$$

Using the trigonometric identity given in Eq (B3), we obtain

$$\hat{w}_l(t)=\sum_{n=0}^{N-1}\{\cos(2[nH-wt]+wT+H)+\cos(wT-H) \\ -\cos(2[nH-wt]+wT)-\cos(wT) \\ -\cos(2[nH-wt]+H)-\cos(H) \\ +\cos(2[nH-wt])+1\}K_n\sin^2(a)/(2\pi T). \tag{3.1.38}$$

Using Eq (B8), we obtain an estimate of the head velocity that is independent of time

$$\hat{w}_l=\sum_{n=0}^{N-1}\{\cos(wT-H)-\cos(wT)-\cos(H)+1\}K_n\sin^2(a)/(2\pi T). \tag{3.1.39}$$

By using the trigonometric identity given in Eq (B4), the expression given in Eq (3.1.39) can be simplified

$$\hat{w}_l=N\{\sin(wT-H/2)\sin(H/2)+\sin^2(H/2)\}/(\pi T). \tag{3.1.40}$$

Factoring out sin(H/2), using the formula $H=2\pi/N$, and using the trigonometric identity given in Eq (B5) the following expression can be obtain for the estimate of the head velocity due to sequential excitation of N cells at present and delayed times:

$$\hat{w}_l=w\{\sin(H/2)/(H/2)\}\{2\sin(wT/2)\cos([wT-H]/2)/(wT)\}. \tag{3.1.41}$$

By use of symmetry and Eq (3.1.32), the estimate of head velocity utilizing information from the right macula can be given by

$$\hat{w}_r=w\{-\sin(H/2)/(H/2)\}\{2\sin(wT/2)\cos([wT+H]/2)/(wT)\}. \tag{3.1.42}$$

Substituting Eqs (3.1.41) and (3.1.42) into Eq (3.1.33), an estimate of the head velocity is given by

$$\hat{w}=w\{\sin(H)/H\}\{\sin(wT)/wT\}. \qquad (3.1.43)$$

Taking the limit as H->0 in Eq (3.1.43), we obtain the following estimate of head velocity:

$$\hat{w}=w\{\sin(wT)/(wT)\} \qquad (3.1.44)$$

or

$$\hat{w}=wSa(wT) \qquad (3.1.45)$$

where Sa(.) is the sampling function. In the limit as T->0 the estimate becomes w, the head velocity.

3.1.3 Model Simulations and Comparison with Physiological Data

The model was tested for steps of input velocities and both the steady state and dynamic characteristics of the estimated velocities were compared to results obtained during OVAR in the monkey (Fig. 3.1.7). If an animal is rotated about a vertical axis until per-rotatory nystagmus decays to zero followed by a tilt of the axis of rotation, the nystagmus returns slowly to a steady state level after approximately a one second delay (Fig. 3.1.7A). During the period of OVAR there is a sustained horizontal nystagmus for as long as rotation persists. Superimposed on the steady state slow phase velocity are oscillations that are phase locked to head position (Fig. 3.1.7A). When the animal is returned to the upright position, the nystagmus decays to zero with a time constant approximately equal to that of OKAN and per- and post-rotatory nystagmus (Benson & Bodin, 1966a; Guedry, 1965; Raphan et al. 1981; Young & Henn, 1975) (Fig. 3.1.7A). The steady state velocity is related approximately linearly to head velocity up to 50 deg/sec. For head velocities greater than 50 deg/sec steady state eye velocity declines toward zero (Fig. 3.1.7B).

In simulating these response characteristics, the N cells were assumed to be uniformly spaced and divided into M cell groups with M chosen equal to 30. Each cell group represents n consecutively-numbered cells such that nM=N. The excitation of a cell

Fig. 3.1.7 A. Response to off-vertical axis rotation. The animal was rotating in darkness and the slow phase velocity had declined to zero. When the animal is tilted at $t=t_0$, there is a delay of approximately one second followed by a slow rise in slow phase velocity to a steady state level. As long as rotation persists there is a sustained horizontal nystagmus. There is a modulation of the slow phase eye velocity such that the dominant harmonic is phase locked to head position. When the animal is tilted back to the vertical at $t=t_1$, slow phase velocity declines to zero. The time constants of rise and fall in slow phase velocity are consistent with the charging and discharging of the velocity storage integrator.
B. Steady state slow-phase eye velocity as a function of head velocity during rotation about an off-vertical axis (50 degrees) in darkness. Eye velocity rises linearly with head velocity to about 50-60 deg/sec and then declines toward zero as head velocity increases.

A

EYE VELOCITY RESPONSE TO TILTING
DURING PROLONGED ROTATION

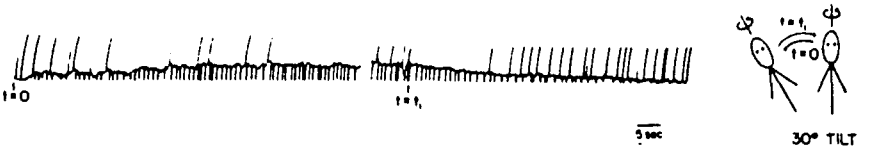

B

STEADY STATE EYE VELOCITY
VS
HEAD VELOCITY

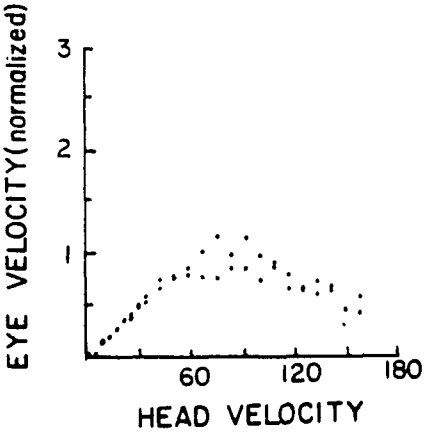

Fig. 3.1.7

group will be the median excitation of the corresponding n cells. It is assumed that the difference between the angular orientations (h) of the end cells associated with a cell group is small compared to 180 degrees. Therefore, the excitation of the cell group with a weight of n is a good approximation to the excitations of the n cells.

A plot of estimated velocity ($\hat{w}$) as a function of head velocity (w) is shown in Fig. 3.1.8A. The simulations suggest that for $0 \leq w << 90/T$ deg/sec the estimate of head velocity rises approximately linearly with unit slope as a function of w. The estimated head velocity peaks at w=90/T deg/sec having a value $1/T(180/\pi\pi)$ deg/sec and then declines for larger values of head velocity. These relationships are maintained for rotations in either direction. This behavior approximates the steady state eye velocity as a function of head velocity during off vertical axis rotation (Fig. 3.1.7B; Raphan et al. 1981). The model predictions were superimposed on the data of Fig. 3.1.7B replotted to take into account the direction of rotation. The data were best fit by a sinusoid with a period T=0.85 seconds, corresponding to a delay in the processing of the pattern for template matching of approximately one second. This is consistent with the one second delay in the buildup of the bias component of OVAR. It suggests that the fall off in the steady state eye velocity at higher stimulus velocities is related to the delay in processing within the velocity estimator. Fig. 3.1.8B shows how the estimated velocity vs. head velocity curve is modified by considering only one macula. The

Fig. 3.1.8 Effects of delay time on the steady state estimate of head velocity.
A. The data of Fig. 7B were best simulated by the estimator with a delay time of 0.85 seconds. The use of the two-sided formula for the estimated velocity resulted in a symmetrical curve that fitted the data.
B. When the one-sided formula (solid curve) with a time-delay of 0.85 seconds was used, there was an asymmetry about the origin. The simulation is shifted up and to the right compared to the simulation in A.
C. When the delay time in the two-sided formula was increased the peak steady state velocity and the linear range of operation was reduced.
D. Decreasing the delay time, T, in the two-sided formula increased the peak steady state velocity and extended the linear range of head velocity estimation. These simulations (solid curves) were performed using 30 cell groups.

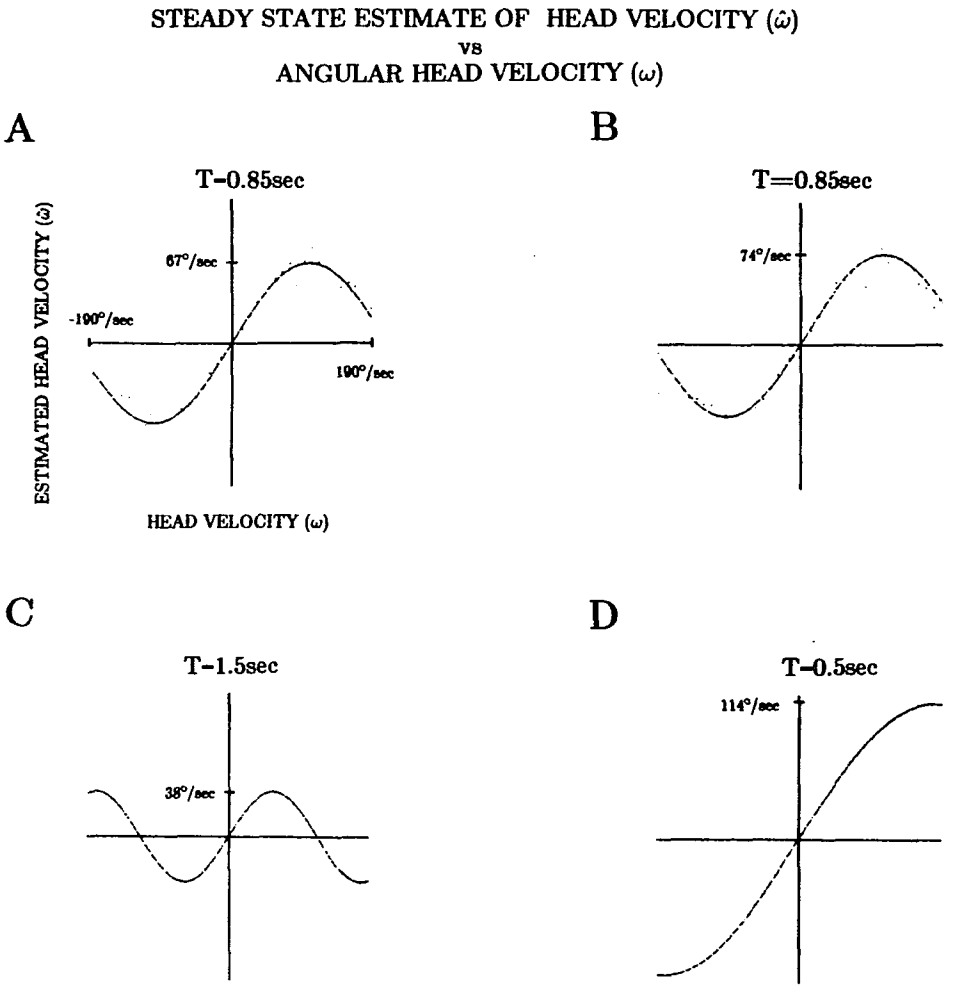
STEADY STATE ESTIMATE OF HEAD VELOCITY ($\hat{\omega}$)
VS
ANGULAR HEAD VELOCITY (ω)
A
T-0.85sec
67°/sec
-190°/sec
190°/sec
ESTIMATED HEAD VELOCITY ($\hat{\omega}$)
HEAD VELOCITY (ω)
B
T=0.85sec
74°/sec
C
T-1.5sec
38°/sec
D
T-0.5sec
114°/sec

Fig. 3.1.8

effect is to shift the curve up and to the right by amounts dependent on the resolution of the position sensing. The range over which the velocity estimator can compute a good estimate of head velocity is diminished as the delay, T, increases (Fig. 3.1.8C). As T decreases, the linear range is enhanced (Fig. 3.1.8D).

Model simulations show how the estimate of head velocity responds to a step in head velocity (Fig. 3.1.9). When the head starts to rotate, the present otolith excitation pattern is the same as the delayed pattern giving an initial estimate of head velocity $\hat{w}=0$. As the head moves, the present pattern shifts but the delayed pattern is unchanged for T seconds. If the head velocity is such that $w<90/T$ deg/sec then the estimate of head velocity increases for the first T seconds and then reaches its steady state value (Fig. 3.1.9B). For a stimulus velocity of $w>90/T$ deg/sec, the estimate of velocity rises to a maximum value and then declines to its steady state value (Fig. 3.1.9C). Fig. 3.1.9D shows the eye velocity response when the estimated velocity of Fig. 3.1.9B is used as an input to the velocity storage integrator. Initially there is a parabolic buildup in eye velocity for T seconds. When the estimated velocity reaches a constant value, the velocity storage integrator charges with its characteristic time constant. When the rotation is stopped, the velocity decays to zero. This behavior is similar to the slow buildup of velocity during OKAN and closely approximates the buildup of the bias component during OVAR (Fig. 3.1.7A). The stored velocity would

Fig. 3.1.9 The dynamic response of the system to a step in head velocity during off-vertical axis rotation.
A. The head velocity versus time curve.
B. The reponse of the pattern velocity estimator due to the input shown in A with a head velocity such that when the system reaches a steady state at time T, the patterns are separated by less than 90 degrees. During rotation, the estimation of velocity rises approximately linearly reaches a steady state and declines linearly when the head is stopped.
C. The reponse of the pattern velocity estimator due to the input shown in A with a head velocity such that the system reaches a steady state velocity when the patterns are separated by more than 90 degrees. For higher velocities of rotation there are transient overshoots in velocity estimation. The velocity storage integrator tends to smooth out these overshoots.
D. The predicted output (state) of the velocity storage integrator when it is driven only by the pattern velocity estimator. The step in head velocity occurs at time zero, but the step down in head velocity occurs at 50 seconds and the velocity remains zero for the next 50 seconds. For the first 0.85 seconds the plot of the integrator state versus time is convex. This is in response to a velocity estimate which is approximately rising at a constant rate (B) due to the constant rate at which the present pattern is separating from the delayed pattern. At the end of the first 0.85 seconds the pattern velocity estimator using the two-sided formula gives an estimate of about 52 deg/sec. After the estimated velocity reaches steady state the integrator charges in response to this constant input. A similar kind of response characteristic is found when the head rotation is stopped. The time constant of the integrator was chosen to be 13.3 seconds.

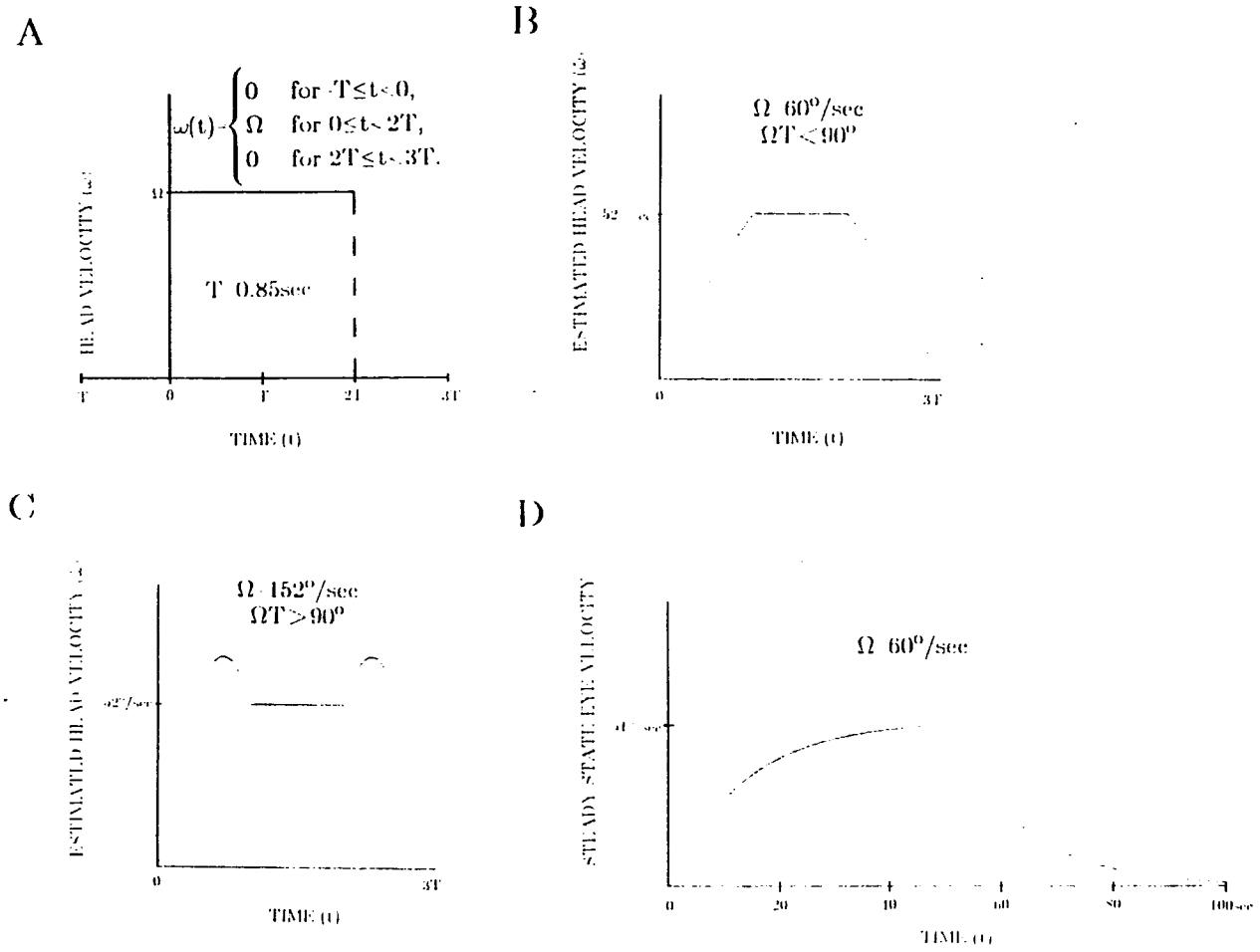
A
$\omega(t) = \begin{cases} 0 & \text{for } -T \le t < 0, \\ \Omega & \text{for } 0 \le t < 2T, \\ 0 & \text{for } 2T \le t < 3T. \end{cases}$
T 0.85sec
TIME (t)
B
Ω 60°/sec
ΩT<90°
TIME (t)
C
Ω 152°/sec
ΩT>90°
TIME (t)
D
Ω 60°/sec
TIME (t)

Fig. 3.1.9

cancel the post-rotatory nystagmus when an animal is stopped during OVAR (Raphan et al. 1981).

The delay in processing, T, used in the estimation of the head velocity was also important in explaining the delay in response characteristics of the buildup in slow phase velocity during OVAR when animals are tilted after having been rotated about a vertical axis at a constant velocity (Fig. 3.1.7A; Raphan et al. 1981). During prolonged rotation about a vertical axis both the present and delayed patterns are at a zero level. When the head is tilted, the present pattern becomes approximately sinusoidally distributed while the delayed pattern remains zero for T seconds. Under these circumstances, the head velocity estimator, defined by Eq (29), gives a zero estimate for T seconds which then steps up to the steady state estimate as when the animal was rotated off axis. This signal charges the velocity storage integrator. When the head is tilted back to the vertical, the present pattern is zero and the estimator outputs a zero velocity estimate. This causes the velocity storage integrator to discharge. The experiment was simulated for a T=0.85 seconds and a head velocity of 60 deg/sec (Fig. 3.1.10). The results agree with the experimental findings (Fig. 3.1.7A).

Fig. 3.1.10 The dynamic response of the velocity storage integrator to a sudden tilt when driven by the estimator. The two-sided formula with a delay time of 0.85 seconds and 30 cell groups was used for this simulation. Initially, the stimulus velocity is 60 deg/sec about the vertical axis. At time zero there is a tilt. At the time just after the tilt, the delayed pattern is zero while the present pattern is sinusoidal. The velocity estimator gives zero as the estimate of the rotational velocity for the first 0.85 seconds and therefore during this period the state (output) of the integrator is, zero. When the delayed pattern becomes sinusoidal, the estimator gives a constant estimate of about 52 deg/sec based on the constant separation between the template pattern and the present pattern. The integrator charges in response to this constant input. At a time equal to 50 seconds there is a tilt back to a vertical position while rotation is maintained. For the first 0.85 seconds after tilting back, the present pattern is zero while the delayed pattern is sinusoidal. For the remainder of the 50 second period both patterns are zero. The estimator in either case gives zero as the estimate of the head velocity and therefore the integrator discharges.

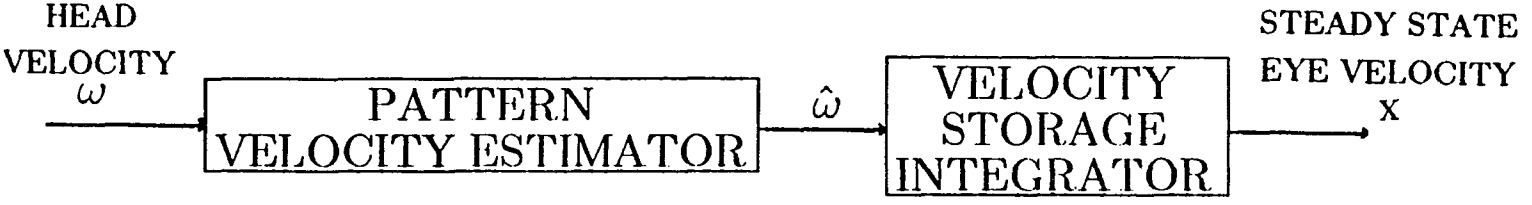
HEAD
VELOCITY
ω
PATTERN
VELOCITY ESTIMATOR
$\hat{\omega}$
VELOCITY
STORAGE
INTEGRATOR
STEADY STATE
EYE VELOCITY
X

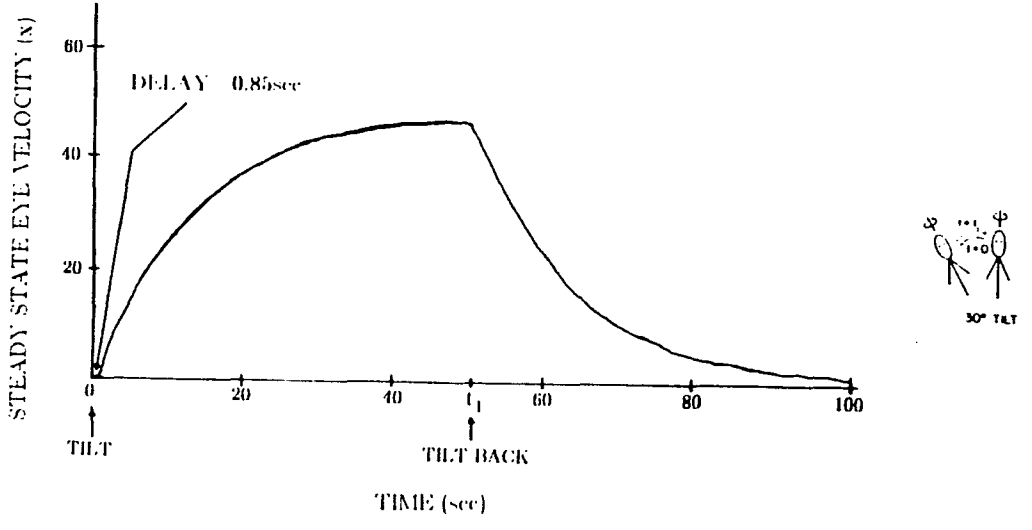
STEADY STATE EYE VELOCITY (x)
60
40
20
DELAY 0.85sec
0
20
40
t_1
60
80
100
TILT
TILT BACK
TIME (sec)
30° TILT

Fig. 3.1.10

3.1.4 Effects on Estimation of Nonuniform Otolith Polarization Angle Spacing

In the development of the model for estimation of head velocity from patterns of otolith activations, it was assumed that the polarization vectors associated with a class of cells were equally spaced over 360 degrees. However, single cell recordings from otolith afferents (Fernandez & Goldberg, 1976a) suggests that polarization vectors are not uniformly spaced. The nonuniformly spaced distribution assumed for the left utricular macula (Fig. 3.1.11) is based on a polar graph by Fernandez & Goldberg (1976a) (Fig. 2.15B). The graph shows some of the left utricular macula's polarization vectors. Each of the polarization vectors lies approximately in a horizontal plane. The distribution has two local maximums directed to either side of the left ear. The number of vectors with a leftward directed component is approximately three times the number of vectors with a rightward directed component. The nonuniformly spaced distribution assumed for the right utricular macula is the mirror image, as seen in a sagittal plane, of the distribution of the left utricular macular.

The model developed in section 3.1.1 will be modified in accordance with the nonuniformly spaced polarization vectors. A left-sided estimate for this model, based on Eq (3.1.24), is given as follows:

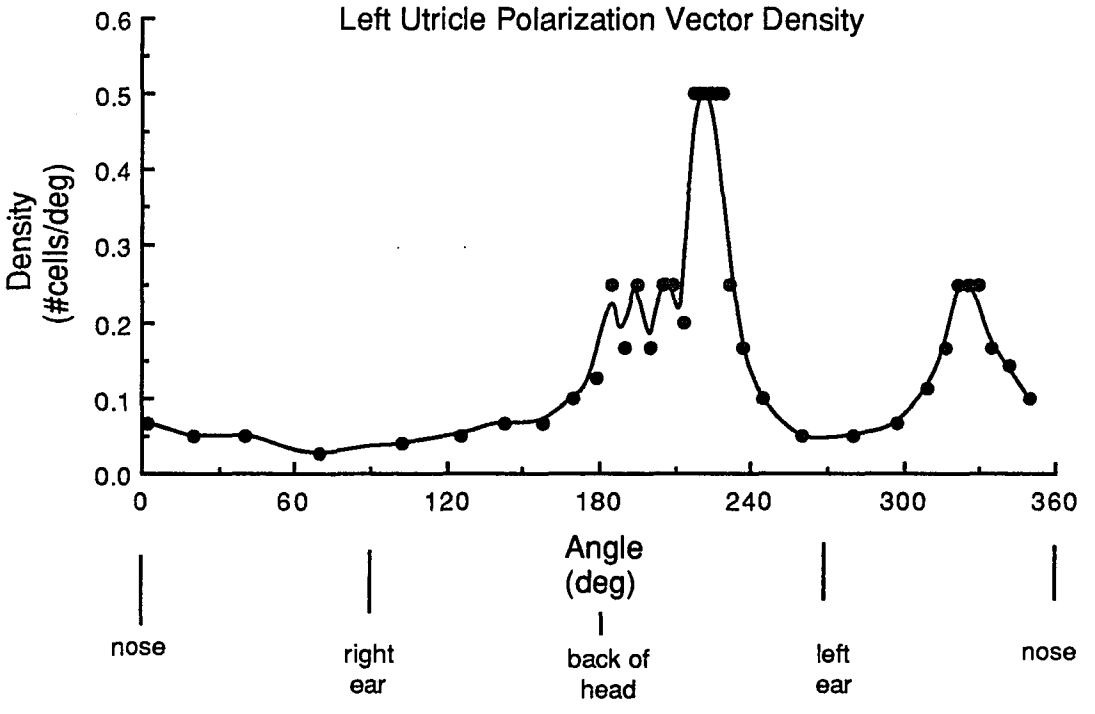

Fig. 3.1.11 Polarization vector distribution based on the graph obtained by Fernandez & Goldberg, 1976a, shown in Fig. 2.14B

$$\hat{w}_l=\left(\sum_{i=0}^{N-1}\{r_{li}(t-T)-r_{li}(t)\}\{[r_{li+1}(t)-r_{li}(t)]/[h_{li+1}-h_{li}]\}\right) \quad (3.1.46)$$

$$\Big/\left(\sum_{i=0}^{N-1}\{[r_{li+1}(t)-r_{li}(t)]/[h_{li+1}-h_{li}]\}^2/T\right).$$

This equation is a generalization of Eq (3.1.34) in which the polarization angle differences are constant and equal to H.

A corresponding right-side estimate, similar to Eq (3.1.46), is given as follows:

$$\hat{w}_r=\left(\sum_{i=0}^{N-1}\{r_{ri}(t-T)-r_{ri}(t)\}\{[r_{ri+1}(t)-r_{ri}(t)]/[h_{ri+1}-h_{ri}]\}\right) \quad (3.1.47)$$

$$\Big/\left(\sum_{i=0}^{N-1}\{[r_{ri+1}(t)-r_{ri}(t)]/[h_{ri+1}-h_{ri}]\}^2/T\right).$$

The two-sided estimate, is obtained by substituting Eqs (3.1.46) and (3.1.47) into Eq (3.1.33).

Using a time delay constant of 0.85 seconds, simulations show that the estimate oscillates as the head rotates (in a barbicue-spit fashion) in a gravitational field (Fig. 3.1.12). The frequency of

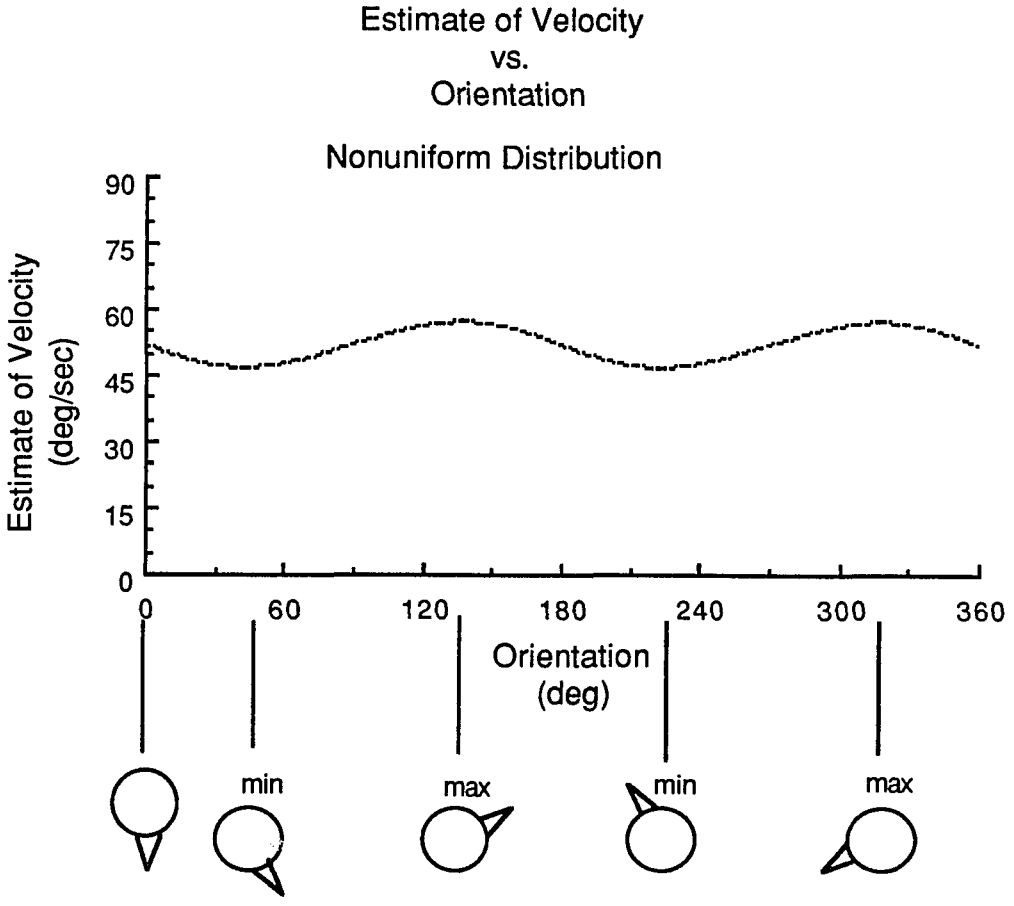

Fig. 3.1.12 Estimate of the head angular velocity: The head angular velocity is 60 degrees/second to the left. The nonuniform distribution of polarization vectors is that shown in Fig. 3.1.11. The estimate oscillates at twice the frequency of the head rotation. The peak-to-peak value of the oscillations is approximately 12 degrees/second. The minimums of the oscillations occur when the head orientation is approximately 45 degrees and again at approximately 225 degrees. The maximums of the oscillations occur when the head orientation is approximately 135 degrees and again at approximately 315 degrees.

oscillation is twice the rotational frequency of the head. In one simulation, as the head rotates at a velocity of 60 degrees/second (to the left) the estimate oscillates between a maximum of about 57 degrees/second and a minimum of about 47 degrees/second. A minimum estimate is obtained when the head orientation, with respect to the acceleration due to gravity, is approximately 45 degrees and at approximately 225 degrees and a maximum estimate is obtained when the head orientation is approximately 135 degrees as well as at approximately 315 degrees.

The average, the maximum, and the minimum estimates, for one head rotation, as a function of the head angular velocity (to the left) is given in Fig. 3.1.13. The average estimate is in agreement with the estimate generated by the ideal estimator developed in section 3.1.2. The difference between the maximum and the minimum estimates as a function of the head angular velocity, increases from zero as the head angular velocity increases from zero. The difference of the extremum reaches a maximum of approximately 45 degrees/second when, the head angular velocity is approximately 160 degrees/second. The extremum difference remains approximately constant as the head velocity continues to increase toward approximately 250 degrees/second. Then, as the head velocity continues to increase, from 250 degrees/second, the extremum difference decreases toward zero.

The zero-state response of the velocity storage integrator driven by the velocity estimator is shown in Fig. 3.1.14. Simulations show

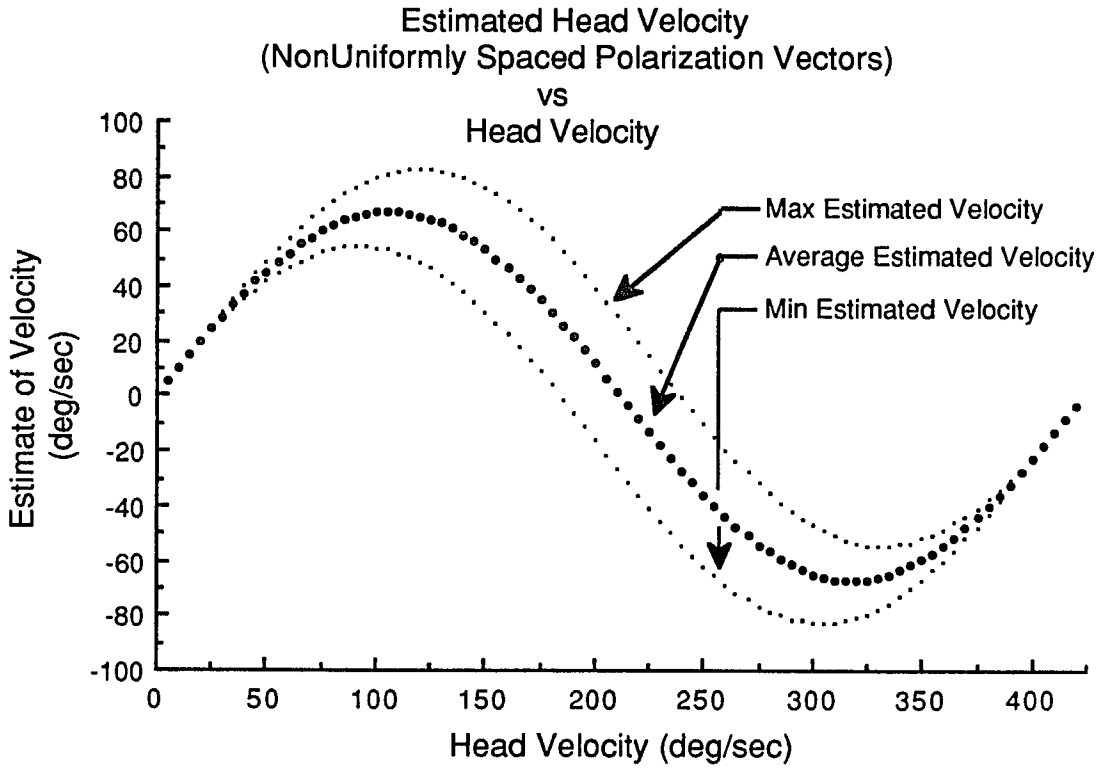

Fig. 3.1.13 The average, the maximum, and the minimum of the estimate for one head rotation of 360 degrees as a function of the head angular velocity: The maximum of the average estimate is approximately 62 degrees/second when the head angular velocity is approximately 100 degrees/second. The difference between the maximum and the minimum as a function of head angular velocity is maximum when the head angular velocity is approximately 160 degrees/second. The extremum difference remains approximately constant for approximately the next 90 degrees/second of increase in head angular velocity.

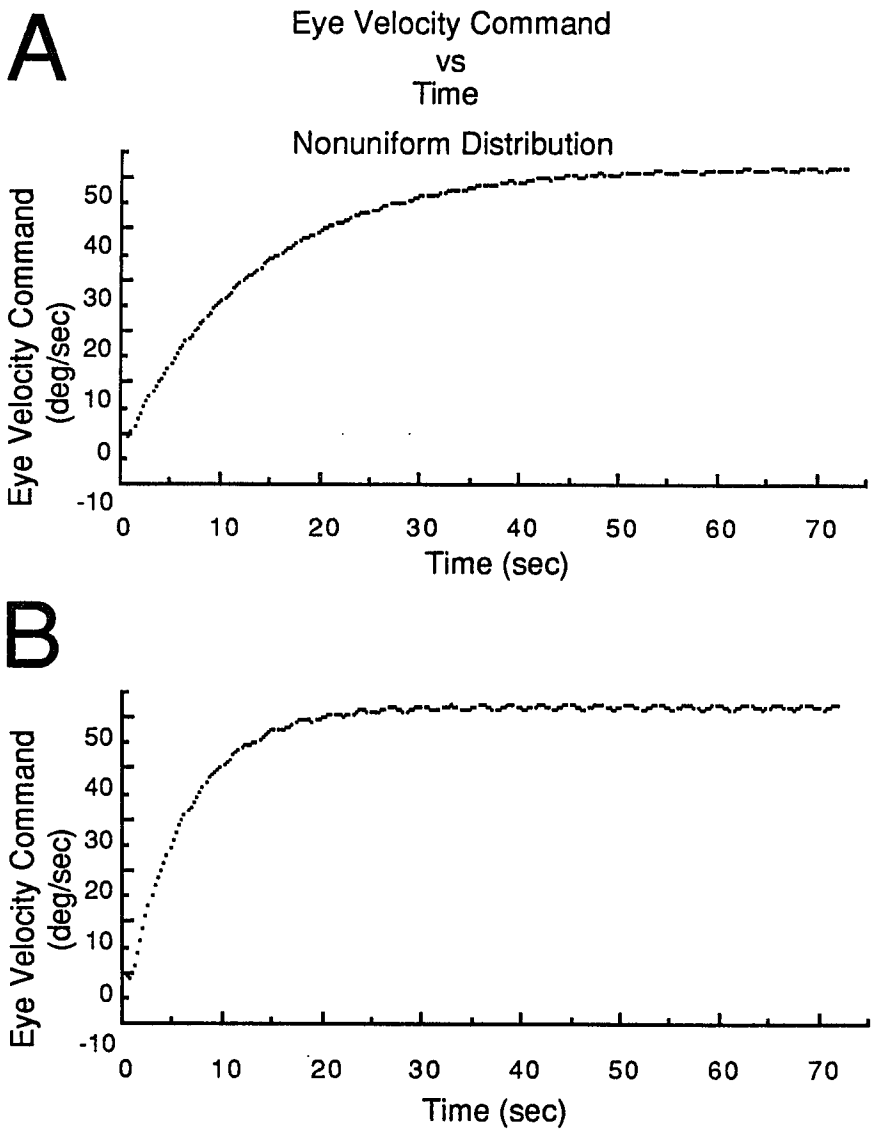

Fig. 3.1.14 The eye velocity command as a function of time: The gain is assumed to equal the reciprocal of the velocity storage integrator time constant. The head angular velocity is 60 degrees/second to the left.
A. The integrator time constant is approximately 13.3 seconds. The initial drop in the eye velocity command is a function of the particular polarization vector distribution. After approximately 50 seconds, the peak-to-peak value of the oscillations is approximately 1 degree/second. The peak-to-peak value of the oscillations output by the estimator is approximately 12 degrees/second. The velocity storage integrator attenuates the variations of the input.
B. The time constant is 6 seconds. After approximately 50 seconds, the peak-to-peak value of the oscillations is approximately 2 degrees/second.

that an oscillating output from the estimator is attenuated by the velocity storage integrator to the point where it is inperceptable. In one simulation, the time constant of the integrator is chosen equal to approximately 13.3 seconds and the gain is chosen equal to the reciprocal of the time constant (Fig. 3.1.14A). The head velocity is 60 degrees/second to the left. As time increases, the zero-state response initially becomes approximately -2 degrees/second and then begins to increase. This behavior is purely a function of the otolith cell distribution and it is not believed to be a major aspect of the model. The response, after approximately fifteen seconds, begins to oscillate as it increases with time. After approximately 50 seconds, the response oscillates with an amplitude much smaller than the amplitude of the oscillating output from the estimator. Further, as time continues to increase the average value of the response is approximately 52 degrees/second.

In another simulation, the time constant of the integrator is chosen to equal to 6 seconds and the gain is again chosen to equal the reciprocal of the time constant (Fig. 3.1.14B). The head velocity is 60 degrees/second to the left. Initially the zero-state response drops to -2 degrees/second within the first second. Then, for approximately the next 20 seconds, the eye velocity command increases more rapidly in Fig. 3.1.14B than in Fig. 3.1.14A. Furthermore, after approximately 50 seconds, the peak-to-peak value of the oscillations of the eye velocity command in Fig. 3.1.14B are greater than in Fig.

3.1.14A. The peak-to-peak value of the oscillations of Fig. 3.1.14B is approximately 2 or 3 degrees/second. The results shown in Fig. 3.1.14 show that the velocity storage integrator plays an important role in damping oscillations due to head velocity estimation and contributes to the robust behavior of the system driving the oculomotor system.

3.1.5 Effects of Nonideal Time Delay on the Estimator

In section 3.1.1, an estimator was developed using an ideal time delay T where T>0 to determine the steady state and dynamic properties of the vestibulo-ocular reflex during OVAR. In this section we will replace this ideal delay by a finite state linear time invariant system to study the effects of a more realistic realization on the estimation characteristics. The ideal delay operator d_T (time domain representation) is defined by the following input output equation (Director & Rohrer, 1972):

$$f(t-T)u(t-T)=d_T(f(t)u(t)). \tag{3.1.48}$$

where u(t) is the unit step function such that

$$u(t)=\begin{cases} 0 \text{ if } t<0 \\ 1 \text{ if } 0\leq t \end{cases} \tag{3.1.49}$$

and f(t) is any input (that has a Laplace transform) defined for t>0.

The ideal delay can be represented in the complex frequency domain by taking the Laplace transform of Eq (3.1.48) giving

$$Y(s)=\exp(-sT)F(s). \tag{3.1.50}$$

From Eq (3.1.50) the system function $D_T(s)$ for an ideal delay operator is identified such that

$$D_T(s)=\exp(-sT). \tag{3.1.51}$$

To obtain a finite state linear time invariant system approximation to $D_T(s)$ we express $\exp(-sT)$, where $T>0$, in the following form:

$$\exp(-sT)=\exp(-sT_2)/\exp(sT_1), \tag{3.1.52}$$

such that

$$T=T_1+T_2. \tag{3.1.53}$$

The parameters, T_1 and T_2 are to be chosen so as to agree with experimental data.

Approximation by a First Order System

In order to obtain a first order system approximating an ideal delay, we expand each exponential in Eq (3.1.52) about s=0 and retain the first two terms obtaining

$$\exp(-sT)\approx(1-sT_2)/(1+sT_1). \tag{3.1.54}$$

Let $H_{T1}(s)$ be equal to the right-hand side of Eq (3.1.54)

$$H_{T1}(s)=(1-sT_2)/(1+sT_1). \tag{3.1.55}$$

In order for the operator $H_{T1}(s)$ to have a finite state system representation T_1 must not be zero. In addition, in order for a finite state system based on $H_{T1}(s)$ to be stable T_1 must be greater than zero. The following equations represent a first order linear time invariant system and are a realization of $H_T(s)$ (Eq (3.1.55)):

$$D_t x(t)=-x(t)/T_1+f(t)/T_1 \tag{3.1.56A}$$

$$y(t)=(T/T_1)x(t)-T_2/T_1 f(t) \tag{3.1.56B}$$

where $f(t)$ is the input, $x(t)$ is the state at time t, $D_t x(t)$ is the derivative of $x(t)$ at time t, T is the time delay, and $y(t)$ is the output. Eqs (3.1.56A) and (3.1.56B) is defined for $t\geq 0$ and $x(0)$ is a given initial state.

The parameters are to be chosen such that the slow phase horizontal component of the eye angular velocity is approximately zero for approximately one second after suddenly tilting the head which had been rotating in the dark about a vertical axis. Furthermore, T_1 and T_2 are to be chosen such that the steady state eye velocity as a function of head angular velocity agrees with the data given in Fig.

3.1.8A which shows a decrease in eye velocity as the head velocity increases toward 200 degrees/second. For an ideal estimator, the estimate becomes negative when the head angular velocity magnitude becomes greater than approximately 212 degrees/second. It is of interest to see if the estimate becomes negative if the ideal delay operator is replaced by a first order or a second order system.

Left-Sided Estimate given a First Order Approximation

The analytic expression for the head velocity estimate, given a nonideal delay, will be developed by substituting Eqs (3.1.56A) and (3.1.56B) into Eq (3.1.30). First let $h_T[.]$ represent the time domain representation of the approximation, $H_T(s)$, as given in Eqs (3.1.56A) and (3.1.56B). Note that $h_T[.]$ can be defined to operate component wise on an N-dimensional vector and is therefore seen to be an approximation to the ideal time delay operator, Delay(T)[.], in Eq (3.1.30) such that

$$\{\text{Delay}(T)[\underline{r}(t)]\}_i \tilde{=} h_T[r_i(t)] \tag{3.1.57}$$

The argument $r_i(t)$, of $h_T(.)$ in Eq (3.1.57), is a sinusoid

$$r_i(t)=A\cos(wt-b)u(t) \tag{3.1.58}$$

where u(t) is the unit step function. The unit step function is used to represent the assumption that the otolith activation pattern is zero before the head is suddenly tilted at time zero. By expanding Eq (3.1.30), using a tilt angle of $\pi/2$, using the approximation given in Eq (3.1.57), the expression for $r_i(t)$ given in Eq (3.1.58), and letting

$$b=iH, \text{ and} \tag{3.1.59}$$

$$A=g \tag{3.1.60}$$

we obtain the following expression for the left-side head angular velocity estimate:

$$\hat{w}_l(t)= \sum_{i=0}^{N-1} \{h_T[g\cos(wt-iH)u(t)]-g\cos(wt-iH)u(t)\} \\ [g\cos(wt-iH-H)u(t)-g\cos(wt-iH)u(t)]/(\pi T g^2). \tag{3.1.61}$$

In Eq (3.1.61), since $h_T[.]$ is linear, g^2 is a common factor of the numerator and of the denominator. Therefore, the estimate can be expressed as

$$\hat{w}_1(t)=\sum_{i=0}^{N-1}\{h_T[\cos(wt-iH)u(t)]-\cos(wt-iH)u(t)\}\,[\cos(wt-iH-H)u(t)-\cos(wt-iH)u(t)]/(\pi T). \tag{3.1.62}$$

The expression for the left-side estimate in Eq (3.1.62) can be expressed as the sum of two terms

$$\hat{w}_1(t)=Q_1(t)+Q_2(t), \tag{3.1.63}$$

where

$$Q_1(t)=\sum_{i=0}^{N-1}h_T[\cos(wt-iH)u(t)]\,[\cos(wt-iH-H)u(t)-\cos(wt-iH)u(t)]/(\pi T) \tag{3.1.64}$$

and

$$Q_2(t)=\sum_{i=0}^{N-1}-\cos(wt-iH)u(t)\,[\cos(wt-iH-H)u(t)-\cos(wt-iH)u(t)]/(\pi T). \tag{3.1.65}$$

The response of the first order approximation (Eqs (3.1.56A) and (3.1.56B)) of an ideal delay to the sinusoid in Eq (3.1.58) (see Eqs (3.1.59) and (3.1.60)) is given by (Javid & Brenner, 1963)

$$h_T[r_i(t)]=(1+T_2/T_1)/[1+(wT_1)^2] \qquad (3.1.66)$$
$$\{\ [-\cos(iH)+wT_1\sin(iH)]\exp(-t/T_1)+\cos(wt-iH)+wT_1\sin(wt-iH)\ \}$$
$$-(T_2/T_1)A\cos(wt-iH).$$

First we will find a simplified expression for Q_1. Substituting Eq (3.1.66) into Eq (3.1.64), for t greater than zero, we obtain

$$Q_1(t)=\sum_{i=0}^{N-1}[(1+T_2/T_1)/[1+(wT_1)^2] \qquad (3.1.67)$$
$$\{\ [-\cos(iH)+wT_1\sin(iH)]\exp(-t/T_1)$$
$$+\cos(wt-iH)+wT_1\sin(wt-iH)\ \}-(T_2/T_1)\cos(wt-iH)]$$
$$[\cos(wt-iH-H)-\cos(wt-iH)]/(\dagger\dagger T).$$

By using the even property of the cosine function and the odd property of the sine function we can rearrange each argument of the sine and cosine functions in Eq (3.1.67) such that iH appears with a positive sign, obtaining

$$Q_1(t)=\sum_{i=0}^{N-1}[(1+T_2/T_1)/[1+(wT_1)^2] \qquad (3.1.68)$$
$$\{\ [-\cos(iH)+wT_1\sin(iH)]\exp(-t/T_1)$$
$$+\cos(iH-wt)-wT_1\sin(iH-wt)\ \}-(T_2/T_1)\cos(iH-wt)]$$
$$[\cos(iH-wt+H)-\cos(iH-wt)]/(\dagger\dagger T).$$

By expanding the product in Eq (3.1.68) we obtain

$$
\begin{aligned}
Q_1(t) = \sum_{i=0}^{N-1} \Big\{ & (1+T_2/T_1)/[1+(wT_1)^2] \\
& \Big(\{ -\cos(iH)\cos[iH-(wt-H)] + wT_1 \sin(iH)\cos[iH-(wt-H)] \\
& \quad + \cos(iH)\cos(iH-wt) - wT_1 \sin(iH)\cos(iH-wt) \} \exp(-t/T_1) \\
& \quad + \cos(iH-wt)\cos[(iH-wt)+H] - wT_1 \sin(iH-wt)\cos[(iH-wt)+H] \\
& \quad - \cos(iH-wt)\cos(iH-wt) + wT_1 \sin(iH-wt)\cos(iH-wt) \Big) \\
& - (T_2/T_1)[\cos(iH-wt)\cos[(iH-wt)+H] - \cos(iH-wt)\cos(iH-wt)] \\
& \Big\} / (TTT).
\end{aligned}
\tag{3.1.69}
$$

By using the trigonometric identity given in Eq (B2) in Eq (3.1.69) we obtain

$$
\begin{aligned}
Q_1(t) = \sum_{i=0}^{N-1} \{ & (1+T_2/T_1)/[1+(wT_1)^2] \\
& (\{ \quad -\cos(iH)[\cos(iH)\cos(wt-H)+\sin(iH)\sin(wt-H)] \\
& \quad +wT_1\sin(iH)[\cos(iH)\cos(wt-H)+\sin(iH)\sin(wt-H)] \\
& \quad +\cos(iH)[\cos(iH)\cos(wt)+\sin(iH)\sin(wt)] \\
& \quad -wT_1\sin(iH)[\cos(iH)\cos(wt)+\sin(iH)\sin(wt)] \\
& \quad \}\exp(-t/T_1) \\
& \quad +\cos(iH-wt)[\cos(iH-wt)\cos(H)-\sin(iH-wt)\sin(H)] \\
& \quad -wT_1\sin(iH-wt)[\cos(iH-wt)\cos(H)-\sin(iH-wt)\sin(H)] \\
& \quad -\cos(iH-wt)\cos(iH-wt)+wT_1\sin(iH-wt)\cos(iH-wt) \\
& \quad) \\
& -(T_2/T_1)[\cos(iH-wt)[\cos(iH-wt)\cos(H)-\sin(iH-wt)\sin(H)] \\
& \qquad -\cos(iH-wt)\cos(iH-wt)] \\
& \}/(\tau\tau T).
\end{aligned}
\tag{3.1.70}
$$

By using Eqs (B9), (B10), and (B11) in Eq (3.1.70) we obtain

$$
\begin{aligned}
Q_1(t) = (& (1+T_2/T_1)/[1+(wT_1)^2] \\
& \{ [-\cos(wt-H)+wT_1\sin(wt-H)+\cos(wt)-wT_1\sin(wt)]\exp(-t/T_1) \\
& \quad +\cos(H)+wT_1\sin(H)-1 \} \\
& -(T_2/T_1)[\cos(H)-1])N/(2\tau\tau T).
\end{aligned}
\tag{3.1.71}
$$

To simplify Eq (3.1.71) let

$$C=\cos(wt)-\cos(wt-H), \tag{3.1.72}$$

$$S=\sin(wt-H)-\sin(wt), \tag{3.1.73}$$

$$D=\cos(H)-1, \text{ and} \tag{3.1.74}$$

$$E=\sin(H). \tag{3.1.75}$$

Substituting Eqs (3.1.72), (3.1.73), (3.1.74), and (3.1.75) into Eq (3.1.71) we obtain

$$Q_1(t)=\{ (1+T_2/T_1)/[1+(wT_1)^2][(C+wT_1S)\exp(-t/T_1)+D+wT_1E] - (T_2/T_1)D \}N/(2\dagger\dagger T). \tag{3.1.76}$$

By using the trigonometric identities Eqs (B1), (B2), (B4) and (B6) in Eqs (3.1.72), (3.1.73), (3.1.74), and (3.1.75) we obtain

$$C=-2\sin(H/2)\sin(wt-H/2), \tag{3.1.77}$$

$$S=-2\sin(H/2)\cos(wt-H/2), \tag{3.1.78}$$

$$D=-2\sin^2(H/2), \text{ and} \tag{3.1.79}$$

$$E=2\sin(H/2)\cos(H/2). \tag{3.1.80}$$

Substituting Eqs (3.1.77), (3.1.78), (3.1.79), and (3.1.80) into Eq (3.1.76) we obtain

$$Q_1(t)=\{\ (1+T_2/T_1)/[1+(wT_1)^2] \qquad (3.1.81)$$
$$[\ (-2\sin(H/2)\sin(wt-H/2)-wT_1 2\sin(H/2)\cos(wt-H/2))\exp(-t/T_1)$$
$$-2\sin^2(H/2)+wT_1 2\sin(H/2)\cos(H/2)]$$
$$+(T_2/T_1)2\sin^2(H/2)\ \}N/(2\uparrow\uparrow T).$$

In Eq (3.1.81) by factoring out 2sin(H/2) we obtain

$$Q_1(t)=\{\ (1+T_2/T_1)/[1+(wT_1)^2] \qquad (3.1.82)$$
$$[\ (-\sin(wt-H/2)-wT_1\cos(wt-H/2))\exp(-t/T_1)$$
$$-\sin(H/2)+wT_1\cos(H/2)]$$
$$+(T_2/T_1)\sin(H/2)\ \}N\sin(H/2)/(\uparrow\uparrow T).$$

Next we will find a simplified expression for Q_2 given in Eq (3.1.65). By setting the time t to be geater than zero in Eq (3.1.65) we obtain

$$Q_2(t)=\sum_{i=0}^{N-1} -\cos(wt-iH)[\cos(wt-iH-H)-\cos(wt-iH)]/(\uparrow\uparrow T). \qquad (3.1.83)$$

By using the even property of the cosine function and the odd property of the sine function we can rearrange each argument of the sine and

cosine functions in Eq (3.1.83) such that iH appears with a positive sign, obtaining

$$Q_2(t)= \sum_{i=0}^{N-1} -\cos(iH-wt)\{\cos[(iH-wt)+H]-\cos(iH-wt)\}/(\pi\pi T). \qquad (3.1.84)$$

By expanding the product in Eq (3.1.84) we obtain

$$Q_2(t)= \sum_{i=0}^{N-1} \{-\cos(iH-wt)\cos[(iH-wt)+H]+\cos(iH-wt)\cos(iH-wt)\} /(\pi\pi T). \qquad (3.1.85)$$

By using the trigonometric identity given in Eq (B2) in Eq (3.1.85) we obtain

$$Q_2(t)= \sum_{i=0}^{N-1} \{ -\cos(iH-wt)[\cos(iH-wt)\cos(H)-\sin(iH-wt)\sin(H)] +\cos(iH-wt)\cos(iH-wt) \}/(\pi\pi T). \qquad (3.1.86)$$

By using Eqs (B9), (B10), and (B11) in Eq (3.1.86) we obtain

$$Q_2=N[1-\cos(H)]/(2\pi\pi T). \qquad (3.1.87)$$

By using Eqs (3.1.74) and (3.1.79) in Eq (3.1.87) we obtain

$$Q_2=N\sin^2(H/2)/(\dagger\dagger T). \tag{3.1.88}$$

Substituting Eqs (3.1.82) and (3.1.88) into Eq (3.1.63) we obtain

$$\begin{aligned}\hat{w}_1(t)=\{\ & (1+T_2/T_1)/[1+(wT_1)^2] \\ & [\ (-\sin(wt-H/2)-wT_1\cos(wt-H/2))\exp(-t/T_1) \\ & \ -\sin(H/2)+wT_1\cos(H/2)] \\ & +(T_2/T_1)\sin(H/2)\ \}N\sin(H/2)/(\dagger\dagger T)+N\sin^2(H/2)/(\dagger\dagger T).\end{aligned} \tag{3.1.89}$$

By factoring out the term $N\sin(H/2)/(\dagger\dagger T)$ in Eq (3.1.89) we obtain

$$\begin{aligned}\hat{w}_1(t)=\{\ & (1+T_2/T_1)/[1+(wT_1)^2] \\ & [\ (-\sin(wt-H/2)-wT_1\cos(wt-H/2))\exp(-t/T_1) \\ & \ -\sin(H/2)+wT_1\cos(H/2)] \\ & +(1+T_2/T_1)\sin(H/2)\ \}N\sin(H/2)/(\dagger\dagger T).\end{aligned} \tag{3.1.90}$$

By factoring out the expression $(1+T_2/T_1)$ in Eq (3.1.90) we obtain the left-sided estimate of the head angular velocity given a first order approximation to an ideal delay

$$\hat{w}_1(t)=\{\ 1/[1+(wT_1)^2]\{\ [-\sin(wt-H/2)-wT_1\cos(wt-H/2)]\exp(-t/T_1) \qquad (3.1.91)$$
$$-\sin(H/2)+wT_1\cos(H/2)\ \}$$
$$+\sin(H/2)\ \}N\sin(H/2)(1+T_2/T_1)/(\dagger\dagger T).$$

Two-Sided Estimate given a First Order Approximation

From Eq (3.1.91) with H replaced by -H we obtain the right-sided estimate

$$\hat{w}_r(t)=-\{\ 1/[1+(wT_1)^2]\{ \qquad (3.1.92)$$
$$[-\sin(wt+H/2)-wT_1\cos(wt+H/2)]\exp(-t/T_1)$$
$$+\sin(H/2)+wT_1\cos(H/2)\ \}$$
$$-\sin(H/2)\ \}N\sin(H/2)(T/T_1)/(\dagger\dagger T).$$

Substituting Eqs (3.1.91) and (3.1.92) into Eq (3.1.33) we obtain

$$\hat{w}(t)=N\sin(H/2)(1+T_2/T_1)/\{(2\dagger\dagger T)[1+(wT_1)^2]\} \qquad (3.1.93)$$
$$\{\ [-\sin(wt-H/2)-\sin(wt+H/2)$$
$$-wT_1\cos(wt-H/2)-wT_1\cos(wt+H/2)]\exp(-t/T_1)$$
$$+2wT_1\cos(H/2)\ \}.$$

Let

$$C=\cos(wt+H/2)+\cos(wt-H/2), \text{ and} \qquad (3.1.94)$$

$$S=\sin(wt+H/2)+\sin(wt-H/2). \tag{3.1.95}$$

Substituting Eqs (3.1.94) and (3.1.95) into Eq (3.1.93) we obtain

$$\hat{w}(t)=N\sin(H/2)(1+T_2/T_1)/\{(2\pi T)[1+(wT_1)^2]\} \tag{3.1.96}$$
$$\{\,[-S-wT_1C]\exp(-t/T_1)+2wT_1\cos(H/2)\,\}.$$

By using the trigonometric identities of Eqs (B1) and (B2) in Eqs (3.1.94) and (3.1.95) we obtain

$$C=2\cos(wt)\cos(H/2), \text{ and} \tag{3.1.97}$$

$$S=2\sin(wt)\cos(H/2). \tag{3.1.98}$$

By substituting Eqs (3.1.97) and (3.1.98) into Eq (3.1.96) we obtain

$$\hat{w}(t)=N\sin(H/2)(1+T_2/T_1)/\{(2\pi T)[1+(wT_1)^2]\} \tag{3.1.99}$$
$$\{\,[-2\sin(wt)\cos(H/2)-2wT_1\cos(wt)\cos(H/2)]\exp(-t/T_1)$$
$$+2wT_1\cos(H/2)\,\}.$$

By factoring out $2\cos(H/2)$ from Eq (3.1.99) we obtain

$$\hat{w}(t)=N\sin(H/2)\cos(H/2)(1+T_2/T_1)/\{(\pi T)[1+(wT_1)^2]\} \tag{3.1.100}$$
$$\{\,[-\sin(wt)-wT_1\cos(wt)]\exp(-t/T_1)+wT_1\,\}.$$

In Eq (3.1.100) by using $NH=2\pi$ we obtain

$$\hat{w}(t)=w[\sin(H/2)/(H/2)]\cos(H/2)(1+T_2/T_1)/\{wT[1+(wT_1)^2]\} \quad (3.1.101)$$
$$\{\ [-\sin(wt)-wT_1\cos(wt)]\exp(-t/T_1)+wT_1\ \}.$$

Let,

$$C(H)=[\sin(H/2)/(H/2)]\cos(H/2). \quad (3.1.102)$$

By using trigonometric identity Eq (B5) with both A and B set equal to H/2 we obtain

$$C(H)=\sin(H)/H. \quad (3.1.103)$$

By substituting Eq (3.1.102) into Eq (3.1.101) we obtain

$$\hat{w}(t)=wC(H)(1+T_2/T_1)/\{wT[1+(wT_1)^2]\} \quad (3.1.104)$$
$$\{\ [-\sin(wt)-wT_1\cos(wt)]\exp(-t/T_1)+wT_1\ \}.$$

The factor, C(H), can be dropped from Eq (3.1.104). If H is small then, from Eq (3.1.103), C(H) is approximately one. If H is not small then divide Eq (3.1.104) by the constant C(H). We therefore obtain

$$\hat{w}(t)=w(1+T_2/T_1)/\{wT[1+(wT_1)^2]\} \qquad (3.1.105)$$
$$\{\ [-\sin(wt)-wT_1\cos(wt)]\exp(-t/T_1)+wT_1\ \}.$$

By using Eq (3.1.53) in Eq (3.1.105) we obtain

$$\hat{w}(t)=w/\{wT_1[1+(wT_1)^2]\} \qquad (3.1.106)$$
$$\{\ [-\sin(wt)-wT_1\cos(wt)]\exp(-t/T_1)+wT_1\ \},$$

The output of the estimator given in Eq (3.1.106) with T_1 equal to T which in turn is set equal to 0.85 seconds, as a function of time, is shown in Fig. 3.1.15. The head is suddenly tilted at time zero and the head angular velocity is 60 degrees/second to the left. The estimate rises from zero to a maximum value of approximately 35 degrees/second which occurs at approximately 2.3 seconds. After approximately 5 seconds the estimate is approximately 33 degrees/second.

Estimate for Small Time t given a First Order Approximation

To examine this estimate, which was derived using a first order approximation to an ideal delay, we will first consider the form of Eq (3.1.106) for small t. By finding the Taylor expansion of Eq (3.1.106) and retaining terms up to the second degree in time t (see Eqs (B12), (B13), and (B14)) we obtain

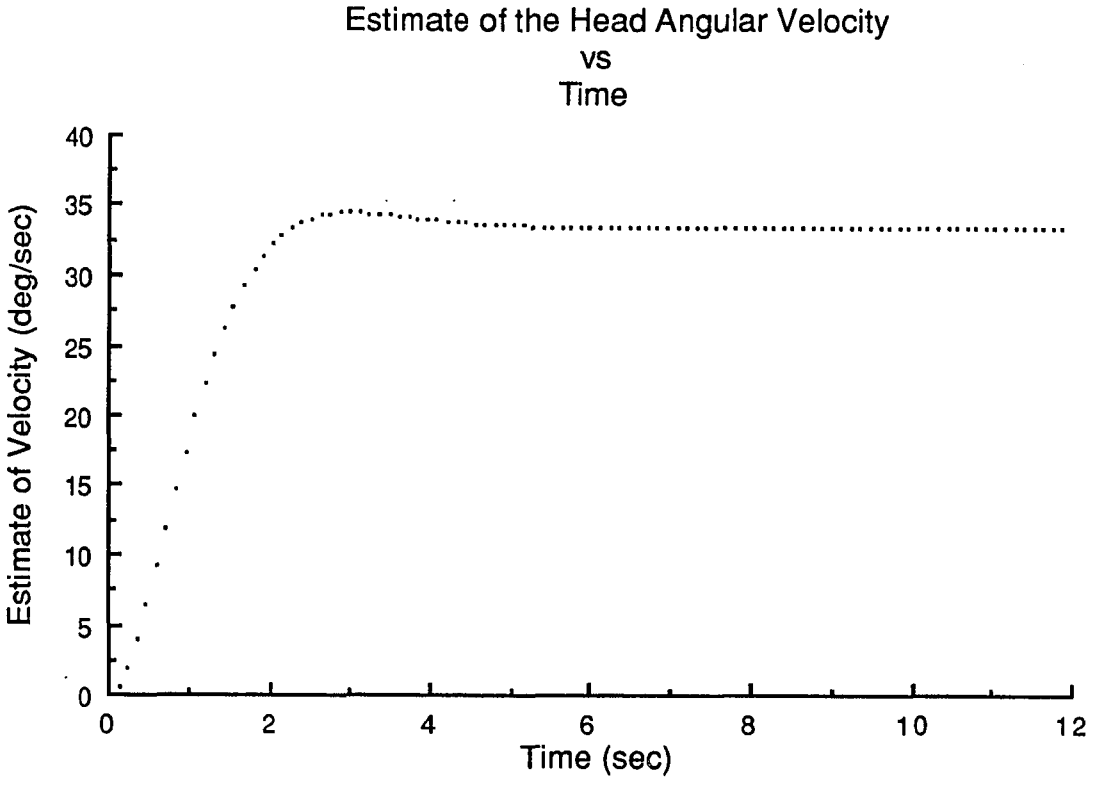

Fig. 3.1.15 Estimate of the head angular velocity: The head angular velocity is 60 degrees/second to the left. The first order system time constant, T_1, is equal to 0.85 seconds and the other time constant, T_2, is equal to 0.0. The head is suddenly tilted at time 0.0. The estimate rises to a maximum of approximately 35 degrees/second after approximately 2.3 seconds and then, after approximately 5 seconds, falls to an constant value of approximately 33 degrees/second.

$$\hat{w}(t)\simeq w/\{wT_1[1+(wT_1)^2]\} \qquad (3.1.107)$$
$$\{\ -wT_1 t/T_1+wT_1(t/T_1)^2-wT_1\{1-t/T_1+[1-(wT_1)^2](t/T_1)^2/2\}+wT_1\ \}.$$

By combining terms of equal degree in t we obtain

$$\hat{w}(t)\simeq w(t/T_1)^2/2, \qquad (3.1.108)$$

Therefore, the estimate in Eq (3.1.106) initially increases quadratically with time as shown in Eq (3.1.108). The coefficient of the t^2 term in Eq (3.1.108) is $(w/T_1^{\ 2})/2$. The larger T_1 is, the more slowly the estimate intially increases. If T_1 is equal to T, T_1's maximum value, in Eq (3.1.108) we obtain

$$\hat{w}(t)\simeq w/(2T^2)t^2. \qquad (3.1.109)$$

Therefore if the estimate given in Eq (3.1.106) is input to the velocity storage integrator, the output of the velocity storage integrator will initially increase cubically with time t. The estimate derived from an ideal delay operator, given in section 3.1.1, is zero for the first T seconds and the output of the integrator is also zero for the first T seconds.

The output of the velocity storage integrator, assuming that its initial state is zero, as a function of time, is shown in Fig. 3.1.16. The input of the integrator is assumed to be the output of the

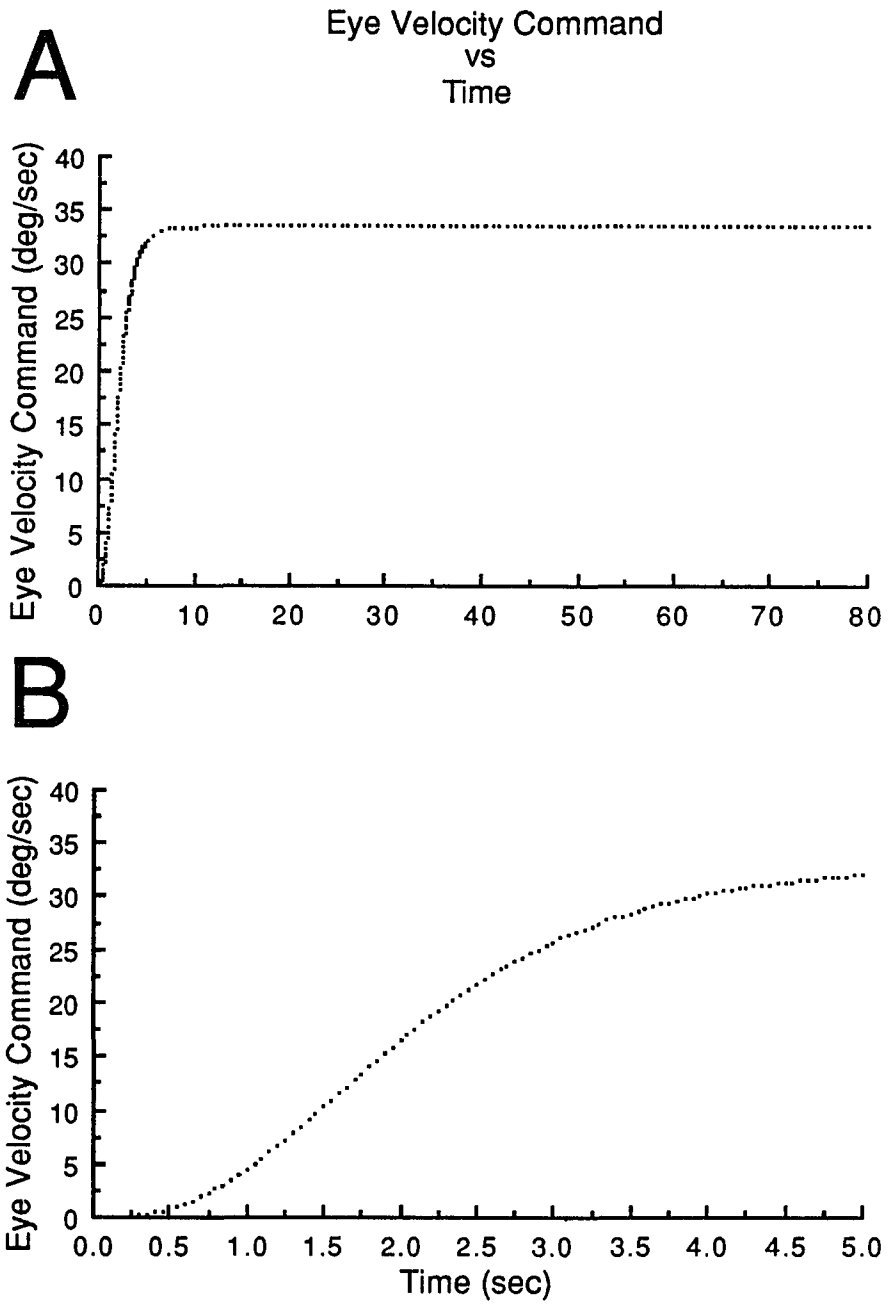

Fig. 3.1.16 The eye velocity command as a function of time: The velocity storage integrator time constant is approximately 13.3 seconds. The head angular velocity is 60 degrees/second to the left.
A. The eye velocity command rises to 33 degrees/second at approximately 8 seconds..
B. The first 5 seconds of the results shown in A. The eye velocity command is 4 degrees/second after approximately 1 second.

estimator given in Eq (3.1.106) with T_1 equal to T which in turn is set equal to 0.85 seconds. The head is suddenly tilted at time zero and the head angular velocity is 60 degrees/second to the left. The eye velocity command reaches a maximum of approximately 33 degrees/second at 8 seconds (Fig. 3.1.16A). From then on the eye velocity command is approximately constant. The first five seconds of the eye velocity command of Fig. 3.1.16A are shown in Fig. 3.1.16B. Initially the eye velocity command is zero and is increasing slowly (Fig. 3.1.16B). At approximately one second the eye velocity command is 4 degrees/second.

Steady State Estimate given a First Order Approximation

Next consider the form of the estimate for large t. Therefore, from Eq (3.1.106) we obtain the steady state solution

$$\hat{w}_s = w/[1+(wT_1)^2] \qquad (3.1.110)$$

First we will examine Eq (3.1.110) for small w. From Eq (3.1.110), for sufficiently small head angular velocity w we obtain

$$\hat{w}_s \tilde{} w. \qquad (3.1.111)$$

Therefore, as w increases from zero the estimate in Eq (3.1.110) will

initially equal w, the head angular velocity. This is the same behavior exhibited by the data shown in Fig. 3.1.8A. As w continues to increase, the estimate, based on the approximation to an ideal delay, will increase, reaching a maximum of $1/(2T_1)$ at which point the head angular velocity equals $1/T_1$. If T_1 is equal to T/2, then the maximum, based on the approximation, is equal to the maximum obtained by the ideal estimate. If T_1 is equal to $2T/\pi$, then the maximum, based on the approximation, occurs at the same head velocity as the ideal estimate's maximum. This behavior distinguishes between the ideal estimate and the esimate given in Eq (3.1.106).

From the data shown in Fig. 3.1.8A a maximum of approximately 67 degrees/second occurs at a head angular velocity magnitude of approximately 105 degrees/second. Therefore, using a maximum estimate of 67 degrees/second fixes T_1 at approximately 0.43 seconds and therefore, the maximum estimate location occurs at a head angular velocity magnitude of approximately 133 degrees/second. Using a maximum estimate location of 105 degrees/second fixes T_1 at approximately 0.55 seconds and therefore, the maximum estimate is approximately 52 degrees/second. Furthermore, from Fig. 3.1.16 the value of T_1 should be increased from 0.85 seconds and not decreased so that the estimate is approximately zero for the first second. This suggests that there is no value of T_1 such that the steady state estimate given in Eq (3.1.110) can be made to agree with the data given in Fig. 3.1.8A and the restriction that the eye velocity command

be approximately zero during approximately the first second after the sudden tilt.

For larger w, the estimate based on the approximation to an ideal delay will begin to decrease as w continues to increase. As w increases the estimate will approach $1/(wT_1)(1/T_1)$ as it decays toward zero. Note that the estimate never goes negative. The ideal estimate, as w increases will oscillate indefinitely about zero at a constant amplitude of $1/T$ with a period of $2\pi/T$.

The steady state estimate given in Eq (3.1.110), with T_1 equal to 0.85 seconds, as a function of the head angular velocity magnitude is shown in Fig. 3.1.17. The maximum value of the estimate is approximately 34 degrees/second which occurs at a head angular velocity magnitude of approximately 70 degrees/second. The estimate then decreases toward zero (Eq (3.1.110)) as the head angular velocity magnitude increases.

In summary, for a small head angular velocity, the estimate, based on the first order approximation to an ideal delay, is approximately equal to the head velocity. The estimate will initially increase as w increases reaching a maximum. The location of the maximum or the maximum itself does not agree with the data shown in Fig. 3.1.8A. Furthermore, to try and fit the maximum estimate or the maximum location requires that T_1 be less than 0.85 seconds by a significant fraction. Therefore, the eye velocity command during the first second after the sudden tilt would be greater than that shown in

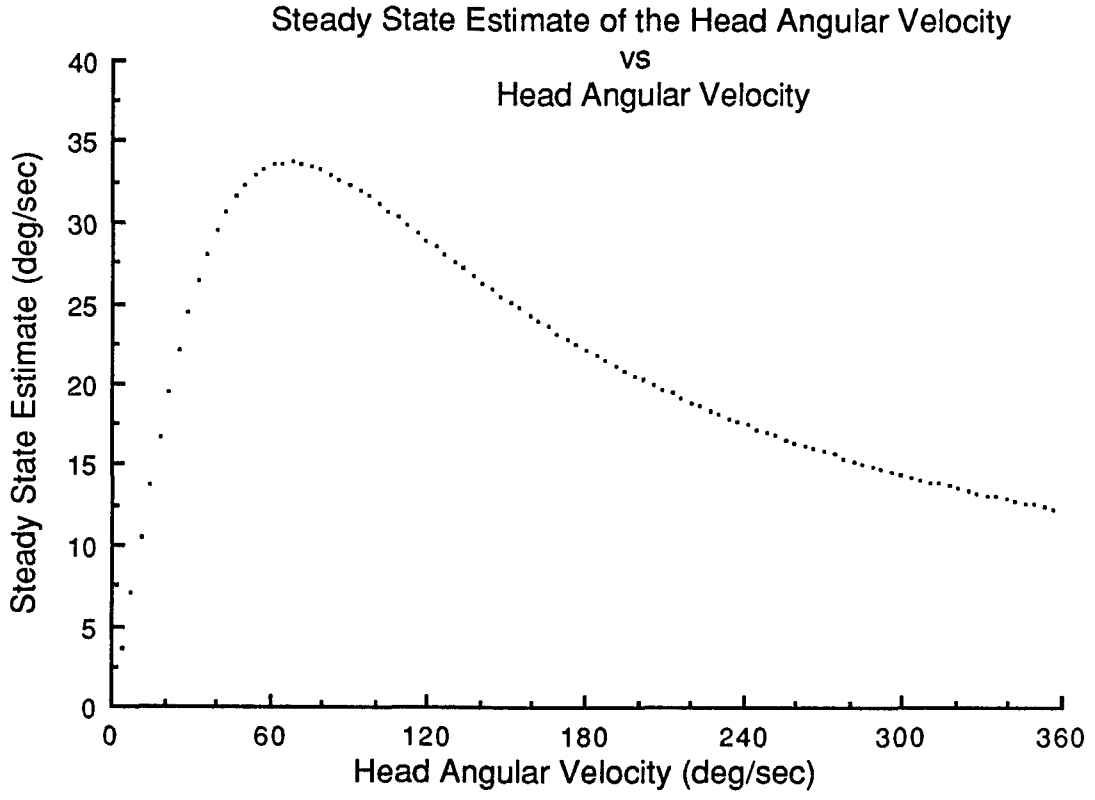

Fig. 3.1.17 The steady state estimate as a function of head angular velocity. The first order system time constant, T_1, is 0.85 seconds and the other time constant, T_2, is equal to 0.0. A maximum estimate of approximately 34 degrees/second which occurs at a head angular velocity of approximately 70 degrees/second.

Fig. 3.1.16. As w continues to increase, beyond the location of the maximum estimate, the estimate will decay toward zero, never turning negative. Therefore, a first order approximation to a delay cannot model the estimation process accurately.

Approximation by a Second Order System

Next we will investigate the effects of approximating the ideal delay operator by a second order linear time invariant system. In Eq (3.1.52) we expand each exponential about s=0 and retain terms up to the second degree in s. Therefore, we obtain

$$\exp(-sT)\simeq[1-sT_2+(sT_2)^2/2]/[1+sT_1+(sT_1)^2/2]. \qquad (3.1.112)$$

The expression given in Eq (3.1.112) is a "frequency" domain approximation to the ideal delay operator which we shall refer to as $H_{T1}(s)$ such that

$$H_{T1}(s)=[1-sT_2+(sT_2)^2/2]/[1+sT_1+(sT_1)^2/2] \qquad (3.1.113)$$

The following state variable representation of a second order linear time invariant system is a realization of $HT_1(s)$:

$$D_t x_1=x_2 \qquad (3.1.114A)$$

$$D_t x_2(t)=-(2/T_1^2)x_1(t)-(2/T_1)x_2(t)+(2/T_1^2)f(t) \qquad (3.1.114B)$$

$$y(t)=[1-(T_2/T_1)^2]x_1(t)-T_2(1+T_2/T_1)x_2(t)+(T_2/T_1)^2 f(t) \qquad (3.1.114C)$$

where at any time t greater than or equal to zero: f(t) is the input, $(x_1(t),x_2(t))$ is the state, $D_t x_1(t)$ and $D_t x_2(t)$ are the derivatives of $x_1(t)$ and x2(t) respectively, T is the time delay constant (see Eq (3.1.53), and y(t) is the output. In Eqs (3.1.114A), (3.1.114B) and (3.1.114C), $(x_1(0),x_2(0))$ is a given initial state.

Left-Sided Estimate given a Second Order Approximation

Next we will examine the output from the estimator assuming that the ideal delay operator is replaced by the linear second order time invariant system, $hT_1[.]$, given in Eqs (3.1.114A), (3.1.114B), and (3.1.114C). The starting point we shall use to calculate the left-sided estimate is Eq (3.1.30). Let $h_T[.]$ represent the time domain representation of the approximation, $H_T(s)$, as given in Eqs (3.1.114A), (3.1.114B), and (3.1.114C). Note that $h_T[.]$ can be defined to operate componentwise on an N-dimensional vector and is therefore seen to be an approximation to the ideal time delay operator, Delay(T)[.] given in Eq (3.1.13), such that

$$\{\text{Delay}(T)[\underline{r}(t)]\}_i \tilde{} h_T[r_i(t)] \qquad (3.1.115)$$

The argument $r_i(t)$, of $h_T[.]$ in Eq (3.1.115), is a sinusoid and is given in Eq (3.1.58). By expanding Eq (3.1.30), using a tilt angle of $\uparrow\uparrow/2$, using the approximation given in Eq (3.1.115), the expression

for $r_i(t)$ given in Eq (3.1.58) and using Eqs (3.1.59) and (3.1.60), we obtain the following expression for the left-sided head angular velocity estimate:

$$\hat{w}_l(t) = \sum_{i=0}^{N-1} \{h_T[g\cos(wt-iH)u(t)]-g\cos(wt-iH)u(t)\} \quad (3.1.116)$$
$$[g\cos(wt-iH-H)u(t)-g\cos(wt-iH)u(t)]/(\tau\tau Tg^2).$$

Since $h_T[.]$ is linear, g^2 is a common factor of the numerator and of the denominator. Therefore, the estimate can be expressed as

$$\hat{w}_l(t) = \sum_{i=0}^{N-1} \{h_T[\cos(wt-iH)u(t)]-\cos(wt-iH)u(t)\} \quad (3.1.117)$$
$$[\cos(wt-iH-H)u(t)-\cos(wt-iH)u(t)]/(\tau\tau T).$$

The expression for the left-sided estimate in Eq (3.1.117) can be expressed as the sum of two terms

$$\hat{w}_l = Q_1 + Q_2, \quad (3.1.118)$$

where

$$Q_1 = \sum_{i=0}^{N-1} h_T[\cos(wt-iH)u(t)] \quad [\cos(wt-iH-H)u(t)-\cos(wt-iH)u(t)]/(\dagger\dagger T) \tag{3.1.119}$$

and

$$Q_2 = \sum_{i=0}^{N-1} -\cos(wt-iH)u(t) \quad [\cos(wt-iH-H)u(t)-\cos(wt-iH)u(t)]/(\dagger\dagger T). \tag{3.1.120}$$

The expression in Eq (3.1.121) is the same as the expression in Eq (3.1.65). Therefore, Q_2 is given in Eq (3.1.88). The response of the second order approximation (Eqs (3.1.114A), (3.1.114B), and (3.1.114C)) of an ideal delay to the sinusoid in Eq (3.1.58) (see Eqs (3.1.59) and (3.1.60)) is given by (Javid & Brenner, 1963)

$$\begin{aligned} h_T[r_i(t)] = {} & 2/[(wT_1)^4+4]T/T_1\{ \\ & (\{[(wT_1)^2T/T_1-2(1-T_2/T_1)]\cos(iH)+wT_1(2-wT_1wT_2)\sin(iH)\}\cos(t/T_1) \\ & +\{[-(wT_1)^2(1-T_2/T_1)-2T/T_1]\cos(iH)+[(wT_1)^3+2wT_2]\sin(iH)\}\sin(t/T_1) \\ &)\exp(-t/T_1) \\ & +[-(wT_1)^2T/T_1+2(1-T_2/T_1)]\cos(wt-iH) \\ & +wT_1(2-wT_1wT_2)\sin(wt-iH) \}+(T_2/T_1)^2\cos(wt-iH). \end{aligned} \tag{3.1.121}$$

We will now find a simplified expression for Q_1 given in Eq (3.1.119).

Substituting Eq (3.1.121) into Eq (3.1.119), for t greater than zero, we obtain

$$
\begin{aligned}
Q_1 = \sum_{i=0}^{N-1} \{\, & 2/[(wT_1)^4+4](1+T_2/T_1)[\\
& (\{ [(wT_1)^2(1+T_2/T_1)-2(1-T_2/T_1)]\cos(iH) \\
& \quad +wT_1(2-wT_1wT_2)\sin(iH)\}\cos(t/T_1) \\
& \quad +\{ [-(wT_1)^2(1-T_2/T_1)-2(1+T_2/T_1)]\cos(iH) \\
& \quad +[(wT_1)^3+2wT_2]\sin(iH)\}\sin(t/T_1))\exp(-t/T_1) \\
& +[-(wT_1)^2(1+T_2/T_1)+2(1-T_2/T_1)]\cos(wt-iH) \\
& +wT_1(2-wT_1wT_2)\sin(wt-iH)]+(T_2/T_1)^2\cos(wt-iH) \,\} \\
& \qquad [\cos(wt-iH-H)-\cos(wt-iH)]/[\dot{T}\dot{T}T].
\end{aligned}
\tag{3.1.122}
$$

By using the even property of the cosine function and the odd property of the sine function we can rearrange each argument of the sine and cosine functions in Eq (3.1.122) such that iH appears with a positive sign, obtaining

$$Q_1 = \sum_{i=0}^{N-1} \{ 2/[(wT_1)^4+4](1+T_2/T_1)[\quad (3.1.123)$$

$$(\{ [(wT_1)^2(1+T_2/T_1)-2(1-T_2/T_1)]\cos(iH)$$

$$+wT_1(2-wT_1wT_2)\sin(iH)\}\cos(t/T_1)$$

$$+\{ [-(wT_1)^2(1-T_2/T_1)-2(1+T_2/T_1)]\cos(iH)$$

$$+[(wT_1)^3+2wT_2]\sin(iH)\}\sin(t/T_1))\exp(-t/T_1)$$

$$+[-(wT_1)^2(1+T_2/T_1)+2(1-T_2/T_1)]\cos(iH-wt)$$

$$-wT_1(2-wT_1wT_2)\sin(iH-wt)]+(T_2/T_1)^2\cos(iH-wt) \}$$

$$[\cos(iH-wt+H)-\cos(iH-wt)]/[\dagger\dagger T].$$

By using the trigonometric identities in Eqs (B1) and (B2) in Eq (3.1.123) we obtain

$$Q_1 = \sum_{i=0}^{N-1} \{ 2/[(wT_1)^4+4](1+T_2/T_1)[\quad (3.1.124)$$

$$(\{ [(wT_1)^2(1+T_2/T_1)-2(1-T_2/T_1)]\cos(iH)$$

$$+wT_1(2-wT_1wT_2)\sin(iH)\}\cos(t/T_1)$$

$$+\{ [-(wT_1)^2(1-T_2/T_1)-2(1+T_2/T_1)]\cos(iH)$$

$$+[(wT_1)^3+2wT_2]\sin(iH)\}\sin(t/T_1))\exp(-t/T_1)$$

$$+[-(wT_1)^2(1+T_2/T_1)+2(1-T_2/T_1)][\cos(wt)\cos(iH)+\sin(wt)\sin(iH)]$$

$$+wT_1(2-wT_1wT_2)[\sin(wt)\cos(iH)-\cos(wt)\sin(iH)]]$$

$$+(T_2/T_1)^2[\cos(wt)\cos(iH)+\sin(wt)\sin(iH)] \}$$

$$[\cos(iH)\cos(wt-H)+\sin(iH)\sin(wt-H)$$

$$-\cos(iH)\cos(wt)-\sin(iH)\sin(wt)]/[\dagger\dagger T].$$

By using Eqs (B9), (B10), and (B11) in Eq (3.1.124) we note that there will be terms

$$z_1=\cos^2(iH)[\cos(wt-H)-\cos(wt)], \tag{3.1.125}$$

$$z_2=\sin^2(iH)[\sin(wt-H)-\sin(wt)], \tag{3.1.126}$$

as well as terms involving sin(iH)cos(iH). Summing these terms over the index i we obtain zero for the terms involving sin(iH)cos(iH) and for the z_1 and z_2 terms we obtain

$$\sum_{i=0}^{N-1} z_1=N/2[\cos(wt-H)-\cos(wt)], \text{ and} \tag{3.1.127}$$

$$\sum_{i=0}^{N-1} z_2=N/2[\sin(wt-H)-\sin(wt)]. \tag{3.1.128}$$

Using the trigonometric identities given in Eqs (B4) and (B6) in Eqs (3.1.127) and (3.1.128) we obtain

$$\sum_{i=0}^{N-1} z_1 = N\sin(H/2)\sin(wt-H/2), \text{ and} \tag{3.1.129}$$

$$\sum_{i=0}^{N-1} z_2 = -N\sin(H/2)\cos(wt-H/2). \tag{3.1.130}$$

Using the trigonometric identities given in Eqs (B1) and (B2) in Eqs (3.1.129) and (3.1.130) we obtain

$$\sum_{i=0}^{N-1} z_1 = N\sin(H/2)[\sin(wt)\cos(H/2)-\cos(wt)\sin(H/2)], \text{ and} \tag{3.1.131}$$

$$\sum_{i=0}^{N-1} z_2 = -N\sin(H/2)[\cos(wt)\cos(H/2)+\sin(wt)\sin(H/2)]. \tag{3.1.132}$$

Combining Eqs (3.1.124) through (3.1.132) we obtain

$$
\begin{aligned}
Q_1 = N\sin(H/2)\{\ & 2/[(wT_1)^4+4](1+T_2/T_1)[\\
& (\{ [(wT_1)^2(1+T_2/T_1)-2(1-T_2/T_1)][\sin(wt)\cos(H/2)-\cos(wt)\sin(H/2)] \\
& \quad -wT_1(2-wT_1wT_2)[\cos(wt)\cos(H/2)+\sin(wt)\sin(H/2)] \}\cos(t/T_1) \\
& \quad +\{ [-(wT_1)^2(1-T_2/T_1)-2(1+T_2/T_1)][\sin(wt)\cos(H/2)-\cos(wt)\sin(H/2)] \\
& \quad -[(wT_1)^3+2wT_2][\cos(wt)\cos(H/2)+\sin(wt)\sin(H/2)]\}\sin(t/T_1) \\
&)\exp(-t/T_1) \\
& +[-(wT_1)^2(1+T_2/T_1)+2(1-T_2/T_1)] \\
& \{ \cos(wt)[\sin(wt)\cos(H/2)-\cos(wt)\sin(H/2)] \\
& \quad -\sin(wt)[\cos(wt)\cos(H/2)+\sin(wt)\sin(H/2)] \} \\
& +wT_1(2-wT_1wT_2)\{ \sin(wt)[\sin(wt)\cos(H/2)-\cos(wt)\sin(H/2)] \\
& \qquad +\cos(wt)[\cos(wt)\cos(H/2)+\sin(wt)\sin(H/2)] \} \ ] \\
& +(T_2/T_1)^2\{ \cos(wt)[\sin(wt)\cos(H/2)-\cos(wt)\sin(H/2)] \\
& \qquad -\sin(wt)[\cos(wt)\cos(H/2)+\sin(wt)\sin(H/2)] \} \\
& \qquad \}/[TTT].
\end{aligned}
\tag{3.1.133}
$$

By canceling the terms that are equal in magnitude but opposite in sign in Eq (3.1.133) we obtain

$$
\begin{aligned}
Q_1 = N\sin(H/2)\{\ & 2/[(wT_1)^4+4](1+T_2/T_1)[\\
& (\{ [(wT_1)^2(1+T_2/T_1)-2(1-T_2/T_1)][\sin(wt)\cos(H/2)-\cos(wt)\sin(H/2)] \\
& \quad -wT_1(2-wT_1wT_2)[\cos(wt)\cos(H/2)+\sin(wt)\sin(H/2)] \}\cos(t/T_1) \\
& \quad +\{ [-(wT_1)^2(1-T_2/T_1)-2(1+T_2/T_1)][\sin(wt)\cos(H/2)-\cos(wt)\sin(H/2)] \\
& \quad -[(wT_1)^3+2wT_2][\cos(wt)\cos(H/2)+\sin(wt)\sin(H/2)]\}\sin(t/T_1) \\
&)\exp(-t/T_1) \\
& -[-(wT_1)^2(1+T_2/T_1)+2(1-T_2/T_1)]\{\cos^2(wt)\sin(H/2)-\sin^2(wt)\sin(H/2)\} \\
& +wT_1(2-wT_1wT_2)\{\sin^2(wt)\cos(H/2)+\cos^2(wt)\cos(H/2)\} \\
& \qquad\qquad\qquad\qquad\qquad\qquad\qquad\qquad\qquad\qquad] \\
& +(T_2/T_1)^2\{-\cos^2(wt)\sin(H/2)-\sin^2(wt)\sin(H/2)\ \} \\
& \qquad\qquad \}/[\dagger\dagger T].
\end{aligned}
\tag{3.1.134}
$$

By factoring a sin(H/2) or a cos(H/2) in three terms of Eq (3.1.134) and noting that the sum of $\cos^2(wt)$ and $\sin^2(wt)$ is one we obtain

$$Q_1=[N/(\dagger\dagger T)]\sin(H/2)\{\ 2/[(wT_1)^4+4](1+T_2/T_1)[\qquad (3.1.135)$$
$$(\ \{\ [(wT_1)^2(1+T_2/T_1)-2(1-T_2/T_1)][\sin(wt)\cos(H/2)-\cos(wt)\sin(H/2)]$$
$$-wT_1(2-wT_1wT_2)[\cos(wt)\cos(H/2)+\sin(wt)\sin(H/2)]\ \}\cos(t/T_1)$$
$$+\{\ [-(wT_1)^2(1-T_2/T_1)-2(1+T_2/T_1)][\sin(wt)\cos(H/2)-\cos(wt)\sin(H/2)]$$
$$-[(wT_1)^3+2wT_2][\cos(wt)\cos(H/2)+\sin(wt)\sin(H/2)]\ \}\sin(t/T_1)$$
$$)\exp(-t/T_1)$$
$$-[-(wT_1)^2(1+T_2/T_1)+2(1-T_2/T_1)]\sin(H/2)$$
$$+wT_1(2-wT_1wT_2)\cos(H/2)$$
$$]$$
$$-(T_2/T_1)^2\sin(H/2)$$
$$\}.$$

By combining Eqs (3.1.118), (3.1.88) and (3.1.135) we obtain the following expression for the left-sided estimate of the head angular velocity:

$$\hat{w}_1=[N/(\dagger\dagger T)]\sin(H/2)\{\ 2/[(wT_1)^4+4](1+T_2/T_1)\ [\qquad (3.1.136)$$
$$(\ \{\ [(wT_1)^2(1+T_2/T_1)-2(1-T_2/T_1)][\sin(wt)\cos(H/2)-\cos(wt)\sin(H/2)]$$
$$-wT_1(2-wT_1wT_2)[\cos(wt)\cos(H/2)+\sin(wt)\sin(H/2)]\ \}\cos(t/T_1)$$
$$+\{\ [-(wT_1)^2(1-T_2/T_1)-2(1+T_2/T_1)][\sin(wt)\cos(H/2)-\cos(wt)\sin(H/2)]$$
$$-[(wT_1)^3+2wT_2][\cos(wt)\cos(H/2)+\sin(wt)\sin(H/2)]\ \}\sin(t/T_1)$$
$$)\exp(-t/T_1)$$
$$-[-(wT_1)^2(1+T_2/T_1)+2(1-T_2/T_1)]\sin(H/2)$$
$$+wT_1(2-wT_1wT_2)\cos(H/2) \qquad]$$
$$-(T_2/T_1)^2\sin(H/2)\quad\}+N\sin(H/2)/\{\dagger\dagger T\}\sin(H/2).$$

By factoring $[N/(\dagger\dagger T)]\sin(H/2)$ in Eq (3.1.136) we obtain

$$\hat{w}_1=[N/(\dagger\dagger T_1)]\sin(H/2)\{\ 2/[(wT_1)^4+4]\ [\qquad (3.1.137)$$
$$(\ \{\ [(wT_1)^2(T/T_1)-2(1-T_2/T_1)][\sin(wt)\cos(H/2)-\cos(wt)\sin(H/2)]$$
$$-wT_1(2-wT_1wT_2)[\cos(wt)\cos(H/2)+\sin(wt)\sin(H/2)]\ \}\cos(t/T_1)$$
$$+\{\ [-(wT_1)^2(1-T_2/T_1)-2(T/T_1)][\sin(wt)\cos(H/2)-\cos(wt)\sin(H/2)]$$
$$-[(wT_1)^3+2wT_2][\cos(wt)\cos(H/2)+\sin(wt)\sin(H/2)]\ \}\sin(t/T_1)$$
$$)\exp(-t/T_1)$$
$$-[-(wT_1)^2(T/T_1)+2(1-T_2/T_1)]\sin(H/2)$$
$$+wT_1(2-wT_1wT_2)\cos(H/2)$$
$$]$$
$$-(T_2/T_1)^2\sin(H/2)+\sin(H/2)$$
$$\}.$$

Two-Sided Estimate given a Second Order Approximation

From Eq (3.1.137) with H replaced by -H we obtain the right-sided estimate

$$\hat{w}_r=-[N/(\pi T_1)]\sin(H/2)\{\ 2/[(wT_1)^4+4][\qquad (3.1.138)$$
$$(\ \{\ [(wT_1)^2(T/T_1)-2(1-T_2/T_1)][\sin(wt)\cos(H/2)+\cos(wt)\sin(H/2)]$$
$$-wT_1(2-wT_1wT_2)[\cos(wt)\cos(H/2)-\sin(wt)\sin(H/2)]\ \}\cos(t/T_1)$$
$$+\{\ [-(wT_1)^2(1-T_2/T_1)-2(T/T_1)][\sin(wt)\cos(H/2)+\cos(wt)\sin(H/2)]$$
$$-[(wT_1)^3+2wT_2][\cos(wt)\cos(H/2)-\sin(wt)\sin(H/2)]\ \}\sin(t/T_1)$$
$$)\exp(-t/T_1)$$
$$+[-(wT_1)^2(T/T_1)+2(1-T_2/T_1)]\sin(H/2)$$
$$+wT_1(2-wT_1wT_2)\cos(H/2)$$
$$]$$
$$+(T_2/T_1)^2\sin(H/2)-\sin(H/2)$$
$$\}.$$

The two-sided estimate is given in Eq (3.1.33) which is expressed in terms of the left-sided and the right-sided estimates. Substituting Eqs (3.1.137) and (3.1.138) into Eq (3.1.33) we obtain

$$\hat{w}=[N/(\tau\tau T_1)]\sin(H/2)2/[(wT_1)^4+4] \quad [\quad (3.1.139)$$
$$(\{ [(wT_1)^2(T/T_1)-2(1-T_2/T_1)]\sin(wt)\cos(H/2)$$
$$-wT_1(2-wT_1wT_2)\cos(wt)\cos(H/2) \}\cos(t/T_1)$$
$$+\{ [-(wT_1)^2(1-T_2/T_1)-2(T/T_1)]\sin(wt)\cos(H/2)$$
$$-[(wT_1)^3+2wT_2]\cos(wt)\cos(H/2) \}\sin(t/T_1)$$
$$)\exp(-t/T_1)+wT_1(2-wT_1wT_2)\cos(H/2) \quad].$$

By factoring out cos(H/2) from Eq (3.1.139) we obtain

$$\hat{w}=[N/(\tau\tau T_1)]2\sin(H/2)\cos(H/2)/[(wT_1)^4+4][\quad (3.1.140)$$
$$(\{ [(wT_1)^2(T/T_1)-2(1-T_2/T_1)]\sin(wt)-wT_1(2-wT_1wT_2)\cos(wt) \}\cos(t/T_1)$$
$$+\{ [-(wT_1)^2(1-T_2/T_1)-2(T/T_1)]\sin(wt)-[(wT_1)^3+2wT_2]\cos(wt) \}\sin(t/T_1)$$
$$)\exp(-t/T_1)+wT_1(2-wT_1wT_2) \quad].$$

In Eq (3.1.140) by using $NH=2\tau\tau$ we obtain

$$\hat{w}=(2/T_1)[\sin(H/2)/(H/2)]\cos(H/2)/[(wT_1)^4+4][\quad (3.1.141)$$
$$(\{ [(wT_1)^2(T/T_1)-2(1-T_2/T_1)]\sin(wt)-wT_1(2-wT_1wT_2)\cos(wt) \}\cos(t/T_1)$$
$$+\{ [-(wT_1)^2(1-T_2/T_1)-2(T/T_1)]\sin(wt)-[(wT_1)^3+2wT_2]\cos(wt) \}\sin(t/T_1)$$
$$)\exp(-t/T_1)+wT_1(2-wT_1wT_2)].$$

By substituting Eq (3.1.103) (see Eq (102)) into Eq (3.1.141) we obtain the two-sided estimate

$$\hat{w}=(1/T_1)C(H)2/[(wT_1)^4+4]\,[\qquad (3.1.142)$$
$$(\,\{\,[(wT_1)^2(T/T_1)-2(1-T_2/T_1)]\sin(wt)$$
$$-wT_1(2-wT_1wT_2)\cos(wt)\,\}\cos(t/T_1)$$
$$+\{\,[-(wT_1)^2(1-T_2/T_1)-2(T/T_1)]\sin(wt)$$
$$-[(wT_1)^3+2wT_2]\cos(wt)\,\}\sin(t/T_1)$$
$$)\exp(-t/T_1)$$
$$+wT_1(2-wT_1wT_2)\qquad],$$

where C(H) is given in Eq (3.1.103). We will drop the facter C(H) from Eq (3.1.142). Therefore, we obtain

$$\hat{w}=(1/T_1)2/[(wT_1)^4+4][\qquad (3.1.143)$$
$$(\,\{\,[(wT_1)^2(T/T_1)-2(1-T_2/T_1)]\sin(wt)$$
$$-wT_1(2-wT_1wT_2)\cos(wt)\,\}\cos(t/T_1)$$
$$+\{\,[-(wT_1)^2(1-T_2/T_1)-2(T/T_1)]\sin(wt)$$
$$-[(wT_1)^3+2wT_2]\cos(wt)\,\}\sin(t/T_1)$$
$$)\exp(-t/T_1)$$
$$+wT_1(2-wT_1wT_2)\qquad],$$

The output of the estimator given in Eq (3.1.143) with both T_1 and T equal to 0.85 seconds, and T_2 equal to zero, as a function of time, is shown in Fig. 3.1.18. The head is suddenly tilted at time zero and the head angular velocity is 60 degrees/second to the left. The estimate rises from zero to a maximum of approximately 52

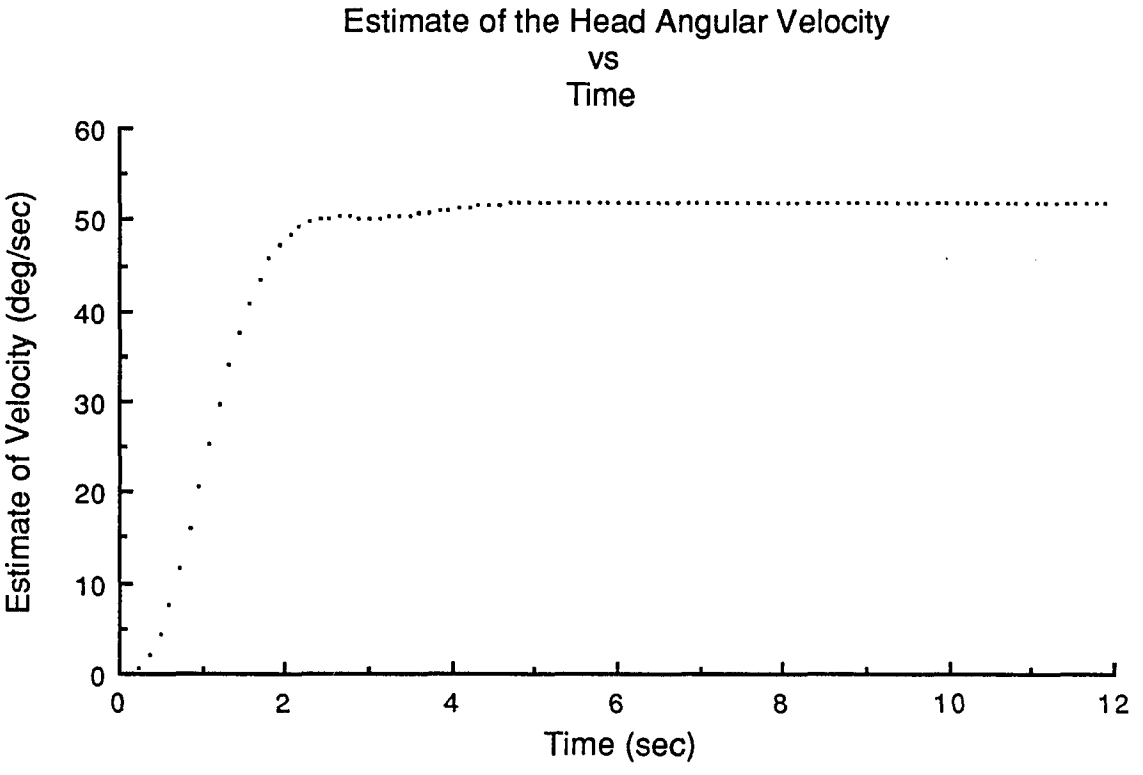

Fig. 3.1.18 Estimate of the head angular velocity: The head angular velocity is 60 degrees/second to the left. The second order system time constant, T_1, is equal to 0.85 seconds and the other time constant, T_2, is equal to 0.0. The head is suddenly tilted at time 0.0. The estimate rises to a maximum of approximately 52 degrees/second after 4.5 seconds.

degrees/second which occurs at approximately 4.5 seconds. The value of the estimate remains approximately constant at 52 degrees/second as time increases.

Estimate for Small Time t given a Second Order Approximation

To investigate this estimate we will first consider its form for small t. By finding the Taylor expansion of Eq (3.1.143), using Eqs (B15), (B16), (B17), and (B18), and retaining terms up to the third degree in t we obtain

$$\hat{w}\tilde{=}(1/T_1)2/[(wT_1)^4+4][\tag{3.1.144}$$
$$[(wT_1)^2(T/T_1)-2(1-T_2/T_1)]$$
$$\{(wT_1)t/T_1-(wT_1)(t/T_1)^2-[(wT_1)^3/6](t/T_1)^3\}$$
$$-wT_1(2-wT_1wT_2)$$
$$\{1-t/T_1-[(wT_1)^2/2](t/T_1)^2+\{[2+3(wT_1)^2]/6\}(t/T_1)^3\}$$
$$+[-(wT_1)^2(1-T_2/T_1)-2(T/T_1)]$$
$$\{(wT_1)(t/T_1)^2-(wT_1)(t/T_1)^3\}$$
$$-[(wT_1)^3+2wT_2]$$
$$\{t/T_1-(t/T_1)^2+\{[2-3(wT_1)^2]/6\}(t/T_1)^3\}$$
$$+wT_1(2-wT_1wT_2)].$$

By collecting the terms that are constant, linear, quadratic, and cubic in time from Eq (3.1.144) we obtain

$$\hat{w}\tilde{=}(1/T_1)2/[(wT_1)^4+4][\qquad (3.1.145)$$
$$-wT_1(2-wT_1wT_2)+wT_1(2-wT_1wT_2)$$
$$+\{[(wT_1)^2(T/T_1)-2(1-T_2/T_1)](wT_1)+wT_1(2-wT_1wT_2)-[(wT_1)^3+2wT_2]\}t/T_1$$
$$+\{-[(wT_1)^2(T/T_1)-2(1-T_2/T_1)](wT_1)+wT_1(2-wT_1wT_2)[(wT_1)^2/2]$$
$$+[-(wT_1)^2(1-T_2/T_1)-2(T/T_1)](wT_1)+[(wT_1)^3+2wT_2]\}(t/T_1)^2$$
$$+\{-[(wT_1)^2(T/T_1)-2(1-T_2/T_1)][(wT_1)^3/6]$$
$$-wT_1(2-wT_1wT_2)[2+3(wT_1)^2]/6$$
$$-[-(wT_1)^2(1-T_2/T_1)-2(T/T_1)](wT_1)$$
$$-[(wT_1)^3+2wT_2]\{[2-3(wT_1)^2]/6\}\ \}(t/T_1)^3].$$

Expanding and then canceling terms in Eq (3.1.145) that are equal in magnitude but opposite in sign and then combining the remaining like terms we obtain

$$\hat{w}\tilde{=}(1/T_1)2/[(wT_1)^4+4]\{ \qquad (3.1.146)$$
$$[-(wT_1)^4wT_2/2-2wT_2](t/T_1)^2$$
$$+[(wT_1)^5/3+(wT_1)^4wT_2/3+4wT_1/3+4wT_2/3](t/T_1)^3\}.$$

By simplifying Eq (3.1.146) we obtain

$$\hat{w}\tilde{=}w2[-T_2/T_1(t/T_1)^2/2+(T/T_1)(t/T_1)^3/3] \qquad (3.1.147)$$

If T_2 is greater than zero (T_2 is less than zero) then the estimate in Eq (3.1.143) initially decreases (increases) quadratically with

time t as shown in Eq (3.1.147). Therefore, if the estimate given in Eq (3.1.143) is input to the velocity storage integrator, the output of the velocity storage integrator will initially decrease (increase) cubically with time t. If T_2 is equal to zero then, the esimate in Eq (3.1.143) initially increases cubically with time t as shown in Eq (3.1.147). Therefore, the output of the integrator will initially increase proportionally to the fourth power of the time t. The estimate, given in section 3.1.2, derived from an ideal delay operator is zero for the first T seconds and therefore, the output of the integrator is also zero for the first T seconds. In summary, the estimate initially changes more slowly for the first T seconds if T_2 is equal to zero (and therefore, T_1 is equal to T) than if T_2 is greater than or less than zero.

The output of the velocity storage integrator, assuming that its initial state is zero, as a function of time is shown in Fig. 3.1.19. The input of the integrator is assumed to be the output of the estimator given in Eq (3.1.143) with T_1 equal to T (T_2 is equal to zero) which in turn is set equal to 0.85 seconds. The head is suddenly tilted at time zero and the head angular velocity is 60 degrees/second to the left. The eye velocity command reaches a maximum of approximately 52 degrees/second at approximately 10 seconds (Fig. 3.1.19A). From then on the eye velocity command is approximately constant. The first five seconds of the eye velocity command of Fig. 3.1.19A are shown in Fig. 3.1.19B. Initially the eye

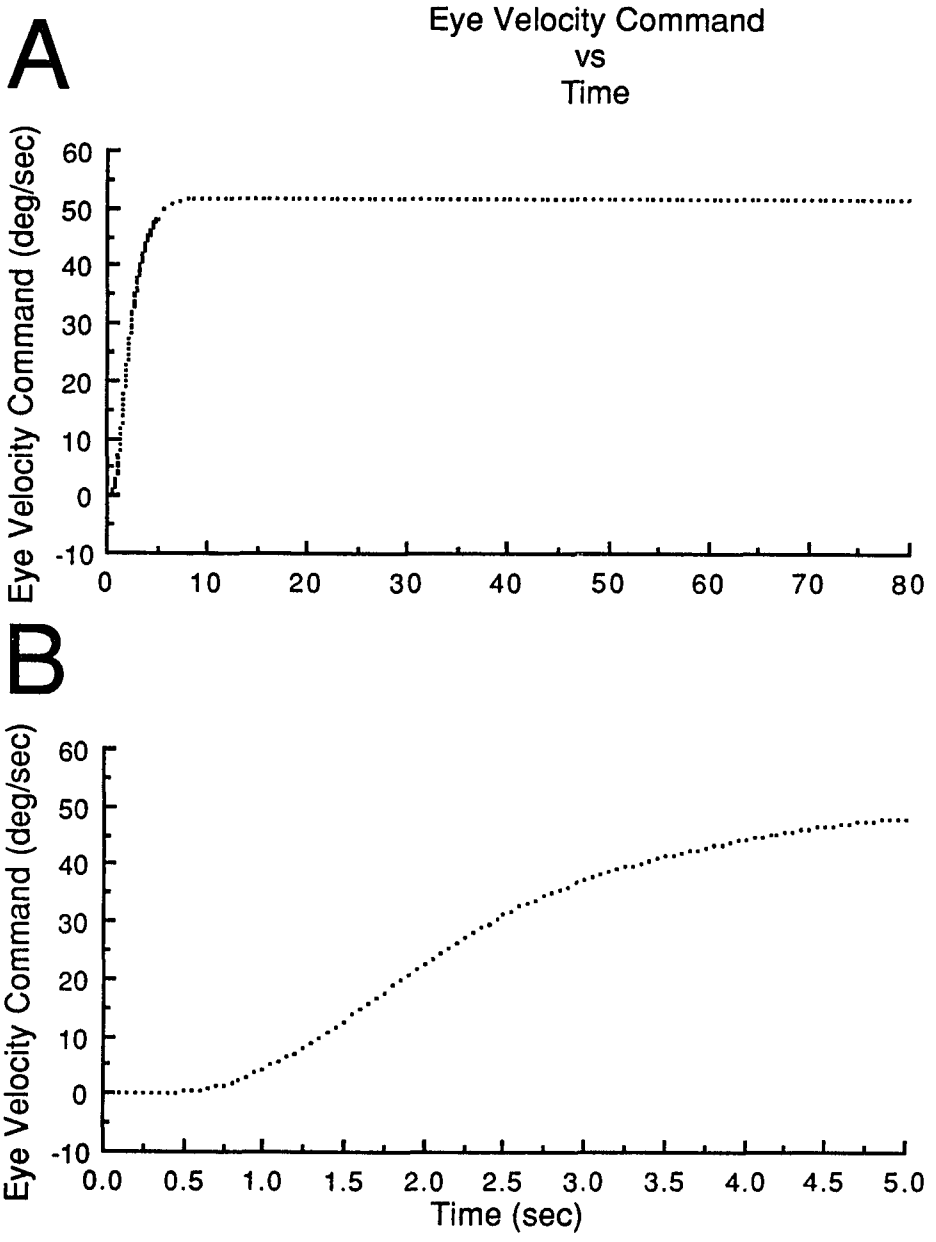

Fig. 3.1.19 The eye velocity command as a function of time: The velocity storage integrator time constant is approximately 13.3 seconds. The head angular velocity is 60 degrees/second to the left.
A. The eye velocity command rises to approximately 52 degrees/second at 10 seconds.
B. The first 5 seconds of the results shown in A. The eye velocity command is approximately 4 degrees/second after 1 second.

velocity command is zero and is increasing slowly (Fig. 3.1.19B). At approximately one second the eye velocity command is approximately 4 degrees/second. This is consistent with the type of delay observed in monkey when it is tilted during constant velocity rotation about the head yaw axis.

Steady State Estimate given a Second Order Approximation

We will examine the behavior of the steady state estimate obtained from Eq (3.1.143) by considering Eq (3.1.143) for large t. The steady state estimate is given by:

$$\hat{w}_s = 2w(2-wT_1 wT_2)/[(wT_1)^4+4]. \qquad (3.1.148)$$

If w is sufficiently small in Eq (3.1.148) we obtain

$$\hat{w}_s \tilde{=} w. \qquad (3.1.149)$$

For small values of the stimulus velocity, w, the steady state estimate in Eq (3.1.148) equals w, the head angular velocity.

The behavior of the steady state estimate for larger values of w depends on T_1 and T_2. If T_2 is greater than zero, then the steady state estimate, $\hat{w}_s$, which is given in Eq (3.1.148) is zero if

$$w=[2/(T_1T_2)]^{1/2}. \tag{3.1.150}$$

As w continues to increase the estimate becomes negative. For very large w the estimate $\hat{w}_s$ is approximately given by

$$\hat{w}_s \tilde{-} -(2T_2/T_1^3)/w, \tag{3.1.151}$$

which approaches zero as w increases. Therefore, the steady state estimate, $\hat{w}_s$, of Eq (3.1.148) has two extremum. The estimate rises to a maximum, and then falls to zero as w increases. The estimate $\hat{w}_s$ falls to some negative minimum, and then increases and asymptotically approaches zero as w continues to increase toward infinity.

When T_2 is less than or equal zero, the steady state estimate $\hat{w}_s$ of Eq (3.1.148) cannot become negative for positive w. For large values of w the estimate asymptotically approaches zero. Therefore, the steady state estimate $\hat{w}_s$ of Eq (3.1.148) has one extremum for positive w. The estimate rises to a maximum, and then falls and asymptotically approaches zero as w increases. The estimate falls to zero more rapidly with increasing w if T_2 is zero than if T_2 is negative.

The data shown in Fig. 3.1.8A taken from monkey is consistent with a maximum estimate of approximately 67 degrees/second and a location of the maximum estimate of approximately 105 degrees/second. However, it should be noted that Fig. 3.1.8A shows considerable

scatter in the data near the apparent maximum estimate. To try and fit the monkey data we consider numeric results from Eq (3.1.148) for T equal to 0.85 and various values of T_1 (Fig. 3.1.20).

If T_2 is equal to zero (Fig. 3.1.20A) (T_1 is equal to T) as the head angular velocity increases the estimate of Eq (3.1.148) increases reaching a maximum of

$$\hat{w}_s=(3/4)(4/3)^{(1/4)}/T, \tag{3.1.152}$$

(which is approximately equal to 54 degrees/second) at which point the head velocity equals

$$w=(4/3)^{(1/4)}/T, \tag{3.1.153}$$

(which is approximately equal to 72 degrees/second.) Setting the maximum estimate to 67 degrees/second fixes T_1 at approximately 0.69 seconds and therefore, the maximum estimate location occurs at a head angular velocity magnitude of approximately 89 degrees/second. This compares favorably with the monkey data shown in Fig. 3.1.8A. Setting the maximum estimate location to 105 degrees/second fixes T_1 at approximately 0.59 seconds and therefore, the maximum estimate is approximately 79 degrees/second. Note that the product of the maximum estimate and T is constant at $(3/4)(4/3)^{(1/4)}$ (Eq (3.1.152)), and that the product of the location of the maximum and T is constant

Fig. 3.1.20 The steady state estimate as a function of head angular velocity using a second order system to approximate an ideal delay.
A. T_1=0.85 seconds, T_2=0.0. A maximum estimate of approximately 54 degrees/second occurs at a head angular velocity of approximately 72 degrees/second. As the head angular velocity continues to increase the estimate decays to zero. The estimate never becomes negative.
B. T_1=0.82 seconds, T_2=+0.03 seconds. A maximum estimate of approximately 55 degrees/second occurs at a head angular velocity of approximately 74 degrees/second. The estimate is equal to 0.0 when the head angular velocity is approximately 517 degrees/second. As the head angular velocity increases, the estimate becomes negative and is a minimum of approximately -0.27 degrees/second when the head angular velocity is approximately 895 degrees/second. As the head angular velocity continues to increase the estimate approaches zero.
C. T_1=0.425 seconds, T_2=0.425 seconds. A maximum estimate of approximately 67 degrees/second occurs at a head angular velocity of approximately 99 degrees/second. The estimate is equal to 0.0 when the head angular velocity is approximately 191 degrees/second. As the head angular velocity increases, the estimate becomes negative and is a minimum of approximately -67 degrees/second when the head angular velocity is approximately 368 degrees/second. As the head angular velocity continues to increase the estimate approaches zero.
D. T_1=0.88 seconds, T_2=-0.03 seconds. A maximum estimate of approximately 54 degrees/second occurs at a head angular velocity of approximately 71 degrees/second. As the head angular velocity continues to increase the estimate decays to zero. The estimate never becomes negative.

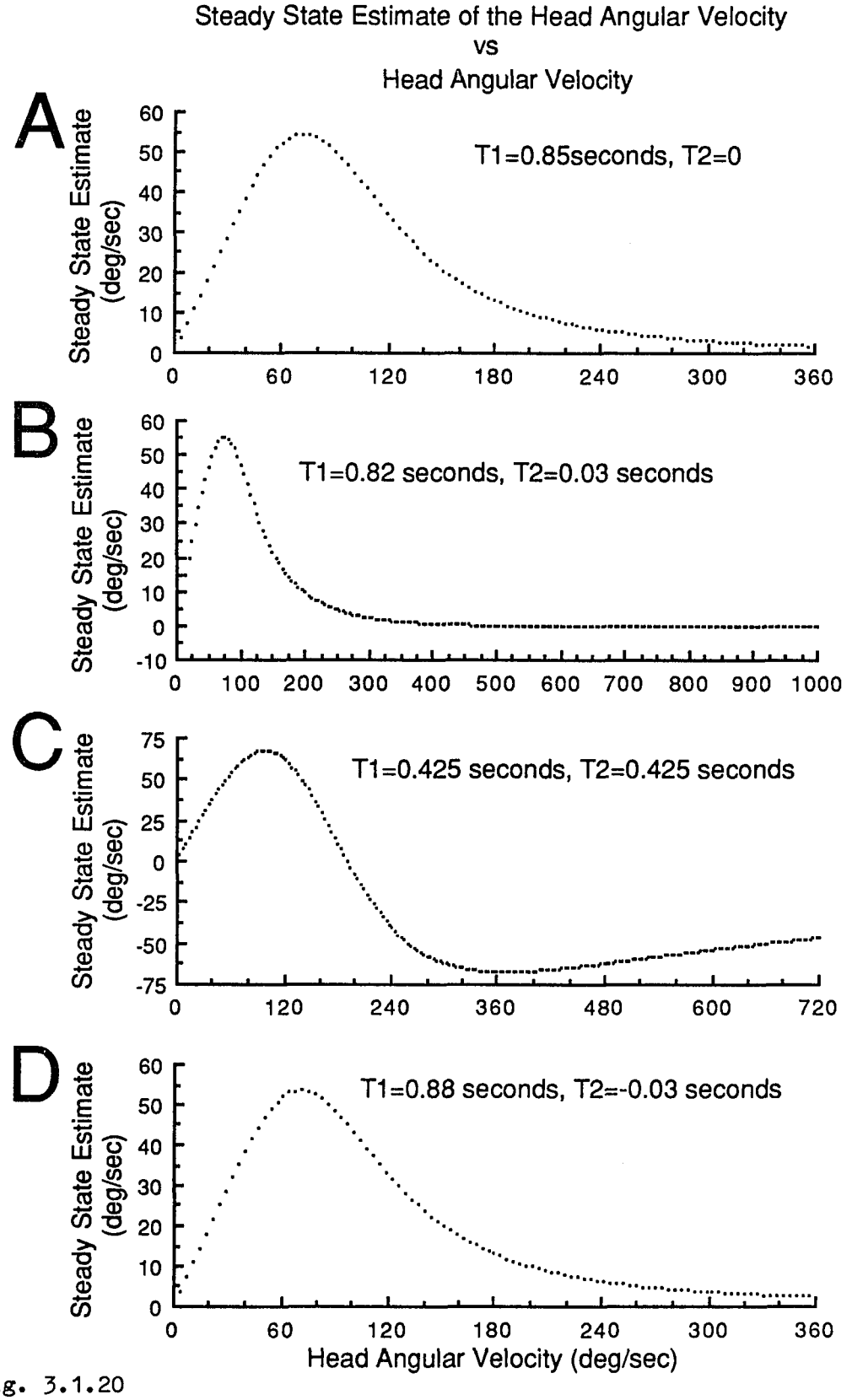
Steady State Estimate of the Head Angular Velocity
vs
Head Angular Velocity
A
B
C
D
Steady State Estimate (deg/sec)
T1=0.85seconds, T2=0
T1=0.82 seconds, T2=0.03 seconds
T1=0.425 seconds, T2=0.425 seconds
T1=0.88 seconds, T2=-0.03 seconds
Head Angular Velocity (deg/sec)

Fig. 3.1.20

at $(4/3)^{(1/4)}$ (Eq (3.1.153)). Therefore, both the location of the maximum estimate and the maximum estimate decrease as T increases.

As w continues to increase the estimate begins to decrease and for larger w it asymptotically approaches

$$\hat{w}_s \tilde{} (4/T^4)/w^3, \tag{3.1.154}$$

(or, for T equal to 0.85 seconds, approximately $(7.7/sec^4)/w^3$) as it decays to zero. Note that the estimate never turns negative.

If T_1 is equal to 0.82 seconds and T_2 is equal to 0.03 seconds (Fig. 3.1.20B), as the head angular velocity increases the estimate increases, reaching a maximum of approximately 55 degrees/second at a head velocity of approximately 74 degrees/second. If T_1 is increased from 0.82 seconds to 0.9 seconds, with T_2 held constant at 0.03 seconds, both the maximum estimate and maximum location decrease to approximately 50.3 degrees/second and 67.5 degrees/second, respectively. If instead, T1 is decreased to 0.78 seconds, with T_2 held constant at 0.03 seconds, then both the maximum estimate and its location increase to approximately 57.9 degrees/second and 77.8 degrees/second, respectively. If T_2 is decreased from 0.03 seconds to 0.01 seconds, with T_1 held constant at 0.82 seconds, then both the maximum estimate and the maximum estimate location increase to approximately 55.9 degrees/second and 74.8 degrees/second. If instead T_2 is increased to 0.05 seconds, with T_1 held constant at 0.82

seconds, then both the maximum estimate and its location decrease to approximately 54.4 degrees/second and 73.3 degrees/second respectively.

As w continues to increase the estimate begins to decrease reaching zero when w is equal to $[2/(T_1T_2)]^{(1/2)}$ (which is approximately equal to 517 degrees/second or approximately 1.5 revolutions/second.) As w continues to increase the estimate continues to decrease reaching a minimum of approximately -0.27 degrees/second at a head velocity of approximately 895 degrees/second, which is approximately 2.5 revolutions/second. As w continues to increase the estimate approaches $-2(T_2/T_1^3)/w$ (which is equal to $-0.11/w$) as it increases toward zero.

If both T_1 and T_2 are equal to 0.425 seconds (Fig. 3.1.20C) as the head angular velocity increases the estimate reaches a maximum of approximately 67 degrees/second at a head angular velocity of approximately 99 degrees/second. As the head angular velocity, w, continues to increase the estimate will fall reaching zero when the head angular velocity, w, is approximately equal to 191 degrees/second. This compares favorably with the monkey data shown in Fig. 3.1.8A. As w continues to increase the estimate decreases reaching a minimum of approximately -67 degrees/second when w is approximately equal to 368 degrees/second. As w continues to increase the estimate increases toward zero.

If T_1 is equal to 0.88 seconds and T_2 is equal to -0.03 seconds

(Fig. 3.1.20D) as the head angular velocity increases the estimate increases reaching a maximum of approximately 54 degrees/second at a head velocity of 71 degrees/second. If T_1 is increased from 0.88 seconds to 0.9 seconds, with T_2 held constant at -0.03 seconds, then both the maximum estimate and maximum location decrease to approximately 52.3 degrees/second and 69.3 degrees/second, respectively. If instead T_1 is decreased from 0.88 seconds to approximately 0.82 seconds, with T_2 held constant at -0.03 seconds, both the maximum estimate and maximum location increase to approximately 57.5 degrees/second and 76.1 degrees/second, respectively. If T_2 is increased from -0.03 seconds to -0.01 seconds, with T_1 held constant at 0.88 seconds, then the maximum estimate and maximum location decrease to approximately 52.8 degrees/second and 70.3 degrees/second, respectively. If instead T_2 is decreased to -0.05 seconds, with T_1 held constant at 0.88 seconds, then both the maximum estimate and maximum location increase to approximately 54.2 degrees/second and 71.5 degrees/second, respectively.

As w continues to increase the estimate decreases and approaches $-2(T_2/T_1^3)/w$ (which is equal to $+0.088/w$) as it decays toward zero.

In summary, for a small head angular velocity, the estimate, based on the second order approximation to an ideal delay, is approximately equal to the head angular velocity. The estimate reaches a maximum as w increases. The maximum estimate and its location depend on the parameters T_1 and T_2. For values of T_1 and T_2

near 0.85 seconds and 0.0 seconds, respectively, if T_1 or T_2 increase with the other held contant then both the maximum estimate and the maximum estimate location decrease, and if T_1 or T_2 decrease with the other held contant then both the maximum estimate and the maximum estimate location increase. The parameters T_1 and T_2 can be chosen such that the maximum estimate and its location, as generated by the model, compare favorably with the monkey data (Fig. 3.1.8A). Furthermore, the one second delay characteristic of the eye velocity command occuring after the sudden tilt of the head is modeled by choosing a value of T_1 equal to approximately 0.85 seconds (Fig. 3.1.7A). The slow phase eye velocity is negative shortly after the sudden tilt in the monkey data shown in Fig. 3.1.7A. This can be modeled by choosing T_2 to be positive. If T_2 is greater than zero then the model steady state estimate becomes negative for sufficiently large w (Figs. 3.1.20B and 3.1.20C).

Therefore, the estimator utilizing a second order approximation to an ideal delay operator provides a better fit to the data than does the estimator utilizing a first order approximation. Futhermore, the second order approximation provides a mechanism through which the estimate can become negative as the head angular velocity magnitude increases and provides more flexibility in predicting the response to OVAR over a wider range of species.

3.1.6 Effects of Noise on the Estimation of Head Velocity

It was assumed that the head angular velocity estimator received signals directly from the otoliths as well as delayed signals. Each of these was assumed to be noiseless. In order to examine the robustness of the estimator under more realistic physiological conditions, we will now assume that each of these signals is contaminated by additive noise, which is independent of the noise in the other signals. We will show that in the presence of noise, the average value of the two-sided estimate is equal to the noiseless two-sided estimate. However, in the presence of noise, the average value of the one-sided estimate is equal to the noiseless one-sided estimate plus a term proportional to the product of the number of cells, N, and the difference between the variance, s_p^2, of the noise in a present signal and the covariance, C_{pd}, of the noise in the present and delayed versions of a signal. The sensitivity to noise of the one-sided estimator is due to 2N terms each of N of these terms is proportional to the square of the present activation of a hair cell and each of another N of these terms is proportional to the product of the present and delayed activations of a hair cell. We will show a one-sided estimator (in which these 2N terms have been replaced) that has the property that, in the presence of noise the average value of the one-sided estimate is equal to the noiseless estimate. To obtain this estimator, we demand that in each product term of the estimator,

the cell refered to in the temporal difference of activations is different from either of the cells refered to in the spatial difference. In the i^{th} product term of the one-sided estimator, the temporal difference refers to cell i. Therefore, we can obtain a one-sided estimator with the above property if in the i^{th} product term, for i=0, ..., N-1, we replace each spatial difference of the activations of cells i+1 and i by the spatial difference of the activations of cells i+1 and i-1.

We will show that the one-sided estimator is sensitive to noise. Let each of the N direct signals be represented by a random variable (see Papoulis, 1984) $R_i(t)$ and let each of the N delayed signals be represented by a random variable $R_i(t-T)$. Let $r_i(t)$ be the signal transmitted by cell i at time t. The random variables, $R_i(t)$ and $R_i(t-T)$ can be represented as follows:

$$R_i(t)=r_i(t)+X_{ip}, \text{ and} \tag{3.1.155}$$

$$R_i(t-T)=\text{Delay}(T)[R_i(t)]=r_i(t-T)+X_{id}, \text{ for i=0 to N-1,} \tag{3.1.156}$$

where Delay(T) is a time delay operator, X_{ip} is the noise in the i^{th} present signal, and where X_{id} is a delayed version of X_{ip}. Each of the terms, X_i, for i=0 to N-1, is a random variable with an assumed mean of zero and a standard deviation of s_i. It is assumed that the N present random variables, X_i, are independent and identically

distributed (see Papoulis, 1984).

To find the effects of noise on the estimator, let $\hat{W}$ represent the random variable associated with the estimate. Therefore from Eq (3.1.34) with a tilt angle of $\pi/2$, let the following be a definition of $\hat{W}_1$:

$$\hat{W}_1 = \sum_{i=0}^{N-1} [\underline{R}_i(t-T)-\underline{R}_i(t)][\underline{R}_{i+1}(t)-\underline{R}_i(t)]/\{\pi\pi Tg^2\}. \qquad (3.1.157)$$

Substituting Eqs (3.1.155) and (3.1.156) into Eq (3.1.157) we obtain

$$\hat{W}_1 = \sum_{i=0}^{N-1} [r_i(t-T)+X_{id}-r_i(t)-X_{ip}] \qquad (3.1.158)$$
$$[r_{i+1}(t)+X_{i+1,p}-r_i(t)-X_{ip}]/\{\pi\pi Tg^2\}.$$

Performing some of the indicated multiplications in Eq (3.1.158) we obtain

$$\hat{W}_1=(1/\{\pi\pi Tg^2\}) \sum_{i=0}^{N-1} [r_i(t-T)-r_i(t)][r_{i+1}(t)-r_i(t)] \qquad (3.1.159)$$
$$+[r_i(t-T)-r_i(t)][X_{i+1p}-X_{ip}]$$
$$+[X_{id}-X_{ip}][r_{i+1}(t)-r_i(t)]$$
$$+[X_{id}-X_{ip}][X_{i+1p}-X_{ip}].$$

Let E(.) be the expected value operator (see Papoulis, 1984). Note that the expected value operator is a linear operator. Applying the linear expected value operator to Eq (3.1.159) we obtain

$$E(\hat{W}_1)=(1/\{\bar{T}\bar{T}Tg^2\}) \sum_{i=0}^{N-1} \begin{aligned} & E([r_i(t-T)-r_i(t)][r_{i+1}(t)-r_i(t)]) \\ & +E([r_i(t-T)-r_i(t)][X_{i+1p}-X_{ip}]) \\ & +E([X_{id}-X_{ip}][r_{i+1}(t)-r_i(t)]) \\ & +E([X_{id}-X_{ip}][X_{i+1p}-X_{ip}]). \end{aligned} \quad (3.1.160)$$

Define A, B, C, D as follows

$$A=(1/\{\bar{T}\bar{T}Tg^2\}) \sum_{i=0}^{N-1} E([r_i(t-T)-r_i(t)][r_{i+1}(t)-r_i(t)]), \quad (3.1.161)$$

$$B=(1/\{\bar{T}\bar{T}Tg^2\}) \sum_{i=0}^{N-1} E([r_i(t-T)-r_i(t)][X_{i+1p}-X_{ip}]), \quad (3.1.162)$$

$$C=(1/\{\bar{T}\bar{T}Tg^2\}) \sum_{i=0}^{N-1} E([X_{id}-X_{ip}][r_{i+1}(t)-r_i(t)]), \text{ and} \quad (3.1.163)$$

$$D=(1/\{\uparrow\uparrow Tg^2\}) \sum_{i=0}^{N-1} E([X_{id}-X_{ip}][X_{i+1p}-X_{ip}]). \qquad (3.1.164)$$

Combining Eqs (3.1.160), (3.1.161), (3.1.162), (3.1.163), and (3.1.164) we obtain

$$E(\hat{W}_1)=A+B+C+D. \qquad (3.1.165)$$

In Eq (3.1.161), the function contained within the expected value operator is independent of the random variables X_{ip} and X_{id}. Therefore, from Eq (3.1.161) we obtain

$$A=(1/\{\uparrow\uparrow Tg^2\}) \sum_{i=0}^{N-1} [r_i(t-T)-r_i(t)][r_{i+1}(t)-r_i(t)], \qquad (3.1.166)$$

Comparing Eq (3.1.166) to Eq (3.1.34) with K_n set to one we obtain

$$A=\hat{w}_1, \qquad (3.1.167)$$

where $\hat{w}_1$ is the left-sided estimate from Eq (3.1.31). Using the linearity of the expected value operator on Eq (3.1.162) we obtain

$$B=(1/\{\tau\tau Tg^2\}) \sum_{i=0}^{N-1} [r_i(t-T)-r_i(t)]\{E(X_{i+1p})-E(X_{ip})\}. \quad (3.1.168)$$

Since the mean of each random variable, X_{ip}, is assumed equal to zero we obtain

$$B=0. \quad (3.1.169)$$

Similarly, it can also be shown that

$$C=0. \quad (3.1.170)$$

Performing the indicated multiplications in Eq (3.1.164) and then using the fact that the expected value operator is linear we obtain

$$D=(1/\{\tau\tau Tg^2\}) \sum_{i=0}^{N-1} E(X_{id}X_{i+1p})-E(X_{ip}X_{i+1p})-E(X_{id}X_{ip})+E(X_{ip}X_{ip}). \quad (3.1.171)$$

In Eq (3.1.171), by assuming that the noise in the $i+1^{th}$ present signal is independent of both the noise in the i^{th} delayed signal and the noise in the i^{th} present signal we obtain

$$D=(1/\{\bar{T}\bar{T}Tg^2\})\sum_{i=0}^{N-1} E(X_{id})E(X_{i+1p})-E(X_{ip})E(X_{i+1p}) \quad (3.1.172)$$
$$-E(X_{id}X_{ip})+E(X_{ip}X_{ip}).$$

Since the average value of each X_{ip} and each X_{id} is zero we obtain

$$D=(1/\{\bar{T}\bar{T}Tg^2\})\sum_{i=0}^{N-1} -E(X_{id}X_{ip})+E(X_{ip}^2). \quad (3.1.173)$$

The nosie sensitivity of the one-sided estimator is due to the presence of term D given in Eq (3.1.173). We can make the following substitutions:

$$E(X_{ip}^2)=m_{2ip}, \quad (3.1.174)$$

where m_{2ip} is the second momemt. Since the mean of X_{ip} is assumed to be zero, the second moment is the variance, s_{ip}^2. Therefore,

$$s_{ip}^2=m_{2ip}. \quad (3.1.175)$$

Since the mean of X_{ip} is zero and assuming that the mean of X_{id} is also zero, we obtain

$$C_{ipd}=E(X_{id}X_{ip}), \tag{3.1.176}$$

where C_{ipd} is the covariance of the random variables, X_{id} and X_{ip}. We assume that the variance and the covariance are independent of i and therefore, we obtain

$$s_{ip}=s_p, \text{ for } i=0, \ldots, N-1, \text{ and} \tag{3.1.177}$$

$$C_{ipd}=C_{pd}, \text{ for } i=0, \ldots, N-1. \tag{3.1.178}$$

Therefore, from Eqs (3.1.173), (3.1.174), (3.1.175), (3.1.176), (3.1.177), and (3.1.178) we obtain

$$D=(N/\{\dagger\dagger Tg^2\})[s_p^2-C_{pd}]. \tag{3.1.179}$$

Combining Eqs (3.1.165), (3.1.167), (3.1.169), (3.1.170), and (3.1.179) we obtain

$$E(\hat{W}_1)=\hat{w}_1+(1/\{\dagger\dagger Tg^2\})N(s_p^2-C_{pd}). \tag{3.1.180}$$

In Eq (3.1.180) it is seen that as the number of cells, N, increases the absolute value of the expected value of the estimate increases, assuming that $s_p^2-C_{pd}$ does not equal zero. A similar expression can be obtained for the right-sided estimator yielding

$$E(\hat{W}_r)=\hat{w}_r+(1/\{\tau\tau Tg^2\})N(s_p^2-C_{pd}). \tag{3.1.181}$$

Forming the two-sided estimate from Eqs (3.1.180) and (3.1.181) we obtain

$$E(\hat{W})=(E(\hat{W}_l)-E(\hat{W}_r))/2=(\hat{w}_l-\hat{w}_r)/2. \tag{3.1.182}$$

This shows that the average value of the two-sided estimate in the presence of noise is equal to the ideal noiseless two-sided estimate.

To eliminate the term proportional to N in the left- or right-sided estimate requires a change in the estimator. One possible change, in which the spatial differnce of the activations of cells i+1 and i is replaced by the spatial difference of the activations of cells i+1 and i-1, to the estimator given in Eq (3.1.157) yields the following:

$$\hat{W}_l'=\sum_{i=0}^{N-1}[\underline{R}_i(t-T)-\underline{R}_i(t)][\underline{R}_{i+1}(t)-\underline{R}_{i-1}(t)]/\{2\tau\tau Tg^2\}. \tag{3.1.183}$$

An analysis similar to that which lead to Eq (3.1.180) from Eq (3.1.157) leads to the following from Eq (3.1.183):

$$E(\hat{W}_1')=\hat{w} \tag{3.1.184}$$

where $\hat{w}$ is the two-sided estimate obtained in section 3.1.2. The right-sided estimator based on Eq (3.1.183) is equal to minus one times the estimator of Eq (3.1.183). Therefore, the two-sided estimate based on the left-sided estimator given in Eq (3.1.183) is equal to the left-sided estimate given in Eq (3.1.183).

From Eq (3.1.184), the average value of the one-sided estimate given additive noise in the signals received by the estimator, is equal to the ideal noiseless one-sided estimate. It also suggests that the noise in eye velocity should increase during unilateral lesions that affect the integrator as well as destroy the otoliths.

3.2 Modelling the Three Dimensional Properties on Velocity Estimation

In section 3.1, a velocity estimator was derived assuming that the angular velocity of the head was normal to the plane of a macula which is approximately in a canal plane (Fig. 3.2.1A). Under these circumstances, the pattern amplitude as a function of rotation angle is approximately the same for all head orientations. However, when the normal to the macular plane is not aligned with the rotation axis, it sweeps out a cone about the rotation axis and consequently complicates the estimation process (Fig. 3.2.1B). The purpose of this section is to study the effects of misalignment of the rotation axis on the patterns generated in the otolith macula and its affects on the head velocity estimator since this is the condition during OVAR when the axis of rotation is along the subject vertical. This will be done by considering an extension of the model to three dimensions based on the principles of motion estimation from patterns of otolith activation in a single plane (Fig. 3.2.2). The input vector, $\underline{g}(t)$, is a uniform acceleration due to gravity or its equivalent. The otoliths transduce $\underline{g}(t)$ into an activation pattern. The three-dimensional angular velocity estimator computes a three-dimensional estimate of the head angular velocity which charges the three-dimensional velocity storage integrator. Signals representing the components of the output of the velocity storage integrator can be observed in the vestibular nucleus (Reisine et al, 1988). In typical OVAR experiments, the

Fig. 3.2.1 A. The normal is parallel to the head velocity and therefore the normal is constant as the head rotates. B. The normal is not parallel to the head velocity. As the head rotates, the direction of the normal changes and sweeps out a conic with regard to the angular head velocity.

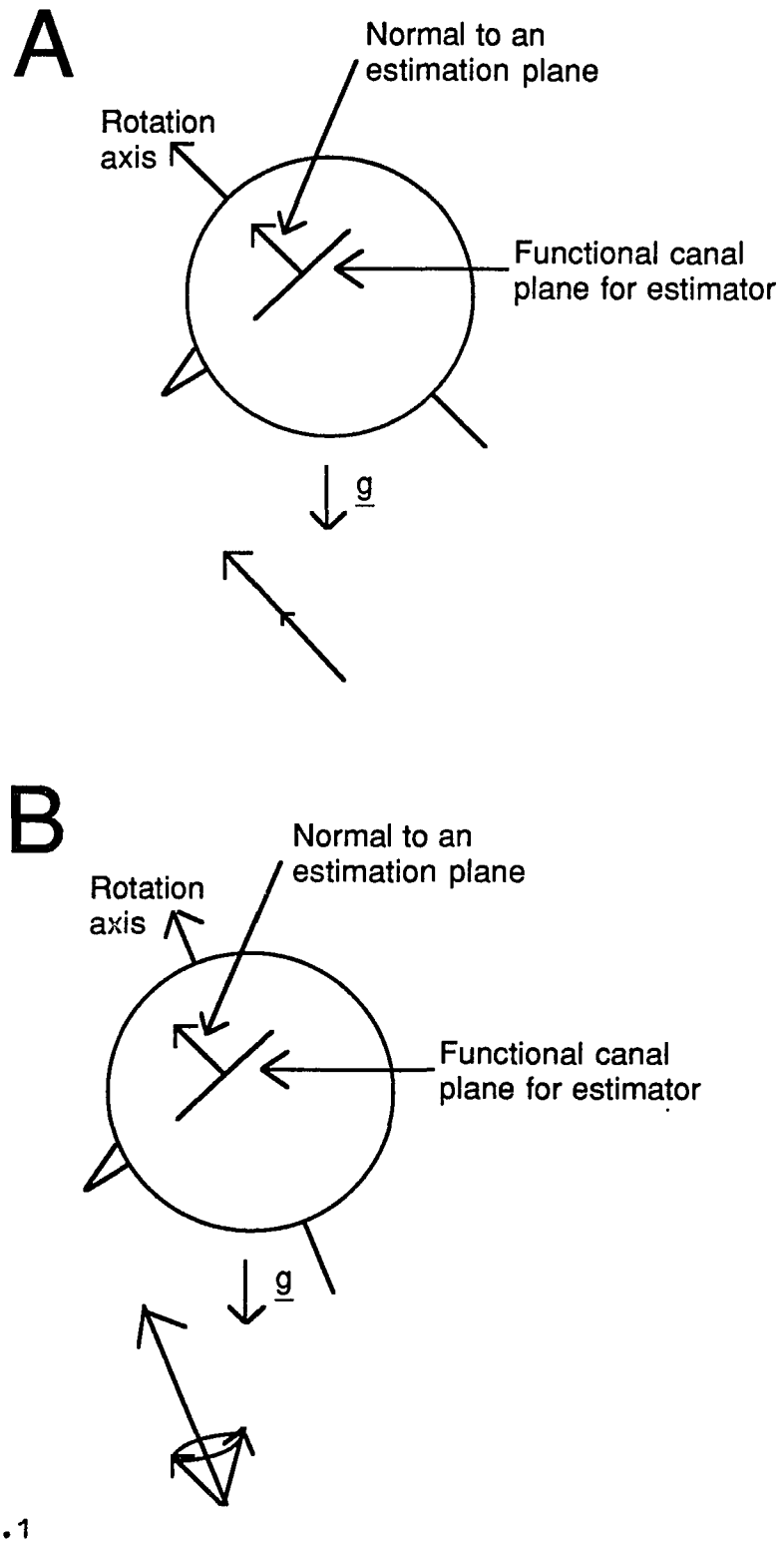
A
Normal to an
estimation plane
Rotation
axis
Functional canal
plane for estimator
g
B
Normal to an
estimation plane
Rotation
axis
Functional canal
plane for estimator
g

Fig. 3.2.1

3-Dimensional System responding to OVAR

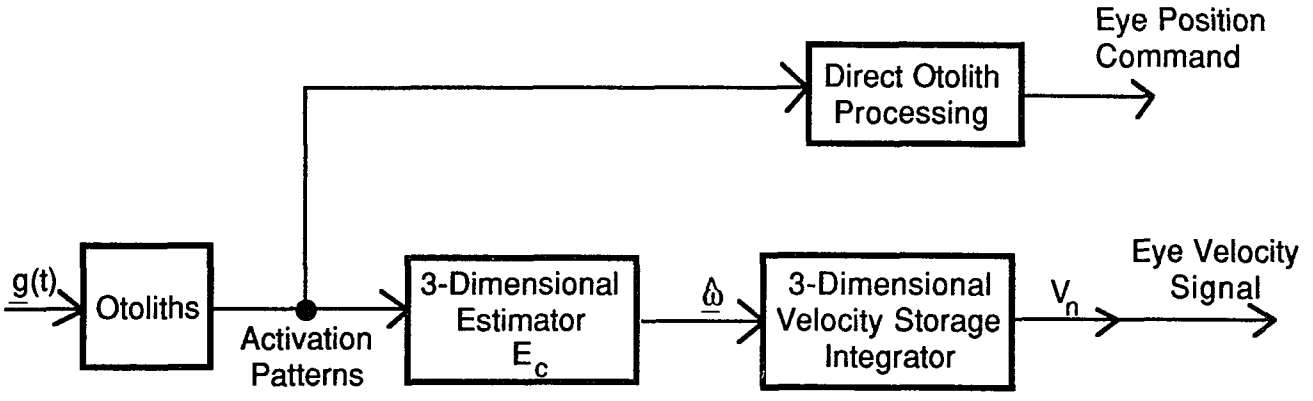

Fig. 3.2.2 Block diagram model of the three-dimensional system responding to OVAR. The components are shown with neither visual nor semicircular canal components, for simplicity.
The otoliths transduce an acceleration due to gravity (or its gravitational equivalent) into a pattern of otolith activation. The three-dimensional estimator, E_c, generates an estimate, $\hat{\omega}$, of the head angular velocity from patterns of otolith activations.
The three-dimensional velocity storage integrator (which is a function of the head orientation with respect to gravity (see Raphan & Cohen, 1988; Sturm & Raphan, 1988)) stores the estimated velocity.
The direct otolith processing unit transforms a pattern of otolith activation into an eye position signal.
The vestibular nuclei receive the signals from the velocity storage integrator (Reisine et al, 1988). This is represented by the signal V_n.

lights are off and the head has been rotating for a long time such that there is zero input from the semicircular canals. Therefore, these signals in the vestibular nucleus represent eye velocity commands. The activation patterns are also input to the direct otolith processing unit which generates eye position commands. Some of the problems and limitations associated with the three-dimensional extension of the model and how it can be modified to give improved estimates of head velocity will be considered. This is important if we are to understand the kinds of compensatory mechanisms that the brain utilizes for matching eye velocity to head velocity for arbitrary rotation of the head in a gravitational environment.

In analogy with the one-dimensional model to three dimensions, it will be first assumed that information available to the three-dimensional velocity estimator, at any time, consists of two activation patterns. The patterns represent the accelerations due to gravity with respect to the head at time t_p and at time t_d, where

$$t_d<t_p, \text{ and} \tag{3.2.1}$$

$$T=t_p-t_d, \tag{3.2.2}$$

where T is a time delay constant (Fig. 3.2.3A).

The problem of estimating the angular velocity of the head in three dimensions, as was the case in one dimension, is to find a

rotation mapping in pattern space that relates the present to the delayed pattern. Each pattern is an N-dimensional representation of a three-dimensional gravity vector relative to the head (Fig. 3.2.3B). This is equivalent to finding a rotation mapping in three dimensions that relates the present orientation of gravity relative to the head to the delayed orientation of gravity relative to the head. There are a variety of finite rotations of the head in space that will correspond to given present and delayed activation patterns. This can be seen by examining two orientations of the head with regard to gravity and considering the various rotations that can bring one orientation into another (Fig. 3.2.4). One orientation axis is the perpendicular to both $g(t_d)$ and $g(t_p)$ (Fig. 3.2.4A). Under this rotation the transformation of $g(t_d)$ to $g(t_p)$ sweeps out a sector of a circle in the plane of these vectors. If the rotation is not orthogonal to the vectors $g(t_d)$ and $g(t_p)$, the circle will not be in the plane of the vectors (Fig. 3.2.4B). In general, any axis which is orthogonal to the difference between the two vectors is a valid rotation axis (Fig. 3.2.4C). Therefore, there is insufficient information in two activation patterns to uniquely determine a finite head rotation. This was handled in the one dimensional case by implementing a correct normalization and is not readily extended to three dimensions. The purpose of this section is to study estimation properties of a two pattern estimator as an extension of the one-dimensional estimator and determine how it might be modified

A

A

N-dimensional patterns for given space orientations

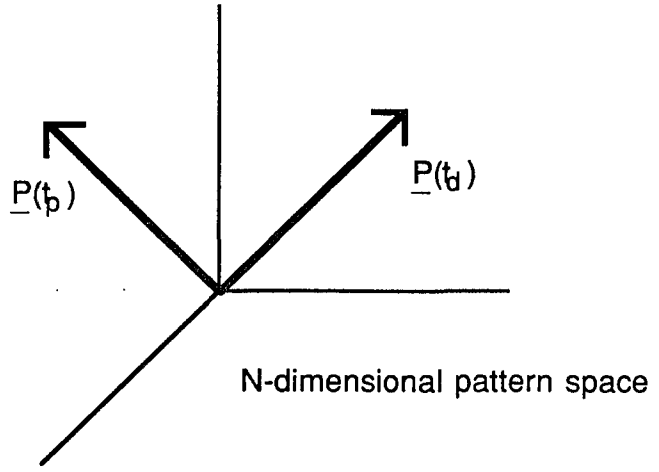

B

Corresponding Gravity vectors relative to the head for given space orientations with respect to the head

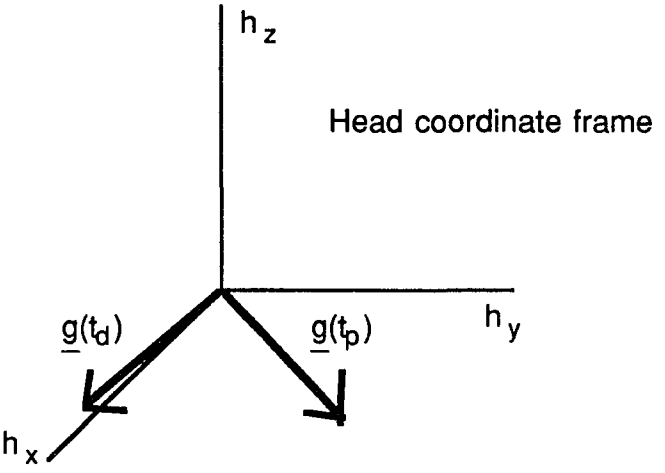

Fig. 3.2.3 A. N-dimensional patterns representing given head orientations with regard to gravity. $\underline{P}(t_p)$ and $\underline{P}(t_d)$ represent the patterns at times t_p and t_d, respectively. B. Corresponding gravity vectors relative to the head at times t_p and t_d, respectively.

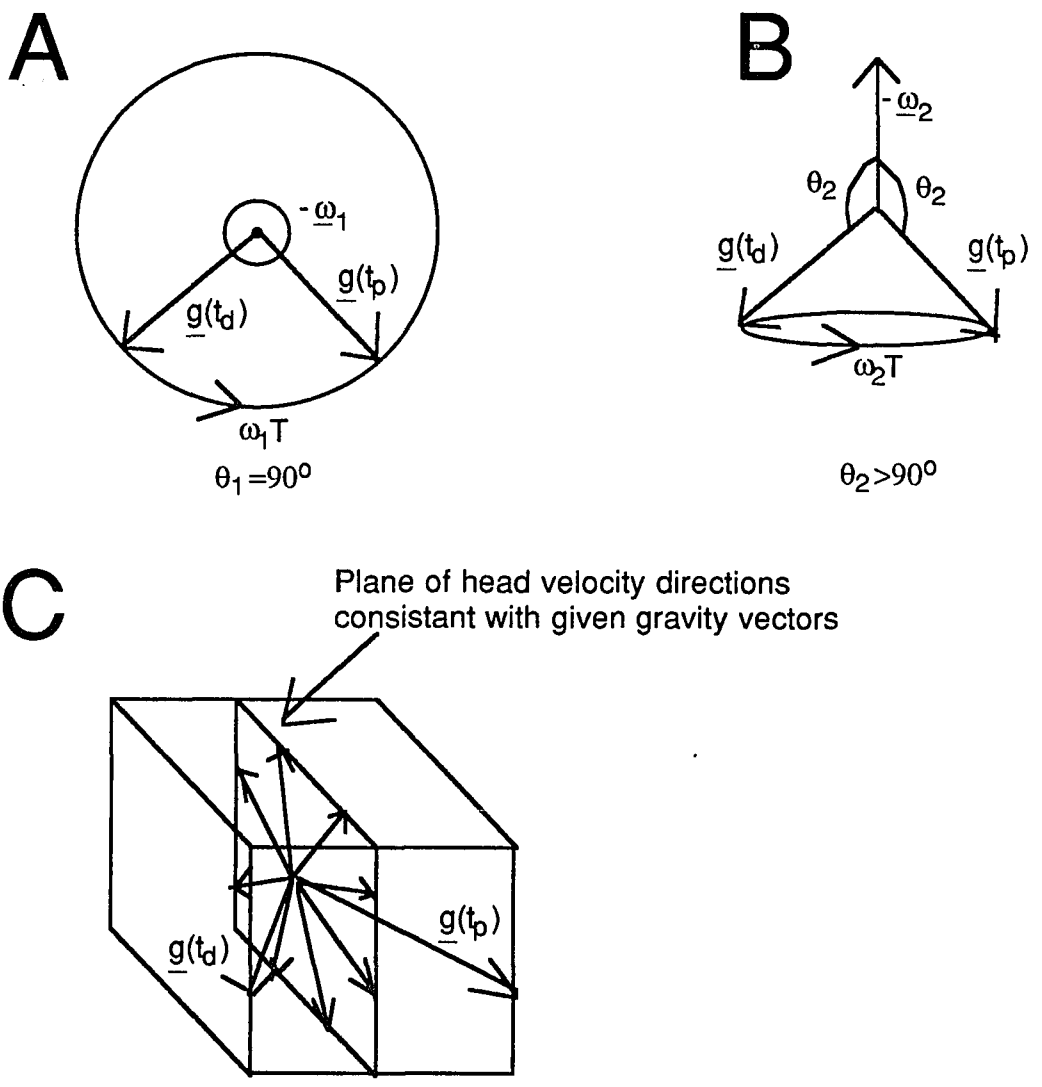

Fig. 3.2.4 There is insufficient information in two otolith activation patterns to uniquely determine the head angular velocity. Each figure shows one or more possible head angular velocity orientations consistant with a pair of accelerations due to gravity represented in a head reference frame.
A. Barbecue-spit rotation of the head consistant with the pair of gravity vectors, $g(t_d)$ and $g(t_p)$.
B. There exists a rotation axis such the angle of head rotation is 180 degrees.
C. In a head reference frame, for any space rotation axis perpendicular to the difference between the two gravity vectors there exists an angle of rotation such that the net rotation is consistant with the gravity vectors.

to implement a better estimator.

3.2.1 Polarization Vectors: Space and Head Representations

In the three-dimensional model, we consider an inertial reference frame defined by a set of orthogonal space axes one of which is in the direction of the gravitational field, $\underline{g}$. Let

$$\underline{\hat{e}}_s^1 = \begin{vmatrix} 1 \\ 0 \\ 0 \end{vmatrix}, \tag{3.2.3a}$$

$$\underline{\hat{e}}_s^2 = \begin{vmatrix} 0 \\ 1 \\ 0 \end{vmatrix}, \text{ and} \tag{3.2.3b}$$

$$\underline{\hat{e}}_s^3 = \begin{vmatrix} 0 \\ 0 \\ 1 \end{vmatrix}. \tag{3.2.3c}$$

be a right-handed sequence of three orthonormal basis vectors fixed in space, such that $\underline{\hat{e}}_s^3$ is opposite in direction to gravity (Fig. 3.2.5A). We can now represent the acceleration due to gravity with respect to the space basis as follows:

$$\underline{g} = -g\underline{\hat{e}}_s^3, \tag{3.2.4}$$

where g is its magnitude.

Next we represent the i^{th} polarization vector, for i=0 to N-1,

Fig. 3.2.5 Comparison of space coordinates and head coordinates.
A. Since gravity usually activates the otolith hair cells, it is natural to consider a space coordinate system in which gravity is opposite in direction to one axis.
B. A polarization vector, fixed with respect to the head, can be decomposed into time dependent space coordinates.
C. Head reference frame in which slow phase eye velocity is measured using pitch, roll, and yaw axes.
D. A polarization vector, fixed with respect to the head, can be decomposed into time independent head coordinates.
E. A head reference frame with left anterior, left posterior, and left lateral canal axes as the coordinate basis.
F. A polarization vector, fixed with respect to the head, decomposed into time independent canal coordinates.

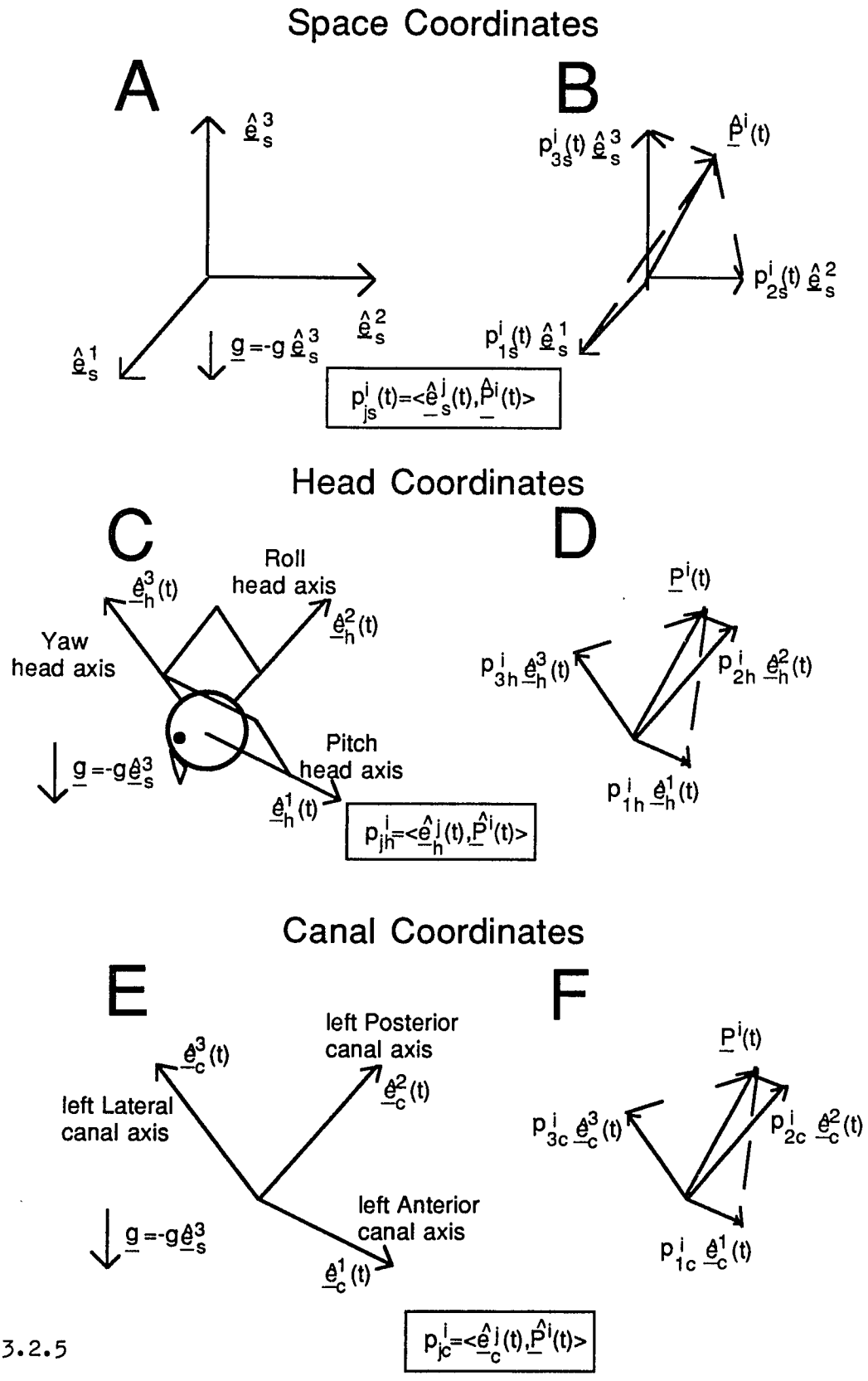
Space Coordinates
A
B
Head Coordinates
C
D
Roll
head axis
Yaw
head axis
Pitch
head axis
Canal Coordinates
E
F
left Posterior
canal axis
left Lateral
canal axis
left Anterior
canal axis

Fig. 3.2.5

with respect to the space basis, at time t, as follows:

$$\underline{\hat{P}}^i(t) = \sum_{j=1}^{3} p^i_{js}(t)\underline{\hat{e}}^j_s, \text{ for } i=0 \text{ to } N-1. \qquad (3.2.5)$$

The coefficients $p^i_{js}(t)$ in Eq (3.2.5) are the projections of the polarization vectors on the space axes and are given by (Fig. 3.2.5B)

$$p^i_{js}(t) = \langle \underline{\hat{e}}^j_s, \underline{\hat{P}}^i(t) \rangle, \text{ for } i=0 \text{ to } N-1 \text{ and } j=1 \text{ to } 3. \qquad (3.2.6)$$

The symbol $\langle , \rangle$, in Eq (3.2.6), is the usual inner product of vectors. Thus, $p^i_{js}(t)$ is the cosine of the angle between $\underline{\hat{e}}^j_s$ and $\underline{\hat{P}}^i(t)$. Because the polarization vectors are constant with respect to the head it is natural to represent the i^{th} polarization vector with respect to a head coordinate system and transform the polarization vectors to the spatial frame of reference.

First, we represent a set of head axes such that they are consistent with how eye movements are measured (Fig. 3.2.5C). At time t, let $\underline{\hat{e}}^1_h(t)$ (x-axis or pitch), $\underline{\hat{e}}^2_h(t)$ (y-axis or roll), and $\underline{\hat{e}}^3_h(t)$ (z-axis or yaw) denote a right-handed sequence of three orthonormal basis vectors fixed in the head and having a specific orientation with respect to gravity. The i^{th} unit polarization vector, for i=0 to N-1, at some time t can be represented with respect to the head basis as

follows:

$$\hat{\underline{P}}^i(t) = \sum_{j=1}^{3} p^i_{jh}\hat{\underline{e}}^j_h(t), \text{ for } i=0 \text{ to } N-1. \qquad (3.2.7)$$

Note that the time dependence arises because of the rotation of the head relative to the inertial space frame. The coefficients in Eq (3.2.7) are given by (Fig. 3.2.5D)

$$p^i_{jh} = \langle \hat{\underline{e}}^j_h(t), \hat{\underline{P}}^i(t) \rangle, \text{ for } i=0 \text{ to } N-1 \text{ and } j=1 \text{ to } 3, \qquad (3.2.8)$$

where, p^i_{1h}, p^i_{2h}, and p^i_{3h}, are the three-dimensional extension of the polarization angle of a hair cell and are called the polarization direction cosines of a hair cell. Note that from the assumption that the polarization vectors with respect to the head are independent of time it follows that the polarization direction cosines are independent of time.

To obtain the relationship, at time t, between the representation of the i^{th} polarization vector in space coordinates (Eq (3.2.5)) to that given in head coordinates (Eq (3.2.7)) we first relate the three head fixed basis vectors, $\hat{\underline{e}}^1_h(t)$, $\hat{\underline{e}}^2_h(t)$, and $\hat{\underline{e}}^3_h(t)$, to the three space fixed basis vectors, $\hat{\underline{e}}^1_s$, $\hat{\underline{e}}^2_s$, and $\hat{\underline{e}}^3_s$ as follows:

$$\underline{\hat{e}}_h^j(t) = \sum_{i=1}^{3} e_{hi}^j(t)\underline{\hat{e}}_s^i, \text{ for } j=1 \text{ to } 3, \tag{3.2.9}$$

where,

$$e_{hj}^i(t) = \langle \underline{\hat{e}}_s^j, \underline{\hat{e}}_h^i(t) \rangle, \text{ for } i=1 \text{ to } 3 \text{ and } j=1 \text{ to } 3. \tag{3.2.10}$$

It is convenient to organize these three unit vectors into a matrix,

$$O_h(t) = \begin{vmatrix} e_{h1}^1(t), & e_{h1}^2(t), & e_{h1}^3(t) \\ e_{h2}^1(t), & e_{h2}^2(t), & e_{h2}^3(t) \\ e_{h3}^1(t), & e_{h3}^2(t), & e_{h3}^3(t) \end{vmatrix}, \tag{3.2.11}$$

The matrix of Eq (3.2.11) represents the orientation of the head with respect to space. It can be interpreted as a representation of an identity operator, that transforms a triple of numbers, representing a vector in head coordinates, into another triple of numbers representing a vector in space coordinates and is given by: (see Goldstein, 1980)

$$\begin{vmatrix} p_{js}^i(t) \\ p_{js}^i(t) \\ p_{js}^i(t) \end{vmatrix} = \begin{vmatrix} e_{h1}^1(t), & e_{h1}^2(t), & e_{h1}^3(t) \\ e_{h2}^1(t), & e_{h2}^2(t), & e_{h2}^3(t) \\ e_{h3}^1(t), & e_{h3}^2(t), & e_{h3}^3(t) \end{vmatrix} \begin{vmatrix} p_{1h}^i \\ p_{2h}^i \\ p_{3h}^i \end{vmatrix}, \quad \text{for } i=0 \text{ to } N-1, \tag{3.2.12}$$

Therefore, knowing the orientation of the head with respect to space

at time t (Eq (3.2.11)), and given the i^{th} polarization direction cosines (Eq (3.2.8)), we can obtain the space coordinate system representation of the i^{th} polarization vector.

3.2.2 Three-Dimensional Estimation by Combining Three One-Dimensional Ideal Noise Free Models

In this section, we examine the performance of a three-dimensional estimator under the restriction that two patterns are processed. We assume that the estimate, generated by the three-dimensional estimator, is in canal coordinates so that the signals can be combined properly with those coding velocity of the head from the semicircular canals or that of the visual system. As a first approximation we will assume that the estimator is composed of three similar one-dimensional estimators each of which operates on information corresponding to a canal axis. Further, we assume that, except for its orientation with respect to the head, each one-dimensional estimator is similar to the one-dimensional estimator developed in section 3.1.

The information available to the estimator consists of two activation patterns and a time delay constant, T. An activation pattern, at any time t, is a sampling of the components of the acceleration due to gravity along N unit polarization vectors. The directions of the polarization vectors, at time t, are distributed in three-dimensional space. However, if it is assumed that they are combined centrally to form functional planes of polarization vectors consistent with canal planes (Fig. 3.2.6A) then, it is possible to obtain a natural extension of the model developed in section 3.1. An

Fig. 3.2.6 The polarization vectors of the otolith organs are distributed in three dimensions.
A. The first stage of processing obtains three functional planes of polarization vectors.
B. In a two-pattern three-dimensional estimator associated with each functional plane of polarization vectors is an activation pattern. Each activation pattern is input to a one-dimensional estimator which includes delay elements. The estimator computes a canal coordinate component of the head angular velocity from a present and a delayed activation pattern. There is no coupling among the three one-dimensional estimators.

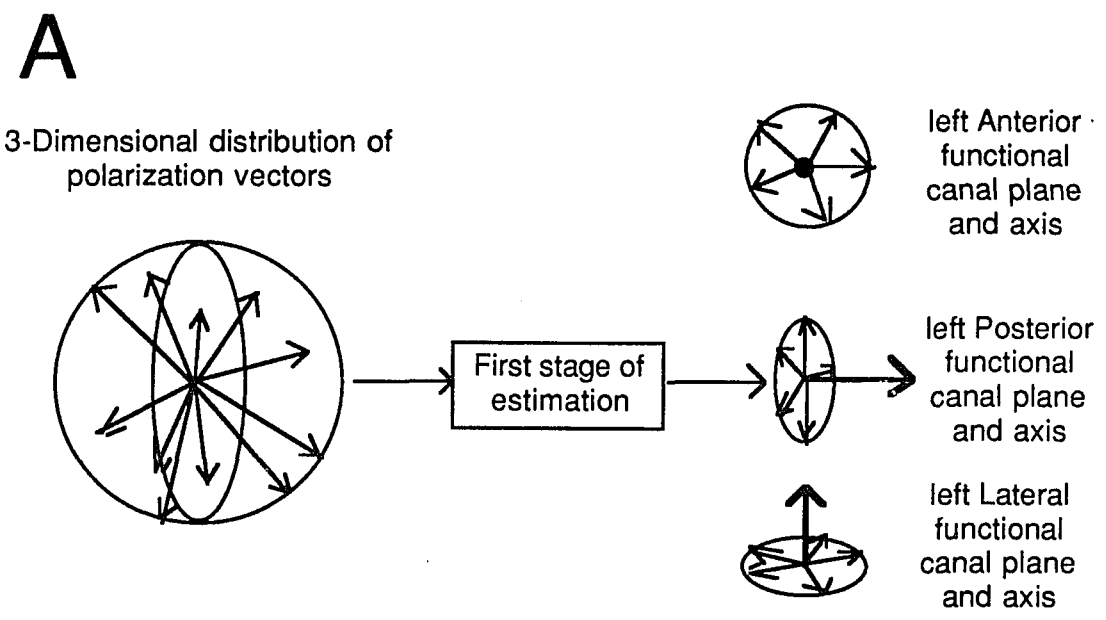
A
3-Dimensional distribution of polarization vectors
First stage of estimation
left Anterior functional canal plane and axis
left Posterior functional canal plane and axis
left Lateral functional canal plane and axis

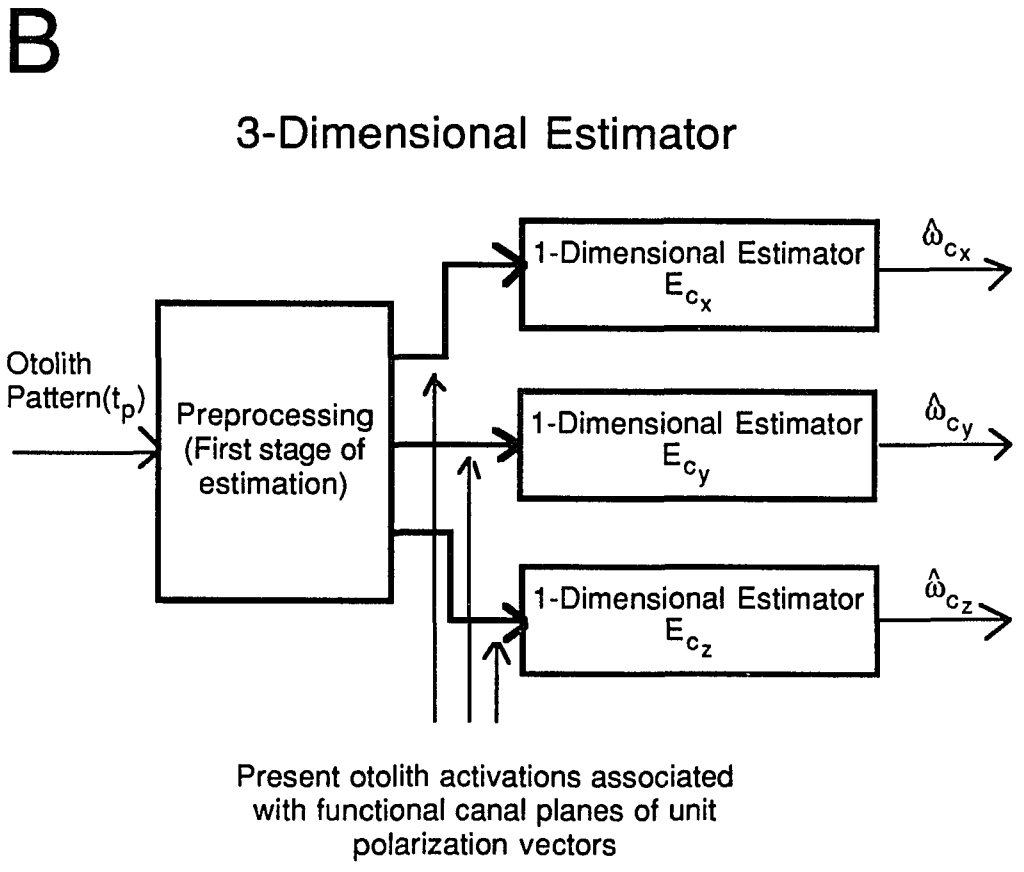
B
3-Dimensional Estimator
Otolith Pattern(t_p)
Preprocessing (First stage of estimation)
1-Dimensional Estimator E_{c_x}
1-Dimensional Estimator E_{c_y}
1-Dimensional Estimator E_{c_z}
$\hat{\omega}_{c_x}$
$\hat{\omega}_{c_y}$
$\hat{\omega}_{c_z}$
Present otolith activations associated with functional canal planes of unit polarization vectors

Fig. 3.2.6

algorithm for defining functional polarization planes is proposed in the next section.

Algorithm for Defining Functional Canal Planes for Otolith Polarization Vectors

At time t let $\underline{\hat{e}}_c^1(t)$ (x-axis or left anterior axis), $\underline{\hat{e}}_c^2(t)$ (y-axis or left posterior axis), and $\underline{\hat{e}}_c^3(t)$ (z-axis or left lateral axis) be a right-handed sequence of three orthonormal vectors fixed in the head (Fig. 3.2.5E), such that each of the three vectors is parallel to a different canal axis. These three canal basis vectors define the directions of the axes of the canal coordinate system with respect to the space coordinate system at time t. The three canal bases vectors, $\underline{\hat{e}}_c^1(t)$, $\underline{\hat{e}}_c^2(t)$, and $\underline{\hat{e}}_c^3(t)$, can be represented in space coordinates as follows

$$\underline{\hat{e}}_c^j(t) = \sum_{i=1}^{3} e_{ci}^j(t)\underline{\hat{e}}_s^i, \text{ for } j=1 \text{ to } 3, \tag{3.2.14}$$

where,

$$e_{cj}^i(t) = \langle \underline{\hat{e}}_s^j, \underline{\hat{e}}_c^i(t) \rangle, \text{ for } i=1 \text{ to } 3 \text{ and } j=1 \text{ to } 3. \tag{3.2.15}$$

Assume that on one side of the head, there are N unit

polarization vectors distributed over a sphere, where the i^{th} polarization vector, for i=0 to N-1, can be represented in canal coordinates as follows (Fig. 3.2.5F)

$$\hat{\underline{P}}^i(t) = \sum_{j=1}^{3} p^i_{jc}\,\hat{\underline{e}}^j_c(t), \text{ for } i=0 \text{ to } N-1. \qquad (3.2.16)$$

The coefficients in Eq (3.2.16) are given by

$$p^i_{jc} = \langle \hat{\underline{e}}^j_c(t), \hat{\underline{P}}^i(t) \rangle, \text{ for } i=0 \text{ to } N-1 \text{ and } j=1 \text{ to } 3, \qquad (3.2.17)$$

Note that from the assumption, that the i^{th} polarization vector with respect to the head is independent of time, it follows that each p^i_{jc}, for i=0 to N-1 and j=1 to 3, is independent of time. Therefore, the angles between the i^{th} unit polarization vector and each of the canal basis vectors, $\hat{\underline{e}}^1_c(t)$, $\hat{\underline{e}}^2_c(t)$, and $\hat{\underline{e}}^3_c(t)$, are independent of time, as they represent a head fixed frame.

The i^{th} unit polarization vector, for i=0 to N-1, can also be represented in three spherical canal coordinate systems each defined by the normal to a canal plane and two orthonormal vectors in the plane of the canal. In the l^{th} coordinate frame, l=1 to 3, the i^{th} unit polarization vector is associated with two angles, theta^i_l and phi^i_l where theta^i_l is a polar angle measured from $\hat{\underline{e}}^l_c(t)$ to $\hat{\underline{P}}^i(t)$ (Fig.

3.2.7A), and phi_1^i is an azimuthal angle measured clockwise about $\hat{\underline{e}}_c^1(t)$ from a reference direction $\hat{\underline{e}}_c^m(t)$ to the component of $\hat{\underline{P}}^i(t)$ perpendicular to $\hat{\underline{e}}_c^1(t)$, for m given by

$$m=\mathrm{mod}(1,3)+1, \tag{3.2.18}$$

where, mod(1,3) is read, 1 modulo 3, and is equal to the integer remainder of 1/3. Consider the otolith hair cells which have unit polarization vectors each of which have an azimuthal angle equal to phi_1^i (Fig. 3.2.7A). Find a subset, S_1^k, of this set of hair cells, such that the sum of all of the polarization vectors associated with the subset S_1^k is perpendicular to $\hat{\underline{e}}_c^1(t)$ (Fig. 3.2.7B). Assume that N_1 of these sums are nonzero. Number each sum, and its corresponding distinct azimuthal angle, from 0 to N_1-1, such that if $0\leq i<j<N_1$ then $phi_1^i<phi_1^j$. Let $\underline{P}_1^i(t)$, for i=0 to N_1-1, represent the i^{th} sum at time t as follows:

$$\underline{P}_1^i=\sum_{j\in S_1^i}\hat{\underline{P}}^j(t). \tag{3.2.19}$$

Let

$$h_1^i=phi_1^i, \text{ for } i=0 \text{ to } N_1-1. \tag{3.2.20}$$

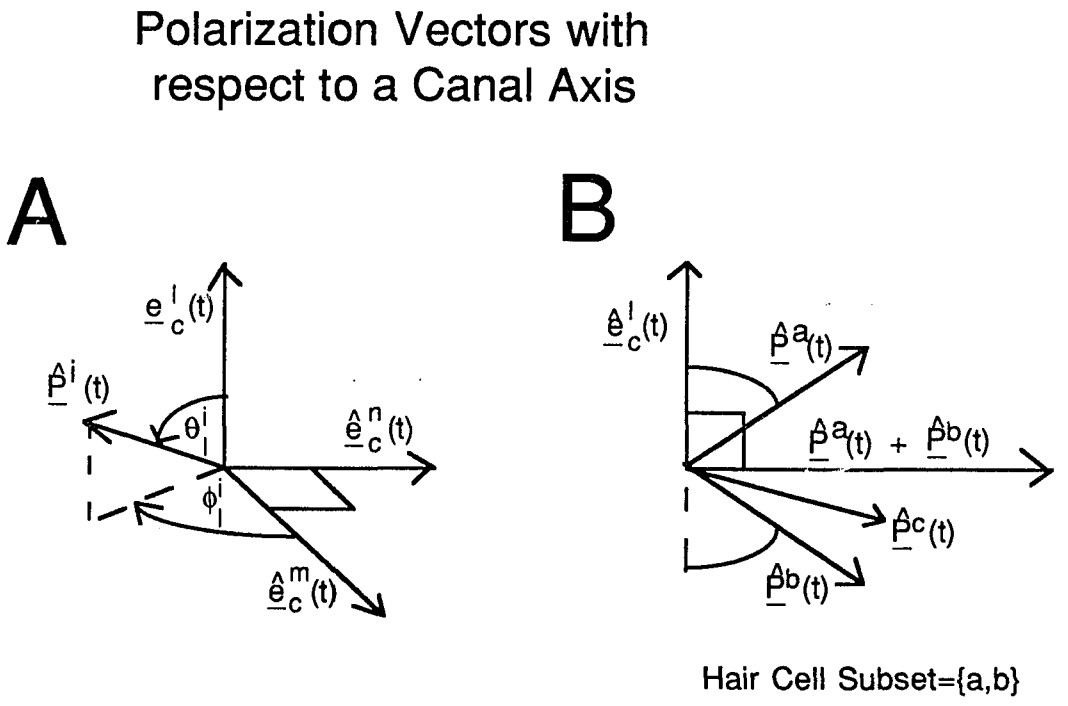

Fig. 3.2.7 To obtain a functional plane of polarization vectors about the l^{th} canal axes, unit polarization vectors must be appropriately combined.
A. Each unit polarization vector can be represented by spherical coordinates which are defined with respect to the l^{th} canal axis (and the m^{th} canal axis).
B. By adding appropriate unit polarization vectors (of otolith hair cells), with equal azimuthal angles about the l^{th} canal axis, a functional polarization vector perpendicular to the l^{th} canal axis can be obtained. The sum of the polar angles (with respect to the l^{th} canal axis) of the polarization vectors, associated which hair cells a and b, is 180 degrees. Therefore, this sum is perpendicular to the l^{th} canal axis.

Therefore, each of the vectors $\underline{P}_l^i(t)$ can be represented as follows Fig. 3.2.8):

$$\underline{P}_l^i(t)=k_l(h_l^i)[\cos(h_l^i)\hat{\underline{e}}_c^m(t)-\sin(h_l^i)\hat{\underline{e}}_c^n(t)], \quad \text{for } i=0 \text{ to } N_l-1 \text{ and } l=1 \text{ to } 3, \tag{3.2.21}$$

where $k_l(h_l^i)$ is the magnitude of $\underline{P}_l^i(t)$, and n is given by

$$n=\text{mod}(l+1,3)+1. \tag{3.2.22}$$

By normalizing each of the vectors in Eq (3.2.21) we obtain the following

$$\hat{\underline{P}}_l^i(t)=\cos(h_l^i)\hat{\underline{e}}_c^m(t)-\sin(h_l^i)\hat{\underline{e}}_c^n(t), \text{ for } i=0 \text{ to } N_l-1, \; l=1 \text{ to } 3. \tag{3.2.23}$$

We call the i^{th} vector, $\hat{\underline{P}}_l^i(t)$, the i^{th} unit polarization vector with respect to $\hat{\underline{e}}_c^l(t)$, for i=0 to N_l-1. At time t, the N_l unit polarization vectors with respect to the l^{th} canal basis vector, of Eq (3.2.23), are distributed in a two-dimensional space, for l=1 to 3.

The one-dimensional estimator of section 3.1, generates its estimate from activation patterns. Each activation value of a pattern at time t is assumed to be equal to the inner product of the corresponding unit polarization vector at time t with the acceleration due to gravity. Similarly, for the l^{th} component of the

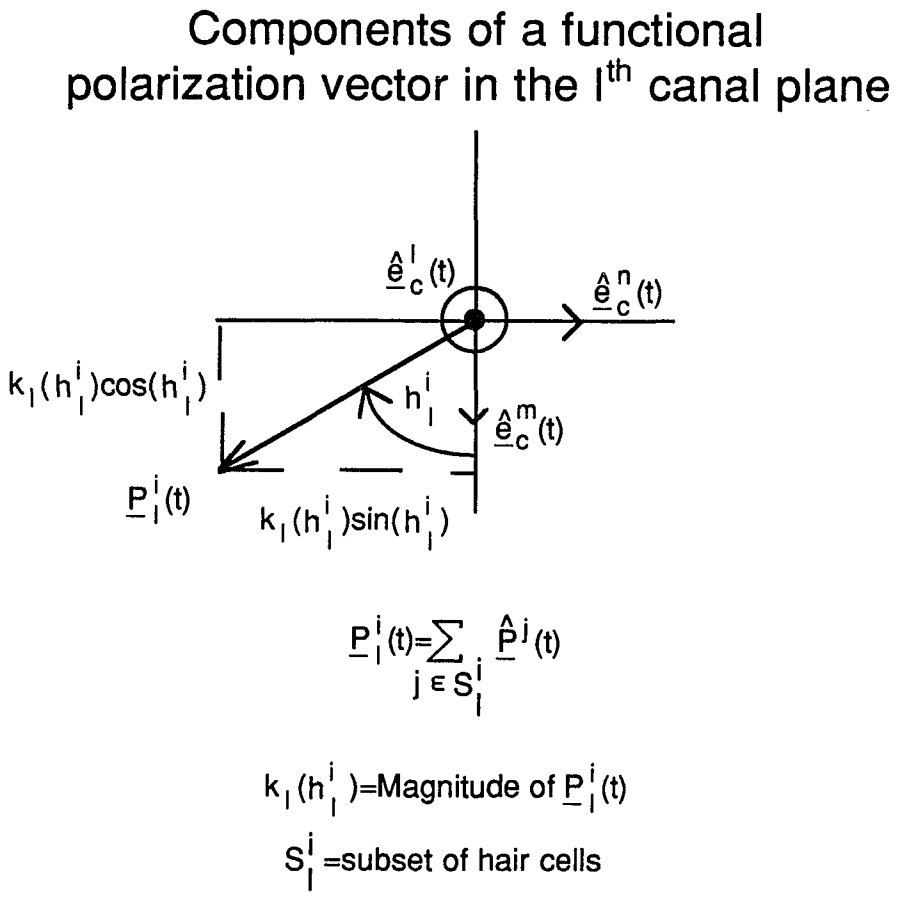

Fig. 3.2.8 A functional polarization vector of the l^{th} functional canal plane is shown decomposed into polar coordinates. The h_l^i correspond to the polarization angles of a one-dimensional estimator.

three-dimensional estimator, the i^{th} activation value of a pattern at time t is assumed to be equal to the inner product of the corresponding unit polarization vector with respect to $\underline{\hat{e}}_c^l(t)$ at time t with the acceleration due to gravity, for i=0 to N_{l-1}, for l=1 to 3, and is given by

$$r_l^i(t)=\langle \underline{g}, \underline{\hat{P}}_l^i(t) \rangle, \text{ for } i=0 \text{ to } N_l-1 \text{ and } l=1 \text{ to } 3. \tag{3.2.24}$$

In Eq (3.2.24), $r_l^i(t)$ is called the i^{th} activation with respect to $\underline{\hat{e}}_c^l(t)$.

It is assumed that the brain computes the i^{th} activation (of the l^{th} functional macula) with respect to $\underline{\hat{e}}_c^l(t)$ by summing the activations of all the hair cells which belong to a given subset S_l^i as defined above, for l=1 to 3 and i=0 to N_l-1. It is further assumed that the i^{th} sum of activations is multiplied by $1/k_l(h_l^i)$ obtaining $r_l^i(t)$, which is given in Eq (3.2.24) where $k_l(h_l^i)$ is a normalizing factor for polarization vector $\underline{P}_l^i(t)$ of Eq (3.2.21). Therefore, $r_l^i(t)$ can also be represented as follows:

$$r_l^i = \Big[\sum_{j \in S_l^i} r_j(t) \Big] / k_l(h_l^i). \tag{3.2.25}$$

How this estimator performs by having two patterns as input is considered next.

Three-Dimensional Estimator based on a Two-Pattern input

Denote the three-dimensional head angular velocity estimator by E_c, and its three one-dimensional components by E_{1c}, E_{2c}, and E_{3c}, (Fig 3.2.6B). Since, at time t, the estimator represents the estimate in canal coordinates, we represent the head angular velocity in canal coordinates as follows:

$$\underline{w} = \sum_{i=0}^{3} w_{ic}\underline{\hat{e}}_c^i(t), \tag{3.2.26}$$

and the estimate of the head angular velocity in canal coordinates as follows:

$$\underline{\hat{w}}(t) = \sum_{i=0}^{3} \hat{w}_{ic}(t)\underline{\hat{e}}_c^i(t), \tag{3.2.27}$$

where, the 1^{th} one-dimensional estimator E_{1c} computes $\hat{w}_{1c}(t_p)$, which is an estimate of $w_{1c}(t)$, for 1=1 to 3.

The 1th estimator, E_{1c}, at time t_p, computes the estimate $\hat{w}_{1c}(t_p)$ from the activations $r_1^i(t_p)$ and $r_1^i(t_d)$ for i=1 to N_1-1, for 1=1 to 3 (see Eqs (3.2.1), (3.2.2), and (3.2.24)). Assume that the azimuthal

angles, h_l^i, are uniformly spaced about $\underline{\hat{e}}_c^l(t)$ with spacing H_l. Therefore, each azimuthal angle h_l^i can be represented as follows:

$$h_l^i = iH_l \text{ for } i=0 \text{ to } N_l-1 \text{ and } l=1 \text{ to } 3. \tag{3.2.28}$$

The following algorithm (derived in section 3.1, Eq (3.1.30)) is used to compute the left-sided estimate of the l^{th} component of the head angular velocity along $\underline{\hat{e}}_c^l(t_p)$, at time t_p (Fig. 3.1.6):

$$\hat{w}_{lc}^L(t_p) = \langle [\text{Delay}(T)-I][\underline{r}_l^L(t_p)], (\text{RotateUp}-I)[\underline{r}_l^L(t_p)] \rangle / (\tau\tau Tg^2), \text{ for } l=1 \text{ to } 3, \tag{3.2.29}$$

where $\underline{r}_l^L(t_p)$ is the N_l^L-dimensional activation pattern vector with respect to $\underline{\hat{e}}_c^l(t_p)$ associated with the left maculae, for l=1 to 3. The operators $\langle,\rangle$, Delay(T)[.], and RotateUp[.] are defined in section 3.1. The l^{th} right-sided estimate of the component of the head velocity along $\underline{\hat{e}}_c^l(t_p)$ is obtained from Eq (3.2.29) by replacing H_l by $-H_l$

$$\hat{w}_{lc}^R(t_p) = \langle [\text{Delay}(T)-I][\underline{r}_l^R(t_p)], (\text{RotateUp}-I)[\underline{r}_l^R(t_p)] \rangle / (\tau\tau Tg^2), \text{ for } l=1 \text{ to } 3, \tag{3.2.30}$$

where $\underline{r}_l^R(t_p)$ is the N_l^R-dimensional activation pattern vector with respect to $\underline{\hat{e}}_c^l(t_p)$ associated with the right maculae, for l=1 to 3.

The estimate of the component of the head angular velocity along $\underline{\hat{e}}_c^l(t_p)$ due to both otoliths is therefore given by

$$\hat{w}_{lc}(t_p)=[\hat{w}^L_{lc}(t_p)-\hat{w}^R_{lc}(t_p)]/2, \text{ for } l=1 \text{ to } 3. \qquad (3.2.31)$$

Normalization of the Two-Pattern Three-Dimensional Estimator

As was stated at the beginning of this section, the horizontal component of the slow phase eye velocity during OVAR about the head yaw axis is approximately equal to the head angular velocity. Therefore, we must expect that the three-dimensional estimator, given in Eq (3.2.31), to generate a good estimate in this case. We choose to normalize the three-dimensional estimate, given in Eq (3.2.31), by normalizing the activations of the l^{th} component of the estimator with respect to the l^{th} canal axis. The normalization of the l^{th} component depends on the tilt of the l^{th} canal axis with respect to the gravitational field (Fig. 3.2.9). Therefore, each component is associated with a different normalization function of head orientation with respect to space.

At time t_p, the l^{th} estimators on each side of the head use information obtained at time t_p and at time t_d, for l=1 to 3. Therefore, to normalize the activations of the l^{th} estimator, the activations at time t_p and the activations at time t_d must separately be normalized. However, the bilinear form given in Eqs (3.2.29) and

Tilt Angles used for Estimate Normalization

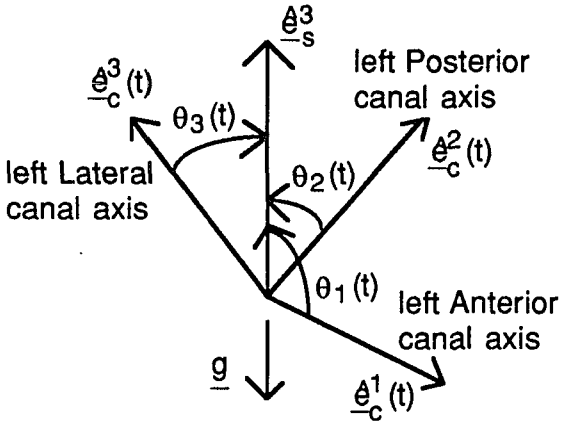

$\theta_1(t)$, $\theta_2(t)$, $\theta_3(t)$: Tilt angles of the canal axes with respect to the space vertical

Fig. 3.2.9 For each component of the estimate, the three-dimensional estimator, computes a normalization from the tilt angle of the corresponding canal axis.

(3.2.30) is the mechanism we have to normalize the estimate. We show that the bilinear form is sufficient to normalize the three-dimensional estimate. We will show that the estimate in Eq (3.2.31) is the sum of products where each product is formed by multiplying an activation at time t_d by a difference of activations at time t_p. Therefore, it is sufficient to multiply each estimate in Eq (3.2.31) by a corresponding normalization factor.

Using the following assumptions, we show that the estimate of Eq (3.2.31) can be computed from a knowledge of $\underline{r}_l^L$, for l=1 to 3. We assumed that for the l^{th} estimator, the corresponding polarization vectors were uniformly spaced, for l=1 to 3. In addition, we assume that the planar polarization vector distribution associated with the l^{th} estimator on the right side of the head is a mirror image of the planar polarization vector distribution associated with the l^{th} estimator on the left side of the head. Therefore, the i^{th} activation of the l^{th} one-dimensional right side estimator is equal to the N_l-i^{th} activation of the l^{th} one-dimensional left side estimator (Fig. 3.1.2A) for i=1 to N_l-1,

$$\underline{r}_{li}^R(t_p)=\underline{r}_{lN_l-i}^L(t_p), \text{ for } i=0 \text{ to } N_l-1 \text{ and } l=1 \text{ to } 3. \qquad (3.2.32)$$

From this it follows that the i^{th} component of RotateUp$[\underline{r}_l^R(t_p)]$ is equal to the N_l-i-1^{th} component of $\underline{r}_l^L(t_p)$. Therefore, we define another operator, RotateDown[.], such that it is the inverse of

RotateUp[.]

$$\text{RotateUp}[\text{RotateDown}(\underline{r})]=\text{RotateDown}[\text{RotateUp}(\underline{r})]=\underline{r}, \qquad (3.2.33)$$

where $\underline{r}$ is an N_1-dimensional vector. Therefore, the i^{th} component of RotateUp$[\underline{r}_1^R(t_p)]$ is equal to the N_1-i^{th} component of RotateDown$[\underline{r}_1^L(t_p)]$

$$\text{RotateUp}[\underline{r}_1^R(t_p)]_i=\text{RotateDown}[\underline{r}_1^L(t_p)]_{N1-i}, \qquad (3.2.34)$$

for i=0 to N_1-1 and 1=1 to 3.

Therefore, in Eq (3.2.30) by substituting Eqs (3.2.32) and (3.2.34) we obtain

$$\hat{w}_{1c}^R(t_p)= <[\text{Delay}(T)-I][\underline{r}_1^L(t_p)],(\text{RotateDown}-I)[\underline{r}_1^L(t_p)]>/(\tau\tau Tg^2), \qquad (3.2.35)$$

for 1=1 to 3,

since the results of the sums (bilinear forms) in Eqs (3.2.30) and (3.2.35) do not depend on the order in which the terms are summed. By substituting Eqs (3.2.29) and (3.2.35) into Eq (3.2.31) we obtain

$$\hat{w}_{lc}(t_p)=\langle[\text{Delay}(T)-I][\underline{r}_l^L(t_p)], \quad (3.2.36)$$
$$(\text{RotateUp}-\text{RotateDown})[\underline{r}_l^L(t_p)]\rangle/(2\tau\tau Tg^2),$$
$$\text{for } l=1 \text{ to } 3.$$

The term, in Eq (3.2.36), corresponding to the bilinear form of the identity operator and the difference of the rotation operators is zero since, the value of the form does not depend on the order in which the product terms are summed. Therefore, Eq (3.2.35) corresponds to a sum of product terms, where each term is the product of an activation at time t_d and a difference of activations at time t_p. Therefore, we choose to normalize the l^{th} estimate given in Eq (3.2.31) by dividing by the product of the sine of the angle of the l^{th} canal axis at time t_p with respect to the acceleration due to gravity and the sine of the angle of the l^{th} canal axis at time t_d with respect to the acceleration due to gravity. We denote the normalization by

$$K^l(t_d,t_p)=1/\{\sin[\measuredangle(-\underline{\hat{e}}_s^3,\underline{\hat{e}}_c^l(t_d)]\sin[\measuredangle(-\underline{\hat{e}}_s^3,\underline{\hat{e}}_c^l(t_p)]\}, \quad (3.2.37)$$
$$\text{for } l=1 \text{ to } 3,$$

where, $-\underline{\hat{e}}_s^3$ is a unit vector in the direction of the acceleration due to gravity and $\measuredangle(,)$ is equal to the smaller angle formed by rotating the first vector argument into the second vector argument. The normalization factor, $K^l(t_d,t_p)$ is positive, since the angle between a

canal axis and the acceleration due to gravity is between 0 and 180 degrees and the minus signs in Eq (3.2.37) can be combined.

The expression for the normalization factor in Eq (3.2.37) has to be modified so that the predictions of the estimate agree with experimental results. In OVAR experiments, the steady state slow phase eye velocity goes to zero as the head tilt goes to zero. Furthermore, for small head angular velocities of up to approximately 60 degrees/second about the head yaw axis and for tilt angles as small as approximately fifteen degrees, the slow phase horizontal eye velocity is approximately equal to the head angular velocity. These experimental results suggest that the normalization factor, given in Eq (3.2.37), should be modified. We assume that the normalization factor has an absolute maximum. In simulations, we choose a maximum value of

$$K^{l}_{max}(t_d,t_p)=1/[\sin(10^o)\sin(10^o)], \text{ for } l=1 \text{ to } 3. \qquad (3.2.38)$$

3.2.3 Estimation as a Function of Gravity, Head Angular Velocity, and Canal Orientation

The estimate, at time t, can be expressed as a function of the head angular velocity, $\underline{w}$, the orientation of the canal axes relative to space, gravity, and the time delay constant, T. Each component of the estimate along a canal axis can be described as a projection onto the canal axis of a linear combination of two space vectors (Fig. 3.2.10A): $\underline{w}_p$, the component of $\underline{w}$ perpendicular to $\underline{g}$ and the vector cross product of $\hat{\underline{e}}_s^3$ and $\underline{w}_p$. A normalization is introduced to compensate for the changing activations of the hair cells in the macula as the angle between the normal to the macula and $\underline{g}$ vary with time (Fig. 3.2.9). The following shows in detail, how this form of the estimate is derived and therefore, represented as a function of $\underline{g}$, $\underline{w}$, and the canal normals (Fig. 3.2.10B).

To obtain the estimate as a function of $\underline{w}$ and the canal orientation, we will consider the information from the left maculae. The bilinear form in Eq (3.2.29) which expresses the one-dimensional estimate can be given as follows:

$$\langle[\text{Delay}(T)-I][\underline{r}_l^L(t_p)],(\text{RotateUp}-I)[\underline{r}_l^L(t_p)]\rangle= \tag{3.2.39}$$

$$\sum_{i=0}^{N_l-1} [\text{Delay}(T)-I][\underline{r}_l^L(t_p)]_i K^l(t_d,t_p)(\text{RotateUp}-I)[\underline{r}_l^L(t_p)]_i,$$

$$\text{for } l=1 \text{ to } 3,$$

Fig. 3.2.10 The estimate of head angular velocity is a function of the head angular velocity, $\underline{w}$, the orientation of the canal axes relative to gravity, and gravity.
A. The estimate is a linear combination of the component of $\underline{w}$ perpendicular to gravity, $\underline{w}_p$, and a vector equal to the cross product of $\underline{w}_p$ with, $\hat{\underline{e}}_g$ or $\underline{g}$.
B. The l^{th} component of the estimate, $\hat{w}_l(t)$, is a normalizied linear combination of the projections of $\underline{w}_p$ and $\hat{\underline{e}}_g \times \underline{w}_p$ onto the l^{th} canal axis, $\hat{\underline{e}}_c$. One of the coefficients of the linear combination is dependent on the component of $\underline{w}$ parallel to $\hat{\underline{e}}_s$ or $\underline{g}$.

Estimate Components

A

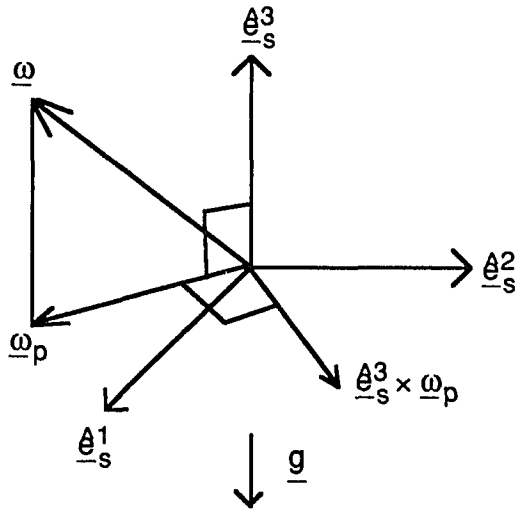

ω_p : component of ω perpendicular to g

B

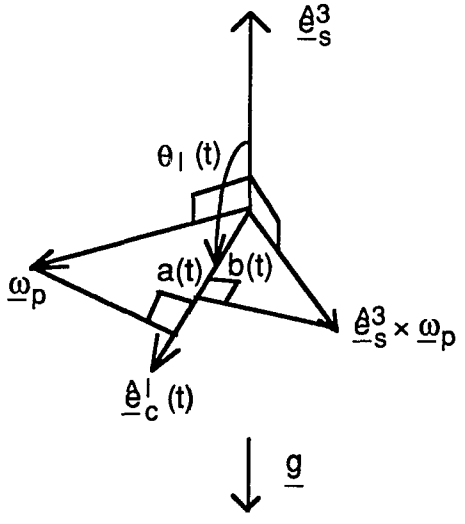

a(t):component of ω_p along $\hat{e}^I_c$ (t)

b(t):component of $\hat{e}^3_s \times \omega_p$ along $\hat{e}^I_c$ (t)

$\hat{\omega}_I$ (t) is a linear combination of a(t) and b(t) normalized with respect to tilt angle θ_I (t)

Fig. 3.2.10

where $K^l(t_d,t_p)$ is a normalization factor. In order to evaluate the bilinear form, the i^{th} component of $[\text{Delay}(T)-I][\underline{r}_l^L(t_p)]$ and the i^{th} component of $(\text{RotateUp}-I)[\underline{r}_l^l(t_p)]$ will be evaluated.

$$[\text{Delay}(T)-I][\underline{r}_l^L(t_p)]_i = r_l^{Li}(t_d) - r_l^{Li}(t_p), \qquad (3.2.40)$$
$$\text{for } i=0 \text{ to } N_l-1 \text{ and } l=1 \text{ to } 3.$$

From Eqs (3.2.24) and (3.2.40) we obtain

$$[\text{Delay}(T)-I][\underline{r}_l^L(t_p)]_i = \langle \underline{g}, \hat{\underline{P}}_l^i(t_d)\rangle - \langle \underline{g}, \hat{\underline{P}}_l^i(t_p)\rangle, \qquad (3.2.41)$$
$$\text{for } i=0 \text{ to } N_l-1 \text{ and } l=1 \text{ to } 3,$$

where, in Eq (3.2.41), $\hat{\underline{P}}^i$ refers to a polarization vector on the left side of the head. Using the bilinear property of the form $\langle,\rangle$, this may be reduced to

$$[\text{Delay}(T)-I][\underline{r}_l^L(t_p)]_i = \langle \underline{g}, \hat{\underline{P}}_l^i(t_d) - \hat{\underline{P}}_l^i(t_p)\rangle. \qquad (3.2.42)$$
$$\text{for } i=0 \text{ to } N_l-1 \text{ and } l=1 \text{ to } 3.$$

The i^{th} component of $(\text{RotateUp}-I)[\underline{r}_l^L(t_p)]$ in Eq (3.2.39) can be expressed as follows:

$$(\text{RotateUp}-I)[\underline{r}_l^L(t_p)]_i = \langle \underline{g}, \hat{\underline{P}}_l^{i+1}(t_p) - \hat{\underline{P}}_l^i(t_p)\rangle, \qquad (3.2.43)$$
$$\text{for } i=0 \text{ to } N_l-1 \text{ and } l=1 \text{ to } 3.$$

Using Eqs (3.2.18) and (3.2.22), the unit polarization vectors in Eqs (3.2.42) and (3.2.43) can be expressed as follows

$$\hat{\underline{P}}_l^i(t_d)=\cos(h_l^i)\hat{\underline{e}}_c^m(t_d)-\sin(h_l^i)\hat{\underline{e}}_c^n(t_d), \tag{3.2.44A}$$

$$\hat{\underline{P}}_l^i(t_p)=\cos(h_l^i)\hat{\underline{e}}_c^m(t_p)-\sin(h_l^i)\hat{\underline{e}}_c^n(t_p), \text{ and} \tag{3.2.44B}$$

$$\hat{\underline{P}}_l^{i+1}(t_p)=\cos(h_l^i+H_l)\hat{\underline{e}}_c^m(t_p)-\sin(h_l^i+H_l)\hat{\underline{e}}_c^n(t_p), \tag{3.2.44C}$$

$$\text{for } i=0 \text{ to } N_l-1 \text{ and } l=1 \text{ to } 3,$$

where the relation between t_p and t_d is given in Eqs (3.2.1) and (3.2.2), and where H_l is the constant difference $h_l^{i+1}-h_l^i$ for i=0 to N_l-1 (see Eq (3.2.28)). Furthermore, in Eqs (3.2.44), the h_l^i refer to angles on the left side of the head. In order to simplify Eq (3.2.39) let

$$\hat{\underline{l}}(t)=\hat{\underline{e}}_c^l(t), \tag{3.2.45A}$$

$$\hat{\underline{m}}(t)=\hat{\underline{e}}_c^m(t), \text{ and} \tag{3.2.45B}$$

$$\hat{\underline{n}}(t)=\hat{\underline{e}}_c^n(t), \tag{3.2.45C}$$

where $\hat{\underline{l}}$, $\hat{\underline{m}}$, and $\hat{\underline{n}}$ are normals to the individual canal planes. Let

$$d\hat{\underline{m}}(t)=\hat{\underline{e}}_c^m(t)-\hat{\underline{e}}_c^m(t-T) \text{ and} \tag{3.2.46A}$$

$$d\hat{\underline{n}}(t)=\hat{\underline{e}}_c^n(t)-\hat{\underline{e}}_c^n(t-T), \tag{3.2.46B}$$

where T is the time delay constant given in Eq (3.2.2). The difference between the two unit polarization vectors with respect to $\hat{\underline{e}}_c^l(t_d)$ and $\hat{\underline{e}}_c^l(t_p)$ in Eq (3.2.42) can be expressed as follows using Eqs (3.2.44) and (3.2.46):

$$\hat{\underline{P}}_l^i(t_d)-\hat{\underline{P}}_l^i(t_p)=-d\hat{\underline{m}}(t_p)\cos(h_l^i)+d\hat{\underline{n}}(t_p)\sin(h_l^i), \tag{3.2.47}$$
$$\text{for } i=0 \text{ to } N_l-1 \text{ and } l=1 \text{ to } 3.$$

The difference between the two unit polarization vectors, each with respect to $\hat{\underline{e}}_c^l(t_p)$ and given in Eq (3.2.43), can be expressed as follows using Eqs (3.2.44) and (3.2.45):

$$\hat{\underline{P}}_l^{i+1}(t_p)-\hat{\underline{P}}_l^i(t_p)= \hat{\underline{m}}(t_p)[\cos(h_l^i+H_l)-\cos(h_l^i)] \tag{3.2.48}$$
$$-\hat{\underline{n}}(t_p)[\sin(h_l^i+H_l)-\sin(h_l^i)],$$
$$\text{for } i=0 \text{ to } N_l-1 \text{ and } l=1 \text{ to } 3.$$

To obtain the ith product in Eq (3.2.39), multiply Eq (3.2.42) by Eq (3.2.43) and replace both unit polarization vector differences by using Eqs (3.2.47) and (3.2.48). Therefore, the following is obtained:

$$[\text{Delay}(T)-I][\underline{r}_1^L(t_p)]_i(\text{RotateUp}-I)[\underline{r}_1^L(t_p)]_i= \tag{3.2.49}$$
$$[-\langle \underline{g}, d\hat{\underline{m}}(t_p)\rangle \cos(h_1^i)+\langle \underline{g}, d\hat{\underline{n}}(t_p)\rangle \sin(h_1^i)]$$
$$\{\langle \underline{g}, \hat{\underline{m}}(t_p)\rangle [\cos(h_1^i+H_1)-\cos(h_1^i)]-\langle \underline{g}, \hat{\underline{n}}(t_p)\rangle [\sin(h_1^i+H_1)-\sin(h_1^i)]\},$$
$$\text{for } i=0 \text{ to } N_1-1 \text{ and } 1=1 \text{ to } 3,$$

where juxtaposition denotes multiplication. The following is obtained by expanding the product in Eq (3.2.49):

$$[\text{Delay}(T)-I][\underline{r}_1^1(t_p)]_i(\text{RotateUp}-I)[\underline{r}_1^1(t_p)]_i= \tag{3.2.50}$$
$$\{ -\langle \underline{g}, d\hat{\underline{m}}(t_p)\rangle \langle \underline{g}, \hat{\underline{m}}(t_p)\rangle [\cos(h_1^i)\cos(h_1^i+H_1)-\cos^2(h_1^i)]$$
$$+\langle \underline{g}, d\hat{\underline{m}}(t_p)\rangle \langle \underline{g}, \hat{\underline{n}}(t_p)\rangle [\cos(h_1^i)\sin(h_1^i+H_1)-\cos(h_1^i)\sin(h_1^i)]$$
$$+\langle \underline{g}, d\hat{\underline{n}}(t_p)\rangle \langle \underline{g}, \hat{\underline{m}}(t_p)\rangle [\sin(h_1^i)\cos(h_1^i+H_1)-\sin(h_1^i)\cos(h_1^i)]$$
$$-\langle \underline{g}, d\hat{\underline{n}}(t_p)\rangle \langle \underline{g}, \hat{\underline{n}}(t_p)\rangle [\sin(h_1^i)\sin(h_1^i+H_1)-\sin^2(h_1^i)] \},$$
$$\text{for } i=0 \text{ to } N_1-1 \text{ and } 1=1 \text{ to } 3.$$

To simplify Eq (3.2.50) replace each sinusoid and each cosine, which has $h_1^i+H_1$ as its argument, with the expansions given in Eqs (B1) and (B2), then sum Eq (3.2.50) from i=0 to N_1-1, and then use Eqs (B9), (B10), and (B11) to simplify the sum of the $\cos^2(h_1^i)$ terms, the sum of the $\sin^2(h_1^i)$ terms, and the sum of the $\sin(h_1^i)\cos(h_1^i)$ terms. After the previous manipulations of Eq (3.2.50) the following is obtained:

$$\sum_{i=0}^{N_l-1} [\text{Delay}(T)-I][\underline{r}_l^L(t_p)]_i(\text{RotateUp}-I)[\underline{r}_l^L(t_p)]_i=(N_l/2) \qquad (3.2.51)$$

$$\{ -\langle \underline{g},d\hat{\underline{m}}(t_p)\rangle\langle \underline{g},\hat{\underline{m}}(t_p)\rangle[\cos(H_l)-1]+\langle \underline{g},d\hat{\underline{l}}(t_p)\rangle\langle \underline{g},\hat{\underline{m}}(t_p)\rangle\sin(H_l)$$
$$-\langle \underline{g},d\hat{\underline{n}}(t_p)\rangle\langle \underline{g},\hat{\underline{m}}(t_p)\rangle\sin(H_l)-\langle \underline{g},d\hat{\underline{m}}(t_p)\rangle\langle \underline{g},\hat{\underline{m}}(t_p)\rangle[\cos(H_l)-1] \},$$
$$\text{for } l=1 \text{ to } 3.$$

To simplify Eq (3.2.51) we use the assumption that NH=2↑↑ and Eq (B1) with both A and B set equal to $H_l/2$, obtaining

$$\sum_{i=0}^{N_l-1} [\text{Delay}(T)-I][\underline{r}_i^L(t_p)]_i(\text{RotateUp}-I)[\underline{r}_l^L(t_p)]_i= \qquad (3.2.52)$$

$$\uparrow\uparrow * [\sin(H_l/2)/(H_l/2)]$$
$$\{ [\langle \underline{g},d\hat{\underline{m}}(t_p)\rangle\langle \underline{g},\hat{\underline{n}}(t_p)\rangle-\langle \underline{g},d\hat{\underline{n}}(t_p)\rangle\langle \underline{g},\hat{\underline{m}}(t_p)\rangle]\cos(H_l/2)$$
$$-[\langle \underline{g},d\hat{\underline{m}}(t_p)\rangle\langle \underline{g},\hat{\underline{m}}(t_p)\rangle-\langle \underline{g},d\hat{\underline{n}}(t_p)\rangle\langle \underline{g},\hat{\underline{n}}(t_p)\rangle]\sin(H_l/2) \},$$
$$\text{for } l=1 \text{ to } 3.$$

To simplify Eq (3.2.52), note that

$$\hat{\underline{m}}(t_d)=R_{\underline{w}}(-wT)\hat{\underline{m}}(t_p) \text{ and} \qquad (3.2.53A)$$

$$\hat{\underline{n}}(t_d)=R_{\underline{w}}(-wT)\hat{\underline{n}}(t_p), \qquad (3.2.53B)$$

where $R_{\underline{w}}(-wT)$ represents a rotation operator that rotates vectors

clockwise about the $\underline{w}$ axis by an angle wT and where $\underline{w}$ is the head angular velocity vector with magnitude w, and T is the time delay constant. Eqs (3.2.53) can be expressed as follows (see Goldstein, 1980):

$$\hat{\underline{m}}(t_d)= \hat{\underline{m}}(t_p)\cos(wT)+(\underline{w}/w)<(\underline{w}/w),\hat{\underline{m}}(t_p)>[1-\cos(wT)] \qquad (3.2.54A)$$
$$-(\underline{w}/w)X\hat{\underline{m}}(t_p)\sin(wT)$$

and

$$\hat{\underline{n}}(t_d)= \hat{\underline{n}}(t_p)\cos(wT)+(\underline{w}/w)<(\underline{w}/w),\hat{\underline{n}}(t_p)>[1-\cos(wT)] \qquad (3.2.54B)$$
$$-(\underline{w}/w)X\hat{\underline{n}}(t_p)\sin(wT),$$

where X represents the usual cross product operator and <,> is the usual inner product. The following expressions for $d\hat{\underline{m}}(t_p)$ and $d\hat{\underline{n}}(t_p)$ can be obtained from Eqs (3.2.46), (B7) and (3.2.54):

$$d\hat{\underline{m}}(t_p)=2\sin(wT/2)\{\ [\hat{\underline{m}}(t_p)-(\underline{w}/w)<(\underline{w}/w),\hat{\underline{m}}(t_p)>]\sin(wT/2) \qquad (3.2.55A)$$
$$+(\underline{w}/w)X\hat{\underline{m}}(t_p)\cos(wT/2)\ \}$$

and

$$d\hat{\underline{n}}(t_p)=2\sin(wT/2)\{\ [\hat{\underline{n}}(t_p)-(\underline{w}/w)<(\underline{w}/w),\hat{\underline{n}}(t_p)>]\sin(wT/2) \qquad (3.2.55B)$$
$$+(\underline{w}/w)X\hat{\underline{n}}(t_p)\cos(wT/2)\ \}$$

Let

$$\hat{\underline{k}}=\hat{\underline{e}}_s^3, \tag{3.2.56A}$$

$$w_z=w_3, \tag{3.2.56B}$$

$$l_z=\langle\hat{\underline{k}},\hat{\underline{l}}(t_p)\rangle, \tag{3.2.56C}$$

$$m_z=\langle\hat{\underline{k}},\hat{\underline{m}}(t_p)\rangle, \text{ and} \tag{3.2.56D}$$

$$n_z=\langle\hat{\underline{k}},\hat{\underline{n}}(t_p)\rangle, \tag{3.2.56E}$$

where $\hat{\underline{l}}(t_p)$, $\hat{\underline{m}}(t_p)$ and $\hat{\underline{n}}(t_p)$ are canal normals at time t_p (see Eq (3.2.45)), $\hat{\underline{e}}_s^3$ is oposite to gravity (see Eqs (3.2.3c) and (3.2.4)), and w_3 is the space vertical component of the head angular velocity. In Eq (3.2.52), replace $d\hat{\underline{m}}(t_p)$ and $d\hat{\underline{n}}(t_p)$ with the expressions given in Eqs (3.2.55), (3.2.56D), and (3.2.56E), and use Eqs (3.2.56B) and (3.2.56A) to obtain the following:

$$\sum_{i=0}^{N_1-1} [\text{Delay}(T)-I][\underline{r}_1^1(t_p)]_i(\text{RotateUp}-I)[\underline{r}_1^1(t_p)]_i = \tag{3.2.57}$$

$$wT[\sin(wT/2)/(wT/2)]\tau g^2[\sin(H_1/2)/(H_1/2)]$$

$$\{ (1/w)[\langle \hat{\underline{k}}, \underline{w}\underline{X}\hat{\underline{m}}(t_p)\rangle n_z - \underline{w}\underline{X}\hat{\underline{n}}(t_p)m_z\rangle]\cos(H_1/2)\cos(wT/2)$$

$$+(w_z/w^2)[\langle \underline{w}, \hat{\underline{n}}(t_p)\rangle m_z - \langle \underline{w}, \hat{\underline{m}}(t_p)\rangle n_z]\cos(H_1/2)\sin(wT/2)$$

$$+(1/w)[\langle \hat{\underline{k}}, \underline{w}\underline{X}\hat{\underline{m}}(t_p)\rangle m_z + \langle \hat{\underline{k}}, \underline{w}\underline{X}\hat{\underline{n}}(t_p)\rangle n_z]\sin(H_1/2)\cos(wT/2)$$

$$+\{m_z^2+n_z^2-(w_z/w^2)[\langle \underline{w}, \hat{\underline{m}}(t_p)\rangle m_z + \langle \underline{w}, \hat{\underline{n}}(t_p)\rangle n_z]\}\sin(H_1/2)\sin(wT/2) \},$$

for $l=1$ to 3.

In Eq (3.2.57), using the assumption that the polarization vectors with respect to $\hat{\underline{e}}_c^1$ are uniformly spaced about $\hat{\underline{e}}_c^1$, it is reasonable to expect that all references to $\hat{\underline{m}}(t_p)$ and $\hat{\underline{n}}(t_p)$ can be eliminated leaving only references to $\underline{w}$, $\underline{g}$, and $\hat{\underline{l}}(t_p)$.

The following are identities involving any three three-dimensional vectors $\underline{A}$, $\underline{B}$, and $\underline{C}$:

$$\underline{A}\underline{X}(\underline{B}\underline{X}\underline{C}) = \underline{B}\langle \underline{A}, \underline{C}\rangle - \underline{C}\langle \underline{A}, \underline{B}\rangle \text{ and} \tag{3.2.58A}$$

$$\langle \underline{A}, \underline{B}\underline{X}\underline{C}\rangle = \langle \underline{C}, \underline{A}\underline{X}\underline{B}\rangle. \tag{3.2.58B}$$

Consider the inner product $\langle \hat{\underline{k}}, \underline{w}\underline{X}\hat{\underline{m}}(t_p)\rangle n_z - \underline{w}\underline{X}\hat{\underline{n}}(t_p)m_z\rangle$ from Eq (3.2.57). In this inner product consider the left expression. In this expression factor out $\underline{w}$ obtaining

$$\langle\hat{\underline{k}},\underline{w}\underline{X}\hat{\underline{m}}(t_p)n_z-\underline{w}\underline{X}\hat{\underline{n}}(t_p)m_z\rangle= \tag{3.2.59}$$
$$\langle\hat{\underline{k}},\underline{w}\underline{X}[\hat{\underline{m}}(t_p)\langle\hat{\underline{k}},\hat{\underline{n}}(t_p)\rangle-\hat{\underline{n}}(t_p)\langle\hat{\underline{k}},\hat{\underline{m}}(t_p)\rangle]\rangle,$$

where m_z and n_z have been expanded according to Eqs (3.2.56D) and (3.2.56E). Compare the expression within the brackets in Eq (3.2.52) with Eq (3.2.58A) and make the following associations:

$$\underline{A}=\hat{\underline{k}}, \tag{3.2.60A}$$

$$\underline{B}=\hat{\underline{m}}(t_p), \text{ and} \tag{3.2.60B}$$

$$\underline{C}=\hat{\underline{n}}(t_p). \tag{3.2.60C}$$

Therefore, from Eqs (3.2.58), (3.2.59), and (3.2.60) the following is obtained:

$$\langle\hat{\underline{k}},\underline{w}\underline{X}\hat{\underline{m}}(t_p)n_z-\underline{w}\underline{X}\hat{\underline{n}}(t_p)m_z\rangle=\langle\hat{\underline{k}},\underline{w}\{\hat{\underline{k}}\underline{X}[\hat{\underline{m}}(t_p)\underline{X}\hat{\underline{n}}(t_p)]\}\rangle. \tag{3.2.61}$$

Since the vectors $\hat{\underline{l}}(t_p)$, $\hat{\underline{m}}(t_p)$, and $\hat{\underline{n}}(t_p)$ form a right-handed sequence of orthonormal vectors the following is obtained:

$$\hat{\underline{l}}(t_p)=\hat{\underline{m}}(t_p)\underline{X}\hat{\underline{n}}(t_p). \tag{3.2.62}$$

Combining Eqs (3.2.61) and (3.2.62) the following is obtained:

$$\langle\hat{\underline{k}},\underline{w}\hat{\underline{X}}\hat{\underline{m}}(t_p)n_z-\underline{w}\hat{\underline{X}}\hat{\underline{n}}(t_p)m_z\rangle=\langle\hat{\underline{k}},\underline{w}\{\hat{\underline{k}}\hat{\underline{X}}\hat{\underline{l}}(t_p)\}\rangle. \tag{3.2.63}$$

From Eq (3.2.63), it can be seen that all references to $\hat{\underline{m}}(t_p)$ and $\hat{\underline{n}}(t_p)$ in the inner product, $\langle\hat{\underline{k}},\underline{w}\hat{\underline{X}}\hat{\underline{m}}(t_p)n_z-\underline{w}\hat{\underline{X}}\hat{\underline{n}}(t_p)m_z\rangle$, can be removed. Eq (3.2.63) can be further manipulated by expanding the triple cross product using the identity in Eq (3.2.58A), then performing the inner product, and then factoring out $\hat{\underline{l}}(t_p)$. Therefore, the following is obtained:

$$\langle\hat{\underline{k}},\underline{w}\hat{\underline{X}}\hat{\underline{m}}(t_p)n_z-\underline{w}\hat{\underline{X}}\hat{\underline{n}}(t_p)m_z\rangle=\langle\hat{\underline{l}}(t_p),\underline{w}-w_z\hat{\underline{k}}\rangle. \tag{3.2.64}$$

In Eq (3.2.57), consider the expression $\langle\underline{w},\hat{\underline{n}}(t_p)\rangle m_z-\langle\underline{w},\hat{\underline{m}}(t_p)\rangle n_z$. By factoring $\hat{\underline{k}}$ we obtain the following:

$$\langle\underline{w},\hat{\underline{n}}(t_p)\rangle m_z-\langle\underline{w},\hat{\underline{m}}(t_p)\rangle n_z=\langle\hat{\underline{k}},\langle\underline{w},\hat{\underline{n}}(t_p)\rangle\hat{\underline{m}}(t_p)-\langle\underline{w},\hat{\underline{m}}(t_p)\rangle\hat{\underline{n}}(t_p)\rangle. \tag{3.2.65}$$

In the right-hand side of Eq (3.2.65), compare the left component of the inner with Eq (3.2.58A) and make the following associations:

$$\underline{A}=\underline{w}, \tag{3.2.66A}$$

$$\underline{B}=\hat{\underline{m}}(t_p), \text{ and} \tag{3.2.66B}$$

$$\underline{C}=\hat{\underline{n}}(t_p). \tag{3.2.66C}$$

Therefore, from Eqs (3.2.58A), (3.2.65), and (3.2.66) the following is obtained:

$$\langle \underline{w},\hat{\underline{n}}(t_p)\rangle m_z-\langle \underline{w},\hat{\underline{m}}(t_p)\rangle n_z=\langle \hat{\underline{k}},\underline{w}X[\hat{\underline{m}}(t_p)X\hat{\underline{n}}(t_p)]\rangle. \tag{3.2.67}$$

From Eqs (3.2.62) and (3.2.67) the following is obtained:

$$\langle \underline{w},\hat{\underline{n}}(t_p)\rangle m_z-\langle \underline{w},\hat{\underline{m}}(t_p)\rangle n_z=\langle \hat{\underline{k}},\underline{w}X\hat{\underline{l}}(t_p)\rangle. \tag{3.2.68}$$

In Eq (3.2.57), consider expression $\langle \hat{\underline{k}},\underline{w}X\hat{\underline{m}}(t_p)\rangle m_z+\langle \hat{\underline{k}},\underline{w}X\hat{\underline{n}}(t_p)\rangle n_z$. Applying the identity in Eq (3.2.58B) to this expression the following is obtained:

$$\langle \hat{\underline{k}},\underline{w}X\hat{\underline{m}}(t_p)\rangle m_z+\langle \hat{\underline{k}},\underline{w}X\hat{\underline{n}}(t_p)\rangle n_z=\langle \hat{\underline{m}}(t_p),\hat{\underline{k}}X\underline{w}\rangle m_z+\langle \hat{\underline{n}}(t_p),\hat{\underline{k}}X\underline{w}\rangle n_z. \tag{3.2.69}$$

By using the symmetric and bilinear properties of the inner product in Eq (3.2.69) the following is obtained:

$$\langle \hat{\underline{k}},\underline{w}X\hat{\underline{m}}(t_p)\rangle m_z+\langle \hat{\underline{k}},\underline{w}X\hat{\underline{n}}(t_p)\rangle n_z=\langle \hat{\underline{k}}X\underline{w},m_z\hat{\underline{m}}(t_p)+n_z\hat{\underline{n}}(t_p)\rangle. \tag{3.2.70}$$

The three vectors $\hat{\underline{l}}(t)$, $\hat{\underline{m}}(t)$, and $\hat{\underline{n}}(t)$, defined in Eq (3.2.45), form a right-handed sequence of orthonormal vectors. Therefore, at any given

time t_p any three-dimensional vector, such as $\hat{\underline{k}}$ (see Eq (3.2.56A)), can be represented as a linear combination of these three vectors. Therefore, $\hat{\underline{k}}$ can be represented as

$$\hat{\underline{k}}=l_z\hat{\underline{l}}(t)+m_z\hat{\underline{m}}(t)+n_z\hat{\underline{n}}(t), \tag{3.2.71}$$

where l_z, m_z, and n_z are given in Eqs (3.2.56C), (3.2.56D), and (3.2.56E). From Eqs (3.2.70) and (3.2.71) the following is obtained:

$$<\hat{\underline{k}},\underline{w}X\hat{\underline{m}}(t_p)>m_z+<\hat{\underline{k}},\underline{w}X\hat{\underline{n}}(t_p)>n_z=<\hat{\underline{k}}X\underline{w},\hat{\underline{k}}-l_z\hat{\underline{l}}(t_p)>. \tag{3.2.72}$$

The cross product $\hat{\underline{k}}X\underline{w}$ is perpendicular to each of its constituent vectors. Therefore, the following is obtained from Eq (3.2.72):

$$<\hat{\underline{k}},\underline{w}X\hat{\underline{m}}(t_p)>m_z+<\hat{\underline{k}},\underline{w}X\hat{\underline{n}}(t_p)>n_z=-<\hat{\underline{k}}X\underline{w},\hat{\underline{l}}(t_p)>l_z. \tag{3.2.73}$$

By using the identity in Eq (3.2.58B) the following is obtained:

$$<\hat{\underline{k}},\underline{w}X\hat{\underline{m}}(t_p)>m_z+<\hat{\underline{k}},\underline{w}X\hat{\underline{n}}(t_p)>n_z=-<\hat{\underline{k}},\underline{w}X\hat{\underline{l}}(t_p)>l_z. \tag{3.2.74}$$

In Eq (3.2.57), consider the expression $m_z^2+n_z^2-(w_z/w^2)(<\underline{w},\hat{\underline{m}}(t_p)>m_z+<\underline{w},\hat{\underline{n}}(t_p)>n_z)$. The subexpression $m_z^2+n_z^2$ can be simplified by using the expansion of $\hat{\underline{k}}$ given in Eq (3.2.71). The square of the magnitude of $\hat{\underline{k}}$ is given by the sum of the squares of the

coefficients in Eq (3.2.71). Since the magnitude of $\hat{\underline{k}}$ is one, the following is obtained:

$$l_z^2+m_z^2+n_z^2=1 \tag{3.2.75}$$

and $m_z^2+n_z^2$ can be expressed as

$$m_z^2+n_z^2=1-l_z^2. \tag{3.2.76}$$

Therefore, the expression in Eq (3.2.57) can be rewritten as follows:

$$m_z^2+n_z^2-(w_z/w^2)(\langle\underline{w},\hat{\underline{m}}(t_p)\rangle m_z+\langle\underline{w},\hat{\underline{n}}(t_p)\rangle n_z)= \tag{3.2.77}$$
$$1-l_z^2-(w_z/w^2)(\langle\underline{w},\hat{\underline{m}}(t_p)\rangle m_z+\langle\underline{w},\hat{\underline{n}}(t_p)\rangle n_z).$$

The references to $\hat{\underline{m}}(t)$ and $\hat{\underline{n}}(t)$ can be eliminated from the righthand side of Eq (3.2.77) as follows: Representing $\underline{w}$ as a linear combination of $\hat{\underline{l}}(t)$, $\hat{\underline{m}}(t)$, and $\hat{\underline{n}}(t)$, the following is obtained:

$$\underline{w}=\langle\underline{w},\hat{\underline{l}}(t)\rangle\hat{\underline{l}}(t)+\langle\underline{w},\hat{\underline{m}}(t)\rangle\hat{\underline{m}}(t)+\langle\underline{w},\hat{\underline{n}}(t)\rangle\hat{\underline{n}}(t). \tag{3.2.78}$$

Consider the inner product of $\hat{\underline{k}}$, as given in Eq (3.2.71), with $\underline{w}$ as given in Eq (3.2.78). Therefore, at time t_p the following is obtained:

$$\langle \underline{w},\hat{\underline{k}}\rangle = \tag{3.2.79}$$
$$\langle \underline{w},\hat{\underline{l}}(t_p)\rangle\langle \hat{\underline{k}},\hat{\underline{l}}(t_p)\rangle+\langle \underline{w},\hat{\underline{m}}(t_p)\rangle\langle \hat{\underline{k}},\hat{\underline{m}}(t_p)\rangle+\langle \underline{w},\hat{\underline{n}}(t_p)\rangle\langle \hat{\underline{k}},\hat{\underline{n}}(t_p)\rangle.$$

Using Eqs (3.2.56C), (3.2.56D), (3.2.56E), (3.2.77), and (3.2.79) the following is obtained:

$$m_z^2+n_z^2-(w_z/w^2)(\langle \underline{w},\hat{\underline{m}}(t_p)\rangle m_z+\langle \underline{w},\hat{\underline{n}}(t_p)\rangle n_z)= \tag{3.2.80}$$
$$1-l_z^2-(w_z/w^2)(\langle \underline{w},\hat{\underline{k}}\rangle-\langle \underline{w},\hat{\underline{l}}(t_p)\rangle\langle \hat{\underline{k}},\hat{\underline{l}}(t_p)\rangle).$$

Combining Eq (3.2.57) with Eqs (3.2.64), (3.2.68), (3.2.74), and (3.2.80) the following is obtained:

$$\sum_{i=0}^{N_l-1}[\text{Delay}(T)-I][\underline{r}_l^L(t_p)]_i(\text{RotateUp}-I)[\underline{r}_l^L(t_p)]_i= \tag{3.2.81}$$
$$wT[\sin(wT/2)/(wT/2)]\tau\tau g^2[\sin(H_l/2)/(H_l/2)]$$
$$\{(1/w)[\langle \underline{w}-\langle \hat{\underline{k}},\underline{w}\rangle\hat{\underline{k}},\hat{\underline{l}}(t_p)\rangle]\cos(H_l/2)\cos(wT/2)$$
$$+(1/w^2)\langle \hat{\underline{k}},\underline{w}\rangle\langle \hat{\underline{k}}X\underline{w},\hat{\underline{l}}(t_p)\rangle\cos(H_l/2)\sin(wT/2)$$
$$-(1/w)\langle \hat{\underline{k}},\hat{\underline{l}}(t_p)\rangle\langle \hat{\underline{k}}X\underline{w},\hat{\underline{l}}(t_p)\rangle\sin(H_l/2)\cos(wT/2)$$
$$+\{1-\langle \hat{\underline{l}}(t_p),\hat{\underline{k}}\rangle^2-(1/w^2)[\langle \hat{\underline{k}},\underline{w}\rangle^2-\langle \hat{\underline{l}}(t_p),\underline{w}\rangle\langle \underline{w},\hat{\underline{k}}\rangle\langle \hat{\underline{k}},\hat{\underline{l}}(t_p)\rangle]\}$$
$$\sin(H_l/2)\sin(wT/2)\},$$
$$\text{for } l=1 \text{ to } 3.$$

Therefore, the estimate of the component of head angular velocity along $\hat{\underline{e}}_c^1(t_p)$ can be expressed as follows by combining Eqs (3.2.29),

(3.2.37), (3.2.39), and (3.2.81):

$$\hat{w}^{L}_{lc}(t_p)=w[\sin(wT/2)/(wT/2)][\sin(H_l/2)/(H_l/2)]K^{l}(t_d,t_p) \quad (3.2.82)$$
$$\{ (1/w)[\langle\hat{\underline{l}}(t_p),\underline{w}\rangle-\langle\hat{\underline{k}},\underline{w}\rangle\langle\hat{\underline{l}}(t_p),\hat{\underline{k}}\rangle]\cos(H_l/2)\cos(wT/2)$$
$$+(1/w^2)\langle\hat{\underline{k}},\underline{w}\rangle\langle\underline{w}\times\hat{\underline{l}}(t_p),\hat{\underline{k}}\rangle\cos(H_l/2)\sin(wT/2)$$
$$-(1/w)\langle\hat{\underline{k}},\hat{\underline{l}}(t_p)\rangle\langle\underline{w}\times\hat{\underline{l}}(t_p),\hat{\underline{k}}\rangle\sin(H_l/2)\cos(wT/2)$$
$$+\{ 1-\langle\hat{\underline{k}},\hat{\underline{l}}(t_p)\rangle\langle\hat{\underline{l}}(t_p),\hat{\underline{k}}\rangle$$
$$-(1/w^2)[\langle\hat{\underline{k}},\underline{w}\rangle\langle\underline{w},\hat{\underline{k}}\rangle-\langle\hat{\underline{k}},\underline{w}\rangle\langle\underline{w},\hat{\underline{l}}(t_p)\rangle\langle\hat{\underline{l}}(t_p),\hat{\underline{k}}\rangle] \}$$
$$\sin(H_l/2)\sin(wT/2) \},$$
$$\text{for } l=1 \text{ to } 3.$$

By the use of symmetry and Eq (3.2.30), the estimate of the component of the head angular velocity along $\hat{\underline{e}}^{l}_{c}(t_p)$ utilizing information from the right maculae can be given by

$$\hat{w}^{R}_{lc}(t_p)=w[\sin(wT/2)/(wT/2)][\sin(H_l/2)/(H_l/2)]K^{l}(t_d,t_p) \quad (3.2.83)$$
$$\{-(1/w)[\langle\hat{\underline{l}}(t_p),\underline{w}\rangle-\langle\hat{\underline{k}},\underline{w}\rangle\langle\hat{\underline{l}}(t_p),\hat{\underline{k}}\rangle]\cos(H_l/2)\cos(wT/2)$$
$$-(1/w^2)\langle\hat{\underline{k}},\underline{w}\rangle\langle\underline{w}\times\hat{\underline{l}}(t_p),\hat{\underline{k}}\rangle\cos(H_l/2)\sin(wT/2)$$
$$-(1/w)\langle\hat{\underline{k}},\hat{\underline{l}}(t_p)\rangle\langle\underline{w}\times\hat{\underline{l}}(t_p),\hat{\underline{k}}\rangle\sin(H_l/2)\cos(wT/2)$$
$$+\{ 1-\langle\hat{\underline{k}},\hat{\underline{l}}(t_p)\rangle\langle\hat{\underline{l}}(t_p),\hat{\underline{k}}\rangle$$
$$-(1/w^2)[\langle\hat{\underline{k}},\underline{w}\rangle\langle\underline{w},\hat{\underline{k}}\rangle-\langle\hat{\underline{k}},\underline{w}\rangle\langle\underline{w},\hat{\underline{l}}(t_p)\rangle\langle\hat{\underline{l}}(t_p),\hat{\underline{k}}\rangle] \}$$
$$\sin(H_l/2)\sin(wT/2) \},$$
$$\text{for } l=1 \text{ to } 3.$$

where the H_1, in Eq. (3.2.83), refer to angles on the right side of the head. By substituting Eqs (3.2.82) and (3.2.83) into Eq (3.2.31), assuming that corresponding H_1 on the left side of the head and on the right side of the head are equal, and using Eq (3.2.58B), the following estimate of the component of the head angular velocity along $\hat{\underline{e}}_c^1(t_p)$ is obtained:

$$\hat{w}_{1c}(t_p)=w[\sin(wT/2)/(wT/2)][\sin(H_1/2)\cos(H_1/2)/(H_1/2)] \quad (3.2.84)$$
$$K^1(t_d,t_p)[\ (1/w)\langle \underline{w}-\langle \underline{w},\hat{\underline{k}}\rangle\hat{\underline{k}},\hat{\underline{l}}(t_p)\rangle\cos(wT/2)$$
$$+(1/w^2)\langle \underline{w},\hat{\underline{k}}\rangle\langle \hat{\underline{k}}X\underline{w},\hat{\underline{l}}(t_p)\rangle\sin(wT/2)\ ],$$
$$\text{for } l=1 \text{ to } 3.$$

Substituting Eqs (3.1.102), (3.2.45A) and (3.2.56A) into Eq (3.2.84), the estimate of the component of the head angular velocity along $\hat{\underline{e}}_c^1(t_p)$ is expressed as

$$\hat{w}_{1c}(t_p)=wC(H_1)[\sin(wT/2)/(wT/2)]K^1(t_d,t_p) \quad (3.2.85)$$
$$[\ (1/w)\langle \underline{w}-\langle \underline{w},\hat{\underline{e}}_s^3\rangle\hat{\underline{e}}_s^3,\hat{\underline{e}}_c^1(t_p)\rangle\cos(wT/2)$$
$$+(1/w^2)\langle \underline{w},\hat{\underline{e}}_s^3\rangle\langle \hat{\underline{e}}_s^3X\underline{w},\hat{\underline{e}}_c^1(t_p)\rangle\sin(wT/2)\ ], \text{ for } l=1 \text{ to } 3.$$

The estimate in three dimensions is given by a linear combination of the components in Eq (3.2.85):

$$\underline{\hat{w}}_c(t_p)=\sum_{l=1}^{3}\hat{w}_{lc}(t_p)\underline{\hat{e}}_c^l(t_p). \tag{3.2.86}$$

The constants, $C(H_l)$ for l=1 to 3, can be eliminated from Eq (3.2.85) by either dividing each component of Eq (3.2.85) by $C(H_l)$ or by noting that if each H_l is small then, $C(H_l)$ is approximately unity.

To gain better insight into the meaning of Eq (85), we allow

$$\underline{w}_p=\underline{w}-\langle\underline{w},\underline{\hat{e}}_s^3\rangle\underline{\hat{e}}_s^3, \tag{3.2.87}$$

where $\underline{w}_p$ is the component of the head angular velocity, $\underline{w}$, perpendicular to the acceleration due to gravity, $\underline{g}$ (Fig. 3.2.10A). It shoud be noted that

$$\langle\underline{g},\underline{w}_p\rangle=0, \tag{3.2.88}$$

and therefore, $\underline{w}$ can be expressed in terms of $\underline{w}_p$ as follows:

$$\underline{w}=\underline{w}_p+w_3\underline{\hat{e}}_s^3, \tag{3.2.89}$$

where w_3 is the component of $\underline{w}$ parallel to gravity (but in the opposite direction), and is given by

$$w_3=\langle \hat{e}_s^3, \underline{w}\rangle. \tag{3.2.90}$$

Let

$$w_p=|\underline{w}_p| \tag{3.2.91}$$

be the magnitude of $\underline{w}_p$. From Eq (3.2.89) it follows that (Fig. 3.2.10A)

$$\hat{e}_s^3 X \underline{w}=\hat{e}_s^3 X \underline{w}_p=\underline{w}_p X \underline{g}/g. \tag{3.2.92}$$

The magnitude of $\hat{e}_s^3 X \underline{w}_p$ is given by

$$|\hat{e}_s^3 X \underline{w}_p|=w_p. \tag{3.2.93}$$

For constant head angular velocity, $\hat{e}_s^3$, $\underline{w}_p$, and $\hat{e}_s^3 X \underline{w}_p$ form a right-handed orthogonal sequence of three vectors fixed in space (Fig. 3.2.10A). Combining Eqs (3.2.87) and (3.2.92) with Eq (3.2.85) we obtain

$$\begin{aligned}\hat{w}_{lc}(t_p)=w[\sin(wT/2)/(wT/2)]K^l(t_d,t_p) \qquad (3.2.94)\\ [\ (1/w)\langle \underline{w}_p, \hat{e}_c^l(t_p)\rangle \cos(wT/2)\\ +(1/w^2)w_3\langle \hat{e}_s^3 X \underline{w}_p, \hat{e}_c^l(t_p)\rangle \sin(wT/2)\ ],\ \text{for } l=1 \text{ to } 3.\end{aligned}$$

Since the sine function lags the cosine function by 90 degrees Eq (3.2.94) can be expressed as follows (Fig. 3.2.10B)

$$\hat{w}_{lc}(t_p)=w[\sin(wT/2)/(wT/2)]K^{l}(t_d,t_p) \qquad (3.2.95)$$
$$[\ (1/w)\langle \underline{w}_p,\underline{\hat{e}}^{l}_{c}(t_p)\rangle\cos(wT/2)$$
$$+(1/w^2)w_3\langle \underline{\hat{e}}^{3}_{s}X\underline{w}_p,\underline{\hat{e}}^{l}_{c}(t_p)\rangle\cos(wT/2-\uparrow\uparrow/2)\ ],\ \text{for } l=1 \text{ to } 3.$$

The estimate in Eq (3.2.95) is composed of two terms

$$\hat{w}_{lc}(t_p)=\hat{w}_{lc1}(t_p)+\hat{w}_{lc2}(t_p), \qquad (3.2.96)$$

where

$$\hat{w}_{lc1}(t_p)=K^{l}(t_d,t_p)[\sin(wT/2)/(wT/2)] \qquad (3.2.97A)$$
$$\langle \underline{w}_p,\underline{\hat{e}}^{l}_{c}(t_p)\rangle\cos(wT/2),\ \text{for } l=1 \text{ to } 3,$$

and

$$\hat{w}_{lc2}(t_p)=K^{l}(t_d,t_p)[\sin(wT/2)/(wT/2)] \qquad (3.2.97B)$$
$$(w_3/w)\langle \underline{\hat{e}}^{3}_{s}X\underline{w}_p,\underline{\hat{e}}^{l}_{c}(t_p)\rangle\cos(wT/2-\uparrow\uparrow/2),\ \text{for } l=1 \text{ to } 3.$$

The three factors, $\langle \underline{w}_p,\underline{\hat{e}}^{l}_{c}(t_p)\rangle$ for l=1 to 3, of the first component, $\hat{w}_{lc1}(t_p)$, of the estimate, $\hat{w}_{lc}(t_p)$, form the component of the head

angular velocity perpendicular to the acceleration due to gravity, $\underline{w}_p$, represented in canal coordinates. Each factor, $\langle \underline{w}_p, \hat{\underline{e}}_c^1(t_p) \rangle$, is normalized by $K^1(t_d,t_p)$ which is determined by the orientation of the 1^{th} canal axis relative to $\underline{g}$. The three factors, $\langle \hat{\underline{e}}_s^3 X \underline{w}_p, \hat{\underline{e}}_c^1(t_p) \rangle$ for 1=1 to 3, of the second component, $\hat{w}_{1c2}(t_p)$, of the estimate form $\hat{\underline{e}}_s^3 X \underline{w}_p$, represented in canal coordinates. Each factor, $\langle \hat{\underline{e}}_s^3 X \underline{w}_p, \hat{\underline{e}}_c^1(t_p) \rangle$, is normalized by $K^1(t_d,t_p)$. Further, the second component of the estimate is multiplied by w_3/w which is equal to the cosine of the angle between $\underline{w}$ and, $\hat{\underline{e}}_s^3$ or $\underline{g}$.

From this analysis, the estimate along each canal plane normal is comprised of two components. One is the projection onto the canal normal of a vector along the head angular velocity component perpendicular to gravity. Another is the projection of a vector which is along the cross product in space of the head angular velocity with gravity. This is shown in Fig. (Fig. 3.2.10B) where the head angular velocity $\underline{w}$, and gravity, $\underline{g}$, have induced spacial vectors $\underline{w}_p$ and $\underline{w}_p x \underline{g}$. A linear combination of these vectors is projected onto the canal normal. Each projection along a canal normal is then normalized according to the tilt angle of the canal axis with regard to gravity.

In the next section we examine the three dimensional estimator and how it behaves for rotations of the head when the angular velocity vector is aligned with a canal plane normal.

3.2.4 Analysis of the Three-Dimensional Estimator for Head Angular Velocity Parallel to a Canal Axis

If the head angular velocity, $\underline{w}$, is parallel to the macular normal $\hat{\underline{e}}_c^1(t_p)$ (Fig. 3.2.1A) then, $\hat{w}_{1c}(t_p)$, for 1=0, 1, or 2, is a time independent estimate of the magnitude of the head angular velocity, w, and corresponds to the one-dimensional estimate obtained in section 3.1.2. We will show that under these circumstances the estimate of head angular velocity given by Eq (3.2.31) along that normal reduces to that of Eq (3.1.44).

Let the head angular velocity be parallel to $\hat{\underline{e}}_c^q$, for q=1, 2, or 3, such that

$$\underline{w}=w\hat{\underline{e}}_c^q(t). \tag{3.2.98}$$

Generally, as $\hat{\underline{e}}_c^q(t)$ rotates its direction changes. The time dependence of $\hat{\underline{e}}_c^q(t)$ comes from the rotating semi-circular canals. Since $\underline{w}$ is an eigenvector of the rotation operator so is $\hat{\underline{e}}_c^q(t)$. Therefore, the direction of $\hat{\underline{e}}_c^q(t)$ is independent of the rotation about $\underline{w}$ and therefore, independent of time t. Furthermore, since $K^q(t_d,t_p)$ depends on the angle between $\hat{\underline{e}}_c^q$ and the acceleration due to gravity. Since $\hat{\underline{e}}_c^q$ is independent of time so is K^q. By substituting Eq (3.2.98) into Eq (3.2.85) the following is obtained:

$$\hat{w}_{1c}(t_p)=wC(H_1)[\sin(wT/2)/(wT/2)]K^1(t_d,t_p) \qquad (3.2.99)$$
$$[\ (1/w)<w\hat{e}^q_c-<w\hat{e}^q_c,\hat{e}^3_s>,\hat{e}^1_c(t_p)>\cos(wT/2)$$
$$+(1/w^2)<w\hat{e}^q_c,\hat{e}^3_s><\hat{e}^3_s X w\hat{e}^q_c,\hat{e}^1_c(t_p)>\sin(wT/2)\ ],\ \text{for } 1=1 \text{ to } 3.$$

If in Eq (3.2.99) q is equal to 3, 1 is equal to 3, and we drop the factor $C(H_1)$ we obtain

$$\hat{w}_{3c}=w[\sin(wT/2)/(wT/2)]K^3 \qquad (3.2.100)$$
$$[\ (1/w)<w\hat{e}^3_c-<w\hat{e}^3_c,\hat{e}^3_s>\hat{e}^3_s,\hat{e}^3_c>\cos(wT/2)$$
$$+(1/w^2)<w\hat{e}^3_c,\hat{e}^3_s><\hat{e}^3_s X w\hat{e}^3_c,\hat{e}^3_c>\sin(wT/2)\ ],$$

where, $\hat{w}_{3c}$ is independent of time. In Eq (3.2.100), $\hat{e}^3_s X w\hat{e}^3_c$ is perpendicular to $\hat{e}^3_c$ and therefore, we obtain

$$\hat{w}_{3c}=w[\sin(wT/2)/(wT/2)]K^3 \qquad (3.2.101)$$
$$[\ (1/w)<w\hat{e}^3_c-<w\hat{e}^3_c,\hat{e}^3_s>\hat{e}^3_s,\hat{e}^3_c>\cos(wT/2)\ ].$$

Using the trigonometric identity given in Eq (B1) with both A and B set equal to wT/2, we obtain

$$\hat{w}_{3c}=w[\sin(wT)/(wT)]K^3[\ (1/w)<w\hat{e}^3_c-<w\hat{e}^3_c,\hat{e}^3_s>\hat{e}^3_s,\hat{e}^3_c>\ ]. \qquad (3.2.102)$$

Since the inner product operator <,> is linear, w can be factored out in Eq (3.2.102) obtaining

$$\hat{w}_{3c}=w[\sin(wT)/(wT)]K^3[\ \langle \underline{\hat{e}}_c^3-\langle \underline{\hat{e}}_c^3,\underline{\hat{e}}_s^3\rangle \underline{\hat{e}}_s^3,\underline{\hat{e}}_c^3\rangle\ ]. \tag{3.2.103}$$

By performing the inner products in Eq (3.2.103) we obtain

$$\hat{w}_{3c}=w[\sin(wT)/(wT)]K^3(1-\langle \underline{\hat{e}}_c^3,\underline{\hat{e}}_s^3\rangle^2). \tag{3.2.104}$$

The expression, $(1-\langle \underline{\hat{e}}_c^3,\underline{\hat{e}}_s^3\rangle^2)$, in Eq (3.2.104) is equal to the square of the sine of the angle between gravity and $\underline{\hat{e}}_c^3$ which is the reciprocal of K^3 (Eq (3.2.37)). Therefore, we obtain

$$\hat{w}_{3c}=w[\sin(wT)/(wT)]. \tag{3.2.105}$$

Eq (3.2.105) is equal to the one-dimensional estimate obtained in section 3.1.2.

Simulations and predictions of the estimator are considered next.

3.2.5 Two-Pattern Estimator, Simulations and Results

In this section, we present the results from simulations of OVAR assuming that the brain utilizes a two-pattern three-dimensional head velocity estimator (Eq (3.2.39)) and a time delay constant, T, of 0.85 seconds for consistency with the one-dimensional estimator. Further, it is assumed that the left canal axes relative to the head are pitched back by 15 degrees and then rotated (to the left) by 45 degrees about the left lateral canal axis. The intial conditions of many simulations correspond to an experiment in which the head is initially pitched forward by 30 degreees and is rotating to the left at 60 degrees/second about the head yaw axis. The results from one simulation corresponding to the given initial conditions are shown in Fig. 3.2.11.

Under these initial conditions and assumptions the angle between the head velocity and the left lateral canal axis is 15 degrees, and the angle between the left anterior (or posterior) canal axis and the head velocity is approximately 100 degrees. The results shown in Fig. 3.2.11 predict that the component of the estimate about this normal oscillates with a period equal to the period of head rotation. The number of extremum in one head rotation is dependent on the head angular velocity. For an angular velocity of 60 degrees/second there are two extremum (see Fig. 3.2.11) but, for a head velocity of 90 degrees/second there are four extremum (see Fig. 3.2.12). This is

Fig. 3.2.11 Output in canal coordinates from the two-pattern estimator as a function of time or head rotation angle: The time delay constant is 0.85 seconds. The left semicircular canals are pitched back by 15 degrees, and then rotated by 45 degrees to the left about the left lateral canal axis, relative to the head. The head is initially pitched forward by 30 degrees. The magnitude of the head angular velocity is 60 degrees/second.
A. The maximum and minimum values of the left anterior signal are approximately 35 and -30 degrees/second, respectively. The bias is approximately zero.
B. The maximum and minimum values of the left posterior signal are approximately 35 and -30 degrees/second, respectively. The bias is approximately zero.
C. The maximum and minimum values of the left lateral signal are approximately 67 and 40 degrees/second, respectively. The bias is approximately 55 degrees/second.

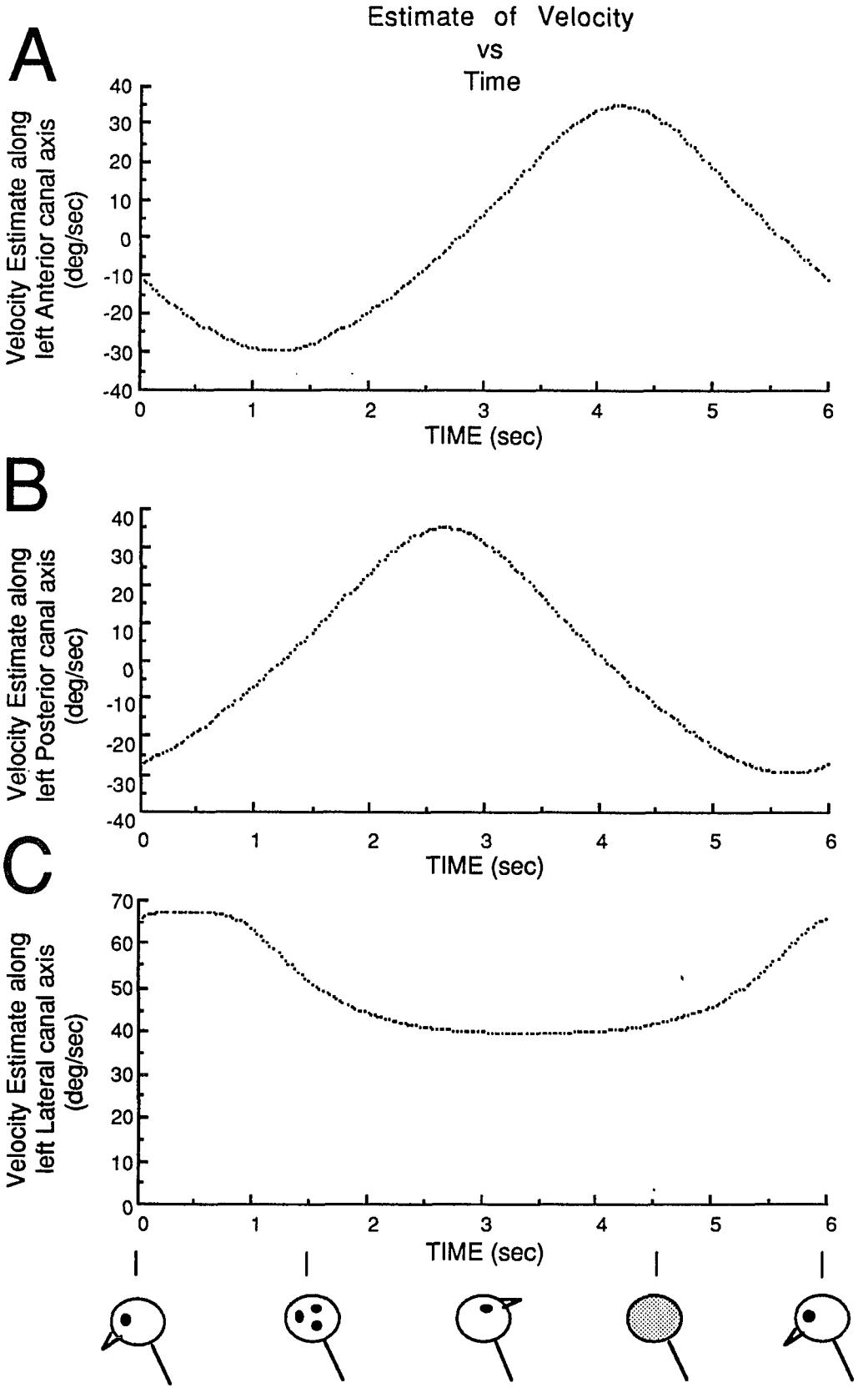
A
Estimate of Velocity
vs
Time
Velocity Estimate along
left Anterior canal axis
(deg/sec)
40
30
20
10
0
-10
-20
-30
-40
0
1
2
3
4
5
6
TIME (sec)
B
Velocity Estimate along
left Posterior canal axis
(deg/sec)
40
30
20
10
0
-10
-20
-30
-40
0
1
2
3
4
5
6
TIME (sec)
C
Velocity Estimate along
left Lateral canal axis
(deg/sec)
70
60
50
40
30
20
10
0
0
1
2
3
4
5
6
TIME (sec)

Fig. 3.2.11

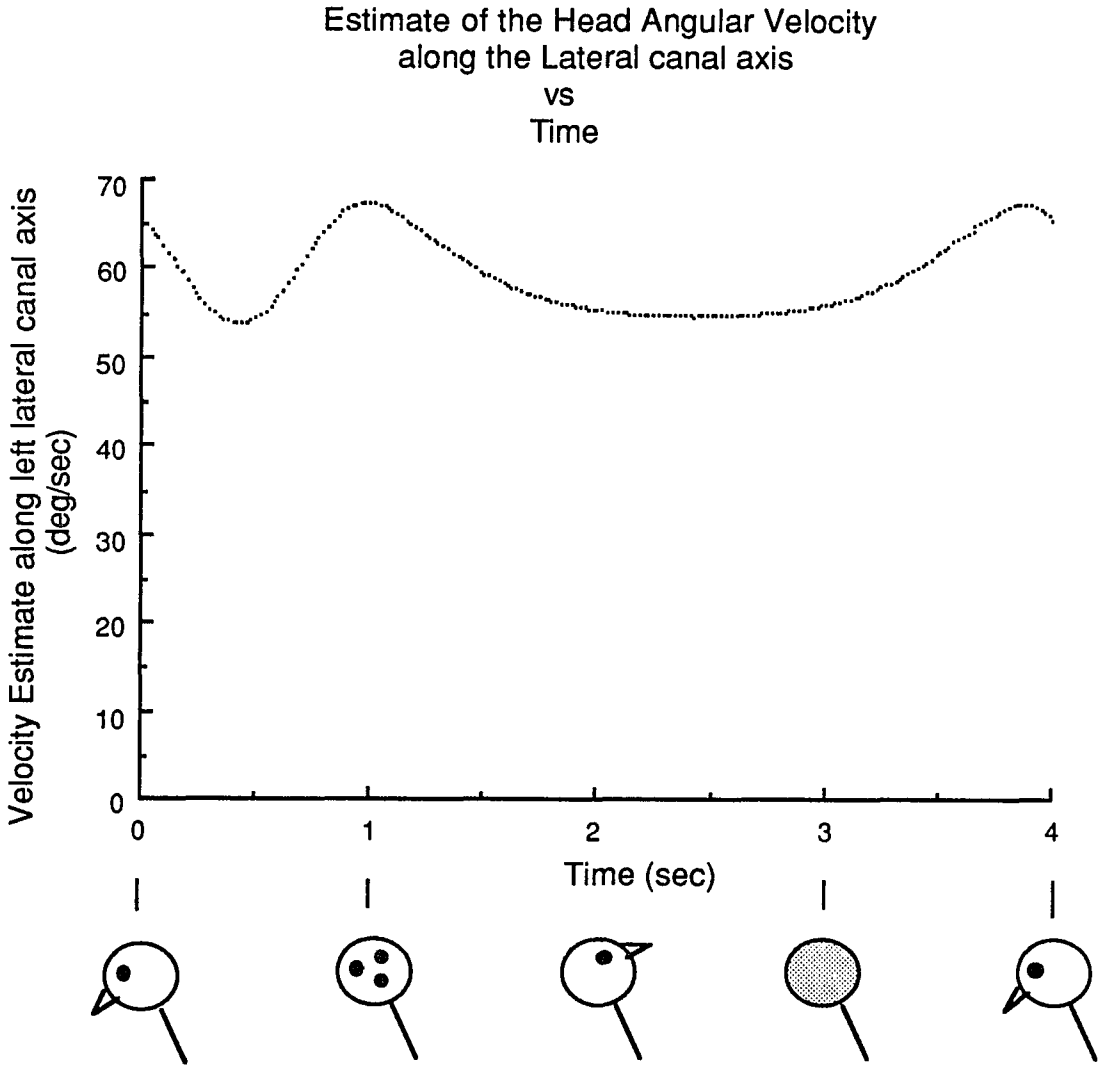

Fig. 3.2.12 The number of extremum in the signal from the two-pattern estimator depends on the magnitude of the head angular velocity. The assumptions for this simulation are same as given in Fig. 3.2.11 except that the magnitude of the head angular velocity is 90 degrees/second. There are two relative maximums and two relative minimums.

probably due to the complex nonlinear interaction of the normalization for each pattern for a given head orientation and the relative phase difference between patterns. The results for the left laterial canal axis shown in Fig. 3.2.11C show that, on the average this component of the estimate is approximately 52 degrees/second, which is in agreement with experimental findings. The results for the left anterior and the left posterior canal axes shown in Figs. 3.2.11A and 3.2.11B show that, on the average these components of the estimate are approximately zero but oscillate with an amplitude of approximately 30 degrees/second. This is due to the large angle between the head velocity vector and the canal normal.

The dependence of the average value of each of the three canal coordinate components of the estimate over one head rotation on the magnitude of the head angular velocity is shown in Fig. 3.2.13. Initially the head is assumed to be pitched forward by 30 degrees and rotating to the left with some given angular velocity. The magnitude varies from zero to a maximum value, w_{max}, such that $w_{max}T$ is equal to 360 degrees. Further increases in head velocity will repeat the estimated head velocity (Fig. 3.2.13). These simulations show that the average of the lateral canal component of the estimate (Fig. 3.2.13C) is in good agreement with experimental findings. The average of the anterior (posterior) canal component of the estimate (Fig. 3.2.13A (B)) is approximately zero.

The dependence of the average value of each of the three canal

Fig. 3.2.13 The average, the maximum, and the minimum of the output from the two-pattern estimator in canal coordinates for one head rotation of 360 degrees as a function of the head angular velocity: The time delay constant is 0.85 seconds. The left semicircular canals are pitched back by 15 degrees, and then rotated by 45 degrees to the left about the left lateral canal axis, relative to the head. The head is initially pitched forward by 30 degrees. If the magnitude of the head angular velocity is 60 degrees/second then, the components of a good estimate along the anterior, posterior, and lateral canal axes are approximately -9, -9, and 51 degrees/second.
A. The angle between the left anterior canal axis and the head velocity is approximately 100 degrees. For each magnitude of the head velocity, the average value of the left anterior component of the head velocity is approximately zero.
B. The angle between the left posterior canal axis and the head velocity is approximately 100 degrees. For each magnitude of the head velocity, the average value of the left posterior component of the head velocity is approximately zero.
C. The angle between the left lateral canal axis and the head velocity is 15 degrees. When the magnitude of the head velocity is approximately 60 degrees/second the average value is approximately 50 degrees/second.

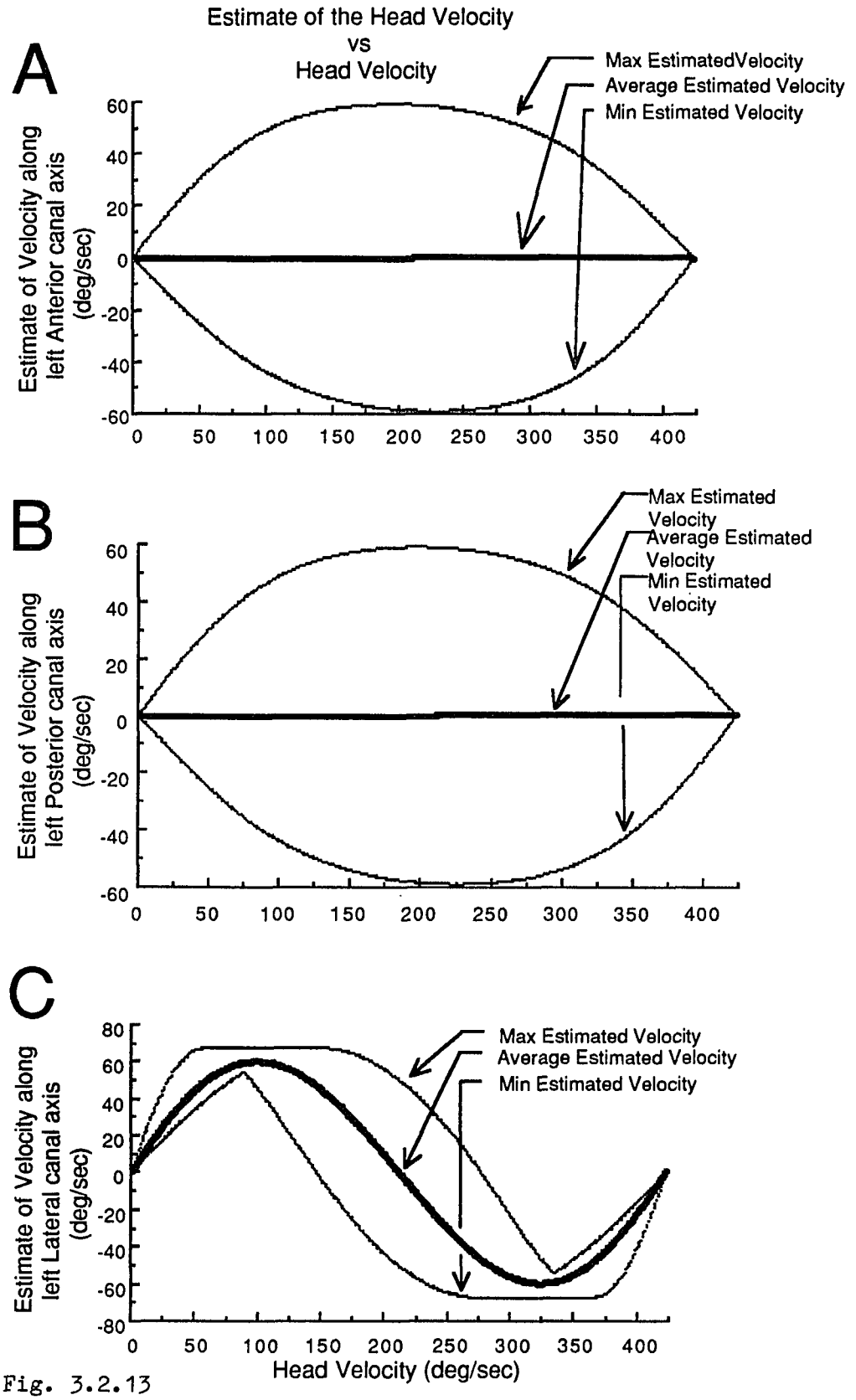
A
Estimate of the Head Velocity
vs
Head Velocity
Max EstimatedVelocity
Average Estimated Velocity
Min Estimated Velocity
Estimate of Velocity along left Anterior canal axis (deg/sec)
60
40
20
0
-20
-40
-60
0
50
100
150
200
250
300
350
400
B
Max Estimated Velocity
Average Estimated Velocity
Min Estimated Velocity
Estimate of Velocity along left Posterior canal axis (deg/sec)
C
Max Estimated Velocity
Average Estimated Velocity
Min Estimated Velocity
Estimate of Velocity along left Lateral canal axis (deg/sec)
80
-80
Head Velocity (deg/sec)

Fig. 3.2.13

coordinate components of the estimate over one head rotation, on the angle of tilt of the head relative to the space vertical is shown in Fig. 3.2.14. The orientation of the head angular velocity vector relative to the head remains constant throughout the simulation. Initially the head is assumed to be pitched forward by some given tilt angle. The head for all cases is rotating to the left at 60 degrees/second about the head yaw axis. These simulations show that the average of the lateral canal component of the estimate (Fig. 3.2.14C) is initially zero when the head is upright. The average of the lateral component of the estimate increases as the head is pitched forward until, the pitch angle reaches approximately 25 degrees. The average of the lateral canal axis component of the estimate remains approximatly constant at about 51 degrees/second as the pitch angle increases. This is in good agreement with experimental findings. The average value of the lateral canal component of the estimate remains approximately constant as the pitch angle continues to increase until, the angle of pitch is approximately 155 degrees. Then the average value of the component of the estimate decreases to zero as the pitch angle increases to 180 degrees.

The average values of the anterior canal axis and of the posterior canal axis components of the estimate over one head rotation, as a function of head tilt is shown in Figs. 3.2.14A and 3.2.14B. The average of the anterior (posterior) canal axis component of the estimate is approximately zero up to a pitch angle of

Fig. 3.2.14 The average, the maximum, and the minimum of the output from the two-pattern estimator in canal coordinates for one head rotation of 360 degrees as a function of the angle between the head yaw axis and the space vertical: The time delay constant is 0.85 seconds. The left semicircular canals are pitched back by 15 degrees, and then rotated by 45 degrees to the left about the left lateral canal axis, relative to the head. The magnitude of the head angular velocity is 60 degrees/second. The direction of the head angular velocity is along the head yaw axis. If the head tilt is greater than approximately 10 degrees then, the components of a good estimate along the anterior, posterior, and lateral canal axes are approximately -9, -9, and 51 degrees/second.
A. The angle between the left anterior canal axis and the head velocity is approximately 100 degrees. Initially, the average value is approximately zero. When the head tilt is approximately 70 degrees the average value is approximately -10 degrees/second.
B. The angle between the left posterior canal axis and the head velocity is approximately 100 degrees. When the head tilt is approximately 70 degrees the average value is approximately -10 degrees/second.
C. The angle between the left lateral canal axis and the head velocity is 15 degrees. Initially, the average value is approximately zero. As the head tilts increase from zero to approximately 25 degrees, the average value increases from zero to approximately 50 degrees/second.

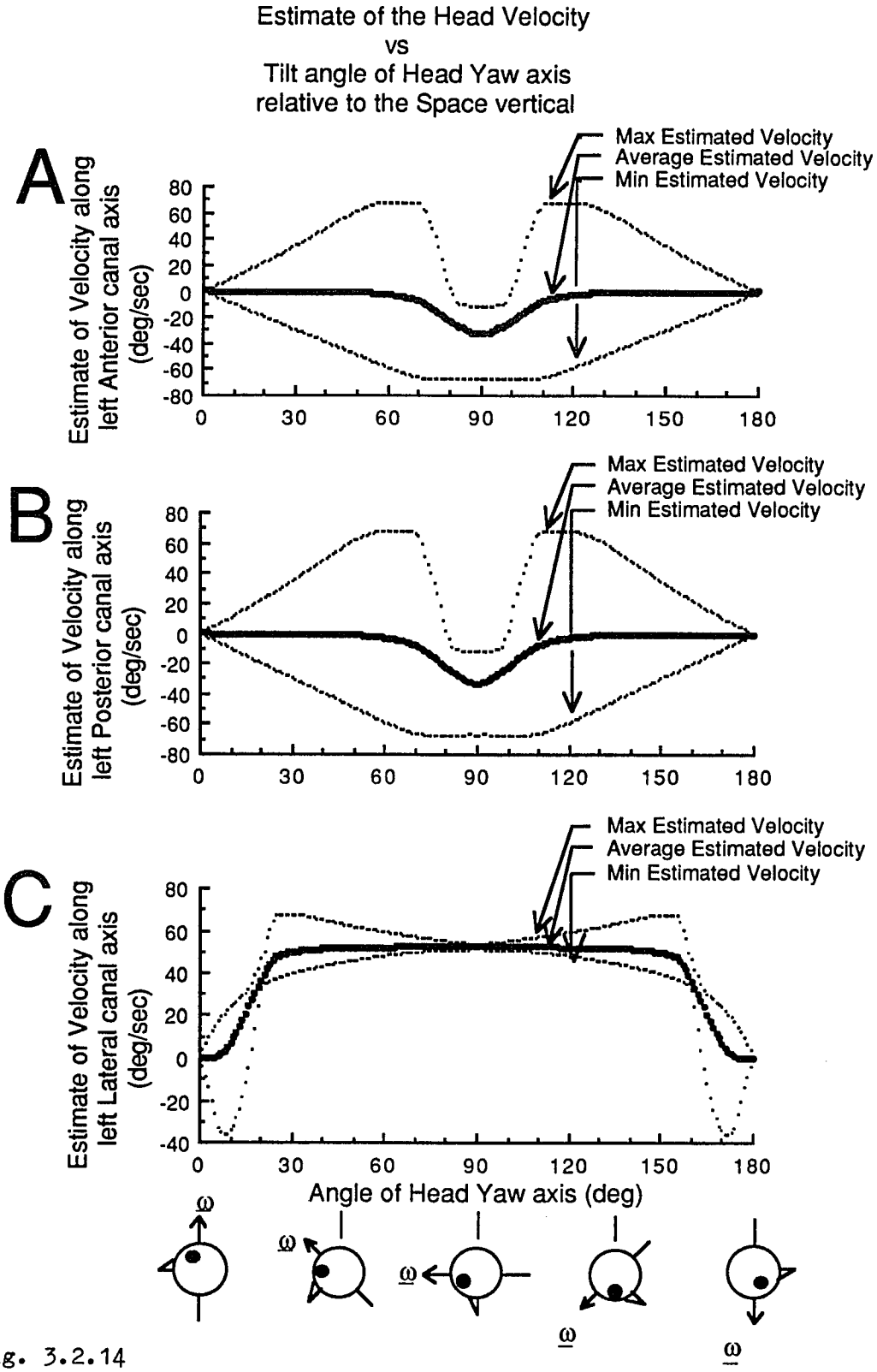
Estimate of the Head Velocity
vs
Tilt angle of Head Yaw axis
relative to the Space vertical
A
Estimate of Velocity along left Anterior canal axis (deg/sec)
Max Estimated Velocity
Average Estimated Velocity
Min Estimated Velocity
80
60
40
20
0
-20
-40
-60
-80
0
30
60
90
120
150
180
B
Estimate of Velocity along left Posterior canal axis (deg/sec)
Max Estimated Velocity
Average Estimated Velocity
Min Estimated Velocity
C
Estimate of Velocity along left Lateral canal axis (deg/sec)
Max Estimated Velocity
Average Estimated Velocity
Min Estimated Velocity
Angle of Head Yaw axis (deg)
ω
ω
ω
ω
ω

Fig. 3.2.14

approximately 60 degrees. The average value of both the anterior and posterior components of the estimate then increase in absolute value as the pitch angle increases, until the pitch angle is 90 degrees. The average value then returns to approximately zero as the pitch angle increases to 120 degrees. The average value remains approximately zero as the pitch angle continues to increase to 180 degress.

The dependence of the average value of the left lateral canal component of the estimate over one head rotation, on the angle between the lateral canal normal and the head angular velocity is shown in Fig. 3.2.15. The head angular velocity is 60 degrees/second and makes an angle of 30 degrees with respect to the space vertical throughout these simulations. Initially the head is assumed to be pitched forward by 15 degrees relative to the head angular velocity. Under the assumption regarding the orientation of the canal axes relative to the head, when the head is tilted by 15 degrees relative to the head angular velocity the left lateral canal axis is aligned with the head angular velocity. The average value of the left lateral canal component of the estimate is initially a maximum of approximately 52 degrees/second. As the head is pitched down from the head angular velocity, the average value decreases. The average value is approximately zero when the head is pitched down relative to the head angular velocity by approximately 55 degrees. As the angle relative to the head angular velocity continues to increase the average value

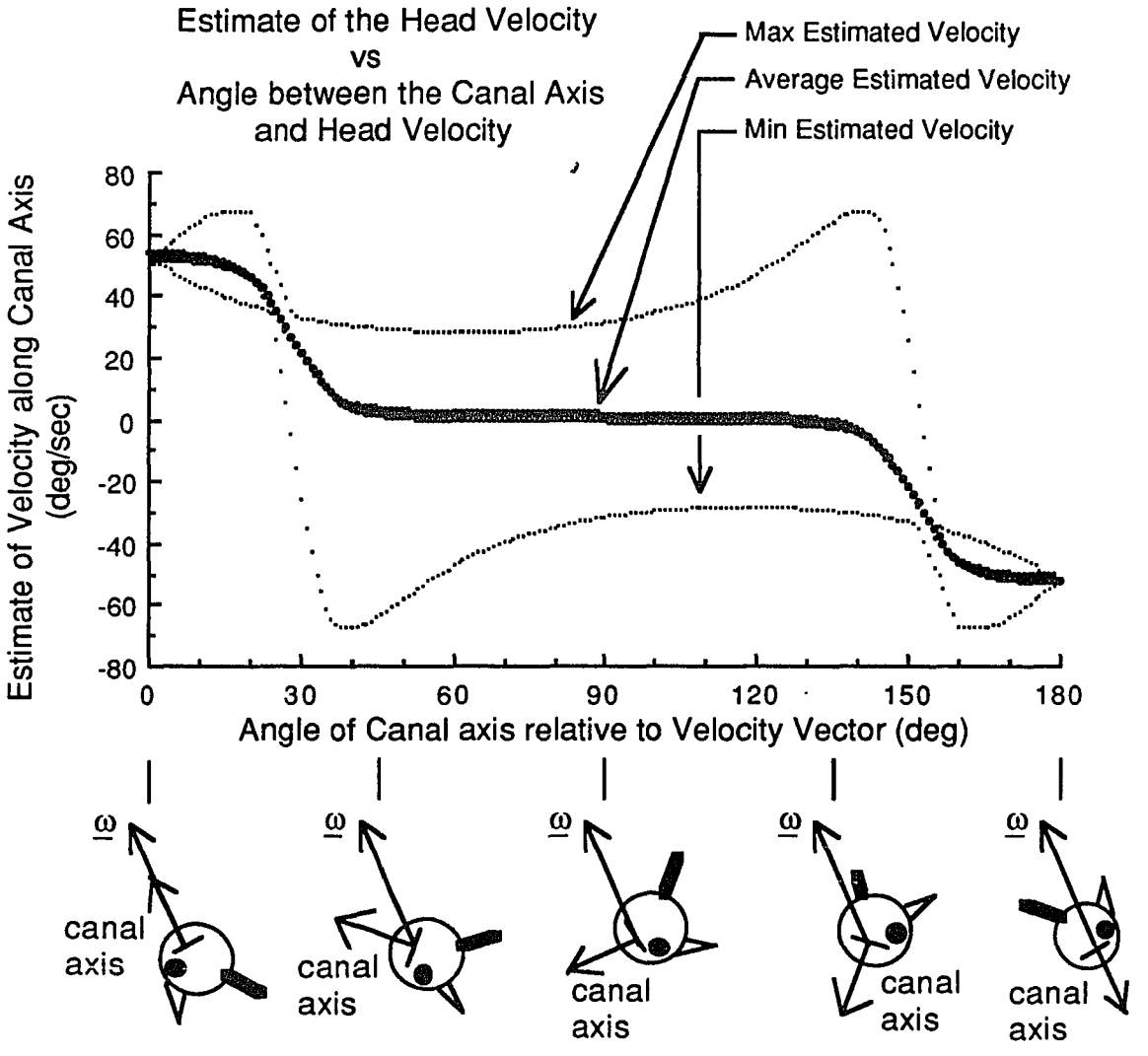

Fig. 3.2.15 A canal component of the average, the maximum, and the minimum of the output from the two-pattern estimator for one head rotation of 360 degrees as a function of the angle between the canal axis and the head angular velocity: The time delay constant is 0.85 seconds. The magnitude of the head angular velocity is 60 degrees/second. The head angular velocity is pitched forward by 30 degrees relative to the space vertical. When the canal axis is along the head angular velocity the average value of the component is approximately 52 degrees/second. The average value of the canal component of the head angular velocity is approximately zero when the angle between the canal axis and the head angular velocity is in the range from approximately 40 to approximately 140 degrees.

remains approximately zero until the angle reaches approximately 155 degrees. As the angle continues to increase the average value decreases.

In the last simulation the important parameter determining the average value is the angle between the left lateral canal axis and the head angular velocity. When the canal axis is aligned with the head angular velocity the average value of the canal component of the estimate is a maximum of approximately 52 degrees/second (Fig. 3.1.15). When the angle between the canal axis and the head velocity is between approximately 40 degrees and approximately 140 degrees the average value is approximately zero.

The following results are of simulations that generate eye velocity command signals in canal coordinates. The output of the two-pattern head angular velocity estimator is used to drive the velocity storage integrator. Intially the head is suddenly pitched forward by 30 degreees after it has been rotationg to the left at 60 degrees/second about a vertical axis long enough so that the state of the velocity storage integrator is zero. It is assumed that the integrator state after the sudden tilt is approximately zero. This is reasonable since the duration of the sudden tilt is less than one second, and the input to the integrator during the sudden tilt is coming from the semicircular canals and the otoliths. Each semicircular canal can be approximated by a system with one integrator. The time constant of the semicircular canal integrator is

approximately 4 seconds. Since the stimulus is short compared to the time constant of the canal system, the response is damped. Further the semicircular canal system is first excited and then inhibited due to the sudden rapid acceleration followed by a rapid deceleration of the sudden-tilt movement. Therefore, during the sudden tilt, the input from each semicircular canal is small and after the sudden tilt the input is approximately zero. The otoliths can be approximated by a one-dimensional system with a very short time constant (16 milliseconds). The output from the otolith velocity estimator, during the sudden tilt, varies in accordance with the separating otolith activation patterns. This output is less than the head velocity and is ignored.

It is assumed that the gain matrix, G, associated with the velocity storage integrator is the negative of the system matrix, H, of the integrator. The representation of H in head coordinates is assumed to be diagonal with time constants of 2, 4, and 13+1/3 seconds along the pitch, roll, and yaw axes, respectively. However, there is OKAN data suggesting that the system matrix varies with the orientation of the head relative to gravity (Raphan & Sturm, 1988).

The eye velocity command signal as a function of time is shown in Fig. 3.2.16. The head is suddenly pitched forward by 30 degrees at time zero. The head angular velocity is 60 degrees/second about the head yaw axis. From a time of approximately 55 seconds, the left anterior and the left posterior command signal components, as shown in

Fig. 3.2.16 Output in canal coordinates from the three-dimensional velocity storage integrator as a function of time: The integrator matrix (system matrix) in head coordinates is assumed to be diagonal. The pitch, roll, and yaw time constants are assumed to be constant and equal to 2, 4, and 13+1/3 seconds. The gain matrix is assumed to be equal to the negative of the system matrix. The input to the integrator is the estimate generated by two-pattern estimator. The time delay constant is 0.85 seconds. The left semicircular canals are pitched back by 15 degrees, and then rotated by 45 degrees to the left about the left lateral canal axis, relative to the head. After the head has rotated a long time at 60 degrees/second about a space vertical the head is suddenly pitched forward by 30 degrees at time zero. The initial state of the integrator is zero. After the sudden tilt, the head angular velocity, with a magnitude of 60 degrees/second, is parallel to the head yaw axis.
A. The peak-to-peak value of the anterior component of the eye velocity command is approximately one-half the peak-to-peak value of the anterior component of the estimate shown in Fig. 3.2.11A. The bias, after approximately 50 seconds, is approximately zero.
B. The peak-to-peak value of the posterior component of the eye velocity command is approximately one-half the peak-to-peak value of the posterior component of the estimate shown in Fig. 3.2.11B. The bias, after approximately 50 seconds, is approximately zero.
C. Initially the lateral component of the eye velocity command becomes negative. The component then increases with time. The component oscillates as time increases. After approximately 50 seconds, the peak-to-peak value of the component is approximately 1/14 of the peak-to-peak value of the lateral component of the estimate shown in Fig. 3.2.11C. The bias, after approximately 50 seconds, is approximately 50 degrees/second.

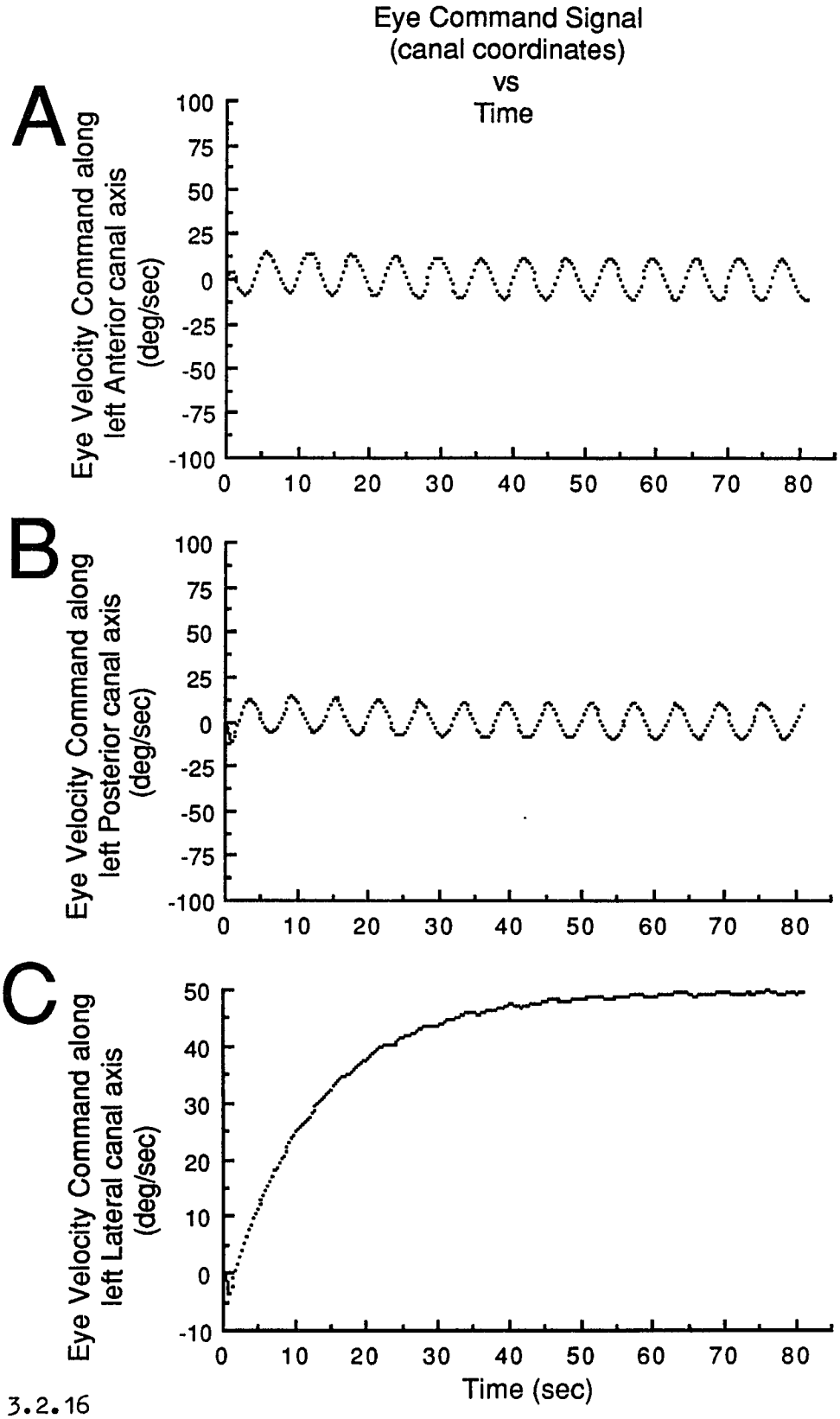
Eye Command Signal
(canal coordinates)
vs
Time
A
Eye Velocity Command along
left Anterior canal axis
(deg/sec)
B
Eye Velocity Command along
left Posterior canal axis
(deg/sec)
C
Eye Velocity Command along
left Lateral canal axis
(deg/sec)
Time (sec)

Fig. 3.2.16

Figs. 3.2.16A and 3.2.16B, oscillate about zero with an amplitude of approximately 10 degrees/second. The zero bias shown in Figs 3.2.16A and 3.2.16B is consistent with the zero bias shown in Fis. 3.2.11A and 3.2.11B, respectively. The left lateral command signal, as shown in Fig. 3.2.16C, for approximately the first one second decreases from zero to approximately -4 degrees/second. Then, as time increases, the left lateral command signal increases toward approximately 50 degrees/second. After approximately 30 seconds, the signal continuously oscillates. The peak-to-peak value of the osillations is approximately 2 degrees/second.

The slow phase eye velocity in pitch, roll, and yaw head coordinates, corresponding to the same simulation shown in Fig. 3.2.16, is shown in Fig. 3.2.17. The head is suddenly pitched forward by 30 degrees at time zero. The head angular velocity is 60 degrees/second about the head yaw axis. The pitch and roll components of the slow phase eye velocity as shown in Figs. 3.2.17A and 3.2.17B oscillate with time. The pitch component oscillates about a bias of approximately zero (Fig. 3.2.17A) with an amplitude of approximately 15 degrees/second. The roll component oscillates about a bias of approximately 13 degrees/second (Fig. 3.2.17B) with an amplitude of approximately 6 degrees/second. The yaw component of the slow phase eye velocity, as shown in Fig. 3.2.17C, for approximately the first one second decreases from zero to approximately -2 degrees/second. As time increases, the yaw component increases toward a bias of

Fig. 3.2.17 Output in head coordinates from the three-dimensional velocity storage integrator as a function of time: All of the assumptions given for Fig. 3.2.17 apply here.
A. The peak-to-peak value of the pitch component of the slow phase eye velocity is approximately 25 degrees/second. The bias is approximately zero.
B. The peak-to-peak value of the roll component of the slow phase eye velocity is approximately 12 degrees/second. The bias, after approximately 30 seconds, is approximately 13 degrees/second.
C. The yaw component of the slow phase eye velocity initially becomes negative. The component then increases with time. As time increases, the component oscillates about an increasing bias. After appoximately 50 seconds, the peak-to-peak value is approximately 5 degrees/second and the bias is approximately 47 degrees/second.

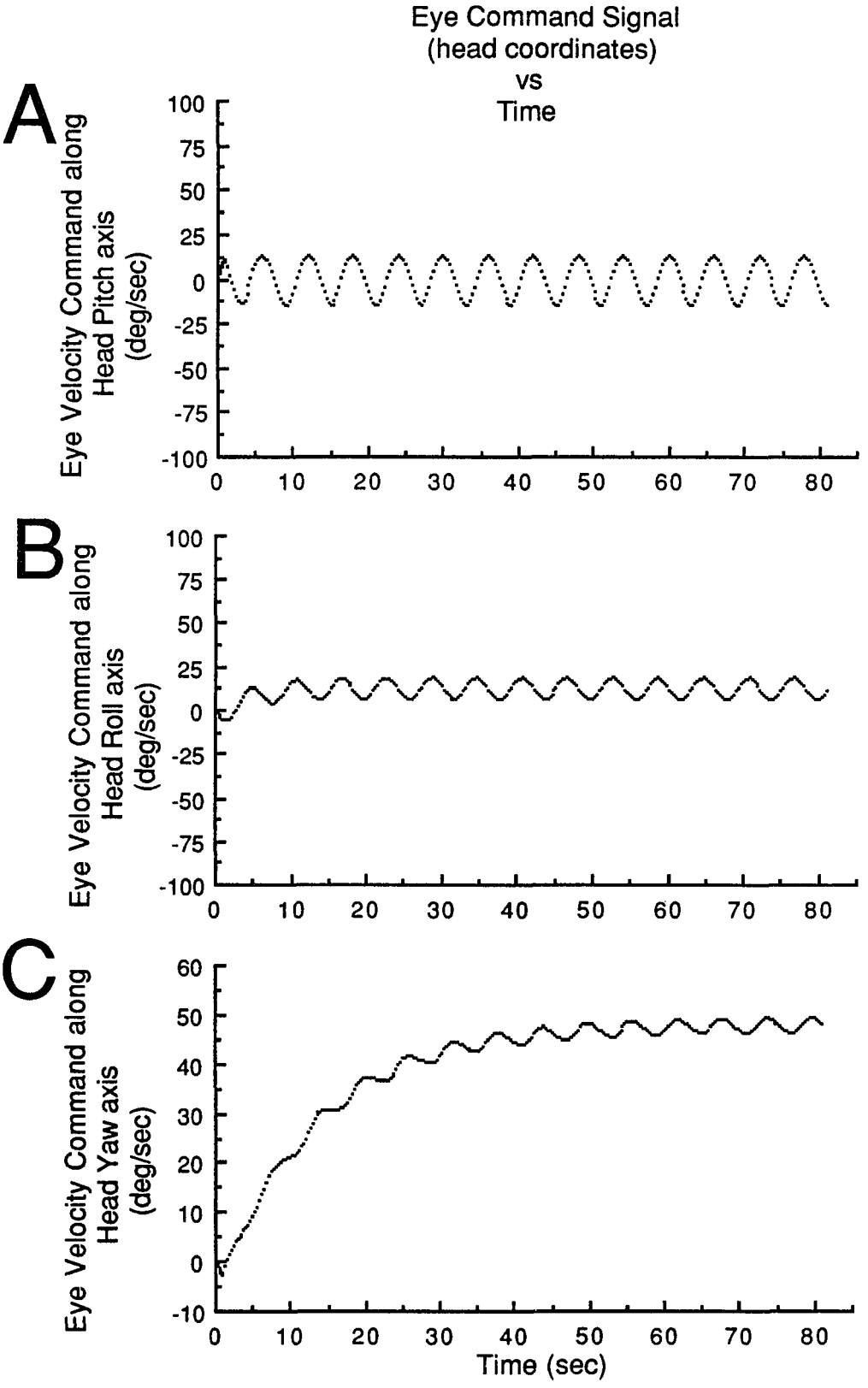
Eye Command Signal
(head coordinates)
vs
Time
A
Eye Velocity Command along
Head Pitch axis
(deg/sec)
B
Eye Velocity Command along
Head Roll axis
(deg/sec)
C
Eye Velocity Command along
Head Yaw axis
(deg/sec)
Time (sec)

Fig. 3.2.17

approximately 48 degrees/second. After approximately 30 seconds, the signal oscillates. The peak-to-peak value of the osillations is approximately 2 degrees/second.

The magnitude of the eye velocity command signal (or the slow phase eye velocity) as a function of time, corresponding to the simulations of Figs. 3.2.16 and 3.2.17, is shown in Fig. 3.2.18. During the first one second, the magnitude rises to approximately 12 degrees/second. The bias of the magnitude increases with time to a value of approximately 50 degrees/second. The magnitude varies with time with a peak-to-peak value of approximately 3 degrees/second.

The effect on the estimate due to a smaller time constant is presented in Figs. 3.2.19 and 3.2.20. The gain matrix, G, is assumed equal to the negative of the system matrix, H. The representation of H in head coordinates is assumed to be diagonal with time constants of 2, 4, and 6 seconds along the pitch, roll, and yaw axes, respectively. Intially the head is suddenly pitched forward by 30 degreees after it has been rotationg to the left at 60 degrees/second about a vertical axis long enough so that the state of the integrator is zero. It is assumed that the integrator state after the sudden tilt is approximately zero. The result, of the simulation, showing the left lateral component of the eye velocity command is shown in Fig. 3.2.19. For the first 50 seconds, the left lateral canal component of the eye velocity command signal of Fig. 3.2.19 is greater than the corresponding part of the signal shown in Fig 3.2.16C. The signal

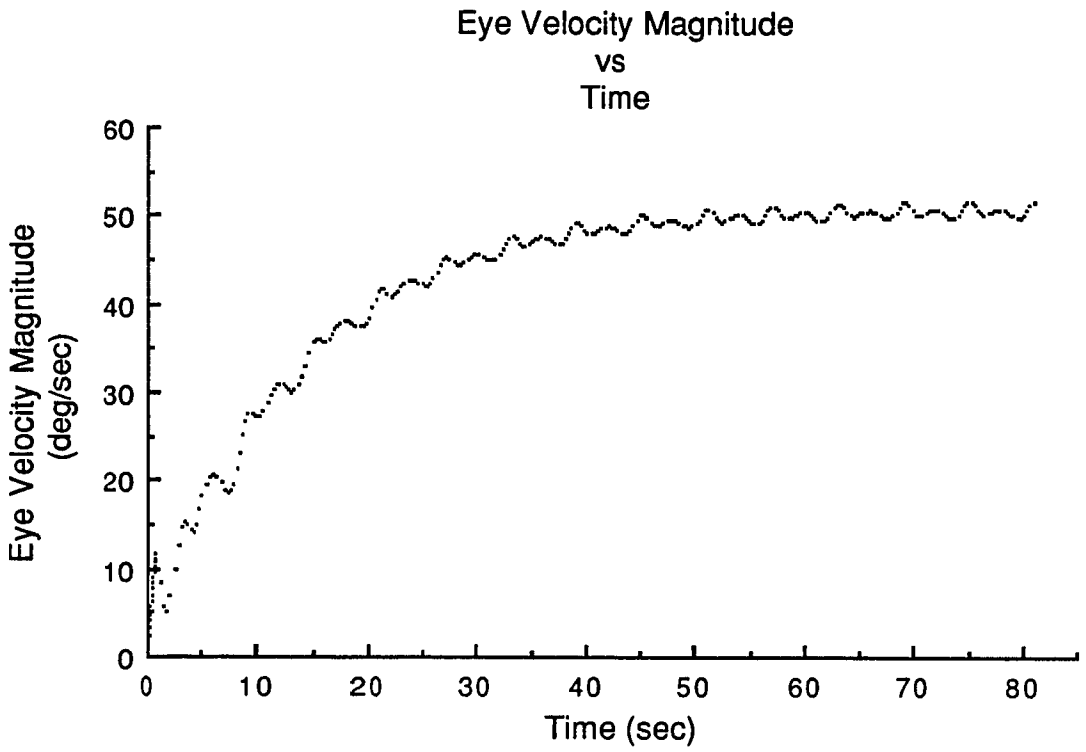

Fig. 3.2.18 Magnitude of the slow phase eye velocity (or eye velocity command), shown in Figs. 3.2.17 and 3.2.18, as a function of time. All of the assumptions given for Fig. 3.2.17 apply here. The magnitude varies but generally increases for the first 50 seconds. The bias of the magnitude, after approximately 50 seconds, is approximately 52 degrees/second.

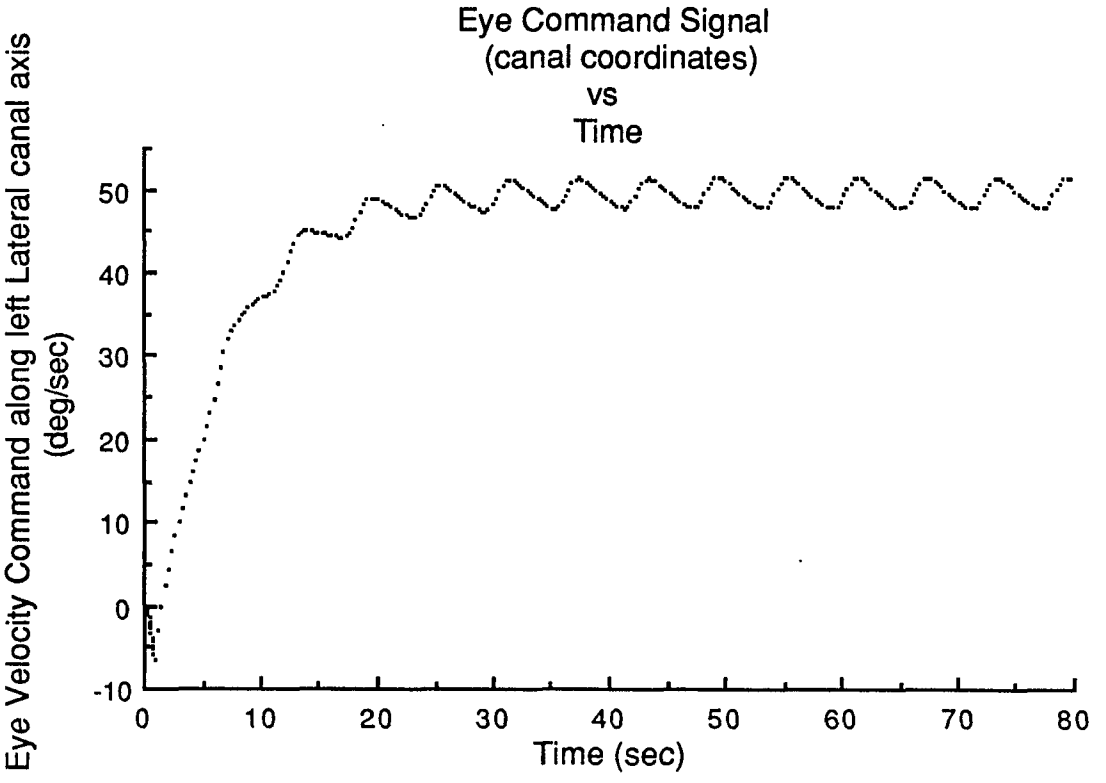

Fig. 3.2.19 The effect of reducing the yaw time constant (and similarly modifying the corresponding component of the gain matrix): The left lateral canal component from the three-dimensional velocity storage integrator as a function of time: All of the assumptions given for Fig. 3.2.17 apply here, except that the integrator yaw time constant is 6 seconds. The gain matrix is equal to the negative of the system matrix. After the first couple of seconds, the initial slope of the 6 second time constant curve is greater than the slope of the corresponding segment of the 13+1/3 second time constant curve in Fig. 3.2.17C. The peak-to-peak values of the oscillations of this 6 second time constant curve are greater than the corresponding peak-to-peak values of the 13+1/3 second time constant curve in Fig. 3.2.17C.

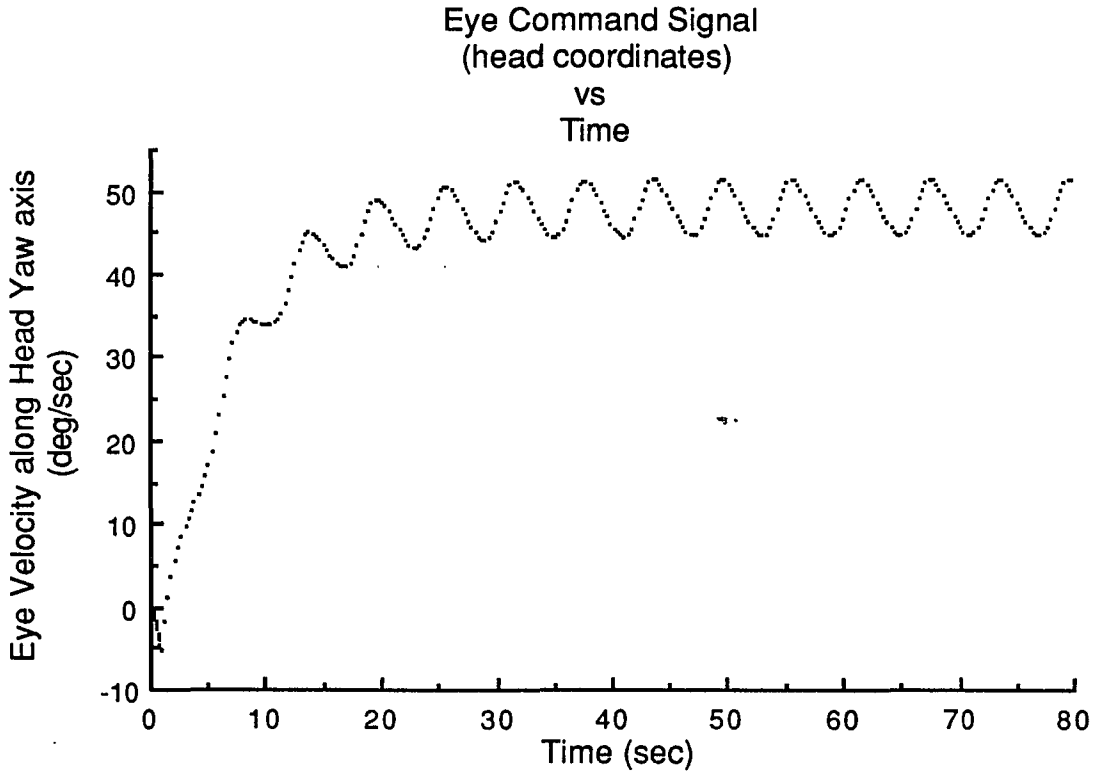

Fig. 3.2.20 The effect of reducing the yaw time constant (and similarly modifying the corresponding component of the gain matrix): The head yaw component of the slow phase eye velocity as a function of time: All of the assumptions given for Fig. 3.2.17 apply here, except that the integrator yaw time constant is 6 seconds. The gain matrix is equal to the negative of the system matrix. After the first couple of seconds, the initial slope of the 6 second time constant curve is greater than the slope of the corresponding segment of the 13+1/3 second time constant curve in Fig. 3.2.18C. The peak-to-peak values of the oscillations of this 6 second time constant curve are greater than the corresponding peak-to-peak values of the 13+1/3 second time constant curve in Fig. 3.2.18C.

shown in Fig. 3.2.19 has a greater peak-to-peak value than the signal shown in Fig. 3.2.16C.

The result of the simulation showing the left yaw component of the eye velocity assuming a time constant of 6 seconds, is shown in Fig. 3.2.20. The comparisons between Figs. 3.2.20 and 3.2.17C are approximately the same as the comparisons pointed out above for Figs. 3.2.19 and 3.2.16C, respectively. The comparisons of Figs. 3.2.19 and 3.2.16C and the comparisons of Figs. 3.2.20 and 3.2.17C are consistant with the known properties of integrators.

Recent OVAR experiments were performed, with initial conditions approximately corresponding to those of the above simulations, in which recording in right anterior, posterior, and lateral canal units were made (Reisine et al, 1988). These experimemtal results show that there is a nonzero bias of approximately 8 degrees/second in the signals from the right anterior unit and also from the right posterior unit. This suggests that the estimation of head angular velocity from otolith activation patterns is processed in canal coordinates and that the estimates of head velocity along anterior and posterior canal axes are better than predicted by a two-pattern estimator. The simulations the using two-pattern estimator suggests that the contribution of the bias component of eye velocity along the anterior and the posterior canal are approximately zero. Moreover, Fig. 3.2.15 shows that if, the head angular velocity vector is tilted by 30 degrees from the space vertical and the angle between a canal axis and the head angular

velocity is between 40 degrees and 140 degrees then, the average value of the component of the estimate along the canal axis is approximately zero.

These experimental results suggest that the computed component of the estimate along a canal axis is a good estimate if the angle between the canal axis and the head velocity is either approximately 15 degrees or 100 degrees. Under the given experimental conditions the brain is able to generate a good estimate of the head angular velocity. Therefore, in the following section we develop a three-dimensional estimator utilizing multiple patterns to correctly estimate head angular velocity in a canal-based coordinate system. We will examine its predictions relative to understanding how units in the central vestibular system would code the estimate of head velocity from position information during OVAR.

3.2.6 Approaches to Multiple Pattern Estimation

In order to gain insight into how to modify the two-pattern estimator so as to obtain an improved three-dimensional estimator, we will express the two-pattern estimator as a function of the acceleration due to gravity relative to the head.

We first express Eq (3.2.36) as a sum obtaining

$$\hat{w}_{lc}(t_p) = \sum_{i=0}^{N_l-1} [\text{Delay}(T)-I][\underline{r}_l^L(t_p)]_i K^l(t_d,t_p) \qquad (3.2.106)$$
$$(\text{RotateUp}-\text{RotateDown})[\underline{r}_l^L(t_p)]i/(2\uparrow\uparrow Tg^2),$$
$$\text{for } l=1 \text{ to } 3.$$

To simplify Eq (3.2.106) we drop the left side designaltion, L. Also, as was pointed out in the discusion following Eq (3.2.36), the term involving the indentity operator is equal to zero and therefore, we obtain

$$\hat{w}_{lc}(t_p) = \sum_{i=0}^{N_l-1} \text{Delay}(T)[\underline{r}_l(t_p)]_i K^l(t_d,t_p) \qquad (3.2.107)$$
$$(\text{RotateUp}-\text{RotateDown})[\underline{r}_l(t_p)]i/(2\uparrow\uparrow Tg^2),$$
$$\text{for } l=1 \text{ to } 3.$$

In Eq (3.2.107) making use of the definitions of the Delay, RotateUp,

and RotateDown operators we obtain

$$\hat{w}_{lc}(t_p)= \sum_{i=0}^{N_l-1} r_l^i(t_d)K^l(t_d,t_p)[r_l^{i+1}(t_p)-r_l^{i-1}(t_p)]/(2\tau\tau Tg^2), \quad \text{for } l=1 \text{ to } 3. \tag{3.2.108}$$

By using the definition given in Eq (3.2.24) we obtain

$$\hat{w}_{lc}(t_p)= \sum_{i=0}^{N_l-1} [K^l(t_d,t_p)/(2\tau\tau Tg^2)]\langle \underline{g},\hat{\underline{P}}_l^i(t_d)\rangle \quad [\langle \underline{g},\hat{\underline{P}}_l^{i+1}(t_p)\rangle-\langle \underline{g},\hat{\underline{P}}_l^{i-1}(t_p)\rangle], \text{ for } l=1 \text{ to } 3. \tag{3.2.109}$$

Next, using Eq (3.2.23) we obtain

$$\hat{w}_{lc}(t_p)= \sum_{i=0}^{N_l-1} [K^l(t_d,t_p)/(2\tau\tau Tg^2)]\langle \underline{g},\cos(h_l^i)\hat{\underline{e}}_c^m(t_d)-\sin(h_l^i)\hat{\underline{e}}_c^n(t_d)\rangle \tag{3.2.110}$$
$$[\ \langle \underline{g},\cos(h_l^{i+1})\hat{\underline{e}}_c^m(t_p)-\sin(h_l^{i+1})\hat{\underline{e}}_c^n(t_p)\rangle$$
$$-\langle \underline{g},\cos(h_l^{i-1})\hat{\underline{e}}_c^m(t_p)-\sin(h_l^{i-1})\hat{\underline{e}}_c^n(t_p)\rangle\ ], \text{ for } l=1 \text{ to } 3.$$

In order to simplify Eq (3.2.110) let

$$g_m(t)=\langle \underline{g},\hat{\underline{e}}_c^m(t)\rangle/g, \text{ and} \tag{3.2.111A}$$

$$g_n(t)=\langle \underline{g}, \underline{\hat{e}}_c^n(t)\rangle/g. \qquad (3.2.111B)$$

Since the inner product operator, <,>, is linear Eq (3.2.110) can be simplified by using the definitions of Eqs (3.2.111), obtaining

$$\hat{w}_{lc}(t_p)= \sum_{i=0}^{N_l-1} [K^l(t_d,t_p)/(2\uparrow\uparrow T)][\cos(h_l^i)g_m(t_d)-\sin(h_l^i)g_n(t_d)] \qquad (3.2.112)$$
$$[\cos(h_l^{i+1})g_m(t_p)-\sin(h_l^{i+1})g_n(t_p)$$
$$-\cos(h_l^{i-1})g_m(t_p)+\sin(h_l^{i-1})g_n(t_p)\ ], \quad \text{for } l=1 \text{ to } 3.$$

From Eq (3.2.28) we obtain

$$\hat{w}_{lc}(t_p)=$$
$$\sum_{i=0}^{N_l-1} [K^l(t_d,t_p)/(2\uparrow\uparrow T)][\cos(iH_l)g_m(t_d)-\sin(iH_l)g_n(t_d)] \qquad (3.2.113)$$
$$[\cos(iH_l+H_l)g_m(t_p)-\sin(iH_l+H_l)g_n(t_p)$$
$$-\cos(iH_l-H_l)g_m(t_p)+\sin(iH_l-H_l)g_n(t_p)\ ], \text{ for } l=1 \text{ to } 3.$$

Using the trigonometric identities given in Eqs (B1) and (B2) we obtain

$$\hat{w}_{lc}(t_p) = \sum_{i=0}^{N_l-1} [K^l(t_d,t_p)/(\pi\pi T)]\sin(H_l) \quad (3.2.114)$$
$$[\sin(iH_l)g_n(t_d)-\cos(iH_l)g_m(t_d)]$$
$$[\sin(iH_l)g_m(t_p)+\cos(iH_l)g_n(t_p)], \text{ for } l=1 \text{ to } 3.$$

Using the identities given in Eqs (B9), (B10), and (B11) we obtain

$$\hat{w}_{lc}(t_p) =$$
$$[N_l K^l(t_d,t_p)/(2\pi\pi T)]\sin(H_l)[g_m(t_p)g_n(t_d)-g_n(t_p)g_m(t_d)], \quad (3.2.115)$$
$$\text{for } l=1 \text{ to } 3.$$

Since $N_l H_l$ is equal to $2\pi\pi$ we obtain

$$\hat{w}_{lc}(t_p) =$$
$$[\sin(H_l)/H_l][K^l(t_d,t_p)][g_m(t_p)g_n(t_d)-g_n(t_p)g_m(t_d)]/T, \quad (3.2.116)$$
$$\text{for } l=1 \text{ to } 3.$$

The factor dependent on H_l can be eliminated by dividing the l^{th} component of Eq (3.2.116) by the factor or by noting that if H_l is small then, the factor is approximately one. Therefore,

$$\hat{w}_{lc}(t_p) =$$
$$K^l(t_d,t_p)[g_m(t_p)g_n(t_d)-g_n(t_p)g_m(t_d)]/T, \text{ for } l=1 \text{ to } 3. \quad (3.2.117)$$

The l^{th} expression in Eq (3.2.117) is the normalized l^{th} componnent of the cross product of $\underline{g}/g$ represented in canal coordinates at time t_p with $\underline{g}/g$ represented in canal coordinates at time t_d. If $\underline{g}/g$ is perpendicular to the head angular velocity, $\underline{w}$, then the estimate given in Eq (3.2.117) would approximately equal $\underline{w}$, for w less than approximately 60 degrees/second. This suggests how to modify the estimator so as to get a good estimate for any orientation of $\underline{w}$ relative to $\underline{g}$. Each of the vectors $\underline{g}/g$, represented in canal coordinates at times t_p and t_d in Eq (3.2.117) can be replaced by a difference of two vectors $\underline{g}/g$. Since each difference vector is perpendicular to $\underline{w}$ (Fig. 3.2.21), the cross product of the two difference vectors has the same direction as $\underline{w}$. Furthermore, if each difference vector is normalized obtaining a unit difference vector then, the magnitude of the cross product is equal to the sine of the angle of rotation from one difference vector to the next.

The two-pattern three-dimensional estimate, at time t_p, can thus be expressed as a normalized cross product of the accelerations due to gravity relative to the head at times t_p and t_d (Eqs (1) and (2)) (Fig. 3.2.4). An activation pattern, at time t, is summarized by the representation of $\underline{g}$ with respect to the canal coordinate system at time t (Fig. 3.2.5E). The axis of any head rotation relating the two representations of $\underline{g}$ is in the plane determined by these representations of $\underline{g}$ (Fig. 3.2.4C). The magnitude of the angle of rotation is then related to the axis of head rotation. Therefore, two

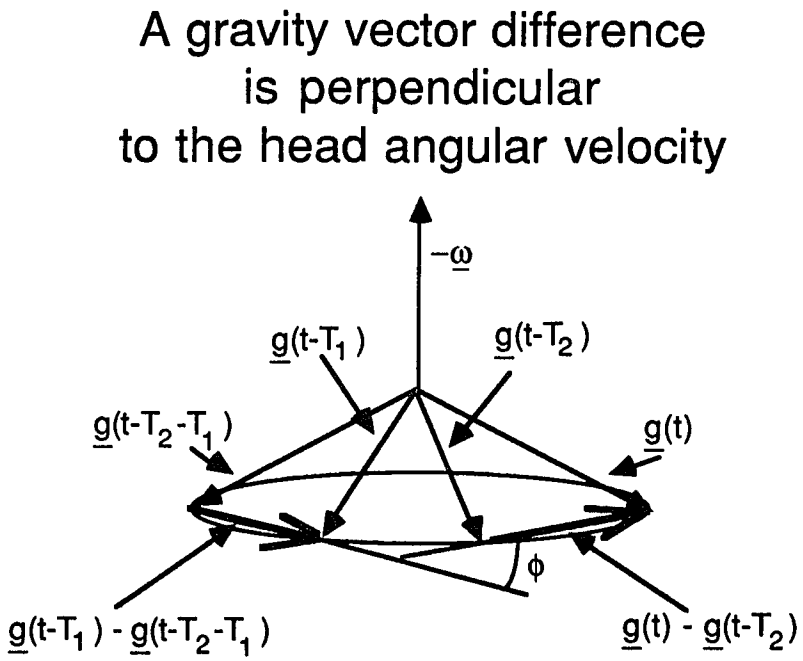

$\underline{\omega}$: the head angular velocity relative to space

$-\underline{\omega}$: the angular velocity of gravity relative to the head

ϕ: angle of rotation in time T_1

$$\phi = \omega T_1$$

Fig. 3.2.21 A difference otolith activation pattern is associated with a difference between two gravity vectors. The gravity vector difference is perpendicular to the space angular velocity relative to the head. The angular velocity of the difference vector is equal to the angular velocity of space relative to the head. The vector cross product of two difference vectors define the direction of the angular velocity, and the angle between the difference vectors and the time interval, T_1, between the difference vectors can be combined to obtain the angular speed of space relative to the head.

activation patterns are not sufficient to determine the head angular velocity, $\underline{w}$, since there are many head rotations relating two representations of $\underline{g}$ at times t_p and t_d.

Therefore, we propose another model of a head angular velocity estimator which uses two otolith activation difference-patterns. The four-pattern estimator, based on a two-sided two-pattern estimator, is given by (Fig. 3.2.22)

$$\hat{w}_{1c}(t)=<[\text{Delay}(T_1)-I][\underline{DP}_1(t)], \quad (\text{RotateUp}-\text{RotateDown})[\underline{DP}_1(t)]>/(2\pi T_1 g^2), \quad \text{for } 1=1 \text{ to } 3, \tag{3.2.118}$$

where

$$\underline{DP}_1(t)=[\text{Delay}(T_2)-I][\underline{r}_1(t)]. \tag{3.2.119}$$

In Eq (3.2.119), $\underline{DP}_1(t)$ is the difference pattern, of the 1^{th} estimator, at time t. There are two time delays associated with the estimator which generate the present and three previous patterns of otolith activation. By an analysis similar to that by which we obtained Eq (3.2.117) from Eq (3.2.36), we obtain the following from Eq (3.2.118):

Fig. 3.2.22 Model of the l^{th} component of the four-pattern three-dimensional head angular velocity estimator. The signals from the first summers from the left in the pattern space model generate a difference pattern, $\underline{DP}(t)$ representing the l^{th} component of the difference between two gravity vectors. All three difference patterns are combined centrally to yield a normalization factor, M(t). The three component estimators are coupled through the M(t) blocks. The difference pattern generated by the M(t) scale factor blocks represents the l^{th} component of a three-dimensional unit vector parallel to the gravity difference vector. The component of the pattern space model to the right of the M(t) scale factor blocks, computes the l^{th} component of the cross product of two three-dimensional unit vectors.

Four-Pattern Estimator

(l th component, l=1 to 3)

$$\hat{\omega}_l(t)=\frac{<[\text{Delay}(T_1)-l][\underline{DP}_l(t)],(\text{RotateUp-RotateDown})[\underline{DP}_l(t)]>}{2\pi T_1 g^2}$$

$$\underline{DP}_l(t)=[\text{Delay}(T_2)-l][\underline{r}_l(t)]$$

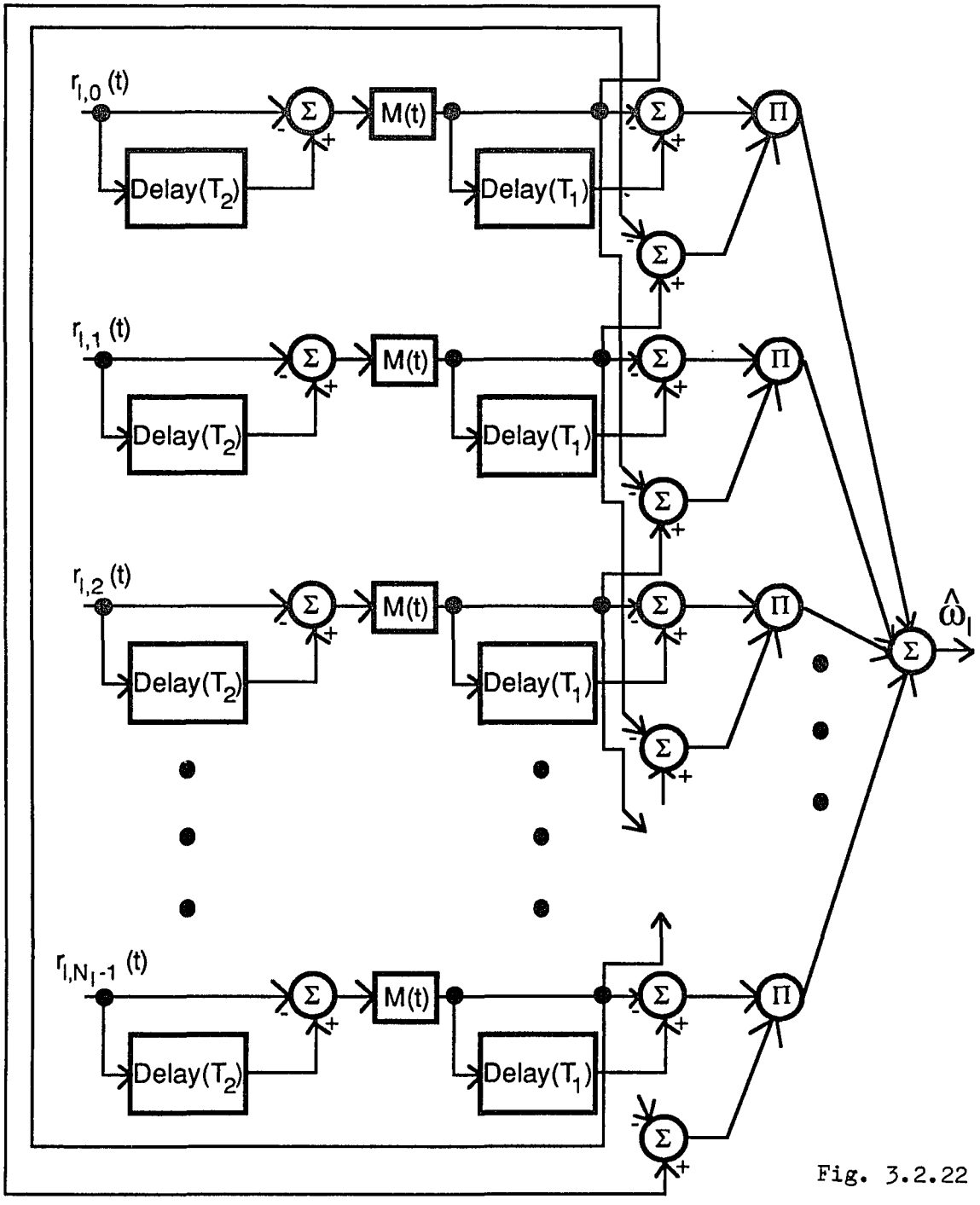

Fig. 3.2.22

$$\hat{w}_{lc}(t)=M'(t,t-T_2,t-T_1,t-T_2-T_1) \qquad (3.2.120)$$
$$\{[g_m(t)-g_m(t-T_2)][g_n(t-T_1)-g_n(t-T_2-T_1)]$$
$$-[g_n(t)-g_n(t-T_2)][g_m(t-T_1)-g_m(t-T_2-T_1)]\}/T_1,$$
$$\text{for } l=1 \text{ to } 3.$$

In Eq (3.2.120) $M'(t,t-T_2,t-T_1,t-T_2-T_1)$ is independent of l and is chosen to equal the reciprocal of the product of the Euclidean norms of the difference vectors:

$$M'(t,t-T_2,t-T_1,t-T_2-T_1)=M(t)M(t-T_1), \qquad (3.2.121)$$

where

$$M(t)|\underline{g}(t)-\underline{g}(t-T_2)|/g=1, \text{ and} \qquad (3.2.122A)$$

$$M(t-T_1)|\underline{g}(t-T_1)-\underline{g}(t-T_2-T_1)|/g=1. \qquad (3.2.122B)$$

Note that $M(t-T_1)$ is a time delayed version of $M(t)$. Therefore, the estimate is given by

$$\underline{\hat{w}}_c(t)=M'(t,t-T_2,t-T_1,t-T_2-T_1) \qquad (3.2.123)$$
$$[\underline{g}(t)-\underline{g}(t-T_2)]X[\underline{g}(t-T_1)-\underline{g}(t-T_2-T_1)]/(g^2T_1),$$

where all vectors are in canal coordinates. The difference vectors $[\underline{g}(t)-\underline{g}(t-T_2)]$ and $[\underline{g}(t-T_1)-\underline{g}(t-T_2-T_1)]$ are related by a rotation angle wT_1 (Fig. 3.2.21). In addition, they are perpendicular to the head angular velocity. Therefore, their cross product is proportional to the $\sin(wT_1)$ and is aligned with the head angular velocity. If the head angular velocity is constant then the estimate given in Eq (3.2.123) can be expressed as follows:

$$\underline{\hat{w}}(t)=\underline{w}\sin(wT_1)/(wT_1). \qquad (3.2.124)$$

In the simulations leading to the results shown in Fig. 3.2.23, we assume that the time delay constant T_1 of the two-difference-pattern estimator is equal to 0.85 seconds. From Eq (3.2.124) it is clear that T_1 is the crucial time delay for determing the steady state bebavior of the estimator. The time delay T_2 is important for fine tuning the dynamic response of the estimator. It can be made small without affecting the steady state estimation process. This parameter may be important for determining the threshold angle for inducing steady state eye velocity during OVAR.

It is assumed that the left canal axes relative to the head are pitched back by 15 degrees and then rotated (to the left) by 45 degrees about the left lateral canal axis. Under these conditions the angle between the left lateral canal axis and the head angular velocity is 15 degrees, and the angle between the left anterior (or

Fig. 3.2.23 The output of the four-pattern three-dimensional estimator as a function of the head angular velocity magnitude: The left semicircular canals are pitched back by 15 degrees, and then rotated by 45 degrees to the left about the left lateral canal axis, relative to the head. The angle between the left anterior (or posterior) canal axis and the head angular velocity is approximately 100 degrees and the angle between the left lateral canal axis and the head angular velocity is 15 degrees. The head is pitched forward from the space vertical and the head angular velocity is along the head yaw axis.
A. The anterior component of the estimate as a function of the head angular speed:
B. The posterior component of the estimate as a function of the head angular speed:
C. The lateral component of the estimate as a function of the head angular speed:
D. The magnitude of the estimate as a function of the head angular speed:

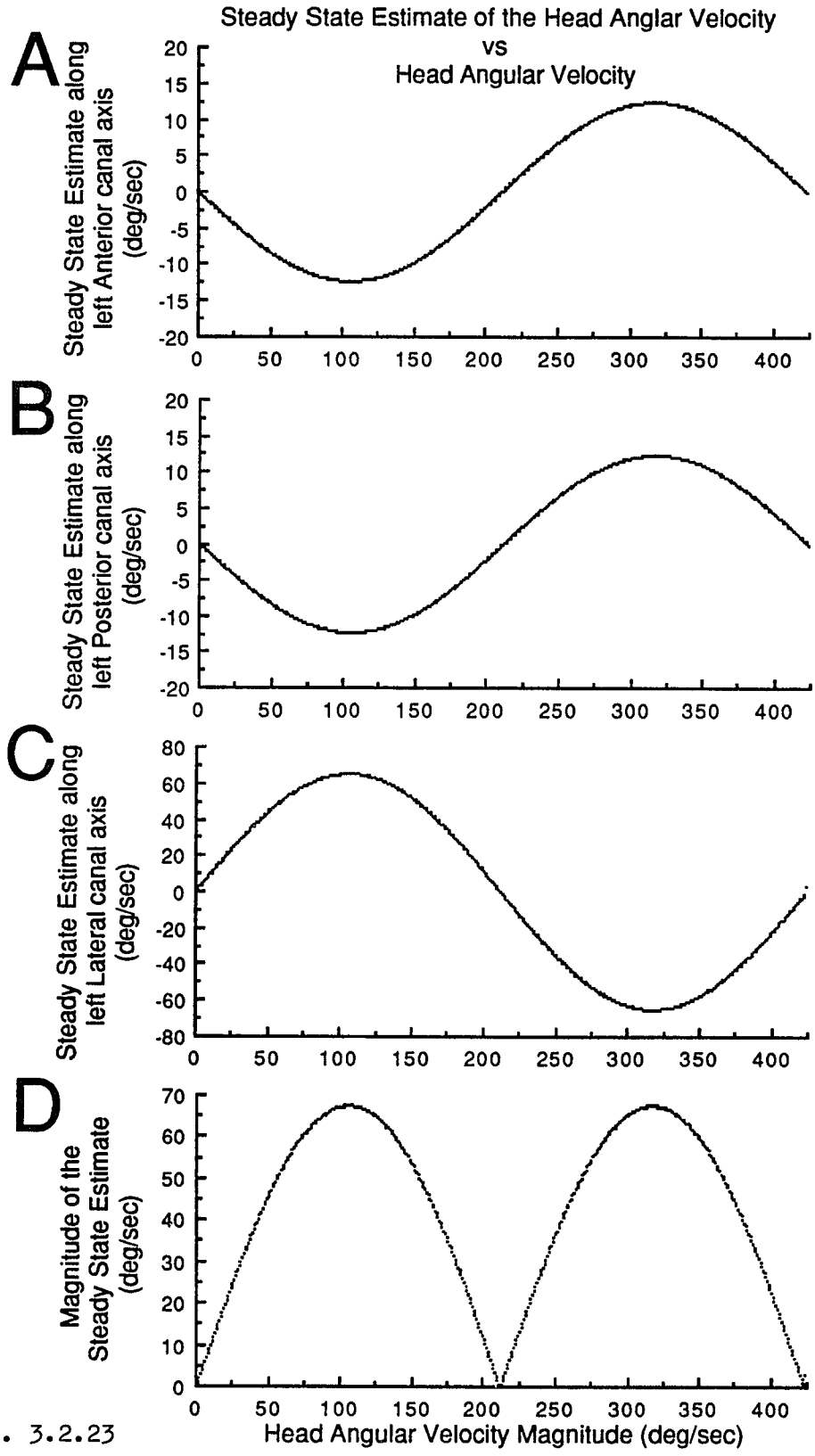
Steady State Estimate of the Head Anglar Velocity
vs
Head Angular Velocity
A
Steady State Estimate along
left Anterior canal axis
(deg/sec)
B
Steady State Estimate along
left Posterior canal axis
(deg/sec)
C
Steady State Estimate along
left Lateral canal axis
(deg/sec)
D
Magnitude of the
Steady State Estimate
(deg/sec)
Head Angular Velocity Magnitude (deg/sec)

Fig. 3.2.23

posterior) canal axis and the head velocity is approximately 100 degrees. It is assumed that the head is pitched forward by an angle between 10 and 170 degrees relative to the space vertical and that the head angular velocity is parallel to the head yaw axis. Note that if the head pitch is zero then each difference pattern associated with a component of the estimate is zero. As the pitch increases, each differnce pattern intially increases. For each head angular velocity, after the first T_2+T_1 seconds, the estimate is constant. Assuming that T_1 is equal to 0.85 seconds which is greater than T_2, the maximum angular speed of the simulation is chosen to cover one period of the estimate. The output of the four-pattern three-dimensional estimator, as a function of the magnitude of the head angular velocity, under the above conditions, is shown in Fig. 3.2.23.

The left anterior (or posterior) component of the estimate as a function of the head angular velocity magnitude is shown in Fig. 3.2.23A (or Fig. 3.2.23B). As the angular speed increases from zero, the component decreases toward a minimum of approximately -12 degrees/second, at which point the head angular velocity is approximately 110 degrees/second. The component of the estimate then begins to increase as the angular velocity increases. The component reaches a maximum of approximately 12 degrees/second, at which point the angular speed is approximately 320 degrees/second.

The left lateral component of the estimate as a function of the head angular velocity magnitude is shown in Fig. 3.2.23C. As the head

angular velocity increases, the component increases toward a maximum of approximately 62 degrees/second, at which point the angular speed is approximately 110 degrees/second. The component of the estimate then begins to decrease as the angular velocity continues to increase. The component reaches a minimum of approximately -62 degrees/second at a velocity of approximately 320 degrees/second.

The magnitude of the estimate as a function of the head angular velocity magnitude is shown in Fig. 3.2.23D. As the angular velocity increases, the estimate magnitude increases toward a maximum of approximately 68 degrees/second, at which point the angular speed is approximately 110 degrees/second. The estimate magnitude then begins to decrease as the angular speed continues to increase. The estimate reaches a minimum of zero, at which point the angular speed is approximately 210 degrees/second. The estimate magnitude then increases as the angular speed increases. The magnitude reaches a maximum of approximately 68 degrees/second, at which point the angular speed is approximately 320 degrees/second.

To compare the effects of the delays, T_1 and T_2, on the estimate, consider a sudden tilt OVAR experiment performed in the dark in which the semicircular canal input is assumed to be negligible. We assume that

$$T_2 < T_1 . \tag{3.2.125}$$

Therefore, the estimate is zero for the first T_1 seconds following the sudden tilt (see Eq (3.2.123)).

We will find the estimate for a time t, such that

$$T_1 \leq t < T_2+T_1 \tag{3.2.126}$$

We assume that the head is tilted by an angle, a, from the vertical and that the head angular velocity is parallel to the head yaw axis. Therefore, by representing gravity and the angular velocity of gravity both with respect to the head at time t, we obtain the following:

$$-\underline{w}=-w\hat{\underline{e}}_h^3, \text{ and} \tag{3.2.127}$$

$$\underline{g}(t)=-g[\ \sin(a)\sin(wt)\hat{\underline{e}}_h^1(t)+\sin(a)\cos(wt)\hat{\underline{e}}_h^2(t) + \cos(a)\hat{\underline{e}}_h^3]. \tag{3.2.128}$$

In Eq (3.2.127) $\underline{w}$ is the head angular velocity with respect to space and therefore, $-\underline{w}$ is the angular velocity of gravity with respect to the head. Since it is assumed that the velocity is aligned with the head yaw axis, $\hat{\underline{e}}_h^3$ is independent of time. The vectors, $\underline{g}(t-T_2)$ and $\underline{g}(t-T_1)$ of Eq (3.2.123) are delayed versions of $\underline{g}(t)$ given in Eq (3.2.128). Since t is less than T_2+T_1 the vector corresponding to $\underline{g}(t-T_2-T_1)$ of Eq (3.2.123) is equal to the head coordinate representation of $\underline{g}$ before the sudden tilt. Therefore,

$$\underline{g}(t-T_2-T_1)=-g\hat{\underline{e}}_h^3, \quad 0\leq t<T_2+T_1. \tag{3.2.129}$$

By substituting the head coordinate representation of $\underline{g}(t)$, $\underline{g}(t-T_2)$, $\underline{g}(t-T_1)$, and $\underline{g}(t-T_2-T_1)$ into Eq (3.2.123) we obtain

$$\begin{aligned}\hat{\underline{w}}(t)=\{ & \sin(a/2)\sin[wt-(wT_2)/2]\hat{\underline{e}}_h^1(t) \\ & +\sin(a/2)\cos[wt-(wT_2)/2]\hat{\underline{e}}_h^2(t) \\ & +\cos(a/2)\cos[wT_1-(wT_2)/2]\hat{\underline{e}}_h^3 \ \}/T_1\end{aligned} \tag{3.2.130}$$

Note that in this equation we assume that w is greater than zero and that the angle of tilt, a, is greater than zero but less than 180 degrees.

Finally, if t is greater than T_2+T_1 then the estimate is given by Eq (3.2.124).

In the following simulations of a sudden tilt experiment, it is assumed that T2 is equal to 0.2 seconds, T1 is equal to 0.85 seconds, a (the angle of head tilt) is equal to 30 degrees, and that the head angular velocity is equal to 60 degrees/second to the left. Furthermore, it is assumed that the left canal axes relative to the head are pitched back by 15 degrees and then rotated (to the left) by 45 degrees about the left lateral canal axis. The output of the two-difference-pattern estimator, as a function of time is shown in Figs. 3.2.24 and 3.2.25.

The interesting aspect of these responses is that for OVAR it

Fig. 3.2.24 Estimate of the head angular velocity in canal coordinates: T_1 is equal to 0.85 seconds and T_2 is equal to 0.20 seconds. The head yaw axis, which is initially opposite in direction to gravity, is suddenly tilted by 30 degrees. The estimate is zero for the first 0.85 seconds. The estimate for next 0.20 seconds depends on the otolith activation pattern before the sudden tilt.
A. The anterior component of the estimate is approximately 8 degrees/second from 0.85 to 1.05 seconds, and from then on it is constant at approximately -10 degrees/second.
B. The posterior component of the estimate varies approximately linearly from approximately -8 degrees/second to approximately -12 degrees/second, from 0.85 to 1.05 seconds, respectively. From then on it is constant at approximately -10 degrees/second.
C. The lateral component of the estimate is approximately 47 degrees/second from 0.85 to 1.05 seconds, and from then on it is constant at approximately 50 degrees/second.

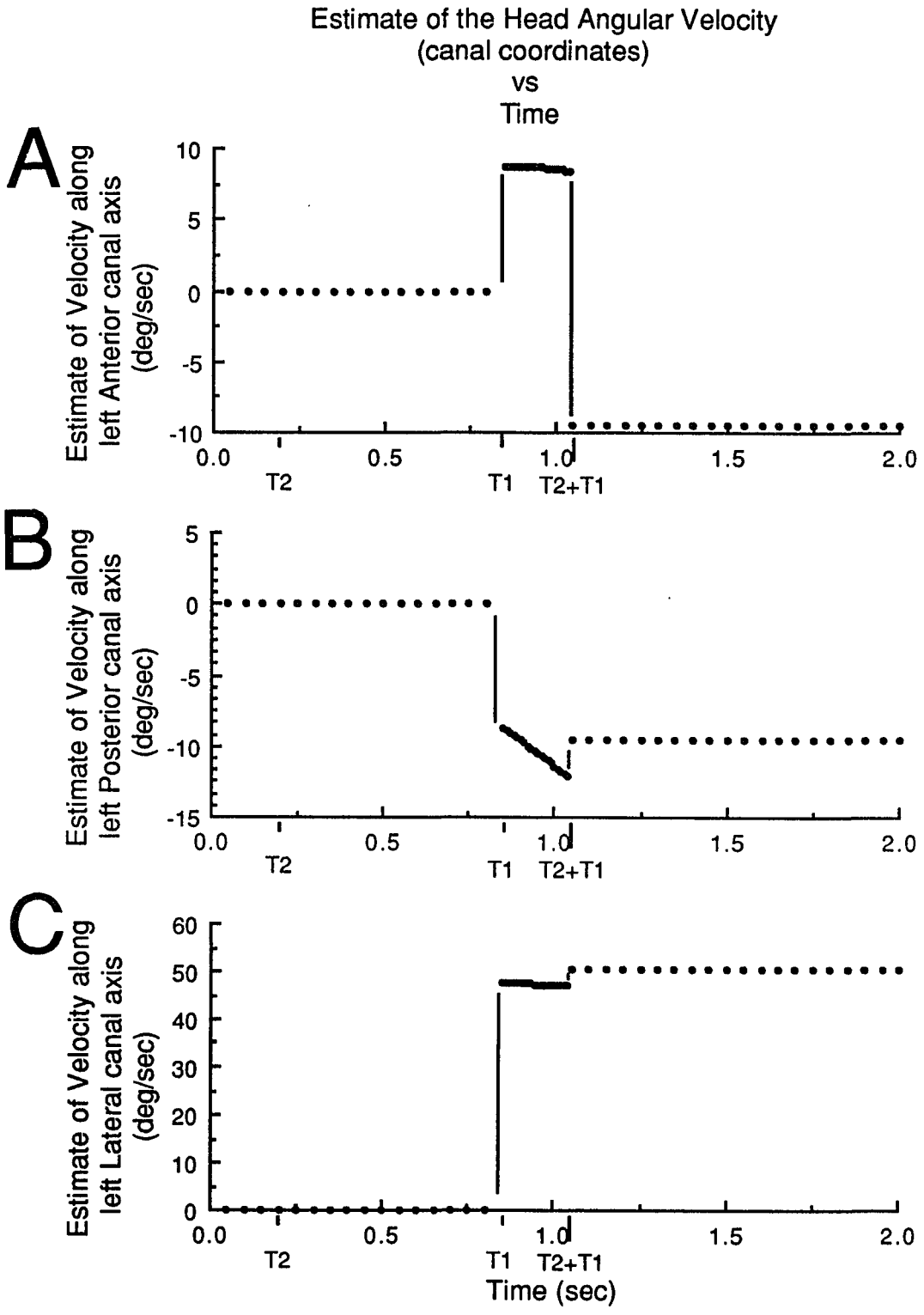
Estimate of the Head Angular Velocity
(canal coordinates)
vs
Time
A
Estimate of Velocity along
left Anterior canal axis
(deg/sec)
10
5
0
-5
-10
0.0
0.5
1.0
1.5
2.0
T2
T1
T2+T1
B
Estimate of Velocity along
left Posterior canal axis
(deg/sec)
5
0
-5
-10
-15
0.0
0.5
1.0
1.5
2.0
T2
T1
T2+T1
C
Estimate of Velocity along
left Lateral canal axis
(deg/sec)
60
50
40
30
20
10
0
0.0
0.5
1.0
1.5
2.0
T2
T1
T2+T1
Time (sec)

Fig. 3.2.24

Fig. 3.2.25 Estimate of the head angular velocity in head coordinates: T_1 is equal to 0.85 seconds and T_2 is equal to 0.20 seconds. The head yaw axis, which is initially opposite in direction to gravity, is suddenly tilted by 30 degrees. The estimate is zero for the first 0.85 seconds. The estimate for next 0.20 seconds depends on the otolith activation pattern before the sudden tilt.
A. The pitch component of the estimate varies approximately linearly from approximately 12 degrees/second to approximately 14 degrees/second, from 0.85 to 1.05 seconds, respectively. From then on it is constant at 0.0 degrees/second.
B. The roll component of the estimate varies approximately linearly from approximately 13 degrees/second to approximately 10 degrees/second, from 0.85 to 1.05 seconds, respectively. From then on it is constant at 0.0 degrees/second.
C. The lateral component of the estimate is constant at approximately 47 degrees/second from 0.85 to 1.05 seconds, and from then on it is constant at approximately 52 degrees/second.

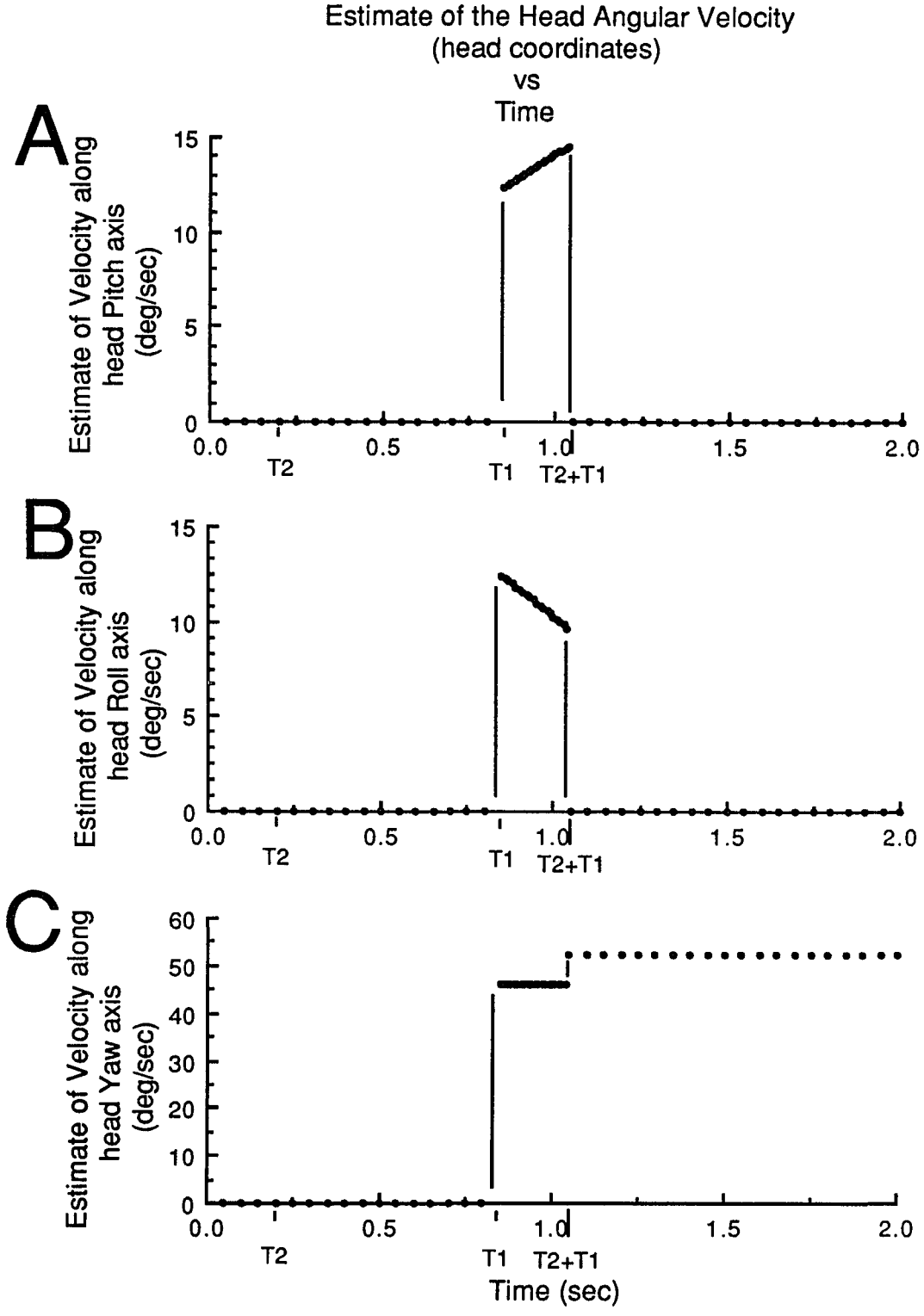
Estimate of the Head Angular Velocity
(head coordinates)
vs
Time
A
Estimate of Velocity along
head Pitch axis
(deg/sec)
15
10
5
0
0.0
0.5
1.0
1.5
2.0
T2
T1
T2+T1
B
Estimate of Velocity along
head Roll axis
(deg/sec)
15
10
5
0
0.0
0.5
1.0
1.5
2.0
T2
T1
T2+T1
C
Estimate of Velocity along
head Yaw axis
(deg/sec)
60
50
40
30
20
10
0
0.0
0.5
1.0
1.5
2.0
T2
T1
T2+T1
Time (sec)

Fig. 3.2.25

gives the estimate of eye velocity in a canal coordinate frame where the anterior, posterior and lateral canal contributions are correctly estimated. This is consistent with recent recordings in the vestibular nuclei which indicate that lateral, anterior and posterior canal related neurons contribute to the bias component of the eye velocity response during OVAR (Reisine et al, 1988). Although the estimator output is consistent with the average firing frequency of neurons in the vestibular nuclei, it does not predict the observed oscillations in frequency of vertical canal related neurons. They may be due to the system matrix which is changing as the head rotates (Sturm & Raphan, 1988; Raphan & Cohen, 1988).

To show that the oscillations may be due to the system matrix and that the bias components of the oscillations are due to the three-pattern estimator, the following rough estimation of the system matrix in canal coordinates is used in our simulations: The system matrix is assumed to be diagonal with time varying 'time constants', varying as a biased sinusoid. Each angular frequency associated with the sinusoids is equal to the head angular velocity magnitude. The left anterior and the left posterior 'time constants' vary from 2 to 10 seconds, and the left lateral 'time constant' varies form 7 to 12 seconds. These values are consistent with the 'time constants' of horizontal and vertical optokinetic after nystagmus (OKAN) when the animal is oriented differently with regard to gravity. The phases of the anterior, posterior, and lateral 'time constants' relative to nose

down, were chosen to be -40, -80, and 0 degrees, respectively to be consistent with the phases of the vertical unit activity recorded (Reisine et al, 1988). Therefore, the system matrix, in canal coordinates, is given by:

$$H(t)=\begin{vmatrix} -1/[6+\cos(wt+40)] & 0 & 0 \\ 0 & -1/[6+\cos(wt+80)] & 0 \\ 0 & 0 & -1/[9.5+\cos(wt)] \end{vmatrix} \quad (3.2.131)$$

The coupling matrix to the velocity storage integrator represented in canal coordinates is assumed to be constant and diagonal. The reciprocal of each diagonal element of the coupling matrix is assumed to be equal to the average value of the correponding 'time constant' of H(t). Therefore, the coupling matrix, in canal coordinates, is given by:

$$G=\begin{vmatrix} 1/6 & 0 & 0 \\ 0 & 1/6 & 0 \\ 0 & 0 & 1/9.5 \end{vmatrix} \quad (3.2.132)$$

The results of the simulations are shown in Fig. 3.2.26 which agree with the results from the unit recordings (Reisine et al, 1988).

A better interpretation of the experimental results, requires a more thorough understanding of the influence of gravity on the velocity storage integrator (Raphan & Cohen, 1988; Raphan and Strum, 1988) and on eye position command signals.

Fig. 3.2.26 Eye velocity command, generated by a three-dimensional gravity dependent velocity storage integrator, as a function of time: The input to the integrator is generated by the four-pattern head angular velocity estimtor.
A. The bias of the anterior component, after approximately 50 seconds, is approximately -7 degrees/second.
B. The bias of the posterior component, after approximately 50 seconds, is approximately -7 degrees/second.
C. The bias of the lateral component, after approximately 50 seconds, is approximately 48 degrees/second.

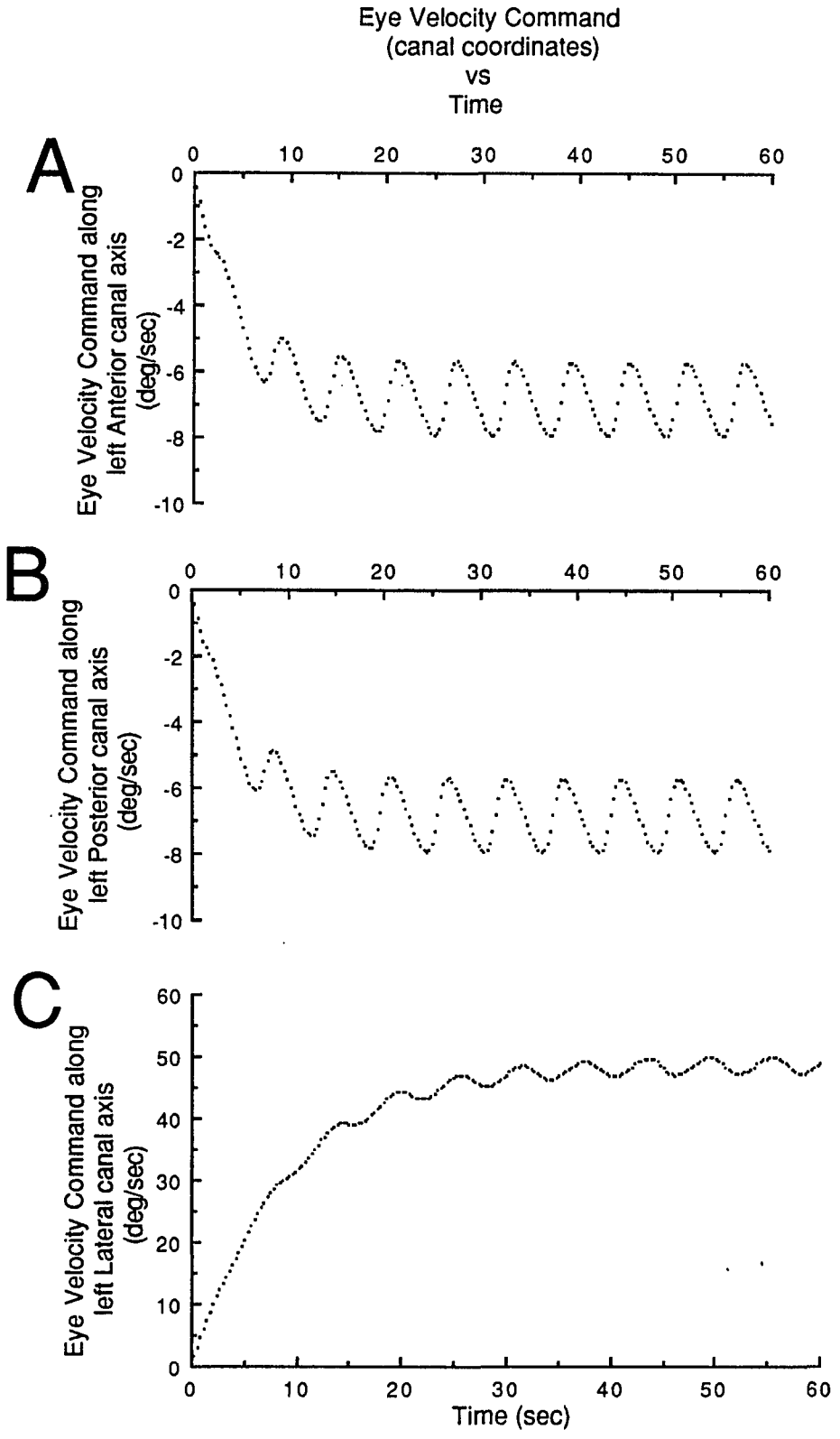
Eye Velocity Command
(canal coordinates)
vs
Time
A
Eye Velocity Command along
left Anterior canal axis
(deg/sec)
0
-2
-4
-6
-8
-10
0
10
20
30
40
50
60
B
Eye Velocity Command along
left Posterior canal axis
(deg/sec)
C
Eye Velocity Command along
left Lateral canal axis
(deg/sec)
0
10
20
30
40
50
60
Time (sec)

Fig. 3.2.26

CHAPTER 4

SUMMARY CONCLUSIONS AND FUTURE RESEARCH

4.1 Summary

In this thesis we have examined the characteristics of a model which would explain the bias response due to off-vertical axis rotation.

Rotation about an off-vertical axis (OVAR) causes continuous unidirectional nystagmus in darkness (Guedry, 1965; Benson & Bodin, 1966a). An analysis of the dynamics of the nystagmus suggests that the continuous slow phase velocity is generated by a signal that is an estimate of the velocity of a traveling wave pattern associated with the excitation and inhibition of the cells of the otolith maculae. The estimated velocity signal then excites the velocity storage integrator (Raphan et al. 1981).

The mathematical model that has been developed shows how the velocity of the traveling wave might be estimated from patterns of otolith activation related to head position. The estimation of velocity is based on a "template matching" algorithm. It is assumed that the signal arising in each cell of the macula is delayed by a certain time (T). As the head rotates in the gravitational field, a delayed pattern representing a previous position of the head is

available as a "template" that can be compared to the pattern associated with the present position of the head.

The delayed signal level for each cell is approximated from the present pattern by a spatial extrapolation in pattern space using information from the given cell and an adjacent one. The value of the displacement that minimizes the mean square error between the extrapolated and the delayed signal values over all cells gives a best estimate of head rotation (d) in time T. The estimated head velocity is proportional to the estimated head displacement ($\hat{d}$) and inversely proportional to the delay time (T).

By using a linear spatial extrapolation function and assuming a uniformly spaced distribution of polarization vectors over 360 degrees, sinusoidal spatial patterns are obtained. The formula for the estimated head velocity ($\hat{w}$) reduces to a sinusoidal function of angular head velocity (w) and delay time (T). For T=0.85 seconds, the model predicts that the steady state estimate of head velocity will rise as a function of stimulus velocity (w) to a peak value at w=50 deg/sec. It then declines for larger values of stimulus velocity (w). This type of behavior is observed in the slow phase velocity characteristics of OVAR in monkeys.

By using a nonuniformly spaced polarization vector distribution, based on the work of Fernandez & Goldberg, the model predicts that the estimate will oscillate at twice the head angular velocity. These ocsillations will be damped by the velocity storage integrator with a

time constant from 6 to approximately 13.3 seconds. The average value of the estimate, over a period of one head rotation, as a function of the head angular velocity is approximately that which was obtained using a uniformly spaced polarization vector distribution.

An estimator utilizing a first order approximation to an ideal delay operator could not account for the steady state characteristics of OVAR. An estimator utilizing a second order approximation to an ideal delay operator produced an estimate which is in closer agreement with the steady state characteristics of OVAR. The connection between the time delay parameters, T_1 and T_2, of the second order system, and the steady state and dynamic characteristics of the estimator, suggested that by choosing T_1 and T_2 such that there would be closer agreement between the steady characteristics of the estimator and of OVAR, required that there be less of an agreement between the dynamic characteristics of the estimator and of OVAR. It suggests that the brain probably implements a higher order system for the delay.

The introduction of additive noise with a mean of zero demonstrated a need to modify the one-sided estimator so as to improve its tolerance to noise. In the presence of noise, the average value of the one-sided estimate was equal to the noiseless estimate plus a term proportional to the number of otolith cells. However, the two-sided estimate is more robust and its average value was equal to the ideal two-sided estimate. This added term due to the noise in the estimate generated by the one-sided estimator was due to the

interaction of an otolith signal with itself and with a its delayed version. A simple modification of the estimator eliminated terms containing squares of an otolith signal and terms containing the product of an otolith signal with its delayed version. The average value of the estimate generated by the modified estimator in the presence of noise is equal to the two-sided estimate generated by the ideal estimator. This suggests that unilateral labyrinthectomy may have a profound effect on the variation of eye velocity during OVAR to the side of the lesion. This is especially true since velocity storage may be affected by such lesions.

By combining three one-dimensional models a three-dimensional estimate was obtained. If the angle between the head angular velocity and a canal normal was within approximately 25 degrees then the estimate was in approximate agreement with experimental findings. In addition, the estimate oscillated with the a frequency equal to the head angular velocity. This was qualitatively in agreement with experimental findings. However, the two-pattern estimator does not contain sufficient information to determine the head angular velocity in space. When the angle between the head angular velocity and a canal normal is greater than approximately 40 degrees then the estimate along that canal normal is approximately zero. This was not in agreement with experimental findings.

A four-pattern three-dimensional estimator was obtained. The

three-dimensional estimate generated by this estimator was in agreement with the bias components in experimental findings generated by experiments in which a head is rotated about the head yaw axis which is not aligned with gravity. If the head angular velocity is constant then the estimate generated by the four-pattern estimator is constant. Therefore, the oscillations seen in experimental findings cannot be due to this ideal four-pattern estimator. In particular, the bias component of the vertical unit recordings was approximately 7 degrees/second. By assuming that the oscillations in the unit recordings were due to the velocity storage integrator an estimate from the model was generated that was in quantitative agreement with the bias components of the OVAR findings.

When animals are tilted after prolonged rotation about a vertical axis the model predicts that the estimate of head velocity is delayed relative to actual head velocity. This accounts for the delay in the buildup of slow phase velocity during the initial second. Once a steady state estimate of head velocity has been established, the rise in slow phase velocity is consistent with the charging of the velocity storage integrator in response to a step in input velocity.

The model predicts many of the characteristics of the steady state slow phase velocity of nystagmus during OVAR. In addition, the computation involved in the model is simple, lends itself to parallel processing, and could utilize circuits involving the vestibular nuclei

and cerebellum. The model defines a mechanism for estimating velocity from position information which could be performed by a wide range of sensory modalities.

4.2 Discussion

This study has examined the computational aspects of estimating head velocity from patterns of otolith activation related to head movement in a gravitational field. The results suggest that otolith cells sample the gravitational field according to their polarization angle and estimate head velocity based on a "template matching" algorithm. If the estimated head velocity is used as an input to the velocity storage integrator it explains many of the dynamic aspects of the bias component of slow phase velocity during OVAR.

An important consideration in conceptualizing the proposed velocity estimator was that the algorithm for the computation of velocity be a function of cell groups with all directions of polarization. The model is consistent with the anatomical and physiological configuration of the otoliths (Spoendelin, 1965; Fernandez & Goldberg, 1976a,b,c) and is useful in determining the effects of the discrete nature of the gravitational information sampling on the response characteristics. This is in contrast to other attempts at modelling the response to OVAR which have used a lumped parameter continuous system approach (Benson & Barnes, 1970;

Hain, 1986) and have not attempted to fit the detailed behavioral responses during OVAR.

The major hypothesis in the model is that the estimation of head velocity is implemented by using a delayed version of the pattern of otolith activation as a "template" and comparing it to the present activation of the otoliths. The delay is an important parameter for determining the dynamic responses as well as the steady state characteristics. A delay of 0.85 seconds causes the steady state estimate of velocity to increase approximately linearly with stimulus velocity, saturate at about 65 deg/sec, and then decline toward zero. This is consistent with the behavior of the steady state component of velocity during OVAR (Raphan, et al. 1981) and is the best fit in the mean square sense to the data obtained from the monkey (Fig. 3.1.8A).

The realization of the delay has important effects on the shape of the estimated head velocity versus head angular velocity curve. For an ideal delay, the phase difference between delayed and present patterns increases linearly with head velocity. The estimation of velocity rises approximately linearly up to 90 degrees of phase shift. When the phase is greater than 90 degrees, the estimation falls and the curve crosses the axis at a head velocity resulting in 180 degrees of phase shift. If the delay is realized by a first order system then the phase delay of neuron signals would approach 180 degrees depending on T_1 and T_2 in Eqs (3.1.56). If T_2 is equal to zero then the phase delay of neuronal signals would approach 90 degrees asymptotically.

If the delay is realized by a second order system then the phase delay of neuronal signals could approach 360 degrees depending on T_1 and T_2 in Eqs (3.1.114). If T_2 is positive then such a realization would cause an inversion in slow phase eye velocity at higher velocities of stimulation. Simulations suggest that the representation of the delay has sufficient flexibility to correlate with the delays observed in neural networks (Schor et al, 1985).

A decrease in the time constant of the velocity storage integrator with rotation velocity would also cause a decline in steady state eye velocity as a function of head velocity. However, such changes in time constant would also not produce an inversion in steady state eye velocity. Although inversions in slow phase eye velocity have been noted (Benson & Bodin, 1966a; Goldberg & Fernandez, 1982) the precise behavior of the bias component of slow phase velocity during OVAR at high velocities of rotation has not been studied. Consequently, the exact structure of the system generating the delay nor what the role the integrator time constant plays in generating the steady state response characteristic is unclear.

It is of interest that the same value of the delay parameter which best fits the steady state eye velocity versus head velocity curve also explains the approximate one second delay observed before the buildup in slow phase velocity during the dynamic tilt paradigm (Raphan et al. 1981). The implication that the steady state and dynamic response characteristics are determined by a common mechanism

is a unifying feature of the model and suggests that the observed delays are not random responses. It predicts that subjects with a wider linear range in their eye velocity vs head velocity curve would have a shorter delay in their time domain response. Although this is experimentally testable, the small intersubject variability in these parameters has made the results difficult to interpret.

The model also gives insight into differences between the role of the otoliths in charging the velocity storage integrator and on tilt suppression (Benson, 1974; Raphan et al. 1981). When a subject is tilted back to the vertical after prolonged rotation about an off-vertical axis, the velocity decays with a time constant of about 10 to 15 seconds. This is in contrast to the rapid 2-3 second decay rates that occur during post rotatory nystagmus following OVAR or when subjects are tilted in various directions during post rotatory nystagmus or OKAN (Correia & Guedry, 1966; Benson & Bodin, 1966b; Benson, 1974; Raphan et al. 1981). In these instances the model predicts a velocity estimate of zero from the otolith input. The differences in response characteristics of the after-nystagmus resulting from tilt suppression as compared to tilting upright during rotation suggests that the mechanism of suppression that shortens the time constant of the integrator utilizes different information than that coming from the velocity estimator. This is supported by the fact that lesions of the nodulus and uvula which affect "dumping" due to tilting and visual suppression do not affect the response to OVAR

(Waespe et al. 1985). Presumably, the vertical semicircular canals which generate continuous nystagmus during pitch while rotating (Raphan et al, 1983) are important factors in the information processing during tilt suppression.

Another interesting aspect of the model was the necessity of introducing bilateral components of otolith macula to explain the characteristics of the steady state eye velocity versus head velocity curve. For a finite number of polarization vectors and a unilateral model of the otoliths, this curve was asymmetrical. The asymmetry depended on the number of classes of polarization angles, their distribution, and the discrete nature of the model. The introduction of a push-pull combination of bilateral components of the velocity estimator cancelled the asymmetry. Thus, for a finite number of polarization classes the model would predict an asymmetrical steady state velocity vs head velocity curve after unilateral lesions. While unilateral labyrinthectomy is known to affect OKN, OKAN, and vestibular nystagmus (Baarsma & Collewijn, 1975), its precise effect on the response characteristics during OVAR is not known.

An extension of the model to three dimensions showed that a two-pattern estimator could only give a reasonable estimate of head velocity over a small range of angles between the otolith macular normals and the head velocity in space. This was true only if appropriate normalization was introduced (Fanelli et al, 1988). One reason for this is that two patterns cannot localize a plane in three

dimensions. An extension to include computation on more delayed patterns led to an improved estimation scheme and suggested that the estimation for each plane was done in a canal coordinate reference frame. This is consistent with data in the vestibular nuclei recorded from alert monkeys (Reisine et al, 1988). This extended model also requires a normalization process to obtain an accurate estimate of head velocity and could be realized by a neural network (Fanelli et al, 1988). Neither the realization of the pattern velocity estimator nor its location is known. The delayed representation of the otolith signal necessary for generating the "template pattern" could be realized by an integrative network whose parameters are such that it gives a phase delay consistent with approximately a one second delay period. The pattern itself could be realized by direct central projections of the afferent otolith signals.

One way to test the feasability of the model at the central level is to identify classes of neurons representing the inputs and the output of the velocity estimator. The input neurons should be comprised essentially of two types. One type of neuron should have a frequency of firing in phase with primary afferent activity and have associated polarization vectors. This class would represent the "present pattern" in the model. Another class should have a frequency of firing phase delayed with respect to the primary afferent activity. This class would represent the "template pattern". The two signal vectors would provide the necessary input to the velocity estimator.

The output neurons should be related to the bias component of eye velocity.

Scattered neurophysiological and anatomical results provide some support for this conceptual organization. Melvill-Jones and Milsum (1969) indicate that central otolith dependent neurons have a broad representation of sensitivity vectors over a complete sphere of solid angle and some neurons show a marked phase delay in their response characteristics. Recently, Schor et al. (1985) have recorded in and around the lateral vestibular nucleus of Deiters and found essentially two classes of neurons. One class of neurons displayed flat gain and phase curves while another class showed almost a linear phase delay up to 180 degrees over the range .01 to 1 Hz. Thus, these neurons could provide the input to the velocity estimator. The cerebellum and its associated nuclei are strong projection areas of Deiters nucleus (Ghelarducci, 1973; Ghelarducci & Magherini, 1975). The cerebellar nuclei also project to the medial vestibular nucleus (Brodal, 1974) where activity related to velocity storage during OKN, OKAN, and vestibular nystagmus has been recorded (Waespe & Henn, 1977a,b). There is also modulation in the activity of canal dependent vestibular nuclei neurons in relation to velocity of rotation during OVAR (Benson et al. 1970). Thus, these vestibular and cerebellar nuclei are good candidates for the central nervous system structures that realize the velocity estimator.

In summary, the model presented is a simple representation of a

mechanism for estimating head velocity from patterns of head position information. The computation involved requires inner products between multidimensional signal vectors. This lends itself to parallel processing and could utilize circuits involving the vestibular nuclei and cerebellum. Thus, while the functional significance of the response to OVAR is not clear, the fact that the central nervous system constructs a velocity estimate from head orientation and stores this information in the velocity storage integrator suggests that this is an important mechanism for ocular and postural stabilization.

4.3 Recommendations for Future Research

The following areas are extensions of this work:

1. To consider the effect on the estimator due to a second or higher order local approximation of a pattern needed for matching the present pattern to the delayed pattern.
2. Include the effects of centrifugal acceleration on otolith activations. The acceleration transduced by an otolith hair cell is a superposition of gravity and the centrifugal acceleration.
3. Replace the instantaneous otolith transduction system used in this thesis with a first or higher order system to more accurately reflect the transduction process.
4. Obtain other possible polarization vector distributions and ascertain how these distributions effect the estimate.
5. Consider the effects on a third order approximation of an ideal delay operator on the estimator.
6. Consider how a nonuniformly spaced polarization vector distribution effects the three-dimensional estimate.
7. Study the effects of approximations to an ideal delay operator on the three-dimensional estimator.

8. Ascertain how additive noise effects the three-dimensional estimate.
9. Find a neural net implementation of the four-pattern estimator. In particular, study how a neural net could be used to implement the normalization of a difference pattern.

APPENDIX A

REDUCTION OF THE COMPUTATIONAL COMPLEXITY OF VELOCITY ESTIMATION

The denominator can be examined for N large and with H small to reduce the computational complexity. Let,

$$X(t)=\|(\text{RotateUp}-I)[\underline{r}(t)]\|^2. \tag{A1}$$

Therefore,

$$X(t)=\sum_{n=0}^{N-1} (r_{n+1}(t)-r_n(t))^2, \tag{A2}$$

where $r_N(t)=r_0(t)$. Using Eqs (3.1.26), (3.1.27), and (3.1.35) we, therefore, obtain

$$X(t)=g^2 \sum_{n=0}^{N-1} \{\cos([n+1]H-wt)-\cos(nH-wt)\}^2. \tag{A3}$$

Expanding Eq (A3) we obtain

$$X(t)=g^2 \sum_{n=0}^{N-1} \{\cos^2(nH-wt+H)-2\cos(nH-wt+H)\cos(nH-wt)+\cos^2(nH-wt)\}. \quad (A4)$$

Using the trigonometric identity given in Eq (B3) we obtain

$$X(t)=(g^2/2) \sum_{n=0}^{N-1} \{\cos[2(nH-wt+H)]+1-2\cos[2(nH-wt)+H] -2\cos[H]+\cos[2(nH-wt)]+1\}. \quad (A5)$$

Using Eq (B8) in Eq (A5) we obtain the following formula for X which is independent of time:

$$X=g^2N(1-\cos(H)). \quad (A6)$$

Using the trigonometric identity given in Eq (B7) we obtain

$$X=2g^2N\sin^2(H/2). \quad (A7)$$

Using the equation, $NH=2\pi$, we therefore, have the following:

$$X=\pi g^2\{\sin^2(H/2)/(H/4)\}. \quad (A8)$$

Substituting Eq (A8) into Eq (A1) we obtain

$$||(\text{RotateUp-I})[\underline{r}(t)]||^2=\pi^2 g^2 H\{\sin(H/2)/(H/2)\}^2, \tag{A9}$$

and therefore,

$$H/||(\text{RotateUp-I})[\underline{r}(t)]||^2=\{(H/2)/\sin(H/2)\}^2/(\pi^2 g^2). \tag{A10}$$

We now take the limit of Eq (A10) for large N (or for small H) and obtain the following result:

$$H/||(\text{RotateUp-I})[\underline{r}(t)]||^2 \xrightarrow[N\to]{} 1/(\pi^2 g^2). \tag{A11}$$

Therefore, the expression for the best estimate of head displacement, $\hat{d}$, is given by

$$\hat{d}=\langle\{\text{DELAY(T)-I}\}[\underline{r}(t)],\{\text{RotateUp-I}\}[\underline{r}(t)]\rangle/(\pi^2 g^2). \tag{A12}$$

APPENDIX B

IDENTITIES AND FORMULAE

USED IN DERIVING ESTIMATION ALGORITHM

$$\sin(A+B)=\sin(A)\cos(B)+\cos(A)\sin(B), \tag{B1}$$

$$\cos(A+B)=\cos(a)\cos(b)-\sin(a)\sin(b), \tag{B2}$$

$$\cos(A+B)+\cos(A-B)=2\cos(A)\cos(B). \tag{B3}$$

$$\cos(A+B)-\cos(A-B)=-2\sin(A)\sin(B). \tag{B4}$$

$$\sin(A+B)+\sin(A-B)=2\sin(A)\cos(B). \tag{B5}$$

$$\sin(A+B)-\sin(A-B)=2\sin(B)\cos(A). \tag{B6}$$

$$\sin^2(H/2)=[1-\cos(H)]/2. \tag{B7}$$

In Eqs (B8), (B9), (B10), and (B11) N>2, $NH=2\pi$, and a is any constant:

$$\sum_{i=0}^{N-1} \cos(2iH-a)=0, \tag{B8}$$

$$\sum_{i=0}^{N-1} \cos^2(iH-a)=N/2, \tag{B9}$$

$$\sum_{i=0}^{N-1} \sin^2(iH-a)=N/2, \tag{B10}$$

$$\sum_{i=0}^{N-1} \sin(iH-a)\cos(iH-a)=0. \tag{B11}$$

$$\sin(x)\simeq x-x^3/6, \tag{B12}$$

$$\cos(x)\simeq 1-x^2/2, \tag{B13}$$

$$\exp(-x)\simeq 1-x+x^2/2-x^3/6. \tag{B14}$$

Using the approximations given in Eqs (B12), (B13), and (B14) we obtain the following:

$$(\sin(wt)\cos(t/T_1)\exp(-t/T_1)\simeq \tag{B15}$$
$$(wT_1)t/T_1-(wT_1)(t/T_1)^2-[(wT_1)^3/6](t/T_1)^3,$$

$$\cos(wt)\cos(t/T_1)\exp(-t/T_1)\simeq \tag{B16}$$
$$1-t/T_1-[(wT_1)^2/2](t/T_1)^2+\{[2+3(wT_1)^2]/6\}(t/T_1)^3,$$

$$\sin(wt)\sin(t/T_1)\exp(-t/T_1)\simeq(wT_1)(t/T_1)^2-(wT_1)(t/T_1)^3, \text{ and} \tag{B17}$$

$$\cos(wt)\sin(t/T_1)\exp(-t/T_1)\simeq \tag{B18}$$
$$t/T_1-(t/T_1)^2+\{[2-3(wT_1)^2]/6\}(t/T_1)^3.$$

APPENDIX C

COMPUTER PROGRAMS USED TO GENERATE

EYE VELOCITY COMMAND IN FIGURES 3.1.10, 3.1.14 AND 3.2.16

Computer Program used to Generate the Eye Velocity Command in Figure 3.1.10

```
1.05 E
1.10 T "ANGULAR VELOCITY IN DEG/SEC"
1.15 S W=60
1.20 T "TIME DELAY IN SEC"
1.25 S T=0.85
1.40 T "DELTA-TIME IN SEC"!
1.45 S DT=0.05
1.50 S PI=3.1415926536
1.55 S WR=W*PI/180
1.60 S WT=WR*T
1.65 S K=180/(PI*PI*T)
1.70 S X=0
1.75 S SX=1023/65
1.80 S BX=5*SX-512
1.85 S SY=1023/120
1.87 S BY=-512
1.90 S MI=1000
1.95 S MA=-1000
1.96 S HO=.075
1.97 S GO=.075
C
1.98 S H=2*PI/30
2.05 F TI=0,DT,T; DO 3.0
2.10 F TI=T+DT,DT,50; DO 5.0
2.12 S NU=0
2.15 F TI=50+DT,DT,100; DO 9.0
2.20 F I=-512,10,511; S L=FDIS(-512,I)+FDIS(I,-512)
2.25 T "MIN X=",MI,"  MAX X=",MA
2.30 Q
C
3.05 S WP=WR*TI
3.10 S NU=0
3.15 F I=0,1,29; DO 4.0
3.20 S NU=K*NU
3.25 DO 9.0
3.30 R
```

```
4.05 S IH=I*H
4.10 S PR=FCOS(IH-WP)
4.15 S AY=0-PR
4.20 S UP=FCOS(IH+H-WP)-PR
4.25 S NU=NU+AY*UP
4.30 R
C
5.05 S WP=WR*TI
5.10 S NU=0
5.15 F I=0,1,29; DO 6.0
5.20 S NU=K*NU
5.25 DO 9.0
5.30 R
C
6.05 S IH=I*H
6.10 S PR=FCOS(IH-WP)
6.15 S AY=FCOS(IH-WP+WT)-PR
6.20 S UP=FCOS(IH+H-WP)-PR
6.25 S NU=NU+AY*UP
6.30 R
C
9.05 S XD=-HO*X+GO*NU
9.10 S X=X+XD*DT
9.15 S L=FDIS(SX*TI+BX,SY*X+BY)
9.20 IF (MA-X)9.25,9.30,9.30
9.25 S MA=X
9.30 IF (X-MI)9.35,9.40,9.40
9.35 S MI=X
9.40 R
```

Computer Program used to Generate the Eye Velocity Command in Figure 3.1.14

```
C     1-DIMENSIONAL, NONUNIFORM DISTRIBUTION, BARBECUE-SPIT
C       ROTATION, SUDDEN TILT AT TIME O, ESTIMATES FROM THE
C       VELOCITY STORAGE INTEGRATOR.

C     EXTERNAL UNITS, TIME:SEC, ANGLE:DEG
C     INTERNAL UNITS, TIME:SEC, ANGLE:RADIANS

C       T:TIME DELAY CONSTANT
C       TC:INTEGRATOR TIME CONSTANT
C       PVAD(.):POLARIZATION VECTOR ANGLE DISTRIBUTION (RAD)
C       PVADDE(.):PVAD DISTRIBUTION IN DEGREES
      REAL T, TC, PVAD(181), PVADDE(181)

C       PVN:NUMBER POLARIZATION VECTORS, .LE. TO 180
      INTEGER PVN

C       TO:INITIAL TIME
C       ORNO:INIT MACULAR ORIENTATION AT TO,
C              RELATIVE TO NOSE DOWN
C       XLRO:INITIAL INTEGRATOR STATE AT TO,
C            LEFT RIGHT ESTIMATE
C       MACVEL:MACULAR VELOCITY, ASSUMED PARALLEL TO NORMAL
      REAL TO, ORNO, XLRO, MACVEL

C       PRSTIM:PRESENT TIME
C       PRSORN:PRESENT MACULAR ORIENTATION
C       DELORN:DELAYED MACULAR ORIENTATION
C       XLR:INTEGRATOR STATE IN RADIANS AT PRSTIM
C           LEFT RIGHT ESTIMATE
      REAL DELORN, PRSORN, PRSTIM, XLR

C       ESTLFT:LEFT ESTIMATE
C       ESTRGT:RIGHT ESTIMATE
C       ESTLR:LEFT RIGHT OR 2 SIDED ESTIMATE
C       LNORM:LEFT SIDE NORMALIZATION DIVISOR
C       RNORM:RIGHT SIDE NORMALIZATION DIVISOR
      REAL ESTLFT, ESTRGT, ESTLR, LNORM, RNORM
C       DT:DELTA TIME, FOR INTEGRATION STEP
      REAL DT
```

```
C       EDTNUM:ESTIMATE DT NUMBER, TIME BETWEEN ESTIMATES
C       ESTNUM:NUMBER ESTIMATES REPORTED, 1 EVERY EDTNUM*DT
      INTEGER EDTNUM, ESTNUM

C       NDT:NUMBER OF DT'S FROM PRSTIM TO T
C       NE:NUMBER OF ESTIMATES FROM PRSTIM TO T
C       ODDDT:ODD NUMBER OF DT'S TO REACH TIME T
C       RMEST:REMAINING ESTIMATES, TO REACH ESTNUM
      INTEGER NDT, NE, ODDDT, RMEST

C       VELT:MACVEL*T
C       VELDT:MACVEL*DT
C       DTDTC:DT/TC
C       PIT:PI*T
C       SPADIF:SPATIAL DIFFERENCE, (ROTATEUP-I)ACTIVATION
C       TEMDIF:TEMPORAL DIFFERENCE, (DELAY-I)ACTIVATION
      REAL VELT, VELDT, DTDTC, PIT, SPADIF, TEMDIF

C       DEGRAD:DEGREES TO RADIANS, CONVERSION FACTOR
C       RADDEG:RADIANS TO DEGREES, CONVERSION FACTOR
C       XD:XLR IN DEGREES
      REAL DEGRAD, RADDEG, XD

C       I,J,K:USED AS INDICES IN DO LOOPS
      INTEGER I, J, K

      REAL PI
        DATA PI/3.14159/
C         2653589793D00/

5       FORMAT(I5)
10      FORMAT(G14.6)

      READ(6,5) PVN
      READ(6,10) (PVADDE(I),I=1,PVN)

C       POLARIZATION COMPONENT PVN+1 IS COMPONENT 1
C       CIRCULAR DISTRIBUTION
      PVADDE(PVN+1)=PVADDE(1)+360.0

      READ(5,10) T, TC, TO, ORNO, XLRO, MACVEL, DT

      READ(5,5) EDTNUM, ESTNUM

      WRITE(4,15)
15      FORMAT(' MACULAR NORMAL PERPENDICULAR TO GRAVITY',/,
     1         ' MACULA ROTATES ABOUT ITS NORMAL')
```

```
      WRITE(4,20) T
20      FORMAT(' TIME DELAY CONSTANT (SEC)=',G14.6)

      WRITE(4,25) TC
25      FORMAT(' INTEGRATOR TIME CONSTANT (SEC)=',G14.6)

      WRITE(4,30) TO
30      FORMAT(' INITIAL TIME (SEC)=',G14.6)

      WRITE(4,35) ORNO
35      FORMAT(
     1          ' INITIAL MACULAR ORIENTATION WRT NOSE DOWN',/,
     2          ' SIGN OF INPUT, +:NOSE LEFT, -:NOSE RIGHT',/,
     3          ' INITIAL MACULAR ORIENTATION (DEG)=',G14.6)

      WRITE(4,40) XLRO
40      FORMAT(' LEFT RIGHT ESTIMATE',/,
     1          ' INITIAL INTEGRATOR STATE (DEG/SEC)=',G14.6)

      WRITE(4,45) MACVEL
45      FORMAT(' MACULAR ANGULAR VELOCITY',/,
     1          ' SIGN OF INPUT, +:ROTATE LEFT, -:ROTATE RIGHT',
     2         /,' ANGULAR VELOCITY (DEG/SEC)=',G14.6)

      WRITE(4,50) DT
50      FORMAT(' INTEGRATION STEP (DELTA-T) (SEC)=',G14.6)

      WRITE(4,55) EDTNUM
55      FORMAT(' ESTIMATE REPORTING INTERVAL IN DT''S',/,
     1          ' NUMBER OF DT''S BETWEEN REPORTS=',I5)

      WRITE(4,60) ESTNUM
60      FORMAT(' SPECIFY NUMBER OF ESTIMATE REPORTS=',I5)

      DEGRAD=PI/180.0
      RADDEG=180.0/PI

C       CONVERT FROM DEGREES TO RADIANS
      DO 65 I=1, PVN+1
        PVAD(I)=PVADDE(I)*DEGRAD
65      CONTINUE

      ORNO=ORNO*DEGRAD
      XLRO=XLRO*DEGRAD
      MACVEL=MACVEL*DEGRAD
```

```
      PRSTIM=TO
      PRSORN=ORNO
      XLR=XLRO

      VELT=MACVEL*T
      VELDT=MACVEL*DT
      DTDTC=DT/TC
      PIT=PI*T

      RMEST=ESTNUM
      WRITE(7,5) ESTNUM
      IF (PRSTIM.GE.T) GOTO 140
C     *ELSE PRSTIM .LT. T, Delayed pattern corresponds to head*
C     *upright*
        NDT=INT((T-PRSTIM)/DT+0.50)
        NE=INT(NDT/EDTNUM)
        IF (NE.GT.ESTNUM) NE=ESTNUM
        DO 90 I=1, NE
          DO 80 J=1, EDTNUM
            PRSTIM=PRSTIM+DT
            PRSORN=PRSORN+VELDT
            ESTLFT=0.0
            ESTRGT=0.0
            LNORM=0.0
            RNORM=0.0
            DO 70 K=1, PVN
C              ADD NEXT TERM TO LEFT-SIDED ESTIMATE AND NORMALIZATION
              TEMDIF=-COS(PRSORN-PVAD(K))
              SPADIF=COS(PRSORN-PVAD(K+1))-COS(PRSORN-PVAD(K))
              ESTLFT=ESTLFT+TEMDIF*SPADIF/(PVAD(K+1)-PVAD(K))
              LNORM=LNORM+(SPADIF/(PVAD(K+1)-PVAD(K)))**2

C              ADD NEXT TERM TO RIGHT-SIDED ESTIMATE AND NORMALIZATION
              TEMDIF=-COS(PRSORN+PVAD(K))
              SPADIF=COS(PRSORN+PVAD(K+1))-COS(PRSORN+PVAD(K))
              ESTRGT=ESTRGT+TEMDIF*SPADIF/(PVAD(K+1)-PVAD(K))
              RNORM=RNORM+(SPADIF/(PVAD(K+1)-PVAD(K)))**2
70            CONTINUE
            ESTLFT=ESTLFT/(T*LNORM)
            ESTRGT=ESTRGT/(T*RNORM)
C            COMPUTE TWO-SIDED ESTIMATE
            ESTLR=(ESTLFT-ESTRGT)/2.0
C            COMPUTE NEXT (TWO-SIDED) INTEGRATOR STATE
            XLR=XLR+(-XLR+ESTLR)*DTDTC
80          CONTINUE
```

```
C          RECORD THE INTEGRATOR STATE
           XD=XLR*RADDEG
           WRITE(4,10) PRSTIM
           WRITE(7,85) PRSTIM, XD
85           FORMAT(' ',G14.6,',',G14.6)
90         CONTINUE
         RMEST=RMEST-NE
         IF (RMEST.EQ.0) GOTO 175
         ODDDT=NDT-NE*EDTNUM
         IF (ODDDT.EQ.0) GOTO 140
         DO 110 J=1, ODDDT
           PRSTIM=PRSTIM+DT
           PRSORN=PRSORN+VELDT
           ESTLFT=0.0
           ESTRGT=0.0
           LNORM=0.0
           RNORM=0.0
           DO 100 K=1, PVN
             TEMDIF=-COS(PRSORN-PVAD(K))
             SPADIF=COS(PRSORN-PVAD(K+1))-COS(PRSORN-PVAD(K))
             ESTLFT=ESTLFT+TEMDIF*SPADIF/(PVAD(K+1)-PVAD(K))
             LNORM=LNORM+(SPADIF/(PVAD(K+1)-PVAD(K)))**2

             TEMDIF=-COS(PRSORN+PVAD(K))
             SPADIF=COS(PRSORN+PVAD(K+1))-COS(PRSORN+PVAD(K))
             ESTRGT=ESTRGT+TEMDIF*SPADIF/(PVAD(K+1)-PVAD(K))
             RNORM=RNORM+(SPADIF/(PVAD(K+1)-PVAD(K)))**2
100          CONTINUE
           ESTLFT=ESTLFT/(T*LNORM)
           ESTRGT=ESTRGT/(T*RNORM)
           ESTLR=(ESTLFT-ESTRGT)/2.0
           XLR=XLR+(-XLR+ESTLR)*DTDTC
110        CONTINUE

C      DELAYED PATTERN CORRESPONDS TO TILTED HEAD
         DO 130 J=1, EDTNUM-ODDDT
           PRSTIM=PRSTIM+DT
           PRSORN=PRSORN+VELDT
           DELORN=PRSORN-VELT
           ESTLFT=0.0
           ESTRGT=0.0
           LNORM=0.0
           RNORM=0.0
           DO 120 K=1, PVN
             TEMDIF=COS(DELORN-PVAD(K))-COS(PRSORN-PVAD(K))
             DPADIF=COS(PRSORN-PVAD(K+1))-COS(PRSORN-PVAD(K))
             ESTLFT=ESTLFT+TEMDIF*SPADIF/(PVAD(K+1)-PVAD(K))
             LNORM=LNORM+(SPADIF/(PVAD(K+1)-PVAD(K)))**2
```

```
            TEMDIF=COS(DELORN+PVAD(K))-COS(PRSORN+PVAD(K))
            SPADIF=COS(PRSORN+PVAD(K+1))-COS(PRSORN+PVAD(K))
            ESTRGT=ESTRGT+TEMDIF*SPADIF/(PVAD(K+1)-PVAD(K))
            RNORM=RNORM+(SPADIF/(PVAD(K+1)-PVAD(K)))**2
120         CONTINUE
          ESTLFT=ESTLFT/(T*LNORM)
          ESTRGT=ESTRGT/(T*RNORM)
          ESTLR=(ESTLFT-ESTRGT)/2.0
          XLR=XLR+(-XLR+ESTLR)*DTDTC
130       CONTINUE

        XD=XLR*RADDEG
          WRITE(4,10) PRSTIM
        WRITE(7,135) PRSTIM, XD
135       FORMAT(' ',G14.6,',',G14.6)
        RMEST=RMEST-1
        IF (RMEST.EQ.0) GOTO 175
C      *END ELSE*
C     DELAYED PATTERN CORRESPONDS TO TILTED HEAD
140   DO 170 I=1, RMEST
        DO 160 J=1, EDTNUM
          PRSTIM=PRSTIM+DT
          PRSORN=PRSORN+VELDT
          DELORN=PRSORN-VELT
          ESTLFT=0.0
          ESTRGT=0.0
          LNORM=0.0
          RNORM=0.0
          DO 150 K=1, PVN
            TEMDIF=COS(DELORN-PVAD(K))-COS(PRSORN-PVAD(K))
            SPADIF=COS(PRSORN-PVAD(K+1))-COS(PRSORN-PVAD(K))
            ESTLFT=ESTLFT+TEMDIF*SPADIF/(PVAD(K+1)-PVAD(K))
            LNORM=LNORM+(SPADIF/(PVAD(K+1)-PVAD(K)))**2

            TEMDIF=COS(DELORN+PVAD(K))-COS(PRSORN+PVAD(K))
            SPADIF=COS(PRSORN+PVAD(K+1))-COS(PRSORN+PVAD(K))
            ESTRGT=ESTRGT+TEMDIF*SPADIF/(PVAD(K+1)-PVAD(K))
            RNORM=RNORM+(SPADIF/(PVAD(K+1)-PVAD(K)))**2
150         CONTINUE
          ESTLFT=ESTLFT/(T*LNORM)
          ESTRGT=ESTRGT/(T*RNORM)
          ESTLR=(ESTLFT-ESTRGT)/2.0
          XLR=XLR+(-XLR+ESTLR)*DTDTC
160       CONTINUE
```

```
        XD=XLR*RADDEG
          WRITE(4,10) PRSTIM
        WRITE(7,165) PRSTIM, XD
165       FORMAT(' ',G14.6,',',G14.6)
170     CONTINUE
175    PRSORN=PRSORN*RADDEG
       XLR=XLR*RADDEG
       WRITE(4,180) PRSTIM, PRSORN, XLR
       WRITE(8,180) PRSTIM, PRSORN, XLR
180      FORMAT(/,' FINAL TIME=',G14.6,/,
     1          ' FINAL ORIENTATION=',G14.6,/,
     2          ' LEFT RIGHT, FINAL STATE=',G14.6)

       ORNO=ORNO*RADDEG
       XLRO=XLRO*RADDEG
       WRITE(8,185) TO, ORNO, XLRO
185      FORMAT(' INITIAL TIME IN SEC=',G14.6,/,
     1          ' INITIAL MACULAR ORIENTATION IN DEG=',G14.6,/,
     2          ' LEFT RIGHT, INITIAL STATE=',G14.6)

       WRITE(8,190) T, TC
190      FORMAT(' TIME DELAY CONSTANT IN SEC=',G14.6,/,
     1          ' INTEGRATOR TIME CONSTANT IN SEC=',G14.6)

       MACVEL=MACVEL*RADDEG
       WRITE(8,195) MACVEL, DT, EDTNUM, ESTNUM
195      FORMAT(' MACULAR VELOCITY IN DEG/SEC=',G14.6,/,
     1          ' DELTA TIME FOR INTEGRATOR IN SEC=',G14.6,/,
     2          ' NUMBER OF DT''S PER ESTIMATE=',I5,/,
     3          ' NUMBER OF ESTIMATES=',I5)

       WRITE(8,205) PVN
205      FORMAT(' POLARIZATION ANGLES IN DEGREES',/,
     1          ' O DEG, NOSE DOWN WITH POLARIZATION VECTOR',
     2          ' PARALLEL TO GRAVITY',/,' SMALL POSITIVE',
     3          ' ANGLE, VECTOR POINTS: RIGHT OF NOSE',/,
     4          ' NUMBER OF VECTORS=',I5)

       WRITE(8,210) (PVADDE(I),I=1,PVN)
210      FORMAT(6(3X,G14.6))

       STOP
       END
```

Computer Program used to Generate the Eye Velocity Command in Figure 3.2.16

```
C     3-DIMENSIONAL IDEAL MODEL, BASED ON 3 1-DIMENSIONAL
C       IDEAL MODELS
C       ROTATION ASSUMED ON GOING FOR TIME .GE. T

C       OTOLITH ANGULAR VELOCITY IS SPECIFIED BY AN
C       ORIENTATION WRT SPACE AND A MAGNITUDE.
C       THE ORIENTATION IS GIVEN BY ROTATNG THE SPACE Z-AXIS
C       (COUTER-CLOCKWISE) BY EACH OF THE FOLLOWING ANGLES.
C       THETAV:FIRST, ROTATE BY THETAV ABOUT SPACE X-AXIS
C       PHIV:SECOND, ROTATE BY PHIV ABOUT SPACE Z-AXIS
C       VELMAG:ANGULAR VELOCITY MAGNITUDE
C       TO DESCIRBE THE ESTIMATE RELATIVE TO THE HEAD
C       VELOCITY WE SPECIFY ANOTHER SPACE COORDINATE SYSTEM
C       WITH THE HEAD VELOCITY DEFINING THE CORRESPONDING
C       Z-AXIS.
C       XPHIRF():X-AXIS RELATIVE TO HEAD VELOCITY
C       YPHIRF():Y-AXIS RELATIVE TO HEAD VELOCITY
C       AXSPA():Z-AXIS CORRESPONDING TO HEAD VELOCITY
C       WE CAN SPECIFY THE HEAD VELOCITY BY GIVING ITS THREE
C       SPACE, HEAD, OR CANAL COORDINATES:
C       VELSPA():OTOLITH ANGULAR VELOCITY IN SPACE SYSTEM
C       VELHED():OTOLITH ANGULAR VELOCITY IN HEAD SYSTEM
C       VELCAN():OTOLITH ANGULAR VELOCITY IN CANAL SYSTEM
      REAL THETAV, PHIV, VELMAG,
     1       XPHIRF(3), YPHIRF(3), AXSPA(3),
     2       VELSPA(3), VELHED(3), VELCAN(3)

C       THE INITIAL ORIENTATION OF THE HEAD SYSTEM WRT SPACE.
C       IT IS SPECIFIED BY 3 EULER ANGLES.
C       ROTATIONS ARE COUNTER-CLOCKWISE.
C       PASSIVE VIEW OF THE ROTATION.
C       FIRST ROTATE ABOUT THE HEAD Z-AXIS.
C       SECOND ROTATE ABOUT THE HEAD X-AXIS.
C       THIRD ROTATE ABOUT THE HEAD Z-AXIS.
C       IPHIHS:ROTATE BY IPHIHS ABOUT THE HEAD Z-AXIS
C       ITHEHS:ROTATE BY ITHEHS ABOUT THE HEAD X-AXIS
C       IPSIHS:ROTATE BY IPSIHS ABOUT THE HEAD Z-AXIS
C       IHS(,):MATRIX REPRESENTING THE INITIAL SYSTEM
C              ROTATION FROM SPACE TO HEAD COORDINATES
C              THE ROWS OF IHS(,) REPRESENT THE INITIAL HEAD
C              AXES IN SPACE COORDINATES.
C              ROW 1:INITIAL HEAD X AXIS
```

```
C               ROW 2:INITIAL HEAD Y AXIS
C               ROW 3:INITIAL HEAD Z AXIS
      REAL IPHIHS, ITHEHS, IPSIHS, IHS(3,3)
C       THE ORIENTATION OF THE CANAL SYSTEM WRT HEAD.
C       IT IS SPECIFIED BY 3 EULER ANGLES.
C       ROTATIONS ARE COUNTER-CLOCKWISE.
C       PASSIVE VIEW OF THE ROTATION.
C       TO OBTAIN RCH(,):
C       FIRST ROTATE ABOUT THE CANAL Z-AXIS,
C       SECOND ROTATE ABOUT THE CANAL X-AXIS, AND
C       THIRD ROTATE ABOUT THE CANAL Z-AXIS.
C       PHICH:ROTATE BY PHICH ABOUT THE CANAL Z-AXIS
C       THECH:ROTATE BY THECH ABOUT THE CANAL X-AXIS
C       PSICH:ROTATE BY PSICH ABOUT THE CANAL Z-AXIS
C       RCH(,):MATRIX REPRESENTING THE SYSTEM
C               ROTATION FROM HEAD TO CANAL COORDINATES
      REAL PHICH, THECH, PSICH, RCH(3,3)

C       INITIAL ORIENTATION OF THE CANAL SYSTEM WRT SPACE.
C       PASSIVE VIEW
C       ICS(,):MATRIX REPRESENTING THE INITIAL SYSTEM
C               ROTATION FROM SPACE TO CANAL COORDINATES
C               THE ROWS OF ICS(,) REPRESENT THE INITIAL CANAL
C               AXES IN SPACE COORDINATES.
C               ROW 1:INITIAL CANAL X AXIS
C               ROW 2:INITIAL CANAL Y AXIS
C               ROW 3:INITIAL CANAL Z AXIS
      REAL ICS(3,3)

C       T:TIME DELAY CONSTANT
      REAL T

C       TO:INITIAL TIME
C       PRSTIM:PRESENT TIME
C       PHIO:INITIAL ANGLE OF ROTATION ABOUT THE ROTATION AXIS
C       PHI:PRESENT ANGLE OF ROTATION ABOUT THE ROTATION AXIS
C       DPHI:DELAYED PHI=PHI-VELMAG*T
C       PCS(,):MATRIX REPRESENTING, AT THE PRESENT TIME, A
C               ROTATION TO CANAL FROM SPACE COORDINATES,
C               PASSIVE VIEW.
C               IT ALSO REPRESENTS THE PRESENT ORIENTATION OF
C               THE CANAL SYSTEM WRT SPACE.
C               THE ROWS OF PCS(,) REPRESENT THE PRESENT CANAL
C               AXES IN SPACE COORDINATES.
C               ROW 1:PRESENT CANAL X AXIS
C               ROW 2:PRESENT CANAL Y AXIS
C               ROW 3:PRESENT CANAL Z AXIS
C       DCS(,):MATRIX REPRESENTING, AT THE DELAYED TIME, A
```

```
C              ROTATION TO CANAL FROM SPACE COORDINATES, A
C              PASSIVE VIEW.
C              IT ALSO REPRESENTS THE DELAYED ORIENTATION OF
C              THE CANAL SYSTEM WRT SPACE.
C              THE ROWS OF DCS(,) REPRESENT THE DELAYED CANAL
C              AXES IN SPACE COORDINATES.
C              ROW 1:DELAYED CANAL X AXIS
C              ROW 2:DELAYED CANAL Y AXIS
C              ROW 3:DELAYED CANAL Z AXIS
      REAL TO, PRSTIM, PHIO, PHI, DPHI, PCS(3,3), DCS(3,3)
C       ESTMAG:ESTIMATE MAGNITUDE
C       COSTHE:COS(THETA)
C       COSPHI:COS(PHI)
C       COSPSI:COS(PSI)
C       SINTHE:SIN(THETA)
C       SINPHI:SIN(PHI)
C       SINPSI:SIN(PSI)
C       DOTE(X):DOT PRODUCT OF ESTSPA() AND XPHIRF()
C       DOTE(Y):DOT PRODUCT OF ESTSPA() AND YPHIRF()
C       DOTE(Z):DOT PRODUCT OF ESTSPA() AND AXSPA()
C               (OR ZPHIRF)
C       EPHI:ASIMUTHAL ANGLE ABOUT AXSPA()
C       ETHETA:POLAR ANGLE RELATIVE TO AXSPA()
      REAL ESTMAG,
     1       COSTHE, COSPHI, COSPSI, SINTHE, SINPHI, SINPSI,
     2       DOTE(3), EPHI, ETHETA

C       ESTCAN():VELOCITY ESTIMATE IN THE CANAL SYSTEM
C       ESTHED():VELOCITY ESTIMATE IN THE HEAD SYSTEM
C       ESTSPA():VELOCITY ESTIMATE IN THE SPACE SYSTEM
      REAL ESTCAN(3), ESTHED(3), ESTSPA(3)

C       NORMT():NORMALIZATION FACTOR DIVIDED BY T
C       PNORM():NORMALIZATION FACTORS FOR PRESENT TILT
C       DNORM():NORMALIZATION FACTORS FOR DELAYED TILT
      REAL NORMT(3), PNORM(3), DNORM(3)

C       CRSPRD(,):CROSS PRODUCTS, EACH ROW CONTAINS ONE
C                 PRODUCT
C       DOTPRD():DOT PRODUCTS
      REAL CRSPRD(3,3), DOTPRD(3)

C       DAXSPA(,):DAXSPA(I,J)=DOTPRD(I)*CRSPRD(I,J)
C       VELT:VELMAG*T
C       VELDT:VELT*DT
      REAL DAXSPA(3,3), VELT, VELDT
```

```
C       STRANG:SATURATION ANGLE OF TILT, FOR PURPOSES OF
C         NORMALIZATION ONLY! MEANING ANGLES OF TILT .LT.
C         STRANG WILL BE SET EQUAL TO STRANG
C         (SEE CALCULATION OF NORM())
C       SINSTR:SIN(STRANG)
      REAL STRANG, SINSTR
C       DT:ESTIMATES CALCULATED EVERY DT SECONDS
      REAL DT

C       NUMEST:TOTAL NUMBER OF ESTIMATES TO BE REPORTED
C       ESTNUM:NUMBER OF ESTIMATES TO BE REPORTED, AFTER
C              TIME T
C       EDTNUM:NUMBER OF DT'S BETWEEN ESTIMATE REPORTS
C       DTNUMT:NUMBER OF DTS IN T
      INTEGER NUMEST, ESTNUM, EDTNUM, DTNUMT

      REAL PHID, EPHID, ESTETD, ESTMAD,
     1     DOTED(3), ESTCAD(3), ESTHDD(3), ESTSPD(3)

C       CSTATO():CANAL COORDINATE REP OF INITIAL INTEGRATOR
C                STATE
C       CSTATE():CANAL COORDINATE REP OF INTEGRATOR STATE
C       NSTATE():CANAL COORDINATE REP, NEXT INTEGRATOR STATE
C       HRH(,):SYSTEM OPERATOR IN HEAD COORDINATES
C       HRCDTI(,):SYSTEM OPERATOR IN CANAL COORDINATES
C                 TIMES DT, PLUS I
C       GRH(,):GAIN MATRIX IN HEAD COORDINATES
C       GRCDT(,):GAIN MATRIX IN CANAL COORDINATES TIMES DT
      REAL CSTATO(3), CSTATE(3), NSTATE(3),
     1     HRH(3,3), HRCDTI(3,3), GRH(3,3), GRCDT(3,3)

C       RADDEG:CONVERSION FACTOR, RADIANS TO DEGREES
C       DEGRAD:CONVERSION FACTOR, DEGREES TO RADIANS
      REAL RADDEG, DEGRAD

C       X:X COMPONENT
C       Y:Y COMPONENT
C       Z:Z COMPONENT
      INTEGER X, Y, Z
        DATA X, Y, Z/1, 2, 3/

C       I,J,K,LM,N USED IN AS INDICES
      INTEGER I, J, K, L

C       PI:3.141592653589793...
      REAL PI, TWOPI
        DATA PI, TWOPI/3.14159, 6.28319/
```

```
5     FORMAT(I5)
10    FORMAT(G14.6)

      READ(5,10) T, THETAV, PHIV, VELMAG, DT
      READ(5,5) EDTNUM, ESTNUM
      READ(5,10) IPHIHS, ITHEHS, IPSIHS
      READ(5,10) PHICH, THECH, PSICH, STRANG
      READ(5,10) TO, PHIO
      READ(5,15) (CSTATO(I), I=1, 3)
15      FORMAT(//,3G14.6)
      READ(5,20) ((HRH(I,J), J=1, 3), I=1,3)
20      FORMAT(//,3G14.6,//,3G14.6,//,3G14.6)
      READ(5,20) ((GRH(I,J), J=1, 3), I=1,3)

CL1   ***DISPLAY PARAMETER VALUES
      WRITE(4,23) T, THETAV, PHIV, VELMAG
23      FORMAT(' TIME DELAY=',G14.6,'SEC',/,
     1         ' VEL EULER ANGLE SPACE X-AXIS=',G14.6,'DEG',/,
     2         ' VEL EULER ANGLE SPACE Z-AXIS=',G14.6,'DEG',/,
     3         ' VELOCITY MAGNITUDE=',G14.6,'DEG/SEC')

      WRITE(4,25) DT, EDTNUM, ESTNUM
25      FORMAT(' DELTA T BETWEEN ESTIMATE CALCULATIONS='
     1         ,G14.6,'SEC',/,' NUMBER OF DELTA T''S ',
     2         'BETWEEN ESTIMATE REPORTS=',I5,/,' NUMBER OF'
     3         ' ESTIMATE REPORTS=',I5)

      WRITE(4,30) IPHIHS, ITHEHS, IPSIHS, PHIO
30      FORMAT(' HEAD WRT SPACE Z-AXIS=',G14.6,'DEG',/,
     1         ' HEAD WRT SPACE X-AXIS=',G14.6,'DEG',/
     2         ,' HEAD WRT SPACE Z-AXIS=',G14.6,'DEG',/
     3         ,' HEAD ABOUT ROTATION AXIS=',G14.6,'DEG')

      WRITE(4,35) PHICH, THECH, PSICH, STRANG
35      FORMAT(' CANAL WRT HEAD Z-AXIS=',G14.6,'DEG',/,
     1         ' CANAL WRT HEAD X-AXIS=',G14.6,'DEG',/,
     2         ' CANAL WRT HEAD Z-AXIS=',G14.6,'DEG',/,
     3         ' SATURATION TILT ANGLE=',G14.6,'DEG')
CL1   ***END

      WRITE(4,40) CSTATO
40      FORMAT(' INITIAL X-STATE=',G14.6,'DEG/SEC',/,
     1         ' INITIAL Y-STATE=',G14.6,'DEG/SEC',/,
     2         ' INITIAL Z-STATE=',G14.6,'DEG/SEC')

      WRITE(4,45) ((HRH(I,J), J=1, 3), I=1, 3)
45      FORMAT(' SYSTEM MATRIX IN HEAD COORDINATES',/,
     1        3G14.6,/,3G14.6,/,3G14.6)
```

```
      WRITE(4,50) ((GRH(I,J), J=1, 3), I=1, 3)
50      FORMAT(' GAIN MATRIX IN HEAD COORDINATES',/,
     1         3G14.6,/,3G14.6,/,3G14.6)

      DEGRAD=PI/180.0
      RADDEG=180.0/PI

CL2   ***CONVERT FROM DEGREES TO RADIANS
      STRANG=STRANG*DEGRAD

      PHIV=PHIV*DEGRAD
      THETAV=THETAV*DEGRAD
      VELMAG=VELMAG*DEGRAD

      IPHIHS=IPHIHS*DEGRAD
      ITHEHS=ITHEHS*DEGRAD
      IPSIHS=IPSIHS*DEGRAD
      PHIO=PHIO*DEGRAD

      PHICH=PHICH*DEGRAD
      THECH=THECH*DEGRAD
      PSICH=PSICH*DEGRAD

      DO 52 I=1, 3
        CSTATO(I)=CSTATO(I)*DEGRAD
52      CONTINUE
CL2   ***END

CL3   ***SET SPACE COORDINATE SYSTEM WITH HEAD VELOCITY AS
C        Z-AXIS
      COSPHI=COS(PHIV)
      SINPHI=SIN(PHIV)
      COSTHE=COS(THETAV)
      SINTHE=SIN(THETAV)

      XPHIRF(X)=COSPHI
      XPHIRF(Y)=SINPHI
      XPHIRF(Z)=0.0

      YPHIRF(X)=-COSTHE*SINPHI
      YPHIRF(Y)=COSTHE*COSPHI
      YPHIRF(Z)=SINTHE

C       SET ZPHIRF OR HEAD AXIS OF ROTATION
      AXSPA(X)=SINTHE*SINPHI
      AXSPA(Y)=-SINTHE*COSPHI
      AXSPA(Z)=COSTHE
```

```
CL3   ***END

CL4   ***SET HEAD ANGULAR VELOCITY IN SPACE COORDINATES
      DO 54 I=1, 3
        VELSPA(I)=VELMAG*AXSPA(I)
54      CONTINUE
CL4   ***END
CL5   ***FIND MATRIX REPRESENTING A COORDINATE SYSTEM CHANGE,
C       PASSIVE VIEW,
C       FROM SPACE TO HEAD, AT TIME 0
      COSPHI=COS(IPHIHS)
      SINPHI=SIN(IPHIHS)
      COSTHE=COS(ITHEHS)
      SINTHE=SIN(ITHEHS)
      COSPSI=COS(IPSIHS)
      SINPSI=SIN(IPSIHS)

      IHS(1,1)=COSPSI*COSPHI
     1         -COSTHE*SINPHI*SINPSI
      IHS(2,1)=-SINPSI*COSPHI
     1         -COSTHE*SINPHI*COSPSI
      IHS(3,1)=SINTHE*SINPHI

      IHS(1,2)=COSPSI*SINPHI
     1         +COSTHE*COSPHI*SINPSI
      IHS(2,2)=-SINPSI*SINPHI
     1         +COSTHE*COSPHI*COSPSI
      IHS(3,2)=-SINTHE*COSPHI

      IHS(1,3)=SINPSI*SINTHE
      IHS(2,3)=COSPSI*SINTHE
      IHS(3,3)=COSTHE
CL5   ***END

CL6   ***FIND THE OTOLITH VELOCITY REPRESENTATION IN HEAD
C       COORDINATES
C       THE ANGULAR VELOCITY VECTOR IS CONSTANT IN THE HEAD
C       REFERENCE SYSTEM.  THEREFORE, WE FIND ITS COORDINATES
C       AT TIME 0 BUT, THESE ARE ITS COORDINATES AT ANY TIME.
C       OBTAINED BY MATRIX VECTOR MULTIPLICATION
C       VELHED()=IHS(,)*VELSPA()
      DO 55 I=1,3
        VELHED(I)=0.0
        DO 60 J=1,3
          VELHED(I)=VELHED(I)+IHS(I,J)*VELSPA(J)
60        CONTINUE
55      CONTINUE
CL6   ***END
```

```
CL7   ***FIND MATRIX REPRESENTING A COORDINATE SYSTEM CHANGE,
C       PASSIVE VIEW,
C       FROM HEAD TO CANAL
      COSPHI=COS(PHICH)
      SINPHI=SIN(PHICH)
      COSTHE=COS(THECH)
      SINTHE=SIN(THECH)
      COSPSI=COS(PSICH)
      SINPSI=SIN(PSICH)

      RCH(1,1)=COSPSI*COSPHI
     1         -COSTHE*SINPHI*SINPSI
      RCH(2,1)=-SINPSI*COSPHI
     1         -COSTHE*SINPHI*COSPSI
      RCH(3,1)=SINTHE*SINPHI

      RCH(1,2)=COSPSI*SINPHI
     1         +COSTHE*COSPHI*SINPSI
      RCH(2,2)=-SINPSI*SINPHI
     1         +COSTHE*COSPHI*COSPSI
      RCH(3,2)=-SINTHE*COSPHI

      RCH(1,3)=SINPSI*SINTHE
      RCH(2,3)=COSPSI*SINTHE
      RCH(3,3)=COSTHE
CL7   ***END

CL8   ***FIND THE OTOLITH VELOCITY REPRESENTATION IN CANAL
C       COORDINATES
C       THE ANGULAR VELOCITY VECTOR IS CONSTANT IN THE CANAL
C       REFERENCE SYSTEM.  THEREFORE, WE FIND ITS COORDINATES
C       AT TIME 0 BUT, THESE ARE ITS COORDINATES AT ANY TIME.
C       OBTAINED BY MATRIX VECTOR MULTIPLICATION
C       VELCAN()=RCH(,)*VELHED()
      DO 70 I=1,3
        VELCAN(I)=0.0
        DO 65 J=1,3
          VELCAN(I)=VELCAN(I)+RCH(I,J)*VELHED(J)
65        CONTINUE
70      CONTINUE
CL8   ***END

CL9   ***FIND MATRIX REPRESENTING A COORDINATE SYSTEM CHANGE,
C       PASSIVE VIEW
C       FROM SPACE TO CANAL, AT TIME 0
C       OBTAINED BY MATRIX MATRIX MULTIPLICATION
C       ICS(,)=RCH(,)*IHS(,)
```

```
      DO 85 I=1,3
        DO 80 K=1,3
          ICS(I,K)=0.0
          DO 75 J=1,3
            ICS(I,K)=ICS(I,K)+RCH(I,J)*IHS(J,K)
75          CONTINUE
80        CONTINUE
85      CONTINUE
CL9   ***END
CL10  ***FIND THE CROSS PRODUCTS OF THE AXIS OF ROTATION WITH
C       EACH INITIAL CANAL AXIS
      DO 90 I=1, 3
        CRSPRD(I,X)=AXSPA(Y)*ICS(I,Z)-AXSPA(Z)*ICS(I,Y)
        CRSPRD(I,Y)=AXSPA(Z)*ICS(I,X)-AXSPA(X)*ICS(I,Z)
        CRSPRD(I,Z)=AXSPA(X)*ICS(I,Y)-AXSPA(Y)*ICS(I,X)
90      CONTINUE
CL10  ***END

CL11  ***FIND THE DOT PRODUCTS OF THE AXIS OF ROTATION WITH
C       EACH INITIAL CANAL AXIS
      DO 100 I=1, 3
        DOTPRD(I)=0.0
        DO 95 J=1, 3
          DOTPRD(I)=DOTPRD(I)+ICS(I,J)*AXSPA(J)
95        CONTINUE
100     CONTINUE
CL11  ***END

CL12  ***THE FOLLOWING ARE USED TO REDUCE THE TIME COMPLEXITY
C       OF THE ESTIMATE CALCULATIONS
      VELT=VELMAG*T
      VELDT=VELMAG*DT

      DO 110 I=1, 3
        DO 105 J=1, 3
          DAXSPA(I,J)=DOTPRD(I)*AXSPA(J)
105       CONTINUE
110     CONTINUE

      SINSTR=SIN(STRANG)
CL12  ***END

      PRSTIM=TO
      PHI=PHIO
```

```
      DO 315 I=1, 3
        CSTATE(I)=CSTATO(I)
        DO 310 J=1, 3
          HRCDTI(I,J)=0.0
          GRCDT(I,J)=0.0
          DO 305 K=1, 3
            DO 300 L=1, 3
              HRCDTI(I,J)=HRCDTI(I,J)
     1                    +RCH(I,K)*HRH(K,L)*RCH(J,L)
              GRCDT(I,J)=GRCDT(I,J)
     1                   +RCH(I,K)*GRH(K,L)*RCH(J,L)
300           CONTINUE
305         CONTINUE
          HRCDTI(I,J)=HRCDTI(I,J)*DT
          GRCDT(I,J)=GRCDT(I,J)*DT
310       CONTINUE
        HRCDTI(I,I)=HRCDTI(I,I)+1.0
315     CONTINUE
      IF (PRSTIM.GE.T) GOTO 1395
C     ELSE
      DO 398 J=1, 3
C         ASSUME THAT AT TIME 0 THE HEAD IS UPRIGHT
C         THEREFORE, THE ROWS OF RCH(,) REPRESENT THE CANAL
C         AXES WRT SPACE AT TIME 0.
        DNORM(J)=SQRT((1.0-RCH(J,Z)**2))
        IF (DNORM(J).LT.SINSTR) DNORM(J)=SINSTR
398     CONTINUE
      DTNUMT=INT((T-PRSTIM)/DT+0.5)
      NUMEST=ESTNUM+DTNUMT
      WRITE(6,399) NUMEST
399     FORMAT(' ',I5)

      DO 1000 I=1, DTNUMT
          PRSTIM=PRSTIM+DT

CL13      ***FIND THE CANAL AXES AT THE PRESENT TIME.
C           EACH ROW OF ICS(,) CONTAINS AN INITIAL CANAL
C           AXIS (JUST AFTER THE SUDDEN TILT) IN SPACE
C           COORDINATES.
C           ROTATE EACH INITIAL CANAL AXIS COUNTER
C           CLOCKWISE ABOUT AXSPA() BY PHI.
          PHI=PHI+VELDT
          DO 405 K=1,3
            DO 400 L=1, 3
              PCS(K,L)=ICS(K,L)*COS(PHI)
     1                 +DAXSPA(K,L)*(1.0-COS(PHI))
     2                 +CRSPRD(K,L)*SIN(PHI)
400           CONTINUE
```

```
405         CONTINUE
C           EACH ROW OF PCS(,) NOW CONTAINS A PRESENT ROTATED
C           CANAL AXIS.

C           EACH ROW OF RCH(,) CONTAINS AN INITIAL
C           CANAL AXIS (JUST BEFORE THE SUDDEN TILT).
CL13      ***END

CL14      ***FIND THE ESTIMATED ANGULAR VELOCITY IN CANAL
C           COORDINATES, RGIHT AFTER THE TILT
          DO 420 L=1, 3
            PNORM(L)=SQRT((1.0-PCS(L,3)**2))
            IF (PNORM(L).LT.SINSTR) PNORM(L)=SINSTR
            NORMT(L)=1.0/(T*PNORM(L)*DNORM(L))
            M=MOD(L,3)+1
            N=MOD(L+1,3)+1
            ESTCAN(L)=NORMT(L)*
     1              ( PCS(M,Z)*RCH(N,Z)-PCS(N,Z)*RCH(M,Z) )
420         CONTINUE
          DO 430 K=1, 3
            NSTATE(K)=0.0
            DO 425 L=1, 3
              NSTATE(K)=NSTATE(K)+HRCDTI(K,L)*CSTATE(L)
     1                          +GRCDT(K,L)*ESTCAN(L)
425           CONTINUE
430         CONTINUE
          DO 435 K=1, 3
            CSTATE(K)=NSTATE(K)
435         CONTINUE
CL14      ***END
CL15    ***FIND THE ESTIMATE OF THE OTOLITH VELOCITY IN HEAD
C         COORDINATES
C         OBTAINED BY MATRIX VECTOR MULTIPLICATION
C         ESTHED()=RHC(,)*CSTATE()
C         RHC(,) IS THE TRANSPOSE OF RCH(,)
        DO 505 K=1,3
          ESTHED(K)=0.0
          DO 500 L=1,3
            ESTHED(K)=ESTHED(K)+RCH(L,K)*CSTATE(L)
500         CONTINUE
505       CONTINUE
CL15    ***END

CL16    ***FIND THE ESTIMATE IN SPACE COORDINATES
C         OBTAINED BY MATRIX VECTOR MULTIPLICATION
C         ESTSPA()=PSC(,)*CSTATE()
C         PCS(,) IS THE TRANSPOSE OF PSC(,)
```

```
        DO 515 K=1, 3
          ESTSPA(K)=0.0
          DO 510 L=1, 3
            ESTSPA(K)=ESTSPA(K)+PCS(L,K)*CSTATE(L)
510         CONTINUE
515       CONTINUE
CL16    ***END

CL17  BEGIN
        ESTMAG=0.0
        DO 520 K=1, 3
          ESTMAG=ESTMAG+CSTATE(K)**2
520       CONTINUE
        ESTMAG=SQRT(ESTMAG)
CL17    END

        IF (ESTMAG.NE.0.0) GOTO 530
CE1     ELSE
          EPHI=0.0
          ETHETA=0.0
          DO 525 K=1, 3
            DOTE(K)=0.0
525         CONTINUE
          GOTO 580
CE1       END
CT1     THEN
C         FIND DOT PRODUCT OF ESTSPA() AND AXSPA()
530       DOTE(Z)=0.0
          DO 535 K=1, 3
            DOTE(Z)=DOTE(Z)+ESTSPA(K)*AXSPA(K)
535         CONTINUE
C         FIND THE POLAR ANGLE BETWEEN THE ESTIMATE AND
C         AXSPA()
          COSTHE=DOTE(Z)/ESTMAG
          ETHETA=ACOS(COSTHE)

CL19        FIND DOT PRODUCT OF ESTSPA() AND XPHIRF()
          DOTE(X)=0.0
          DO 540 K=1, 3
            DOTE(X)=DOTE(X)+ESTSPA(K)*XPHIRF(K)
540         CONTINUE
CL19        END

CL20        FIND DOT PRODUCT OF ESTSPA() AND YPHIRF()
          DOTE(Y)=0.0
          DO 545 K=1, 3
            DOTE(Y)=DOTE(Y)+ESTSPA(K)*YPHIRF(K)
545         CONTINUE
```

```
CL20          END

            IF (DOTE(X).NE.0.0) GOTO 560
CE2         ELSE
              IF (DOTE(Y).NE.0.0) GOTO 550
CE3           ELSE
                EPHI=0.0
                GOTO 580
CT3           THEN
550             IF (DOTE(Y).LT.0.0) GOTO 555
CE4             ELSE
                  EPHI=PI/2.0
                  GOTO 580
CT4             THEN
555               EPHI=3.0*PI/2.0
                  GOTO 580
CI4             ENDIF
CI3           ENDIF
CT2         THEN
560           IF (DOTE(Y).NE.0.0) GOTO 570
CE5           ELSE
                IF (DOTE(X).LT.0.0) GOTO 565
CE6             ELSE
                  EPHI=0.0
                  GOTO 580
CT6             THEN
565               EPHI=PI
                  GOTO 580
CI6             ENDIF
CT5           THEN
570             EPHI=ATAN(DOTE(Y)/DOTE(X))
                IF (DOTE(X).GT.0.0) GOTO 575
CE7             ELSE
                  EPHI=EPHI+PI
                  GOTO 580
CT7             THEN
575               IF (DOTE(Y).GT.0.0) GOTO 580
CE8               ELSE
                    EPHI=EPHI+TWOPI
CI8               ENDIF
CI7             ENDIF
CI5           ENDIF
CI2         ENDIF
CT1         END
CI1       ENDIF
580     PHID=PHI*RADDEG
        EPHID=EPHI*RADDEG
        ETHETD=ETHETA*RADDEG
```

```
      ESTMAD=ESTMAG*RADDEG
      DO 585 K=1, 3
        DOTED(K)=DOTE(K)*RADDEG
        ESTCAD(K)=CSTATE(K)*RADDEG
        ESTHDD(K)=ESTHED(K)*RADDEG
        ESTSPD(K)=ESTSPA(K)*RADDEG
585     CONTINUE
      WRITE(6,590) PRSTIM, PHID, ESTCAD(Z), ESTHDD(Z)
590     FORMAT(' ',G14.6,3(',',G14.6))
C     WRITE(6,590) PRSTIM, PHID, EPHID, ETHETD, ESTMAD,
C     1                DOTED, ESTCAD, ESTHDD, ESTSPD
C590    FORMAT(' ',G14.6,16(',',G14.6))
1000    CONTINUE
      GOTO 1397
1395  WRITE(6,1396) ESTNUM
1396    FORMAT(' ',I5)

1397  DO 2000 I=1, ESTNUM
        DO 1495 J=1, EDTNUM
          PRSTIM=PRSTIM+DT

CL13      ***FIND THE CANAL AXES AT THE PRESENT AND DELAYED
C           TIMES.
C           EACH ROW OF ICS(,) CONTAINS AN INITIAL CANAL
C           AXIS IN SPACE COORDINATES.

C           FIRST, ROTATE EACH INITIAL CANAL AXIS COUNTER
C           CLOCKWISE ABOUT AXSPA() BY PHI.
          PHI=PHI+VELDT
          DO 1405 K=1,3
            DO 1400 L=1, 3
              PCS(K,L)=ICS(K,L)*COS(PHI)
     1                 +DAXSPA(K,L)*(1.0-COS(PHI))
     2                 +CRSPRD(K,L)*SIN(PHI)
1400          CONTINUE
1405        CONTINUE
C           EACH ROW OF PCS(,) NOW CONTAINS A PRESENT ROTATED
C           CANAL AXIS.

C           NEXT ROTATE EACH INITIAL CANAL AXIS COUNTER
C           CLOCKWISE ABOUT AXSPA() BY DPHI.
          DPHI=PHI-VELT
          DO 1415 K=1,3
            DO 1410 L=1, 3
              DCS(K,L)=ICS(K,L)*COS(DPHI)
     1                 +DAXSPA(K,L)*(1.0-COS(DPHI))
     2                 +CRSPRD(K,L)*SIN(DPHI)
1410          CONTINUE
```

```
1415        CONTINUE
C           EACH ROW OF DCS(,) NOW CONTAINS A DELAYED ROTATED
C           CANAL AXIS.
CL13      ***END

CL14      ***FIND THE ESTIMATED ANGULAR VELOCITY IN CANAL
C           COORDINATES
          DO 1420 L=1, 3
            PNORM(L)=SQRT((1.0-PCS(L,3)**2))
            IF (PNORM(L).LT.SINSTR) PNORM(L)=SINSTR
            DNORM(L)=SQRT((1.0-DCS(L,3)**2))
            IF (DNORM(L).LT.SINSTR) DNORM(L)=SINSTR
            NORMT(L)=1.0/(T*PNORM(L)*DNORM(L))
            M=MOD(L,3)+1
            N=MOD(L+1,3)+1
            ESTCAN(L)=NORMT(L)*
     1              ( PCS(M,Z)*DCS(N,Z)-PCS(N,Z)*DCS(M,Z) )
1420        CONTINUE
          DO 1430 K=1, 3
            NSTATE(K)=0.0
            DO 1425 L=1, 3
              NSTATE(K)=NSTATE(K)+HRCDTI(K,L)*CSTATE(L)
     1                          +GRCDT(K,L)*ESTCAN(L)
1425          CONTINUE
1430        CONTINUE
          DO 1435 K=1, 3
            CSTATE(K)=NSTATE(K)
1435        CONTINUE
CL14      ***END
1495      CONTINUE

CL15      ***FIND THE ESTIMATE OF THE OTOLITH VELOCITY IN HEAD
C           COORDINATES
C           OBTAINED BY MATRIX VECTOR MULTIPLICATION
C           ESTHED()=RHC(,)*CSTATE()
C           RHC(,) IS THE TRANSPOSE OF RCH(,)
          DO 1505 K=1,3
            ESTHED(K)=0.0
            DO 1500 L=1,3
              ESTHED(K)=ESTHED(K)+RCH(L,K)*CSTATE(L)
1500          CONTINUE
1505        CONTINUE
CL15      ***END

CL16      ***FIND THE ESTIMATE IN SPACE COORDINATES
C           OBTAINED BY MATRIX VECTOR MULTIPLICATION
C           ESTSPA()=PSC(,)*CSTATE()
C           PCS(,) IS THE TRANSPOSE OF PSC(,)
```

```
        DO 1515 K=1, 3
          ESTSPA(K)=0.0
          DO 1510 L=1, 3
            ESTSPA(K)=ESTSPA(K)+PCS(L,K)*CSTATE(L)
1510        CONTINUE
1515      CONTINUE
CL16    ***END

CL17  BEGIN
        ESTMAG=0.0
        DO 1520 K=1, 3
          ESTMAG=ESTMAG+CSTATE(K)**2
1520      CONTINUE
        ESTMAG=SQRT(ESTMAG)
CL17    END

        IF (ESTMAG.NE.0.0) GOTO 1530
CE1     ELSE
          EPHI=0.0
          ETHETA=0.0
          DO 1525 K=1, 3
            DOTE(K)=0.0
1525        CONTINUE
          GOTO 1580
CE1       END
CT1     THEN
C         FIND DOT PRODUCT OF ESTSPA() AND AXSPA()
1530      DOTE(Z)=0.0
          DO 1535 K=1, 3
            DOTE(Z)=DOTE(Z)+ESTSPA(K)*AXSPA(K)
1535        CONTINUE
C         FIND THE POLAR ANGLE BETWEEN THE ESTIMATE AND
C         AXSPA()
          COSTHE=DOTE(Z)/ESTMAG
          ETHETA=ACOS(COSTHE)
CL19        FIND DOT PRODUCT OF ESTSPA() AND XPHIRF()
          DOTE(X)=0.0
          DO 1540 K=1, 3
            DOTE(X)=DOTE(X)+ESTSPA(K)*XPHIRF(K)
1540        CONTINUE
CL19        END

CL20        FIND DOT PRODUCT OF ESTSPA() AND YPHIRF()
          DOTE(Y)=0.0
          DO 1545 K=1, 3
            DOTE(Y)=DOTE(Y)+ESTSPA(K)*YPHIRF(K)
1545        CONTINUE
CL20        END
```

```
          IF (DOTE(X).NE.0.0) GOTO 1560
CE2       ELSE
            IF (DOTE(Y).NE.0.0) GOTO 1550
CE3         ELSE
              EPHI=0.0
              GOTO 1580
CT3         THEN
1550          IF (DOTE(Y).LT.0.0) GOTO 1555
CE4           ELSE
                EPHI=PI/2.0
                GOTO 1580
CT4           THEN
1555            EPHI=3.0*PI/2.0
                GOTO 1580
CI4           ENDIF
CI3         ENDIF
CT2       THEN
1560        IF (DOTE(Y).NE.0.0) GOTO 1570
CE5         ELSE
              IF (DOTE(X).LT.0.0) GOTO 1565
CE6           ELSE
                EPHI=0.0
                GOTO 1580
CT6           THEN
1565            EPHI=PI
                GOTO 1580
CI6           ENDIF
CT5         THEN
1570          EPHI=ATAN(DOTE(Y)/DOTE(X))
              IF (DOTE(X).GT.0.0) GOTO 1575
CE7           ELSE
                EPHI=EPHI+PI
                GOTO 1580
CT7           THEN
1575            IF (DOTE(Y).GT.0.0) GOTO 1580
CE8             ELSE
                  EPHI=EPHI+TWOPI
CI8             ENDIF
CI7           ENDIF
CI5         ENDIF
CI2       ENDIF
CT1       END
CI1     ENDIF
1580  PHID=PHI*RADDEG
      EPHID=EPHI*RADDEG
      ETHETD=ETHETA*RADDEG
      ESTMAD=ESTMAG*RADDEG
```

```
      DO 1585 K=1, 3
        DOTED(K)=DOTE(K)*RADDEG
        ESTCAD(K)=CSTATE(K)*RADDEG
        ESTHDD(K)=ESTHED(K)*RADDEG
        ESTSPD(K)=ESTSPA(K)*RADDEG
1585    CONTINUE
      WRITE(6,1590) PRSTIM, PHID, ESTCAD(Z), ESTHDD(Z)
1590    FORMAT(' ',G14.6,3(',',G14.6))
C     WRITE(6,1590) PRSTIM, PHID, EPHID, ETHETD, ESTMAD,
C     1                 DOTED, ESTCAD, ESTHDD, ESTSPD
C1590   FORMAT(' ',G14.6,16(',',G14.6))
2000    CONTINUE
C     ***CONVERT FROM RADIANS TO DEGREES
      THETAV=THETAV*RADDEG
      PHIV=PHIV*RADDEG
      VELMAG=VELMAG*RADDEG

      IPHIHS=IPHIHS*RADDEG
      ITHEHS=ITHEHS*RADDEG
      IPSIHS=IPSIHS*RADDEG

      PHICH=PHICH*RADDEG
      THECH=THECH*RADDEG
      PSICH=PSICH*RADDEG

      STRANG=STRANG*RADDEG
      PHIO=PHIO*RADDEG
      DO 700 I=1, 3
        CSTATO(I)=CSTATO(I)*RADDEG
700     CONTINUE
C     ***END

      WRITE(7,703)
703     FORMAT(' DATA FROM DY3DIM.FT',/,' OUTPUT:PRESTIM, ',
     1         'PHID, EPHID, ETHETD, ESTMAD,',/,' DOTED(X:Z),',
     2         ' ESTCAD(X:Z), ESTHDD(X:Z), ESTSPD(X:Z)')

      WRITE(7,705) STRANG, CSTATO
705     FORMAT(/,' STATURATION ANGLE=',G14.6,'DEG',
     1         /,' ','INITIAL X-STATE=',G14.6,'DEG/SEC',
     2         /,' ','INITIAL Y-STATE=',G14.6,'DEG/SEC',
     3         /,' ','INITIAL Z-STATE=',G14.6,'DEG/SEC')

      WRITE(7,707) ((HRH(I,J), J=1, 3), I=1, 3)
707     FORMAT(/,' SYSTEM MATRIX IN HEAD COORDINATES (1/SEC)'
     1         ,/,3G14.6,/,3G14.6,/,3G14.6)
```

```
      WRITE(7,709) ((GRH(I,J), J=1, 3), I=1, 3)
709     FORMAT(/,' GAIN MATRIX IN HEAD COORDINATES (1/SEC)'
     1         ,/,3G14.6,/,3G14.6,/,3G14.6)
      WRITE(7,710) TO, DT, EDTNUM, ESTNUM
710     FORMAT(/,' ','INITIAL TIME=',G14.6,'SEC',/,' ',
     1         'DELTA-T=',G14.6,'SEC',/,' ',
     2         'NUMBER OF DELTA-TS PER ESTIMATE=',I5,/,' ',
     3         'NUMBER OF ESTIMATES PER RUN=',I5)

      WRITE(7,715) T, THETAV, PHIV, VELMAG, PHIO
715     FORMAT(/,' ','TIME DELAY CONSTANT=',G14.6,'SEC',/,
     1         ' ','ANGLE VELOCTIY ROTATED ABOUT X-AXIS=',
     2        G14.6,'DEG',/,' ','ANGLE VELOCITY ROTATED ',
     3         'ABOUT Z-AXIS=',G14.6,'DEG',/,' ',
     4         'VELOCITY MAGNITUDE=',G14.6,'DEG/SEC',/,' ',
     5         'INITIAL ANGLE OF ROTATION=',G14.6,'DEG')

      WRITE(7,720) IPHIHS, ITHEHS, IPSIHS
720     FORMAT(/,' ','INITIAL ORIENTATION OF HEAD WRT SPACE',
     1         /,' ','ANGLE OF HEAD ABOUT Z-AXIS=',G14.6,
     2         'DEG',/,' ','NEXT, ANGLE ABOUT X-AXIS=',G14.6
     3         ,'DEG',/,' ','LAST, ANGLE ABOUT Z-AXIS=',G14.6,
     4         'DEG')

      WRITE(7,725) PHICH, THECH, PSICH
725     FORMAT(/,' ','INITIAL ORIENTATION OF CANAL WRT HEAD',
     1         /,' ','ANGLE OF CANAL ABOUT Z-AXIS=',G14.6,
     2         'DEG',/,' ','NEXT, ANGLE ABOUT X-AXIS=',G14.6
     3         ,'DEG',/,' ','LAST, ANGLE ABOUT Z-AXIS=',G14.6,
     4         'DEG')

730   STOP
      END
```

BIBLIOGRAPHY

Baarsma, E.A. & Collewijn, H. (1975). Changes in compensatory eye movements after unilateral labyrinthectomy in the rabbit. Archives oto-rhino-laryngology. 211, 219-230.

Benson, A.J. (1974). Modification of the response to angular accelerations by linear accelerations. In Handbook of sensory Physiology, Psychophysics, applied aspects and general interpretations, vol. VI/2, editor. Kornhuber, H.H., pp. 281-320. New York: Springer-Verlag.

Benson, A.J. & Barnes, G.R. (1970). Response to rotating linear acceleration vectors considered in relation to a model of the otolith organs. In Fifth symposium on the role of the vestibular organs in space exploration, pp. 221-236. Washington D.C.

Benson, A.J. & Bodin, M.A. (1966a). Interaction of linear and angular accelerations on vestibular receptors in man. Aerospace Medicine. 37, 144-154.

Benson, A.J. & Bodin, M.J. (1966b). Comparison of the effect of the direction of gravitational acceleration on postrotational responses in yaw, pith, and roll. Aerospace Medicine. 37, 889-897.

Benson, A.J., Guedry, F.E. & Melvill-Jones, G. (1970). Response of semicircular canal dependent units in vestibular nuclei to rotation of a linear acceleration vector without angular acceleration. Journal of Physiolology. (London) 210, 475-494.

Blanks, R.H.I., Curthoys, I.S. & Markham, C.H. (1975). Planar relationships of the semicircular canals in man. Acta oto-laryngolica. 80, 185-196.

Brodal, A. (1974). Anatomy of the vestibular nuclei and their connections. In Handbook of sensory physiology, Vestibular System, vol. Vi/I, editor. Kornhuber, H.H., pp. 239-352. New York: Springer-Verlag.

Buizza, A. & Schmid, R. (1982). Visual-vestibular interaction in the control of eye movement: Mathematical modelling and computer simulation. Biological Cybernetics. 43, 209-223.

Cohen, B., Matsuo, V. & Raphan, T. (1977). Quantitative analysis of the velocity characteristics of optokinetic nystagmus and optokinetic after-nystagmus. Journal of Physiology. 270, 321-344.

Cohen, B., Suzuki, J.I. & Raphan, T. (1983). Role of the otolith organs in generation of horizontal nystagmus: effects of selective labyrinthine lesions. Brain Research. 276, 159-164.

Cohen, B., Helwig, D. & Raphan, T. (1987). Baclofen and velocity storage: a model of the effects of the drug on the vestibulo-ocular reflex in the rhesus monkey. Journal of Physiology. 393, 703-725.

Correia, M.J. & Guedry, F.E. (1966). Modification of vestibular responses as a function of the rate of rotation about an earth horizontal axis. Acta oto-laryngolica. 62, 297-308.

Correia, M.J. & Money, K.E. (1970). The effect of blockage of all six semi-circular canal ducts on nystagmus produced by dynamic linear acceleration in the cat. Acta oto-laryngolica. 69, 7-16.

Curthoys, I.S., Blanks, R.H.I. & Markham, C.H. (1977). Semicircular canal functional anatomy in cat, guinea pig and man. Acto oto-laryngolica. 83, 258-265.

de Vries, H. (1950). The mechanics of the labyrinth otoliths. Acta oto-laryngol. 38, 262-273.

Diamond, S.G., Markhan, C.H., Simpson, N.E. & Curthoys, I.S. (1979). Binocular counterrolling in humans during dynamic rotation. Acta oto-laryngolica. 87, 490-498.

Director, S. & Rohrer, R. (1972). Introduction to System Theory. New York, New York: McGraw-Hill.

Fanelli, R., Schnabolk, C. & Raphan, T. (1988). Neural Network Modelling of Velocity Generation During Off-Vertical Axis Rotation (OVAR). Society for Neuroscience, 18TH annual meeting. vol 14, part 1, pp 173.

Fernandez, C. & Goldberg, J.M. (1976a). Physiology of peripheral neurons innervating otolith organs of the squirrel monkey. I. Response to static tilts and to long-duration centrifugal force. Journal of Neurophysiology. 39, 970-984.

Fernandez, C. & Goldberg, J.M. (1976b). Physiology of peripheral neurons innervating otolith organs of the squirrel monkey. II. Directional selectivity and force response relations. Journal of Neurophysiology. 39, 985-995.

Fernandez, C. & Goldberg, J.M. (1976c). Physiology of peripheral neurons innervating otolith organs of the squirrel monkey. III. Response dynamics. Journal of Neurophysiology. 39, 996-1008.

Fernandez, C., Goldberg, J.M. & Abend, W.K. (1972). Responses to static tilts of periperal neurons innervating otolith organs of the squirrel monkey. Journal of Neurophysiology. 35, 978-997.

Flock, A. (1964). Structure of the macula utriculi with special reference to directional interplay of sensory responses as revealed by morphological polarization. Journal of Cell Biology. 22, 413-431.

Flock, A. & Wersall, J. (1962). A study of the orientation of the sensory hairs of the receptor cells in the lateral line organs of fish with special reference to the function of the recptors. Journal of Cell Biology. 15, 1-19.

Fuchs, A.F. (1967). Periodic Eye Tracking in the Monkey. Journal of Physiology (London). 193, 161-171.

Ghelarducci, B. (1973). Responses of cerebellar fastigial neurones to tilt. Pfliigers Archives. 344, 195-206.

Ghelarducci, B. & Magherini, P.C. (1975). Macular input to the lateral cerebellar nucleus of the rabbit. Experimental Brain Research. Supplement 23, 75. Abstract. 146.

Goldberg, J.M. & Fernandez, C. (1975). Responses of peripheral vestibular neurons to angular and linear accelerations in the squirrel monkey. Acta oto-laryngolica. 30, 101-110.

Goldberg, J.M. & Fernandez, C. (1980). Efferent vestibular system in the squirrel monkey: Anatomical location and influence on afferent activity. Journal of Neurophysiology. 43, 986-1025.

Goldberg, J.M. & Fernandez, C. (1981). Physiological mechanisms of the nystagmus produced by rotations about an earth-horizontal axis. Annals of the New York Academy of Science. 374, 40-43.

Goldberg, J.M. & Fernandez, C. (1982). Eye movements and vestibular nerve responses produced in the squirrel monkey by rotations about an earth-horizontal axis. Experimental Brain Research. 46, 393-402.

Graybiel, A. & Miller, E.F. (1968). The otolith organs as a primary etiological factor in motion sickness with a note on "off vertical" rotation. In Forth Symposium on the Role of Vestibular Organs in Space Exploration, NASA SP-187, pp. 53-64. Washington, D.C.

Guedry, F.E. (1965). Orientation of the rotation axis relative to gravity: its influence on nystagmus and the sensation of rotation. Acta oto-laryngolica. 60, 30-48.

Guedry, F.E. (1974). Psychophysics of vestibular sensation. In Handbook of Sensory Physiology, vol. 6, editor. Kornhuber, H.H., pp 3-154. Berlin Heidelberg, New York: Springer Verlag.

Hain, T.C. (1986). A model of the nystagmus induced by off vertical axis rotation. Biological Cybernetics. 54, 337-350.

Henn, V., Cohen, B. & Young, L.R. (1980). Visual-vestibular in motion perception and generation of nystagmus. Neurosciences Research Program Bulletin. Cambridge, Massachusetts: M.I.T. Press.

Hudspeth, A.J. & Corey, D.P. (1977). Sensitivity, polarity and conduction change in the response of vertebrate hair cells to controlled mechanical stimuli. Annals of the National Academy of Science. 74:6, 2407-2411.

Janecke, J.B., Jongkees, L.B.W. & Oosterveld, W.J. (1970). Relationship between the otoliths and nystagmus. Acta oto-laryngolica 69, 1-6.

Javid, M. & Brenner, E. (1963). Analysis, transmission, and filtering of signals. New York, New York: McGraw-Hill.

Keller, E.L. (1976). Behavior of horizontal semicircular canal afferents in alert monkey during vestibular and optokinetic stimulation. Experimental Brain Research. 24, 459-471.

Lang, S. (1966). Linear Algebra. Reading, Massachusetts: Addison Wesley.

Ledaux, A. (1949). Activite electrique des neufs des cannaux semicirculaires, du saccule et de l'utricle chez la grenauille. Acta oto-rhino-laryngology. 3, 335-349.

Lindeman, H.H. (1973). Anatomy of the otolith organs. Adv. Oto-rhino-laryngology. 20, 405-433.

Loe, P.R., Tomko, D.L. & Werner, G. (1973). The neural signal of angular head position in primary afferent vestibular nerve axons. Journal of Physiology. 230, 29-50.

Lowenstein, O. & Wersall, J. (1959). A functional interpretation of the electron-microscope structure of the sensory hairs in the crestae of the elasmobranch (Raja clavata) in terms of directional sensitivity. Nature. 184, 1807-1808.

Mach, E. (1886). Beitrage zur Analyse der Empfindungen. Jena: Fisher.

Melvill-Jones, G. & Milsum, J.H. (1969). Neural response of the vestibular system to translational acceleration. In Supplement to conference on systems analysis approach to neurophysiological problems, pp. 8-20. Brainerd, Minnesota.

Mowrer, O.H. (1937). The influence of vision during bodily rotation upon the duration of post-rotational vestibular nystagmus. Acta Otolarynology. 25, 351-364.

Papoulis, A. (1984). Probability, Random Variables, and Stochastic Processes. New York, New York: McGraw-Hill.

Pellionisz, A. (1986). Tensor Network Theory and its Application in Computer Modeling of the Metaorganization of Sensorimotor Hiearchies of Gaze. In Proc. Neuronal Networks for Computing. AIP 151, New York: American Institute of Physics. pp. 339-344.

Pellionisz, A. & Graf, W. (1987). Tensor network model of the "three-neuron vestibulo-ocular reflex-arc" in cat. Journal of Theoretical Neurobiology. 5, 127-151.

Pellionisz, A. & Llinas, R. (1982). Tensor theory of brain function. The cerebellum as a space-time metric. Chapter 23. In Competition and Cooperation in Neural Nets, editors. Amari, S. & Arbib, M.A. Proceedings of the U.S.-Japan Joint Seminar. Kyoto, Japan. Lecture notes in Biomathematics #45 (managing editor. Levin, S.). Springer Verlag: Berlin-Heidelberg-New York. pp. 394-417.

Perachio, A.A. & Correia, M.J. (1983). Responses of semicircular canal and otolith afferents to small angle static head tilts in the gerbil. Brain Research. 280, 287-298.

Raphan, T. & Cohen, B. (1981). The role of integration in oculomotor control. In Models of Oculomotor Behavior and Control, CRC, editor. Zuber, B.L., pp. 91-109.

Raphan, T. & Cohen, B. (1986). Multidimensional organization of the vestibulo-ocular reflex (VOR). In Adaptive Processes in Visual and Oculomotor Systems, vol. 57, editors. Keller, E.L. & Zee, D.S. pp. 285-292. Elmsford, New York: Pergaman Press.

Raphan, T. & Cohen, B. (1985). Velocity storage and the ocular response to multidimensional vestibular stimuli. In Reviews in Oculomotor Research, editors. Berthoz, A. & Melvill-Jones, G. North Holland: Elsevier.

Raphan, T. & Cohen, B. (1988). Organizational principles of velocity storage in three dimensions: the effect of gravity on cross-coupling of optokinetic nystagmus (OKAN). Annals of the New York Academy of Science.

Raphan, T., Cohen, B. & Henn, V. (1981). Effects of gravity on rotatory nystagmus in monkeys. Annals of the New York Academy of Science. 374, 44-55.

Raphan, T., Cohen, B. & Matsuo, V. (1977). A velocity storage mechanism responsible for optokinetic nystagmus (OKN), optokinetic after-nystagmus (OKAN) and vestibular nystagmus. In Control of Gaze by Brainstem Neurons, editors. Baker, R. & Berthoz, A. pp. 37-48. Amsterdam: Elsevier/North-Holland Biomedical Press.

Raphan, T., Cohen, B., Suzuki, J.I. & Henn, V. (1983). Nystagmus generated by sinusoidal pitch while rotating. Brain Research. 276, 165-172.

Raphan, T., Matsuo, V. & Cohen, B. (1979). Velocity Storage in the vestibulo-ocular reflex arc. Experimental Brain Research. 35, 229-248.

Raphan, T., Waespe, W. & Cohen, B. (1983). Labyrinthine activation during rotation about axes tilted from the vertical. Advances in Oto-rhino-laryngology. 30, 226-229.

Reisine, H., Raphan, T., Cohen, B. & Katz, E. (1988). Signal Processing in the Vestibular Nuclei during Off-Vertical Axis Rotation (OVAR). Society for Neuroscience, 18TH annual meeting. vol 14, part 1, pp. 172.

Robinson, D.A. (1964). The Mechanics of Human Saccadic Eye Movements. Journal of Physiology. 174, 245-264.

Robinson, D.A. (1965). The Mechanics of Human Smooth Pursuit Eye Movements. Journal of Physiology 180, 569-591.

Robinson, D.A. (1977). Vestibular and optokinetic symbiosis: an example of explaining by modeling. In Control of gaze by brain stem neurons. Elsevier, pp. 49-58. Amsterdam.

Robinson, D.A. (1980). In Visual-Vestibular Interaction in Motion Perception and the Generation of Nystagmus, ed. Henn, V., Cohen, B. & Young, L.R., Neuroscience Research Program Bulletin, vol. 18, pp. 582-588.

Robinson, D.A. (1982). The use of matrices in analyzing the three-dimensional behavior of the vestibulo-ocular reflex. Biological Cybernetics. 46, 53-66.

Schnabolk, C. & Raphan, T. (1986). A pattern analysis approach to modelling velocity generation during off-vertical axis rotation (OVAR). Society for Neuroscience, Abstract, 12, 774.

Schor, R.H., Miller, A.D., Stephen, J.B., Timerick, J.B. & Tomko, D.L. (1985). Responses to head tilt in cat central vestibular neurons. II. Frequency dependence of neural response vectors. Journal of Neurophysiology. 53, 1444-1452.

Shotwell, S.L., Jacobs, R. & Hudspeth, A.J. (1981). Directional sensitivity of individual vertebrate hair cells to controlled deflection of their linear bundles. Annals of the New York Academy of Science. 374, 1-10.

Simpson, J.I. & Graf, W. (1981). Eye muscle geometry and compensatory eye movements in lateral eyed and frontal eyed animals. In Vestibular and Oculomotor physiology, International Meeting of the Barany Society, pp. 20-30.

Spoendlin, H.H. (1965). Ultrastructural studies of the labyrinth in squirrel monkeys. In The role of the vestibular organs in the exploration of space. NASA SP-77, pp. 7-22. Washington, D.C.

Spoendlin, H.H. (1966). The ultrastructure of the vestibular sense organ. In The Vestibular System and Its Diseases, editor. Wolfson, R.J., pp. 39-68. Philadelphia: University of Pennsylvannia Press.

Steer, R.W. Jr. (1970). Progress in vestibular modelling. Part I: response of semicircular canals to constant rotation in a linear acceleration field. In Fourth symposium of the role of the vestibular organs in space exploration, pp. 353-360. Washington D.C.

Steinhausen, W. (1933). Uber die beobachtung der cupula in den bogengangesampullen des labyrinths des lebenden. Hects. Pflugers Arch. 232, 500-512.

Sturm, D. & Raphan, T. (1988). Modelling the three dimensional structure of velocity storage in the vestibulo-ocular reflex (VOR). In Proceedings of the 14th Bioengineering Conference (IEEE).

Ter Braak, J.W. (1936). Untersuchungen ueber optokinetischen Nystagmus. Arch. Neerl Physiology. 21, 309-376.

Waespe, W., Cohen, B. & Raphan, T. (1985). Dynamic modification of the vestubula-ocular reflex by the nodulus and uvula. Science. 228, 199-202.

Waespe, W. & Henn, V. (1977a). Neuronal activity in the vestibular nuclei of the alert monkey during vestibular and optokinetic stimulation. Experimental Brain Research. 27, 523-538.

Waespe, W. & Henn, V. (1977b). Vestibular nuclei activity during optokinetic after-nystagmus (OKAN) in the alert monkey. Experimental Brain Research. 30, 323-330.

Waespe, W., Cohen, B. & Raphan, T. (1983). Role of the flocculus in optokinetic nystagmus and visual-vestibular interaction: Effects of flocculectomy. Experimental Brain Research. 50, 9-33.

Wall, C. & Black, O.F. (1984). The modulation component of nystagmus during earth horizontal rotation: relationship with gaze angle. Acta oto-laryngolica 97, 193-201.

Wilson, V. & Melvill-Jones, G. (1979). Mammalian vestibular physiology. New York, New York: Plenum Press.

Young, L.R. & Henn, V.S. (1975). Nystagmus produced by pitch and yaw rotation of monkeys about non-vertical axes. Sonderdruck aus "Fortschritte der Zoologie" Band 23, Heft 1 Seiten 235-246.